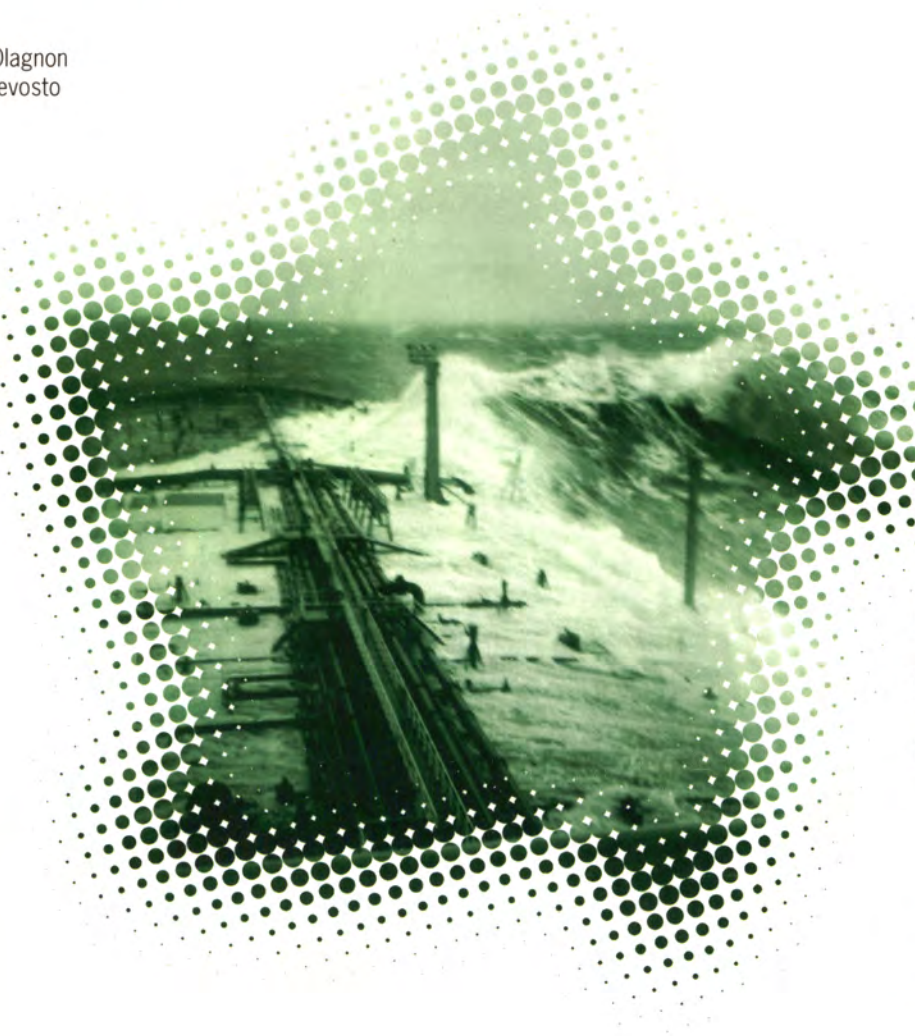


Brest
20-21-22 October 2004



actes de colloques 39

Editors
Michel Olagnon
Marc Prevosto



39


Ifremer

Rogue waves 2004

26 030

Rogue Waves 2004

Michel Ognon & Marc Prevosto
Editors

Proceedings of a Workshop organized by Ifremer
and held in Brest, France
20-21-22 October 2004 within the Brest Sea Tech Week 2004

See also <http://www.ifremer.fr/web-com/stw2004/rw/>



Ifremer



Preface

Every four years, athletes meet at the Olympic games in a friendly competition to raise their performances to higher levels than ever, probably because such a four year duration is the right time interval for efforts to mature into significant progress. Four years after the Rogue Waves 2000 workshop, we thus decided to hold a second Rogue Waves workshop, gathering again researchers, forecasters and industry people to strengthen their work by exchanges in and around a conference room.

We have been very pleased that many of them did respond with evidence of high-quality work carried out since they had gone home after the first workshop. The aim of this second workshop was to assess the state of the art as to conditions of occurrence of waves or groups of waves of unexpected severity, responsible for ship wrecks and damage to offshore oil and gas production systems; and to establish a "road map" as to research actions and collaborations needed to improve the prediction and forecasting abilities in this domain.

We organized the sessions in three groups:

1. Definition, characterization and discussion of the rogueness of waves from their statistics and from the manners in which they affect ships and ocean structures.
2. Generating mechanisms for rogue waves, validation from numerical and physical experiments, observation and comparison between observed and modelled features.
3. Prediction of rogue waves in the short term, through warnings issued with sea conditions forecasts, and in the long term as refinements in the metocean climate descriptions and in the design procedures. What problems are rogue waves facing us with ?

A discussion moderated by Michel Huther concluded the workshop. It stressed that target levels of safety are probably not in jeopardy when global design is considered, but that the problem of how to avoid being caught at the wrong time in the wrong place is still far from being solved.

So we hope to be able to gather participants again in 2008 to discuss their progress on those issues, and may their findings be such that all sailors and workers at sea know afterwards how to keep themselves safe from rogue waves !

September 2005

Michel Olagnon & Marc Prevosto
editors of the proceedings
ROGUE WAVES 2004

Organization

ROGUE WAVES 2004 was organized by the Hydrodynamics and Metocean Group of Ifremer (Institut Français de Recherche pour l'Exploitation de la Mer) and benefitted from the support of the Communauté Urbaine de Brest (now Brest Métropole Océane) and of the Région Bretagne.

It was one of the events of the Brest SeaTechWeek 2004, a week devoted to exchanges between research and industry in marine science and technology.

Our thanks go to all those who supported this workshop by helping finding funding and volunteering their personal time and efforts.

Participants

Pierre Ailliot	email Pierre.Ailliot@univ-ubs.fr
Bertrand Alessandrini	email bertrand.alessandrini@ec-nantes.fr
Fabrice Ardhuin	email ardhuin@shom.fr
Gerassimos Athanassoulis	email mathan@central.ntua.gr
Rolf Baarholm	email Rolf.J.Baarholm@marintek.sintef.no
Sergei Badulin	email bsi@wave.sio.rssi.ru
Nigel Barltrop	email n.barltrop@na-me.ac.uk
Anne Barthelemy	email Anne.Barthelemy@bureauveritas.com
Elzbieta Bitner-Gregersen	email Elzbieta.Bitner-Gregersen@dnv.com
Félicien Bonnefoy	email Felicien.Bonnefoy@ec-nantes.fr
Bas Buchner	email B.Buchner@marin.nl
Alexander Bukhanovsky	email avb@fn.csa.ru
David J.T. Carter	email djc@satobsys.co.uk
Luigi Cavaleri	email luigi.cavaleri@ismar.cnr.it
Lennart Cederberg	email Lennart.Cederberg@smhi.se
Arnaud Coatanhay	email Arnaud.Coatanhay@ensieta.fr
Edmond Coche	email Edmond.Coche@total.fr
Gilbert Damy	email Gilbert.Damy@ifremer.fr
Frédéric Dias	email Frederic.Dias@cmla.ens-cachan.fr
Mark Donelan	email mdonelan@rsmas.miami.edu
Kristian Dysthe	email dysthe@mi.uib.no
Kenneth Johannessen Elk	email kenjo@statoil.com
Pierre Ferrant	email Pierre.Ferrant@ec-nantes.fr
Cyril Frelin	email frelin@actimar.fr
Dorian Fructus	email dorianf@math.uio.no
Richard Gibson	email r.gibson@imperial.ac.uk
E.Brenny van Groesen	email groesen@math.utwente.nl
John Grue	email johng@math.uio.no
Johannes Guddal	email Johannes.Guddal@met.no
Carlos Guedes Soares	email guedess@alfa.ist.utl.pt

Gil-Yong Han
Frédéric Hauville
Sverre Haver
Martin Holt
Michel Hontarrede
Erlend Hovland
René Huijsmans
Keith MacHutchon
Michel Huther
Alastair Jenkins
Lars Johansson
Natanael Karjanto
Christian Kharif
Olivier Kimmoun
Gert Klopman
Harald E. Krogstad
Marc Le Boulluec
Georg Lindgren
Paul C Liu
Leonid Lopatoukhin
Anne Karin Magnusson
Christophe Maisondieu
Gianluca Manes
Bernard Molin
Valérie Monbet
Nobuhito Mori
Alan Murphy
Guillaume Oger
Michel Olagnon
Miguel Onorato
Efim Pelinovsky
D.Howell Peregrine
Marc Prevosto
Igor Rychlik
Henri Savina
Chris Shaw
Hervé Socquet-Juglard
Tarmo Soomere
Christopher Swan
Paul Taylor
Rodolfo Tedeschi
Alessandro Toffoli
Hiroshi Tomita
Karsten Trulsen
Arnaud Vazeille
Arjan Voogt

email gilyonghan@iacs.org.uk
email hauville@ecole-navale.fr
email svha@statoil.com
email Martin.Holt@metoffice.com
email Michel.Hontarrede@meteo.fr
email Erlend.Hovland@stoltoffshore.fr
email r.h.m.huijsmans@marin.nl
email lsi@liebstan.co.za
email michel.huther@bureauveritas.com
email Alastair.Jenkins@bjerknes.uib.no
email Lars.Johansson@smhi.se
email n.karjanto@math.utwente.nl
email kharif@mousson.irphe.univ-mrs.fr
email kimmoun@egim-mrs.fr
email Klopman@math.utwente.nl
email hek@math.ntnu.no
email mlb@ifremer.fr
email georg@maths.lth.se
email paul.c.liu@noaa.gov
email leonid@LL1587.spb.edu
email a.k.magnusson@met.no
email Christophe.Maisondieu@ifremer.fr
email Gianluca.Manes@snamprogetti.eni.it
email molin@egim-mrs.fr
email valerie.monbet@univ-ubs.fr
email mori@urban.eng.osaka-cu.ac.jp
email alan@ship.soton.ac.uk
email guillaume.oger@ec-nantes.fr
email Michel.Olagnon@ifremer.fr
email onorato@ph.unito.it
email Pelinovsky@hydro.appl.sci-nnov.ru
email D.H.Peregrine@bristol.ac.uk
email Marc.Prevosto@ifremer.fr
email igor@maths.lth.se
email Henri.Savina@meteo.fr
email christopher.shaw@shell.com
email Herve.Socquet-Juglard@mi.uib.no
email tarmo@phys.sea.ee
email c.swan@imperial.ac.uk
email paul.taylor@eng.ox.ac.uk
email tedeschi@dinav.unige.it
email Alessandro.Toffoli@bwk.kuleuven.ac.be
email tomita@nmri.go.jp
email karstent@math.uio.no
email Arnaud.Vazeille@bureauveritas.com
email a.j.voogt@marin.nl

Contents

Definition, characterization and discussion of the rogueness of waves from their statistics and from the manners in which they affect ships and ocean structures.

Session 1.1: Large ships and platforms (life-long extremes)

Introductory presentation:

- Sverre Haver (Statoil, Norway) - *Freak Waves - A Suggested Definition and Possible Consequences for Marine Structures*

Regular presentations:

- Bas Buchner and Arjan Voogt (Marin, The Netherlands) - *Wave impacts due to steep fronted waves*
- Rolf Baarholm and Carl Trygve Stansberg (MARINTEK, Norway) - *Extreme Wave Impact on GBS Platform Deck*
- D.Howell Peregrine (School of Mathematics, Bristol University, UK) - *(Abstract) Violent water wave impacts on a wall*
- Nigel Barltrop (Universities of Glasgow and Strathclyde, UK) - *(Abstract) A simple wave front steepness enhancement prediction methodology*
- Bernard Molin, F. Remy, O. Kimmoun, E. Jamois (EGIM, France) - *(Abstract) Enhanced wave effects on the weather side of reflective structures*
- Anne Karin Magnusson (Met.no, Norway), Jaak Monbaliu, Alessandro Toffoli (KU Leuven, Belgium) and Elzbieta Bitner-Gregersen (DNV, Norway) - *(Abstract) On the shape of large waves in the central and southern North Sea*
- Paul C. Liu (NOAA, USA), Keith MacHutchon (Liebenberg & Stander International, South Africa) - *Exploring rogue waves from observations in South Indian Ocean*

Session 1.2: Small crafts, high speed crafts (unexpected highs in operational conditions)

Introductory presentation:

- Bruce Johnson (US Naval Academy, USA) and Stefan Grochowalski (Ottawa, Canada) - *(Abstract - paper not presented due to last minute problem) Development of Operational Guidance Criteria for Small Craft Operating in Dangerous Seas*

Regular presentation:

- Soren Peter Kjeldsen (Trondheim Maritime Academy, Norway) - *Examples of observed freak waves in Norway and related ship accidents (Paper not presented due to last minute problem).*

Generating mechanisms for rogue waves, validation from numerical and physical experiments, observation and comparison between observed and modelled features.

Session 2.1: Theoretical results, numerical and physical simulations

Introductory presentation:

- Paul H. Taylor (University of Oxford, UK) – *(Abstract) Rogue Waves and wave focusing - speculations on theory, numerical results and observations*

Regular presentations:

- Richard Gibson and Chris Swan (Imperial College London, UK) – *The role of resonant wave interactions in the evolution of extreme wave events.*
- J.P. Giovanangeli, C. Kharif (IRPHE, France) and E. Pelinovsky (Institute of Applied Physics, Nizhny Novgorod, Russia) – *Experimental study of the wind effect on the focusing of transient wave groups*
- Dorian Fructus and John Grue (Universitetet i Oslo, Norway) – *A rapid fully nonlinear method in three dimensions with simulations of steep wave event*
- J. Grue, D. Clamond, M. Francius (Universitetet i Oslo, Norway) and C. Kharif (IRPHE, France) – *On the role of downshifting in formation of large wave events*
- Tarmo Soomere and Jüri Engelbrecht (Tallinn Technical University, Estonia) – *Extreme elevations and slopes of interacting Kadomtsev-Petviashvili solitons in shallow water*
- Hervé Socquet-Juglard, Kristian Dysthe (Universitetet i Bergen, Norway), Karsten Trulsen (Matematisk Institutt, Universitetet i Oslo, Norway), Harald E. Krogstad, Jingdong Liu (NTNU, Trondheim, Norway) – *(Abstract) Distribution of extreme waves by simulations*
- Félicien Bonnefoy, Pierre Roux de Reilhac, David Le Touzé, Pierre Ferrant (Ecole Centrale de Nantes, France) – *Numerical & Physical Experiments of Wave focusing in short-crested seas*
- Karsten Trulsen (Matematisk Institutt, Universitetet i Oslo, Norway) – *(Abstract) Transversal crest and group modulation of extreme waves*
- C. Fochesato, F. Dias (ENS Cachan, France), S. Grilli (University of Rhode Island, USA) – *Wave energy focusing in a three-dimensional numerical wave tank*
- Miguel Onorato, Alfred Osborne, Marina Serio (University of Torino, Italy) – *Quasi-resonant interactions and non-Gaussian statistics in long-crested waves*
- Guillaume Oger, Mathieu Doring, Bertrand Alessandrini, Pierre Ferrant (Ecole Centrale de Nantes, France) – *SPH: Towards the simulation of wave-body interactions in extreme seas*

- Sergei Badulin (Russian Academy of Sciences, Moscow, Russia), A. Pushkarev (Waves and Solitons LLC, USA), D. Resio (US Army Engineer R&D Center, USA), V. Zakharov (Russian Academy of Sciences, Moscow, Russia & University of Arizona, USA) - *Self-similarity of wind-wave spectra. Numerical and theoretical studies*

Session 2.2: Comparison with observed results

- Hervé Socquet-Juglard and Kristian B. Dysthe (University of Bergen, Norway), Karsten Trulsen (University of Oslo, Norway), Sébastien Fouques, Jingdong Liu and Harald E. Krogstad (NTNU, Trondheim, Norway) - *Spatial extremes, shapes of large waves and Lagrangian models*
- Chris Swan, Richard Gibson and Peter Tromans (Imperial College London, UK) - *Wave crest statistics calculated using a fully nonlinear spectral response surface method*
- Andonowati and E. van Groesen (Marin, The Netherlands) - *Deterministic Aspects of Nonlinear Modulation Instability*
- Nobuhito Mori, (Osaka City University, Japan) and Peter A.E.M. Janssen (ECMWF, UK) - *Dependence of freak wave occurrence on kurtosis*
- Elzbieta Bitner-Gregersen (DNV, Norway) & Anne Karin Magnusson (Met.no, Norway) - *Extreme Events in Field Data and in a Second Order Wave Model*
- Michel Olagnon (Ifremer, France) & Anne Karin Magnusson (Met.no, Norway) - *Spectral parameters to characterize the risk of rogue waves occurrence in a sea state*
- R. Huijsmans, N. Karjanto, Andonowati, Klopman & E. van Groesen (Marin, The Netherlands) - *Experiments on extreme wave generation using the Soliton on Finite background*
- Alastair D. Jenkins (Universitetet i Bergen, Norway), Anne Karin Magnusson (Met.no, Norway), Andreas Niedermeier (DLR, Germany), Jaak Monbaliu and Alessandro Toffoli (KU Leuven, Belgium), Karsten Trulsen (Matematisk Institutt, Universitetet i Oslo, Norway) - *Rogue waves and extreme events in measured time-series*
- C. Guedes Soares, and E.M. Antão (IST, Portugal) - *Comparison of the characteristics of abnormal waves on the North Sea and Gulf of Mexico*

Prediction of rogue waves in the short term, through warnings issued with sea conditions forecasts, and in the long term as refinements in the metocean climate descriptions and in the design procedures.

Session 3.1: Can sensible warnings be issued ?

Introductory presentation:

- Henri Savina & Jean-Michel Lefèvre (MétéoFrance) - *Sea state in Marine Safety Information : present state, future prospect (Oral Presentation only)*

Regular presentations:

- Martin Holt, Gary Fullerton, Jian-Guo Li (Met Office, UK) - *Forecasting sea state with a spectral wave model (Oral Presentation only)*
- A.V.Boukhanovsky (Institute for High Performance Computing), L.J.Lopatoukhin (State University, Dep. Oceanology) (St. Petersburg, Russia) and C.G.Soares (Instituto Superior Tecnico, Lisboa, Portugal) - *Climatic wave spectra and freak waves probability*
- Mark A. Donelan (university of Miami/RSMAS, USA), Anne Karin Magnusson (Met.no, Norway) and Elzbieta Bitner-Gregersen (DNV, Norway) - *Towards a Global Rogue Wave Warning System (Oral Presentation only)*

Session 3.2: Should we modify design specifications ?

Introductory presentation:

- Gil-Yong Han (IACS - International Association of Classification Societies) - *Ship design rules and regulations, an overview of major themes*

Regular presentations:

- C. Guedes Soares, N. Fonseca and R. Pascoal (IST, Portugal) - *Comparison of present wave induced load criteria with loads induced by an abnormal wave on marine structures*

Our warmest thanks to Professor Laurence Draper and to David Carter for providing reprints of the first known articles about freak waves, to an anonymous former cadet of the Jeanne d'Arc for the report of a near-miss, and to Sverre Haver for clarifying the story of the famous "New Year Wave".

Historical reprints

- Laurence Draper (reprinted from *Oceanus* (X:4), July 1964) - *"Freak" Ocean Waves*
- Laurence Draper (reprinted from *J. Navigation* (24:3), Royal Inst. of Navigation, July 1971) - *Severe Wave Conditions at Sea*

Testimonies

- Cdt. Frédéric-Moreau (Jeanne d'Arc, France) - *The Glorious Three*
- Sverre Haver (Statoil, Norway) - *A possible freak wave event measured at the Draupner Jacket January 1, 1995*

Freak Waves: A Suggested Definition and Possible Consequences for Marine Structures

Sverre Haver

Marine Structures and Risers, Statoil ASA, N-4035 Stavanger, Norway
svha@statoil.com

Abstract. Target annual exceedance probabilities of design loads of offshore structures on the Norwegian Continental shelf are briefly discussed. It is proposed to define freak wave events as events that are well beyond what is typically expected within wave theories utilized for structural design. With this background, the question of whether or not freak waves are of concern for practical design work is discussed. The discussion is not conclusive, and major focus is given to some questions that need to be properly answered before a final conclusion can be made.

1 Introduction

This paper is prepared as an introductory lecture to a session discussing rogue waves and practical problems related to their possible existence. The paper do not present any new evidences of freak waves. The purpose is merely to present some few questions that need to be properly answered before it can be concluded whether or not freak waves represent a threat to structural integrity. Hopefully, these questions and accompanied discussions can act stimulating on those research groups addressing freak waves from a more basic research point of view.

Offshore structures at the Norwegian Continental Shelf are with respect to overload designed against environmental loads corresponding to an annual exceedance probability of 10^{-2} multiplied by a partial load factor of 1.3, Norsok(1999). Provided that the load versus exceedance probability is of a well behaved nature, the design load thus obtained is tacitly assumed to result in a reasonable platform safety against collapse. However, this may not be the case if for some reason the load – exceedance probability relation changes abruptly in a worsening direction for exceedance probabilities between 10^{-2} and 10^{-4} . Such an abrupt change in load pattern could take place if the most extreme waves impact the deck structure. An illustration of the load – exceedance probability relation for a well behaving and a bad behaving response problem is shown in Fig. 1.

In order to ensure that an ill behaving response problem is not slipping unnoticed through the design process, Norwegian Offshore Regulations, NPD(2001), also

requires that the structures shall withstand 10^{-4} -probability¹ environmental loads with at most some local damage. There is not a one-to-one relation between wave crest height and platform loading, but in most cases there is a rather large positive correlation. This means that if we shall be able to predict reasonable estimates for the q -probability loads, $q=10^{-2}$ and 10^{-4} , the wave models used for design should accurately reflect wave events with occurrence probabilities of the order of magnitudes.

Accordingly, a quantity of crucial concern is the very upper tail of the annual distribution function of wave events and loads, i.e. annual exceedance probabilities in the range $10^{-2} - 10^{-5}$. Provided that the sea surface can be modeled as a stationary and homogeneous second order random field, see e.g. Marthinsen and Winterstein (1992), Forristall (2000), it is expected that it is possible to estimate the upper tail of the annual extreme value distributions with a sufficient accuracy. The challenging question, however, is whether or not there exists wave phenomena beyond our adopted design model which may affect the very upper tails significantly.

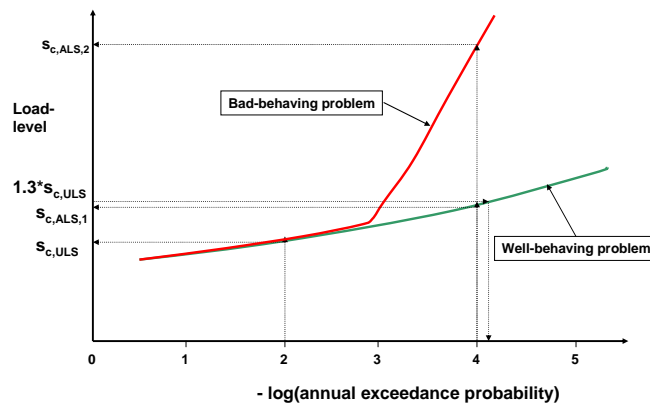


Fig. 1. Illustration of well-behaving and bad-behaving response problem.

2 Are rogue waves a problem for structural design?

The answer to this question depends very much on what is meant by a rogue wave. There is at least two options: i) “Classical” extreme waves and ii) Freak extreme waves. Unfortunately, it is not always clear what people mean when they refer to rogues waves. As an extended introduction, some paragraphs will therefore be spend on clarifying what will be meant throughout this paper.

¹ Q -probability event means an event corresponding to an annual exceedance probability of q .

"Classical" extreme waves

By classical extreme waves, we will herein think of rare members of a population of wave events defined by modeling the surface process as a piecewise stationary and homogeneous slightly non-Gaussian random field. The word "classical" is introduced since this approach is what in principle is available for routine design. Over the years, the so-called "classical" population has evolved somewhat. One to two decades ago, the surface process was often modeled as Gaussian random field. As a consequence of that the "classical" extreme crest height population of those days was shifted slightly to smaller values than those being in agreement with the present definition.

This type of extreme waves are in most cases properly accounted for by the offshore industry, provided some 10^{-4} – probability wave load scenario is implemented. Traditional shipping may have some room for improvements both when it comes to the implementation of a slightly non-Gaussian surface process and the adopted exceedance probabilities for the design loads. The latter is in particular the case when it comes to slamming and green water related problems.

It is important to realize that even within "classical" extreme waves population, wave events which may represent a threat to the integrity of a structure do exist. However, their annual exceedance probability for a given site should be lower than say 10^{-5} if a structure is properly designed.

Freak (extreme) waves

Herein we will define freak waves as typical members of population being defined by physical mechanisms well beyond those underlying "classical" extreme waves.

These types of extreme wave events are not explicitly accounted for in the design process. If such a population exists, it may challenge present design recipes if it significantly affects wave properties (crest heights, wave heights, wave steepness) at a given site corresponding to annual exceedance probabilities of $10^{-3} - 10^{-5}$. It should be noted that we throughout this paper always will refer to the annual extreme value distribution functions at a given site. This because a structure can not simultaneously sample wave events more than at one site. The rule requirements to target maximum exceedance probability of the design loads, therefore refer to annual exceedance probabilities at a particular site. In case of traditional shipping, this site would be a site moving along a given route.

Which out of these populations is the most common adopted definition of rogue waves is hard to say. It seems as if the rogue waves population often is meant to capture both populations referred to above. From a practical point of view that is not convenient, because a major part of the rogue wave population, "classical" extreme waves, does not represent a problem, while the *freak extreme waves* population, if it exists, may represent a challenge.

3 Suggested definition of freak waves

The most common definition of a freak wave, is to define a wave as a freak wave if the wave height to significant wave height ratio or the crest height to significant wave height ratio exceed some thresholds. A factor definition may be useful as a first indicator of possible freak event. In this connection, the recommended thresholds should account for the duration of the observation window, i.e. is the observed maximum a 20-min. maximum, is it a 3-hour maximum or is it a storm maximum.

From a practical point of view it seems more convenient to anchor the definition of a freak wave to mechanisms not captured by the wave models used for design purposes. It is therefore recommended to define freak waves as follows, Haver (2000):

A freak wave event is an event (crest height, wave height, steepness or group of waves) that represent an outlier when seen in view of the population of events generated by a piecewise stationary and homogeneous second order model of the surface process.

The definition is related to major deviations from a second order model because this is the most sophisticated model that is available for routine design work. As more sophisticated model for design is developed, the “classical” extreme wave population will grow on the cost of the *freak wave population*.

If one is to look for freak waves in available measurements, one will need a freak wave indicator as the observations are scanned. For such a purpose a factor threshold is useful. If we are basing the data search on scanning of 20-min. time series, one should establish proper threshold for this experiment. If the sea surface is modeled as a second order process, the 99-percentile of the ratios $c_{20\text{-min.}} / h_s$ and $h_{20\text{-min.}} / h_s$ read about 1.25 and 2.00, respectively, Haver(2000). If an observation exceeds this threshold, one may at a significance level of 1% reject this observation as a realization from a second order process of 20-min. duration. However, further investigations should be carried out before the event is concluded as belonging to the *freak extreme waves* population.

If the observation window is increased to 3-hours, more adequate thresholds would be 1.50 and 2.45, respectively. If a storm is defining the observation window, 1.60 and 2.55 will probably represent adequate thresholds if a 1% significance level is found proper for the freak wave indicator.

The advantage of this definition is that we accept that rather lather freak wave indicator factors occur even within the “classical” extreme waves population. If a separate phenomenon can be excluded, freak wave should be of no concern. If a structure is being hit by an unexpectedly large wave event, it is then merely a matter of being at the wrong place at the wrong time. The annual occurrence probability of this event, however, should be well below the target annual exceedance probabilities of the design loads.

Finally, it should be pointed out that the thresholds recommended above, refer to observations from a given site. If the observation window is extended to also cover spatial domain, the thresholds for the indicator should be significantly increased in order to account for effects discussed by Krogstad et al. (2004).

4 Why should we be concerned about freak waves?

It is seen from Fig. 1 that an ill-behaving response problem being overlooked in the design process could represent a threat to the structural integrity. The figure reflects the airgap problem. In practice this problem is dealt with by requiring that the airgap is sufficiently large for the annual wave-deck impact probability to be less than 10^{-4} . In this connection, the 10^{-4} crest height is estimated using the classical extreme wave population. If a freak wave population exists and if it is realized sufficiently frequent to effect the interesting part of the annual extreme value distribution of the crest height, freak waves may represent a source for an ill-behaving response problem, i.e. a scenario where for a low exceedance probability the load increases abruptly. This is because a fatter tail will make a wave-deck impact more probable. The possible effect of freak waves which we should be concerned about is illustrated in Fig. 2.

If a freak wave population exists, what is the problem? For ships and offshore platforms, a freak wave will mainly represent a problem if its crest hits structural members which is not designed for wave loads. As far as no new members are exposed, the global loading due to a freak wave is most probably smaller than the global loading in connection with a “classical” extreme wave. However, it is recommended that further work are carried out in order to establish some documented knowledge on the freak wave kinematics.

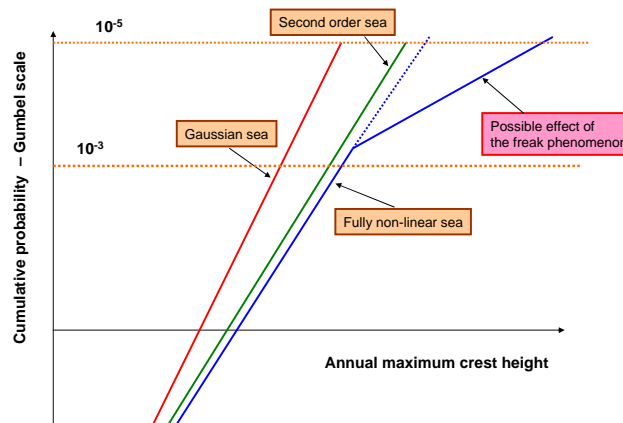


Fig. 2. Possible effect of freak waves of annual extreme value distribution of wave crest height

5 The freak wave challenge

With respect to waves, offshore structures are designed against the q -probability waves from the population referred to herein as the “classical” extreme waves. If the design process also involves a proper check of the structure against accidental waves (10^{-4} – probability waves), a certain robustness against freak wave events is achieved. This is under the assumption that it is not the group involving the worst waves from the “classical” extreme waves that is focused into a single majestic wave. However, if this assumption is not true, freak waves may, if they exist as a separate phenomenon, represent an unknown or unquantified threat to marine structures. At present it is not possible to approach freak waves in a rational way in the design process.

In order to be able to account for possible freak waves in rational design recipe, the following questions need to be answered:

- Does a separate freak wave population exist?
One needs to identify the underlying physical mechanisms that can make a freak wave development possible.
- Given a separate population exists, what is the conditional probability, say per 3-hour duration of a sea state, for a freak wave development given some engineering sea state characteristics?
From a design point of view, a freak wave does not represent a problem unless it at a given site occurs sufficiently frequent to effect our predictions of 10^{-2} - and 10^{-4} – probability wave events.
- Given a freak wave occurs in a 3-hour sea state with given characteristics, what is the conditional distribution for the freak wave amplification factor?
The freak wave amplification factor is defined as the ratio $c_{3hr, freak} / c_{3hr, nonfreak}$. In some cases a freak wave will not be larger than the largest wave in another group of the sea state not being exposed to a freak wave development. On the other hand, if it is the largest group of the sea states that develops into a single majestic wave, the amplification factor may be considerable.

Wave data collection programs will possibly not be the most adequate approach for concluding on the existence of a separate freak wave population. In case of an unexpectedly large observation, one will face the following question, Haver and Andersen (2000): Is the observed wave a very rare realization from the typical slightly non-Gaussian sea surface population, or, is it a typical realization of a very rare and strongly non-Gaussian sea surface population? A more fruitful approach in the long run is to develop mathematical models accounting properly for the underlying physics including the physics that may govern a freak wave development. If such a model becomes available, one should in principle be able to answer the two last equations through time domain simulations of sea surface fields.

A rather qualitative assessment of whether or not freak waves represent a problem for practical design was presented by Haver et al. (2004). The basic idea of that

assessment is that we for any sea state can establish a proper extreme value distribution for $C_{3hr,nonfreak}$, i.e. the 3-hour maximum crest height given no freak wave development took place. The conditional probability of freak wave development is measured by a two outcome variable, K . If no freak wave development take place, $K=0$, while $K=1$ describes a freak wave development. At present we do not know the conditional probability of $K=1$ for the various sea states and in the paper it is simply modeled as a bell shape function of h_s and t_p . An example of $P(K=1 | H_s, T_p)$ is shown in Fig. 3. In the study some sensitivity studies of the parameters of this function are included.

The 3-hour maximum accounting for a possible freak wave development is written on the following form:

$$C_{3hr,freak} = C_{3hr,nonfreak} + K*\Delta C_{3hr,freak} = C_{3hr,nonfreak}(1 + K*\Lambda) \quad (1)$$

$\Delta C_{3hr,freak}$ is the increase of the 3-hour maximum crest height due to the freak wave development. Λ describes the same quantity normalized by the 3-hour maximum if no freak wave development takes place. $\Lambda = 0$ if the freak wave crest height is not the highest crest height of the sea state. This is more or less arbitrarily assumed to be the case in 25% of the cases with a freak wave development. The distribution function for Λ is shown in Fig. 4. The qualitative study indicates that if the chance of a freak wave development is very small, which is what available observations suggest, freak waves will not affect design wave events. However, one has to keep in mind that most of our observations correspond to sea states not much more severe than what the 1- to 10-year contour lines shown in Fig. 5 suggest. However, a wave event is not expected to be critical regarding structural integrity before we approach or exceed the 10000-contour of Fig. 5.

If the conditional probability of $K=1$ is much higher for sea states beyond what are presently observed, freak waves may represent a threat to marine structures. It is therefore recommended that research is continued until it can with reasonable confidence conclude that the freak wave probability is not positively correlated with sea state severity. Severity is in this connection not measured only in significant wave height.

6 Possible mechanisms for a freak wave development

Herein we will not review the various mechanisms that have been proposed as possible freak wave mechanisms. The reader could review other presentations at this workshop or consult proceedings from the previous rogue waves work shop, Olagnon and Athanassoulis (2001). One of the mechanisms, Benjamin-Feir instability, seems to require that surface process need to be rather narrow banded both frequency (wave number) and direction in order to be realized. The real ocean surface is typically short crested suggesting that the real sea surface is less exposed to the self focusing of major wave groups. However, the real ocean is not homogeneous and stationary to the extent that is typically utilized in ocean engineering. Fig. 6 shows an illustration of a

sea surface that is generally of a short crested nature, but where a sub-area is assumed to exist. Is this a possible scenario in the real world? Are we smoothing away these possibilities by our input assumption of piecewise homogeneity and stationarity? One should probably approach these questions rather open minded although if these assumptions have to be skipped, the ergodicity assumption that is underlying much of our work in ocean engineering can be questioned.

Satellite observations of larger areas may prove very useful when it comes to verify our assumption of sea surface homogeneity.

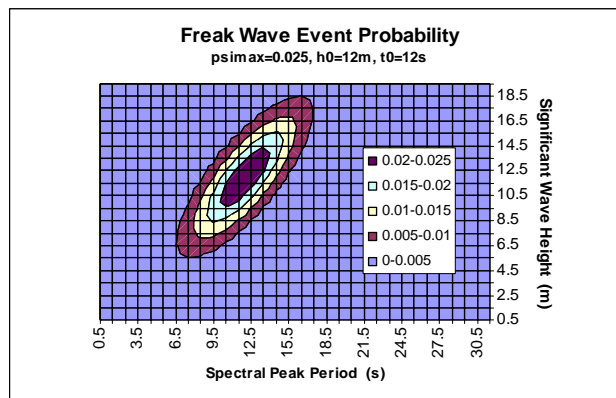


Fig. 3. Illustrative conditional probability of freak wave phenomenon given sea state characteristics.

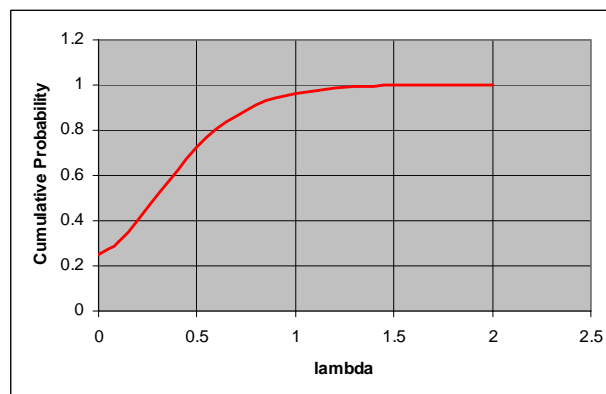


Fig. 4. Illustrative conditional distribution function of the freak wave development factor.

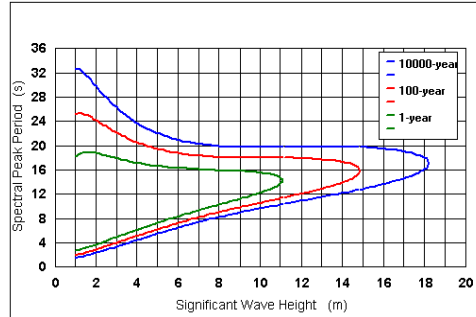


Fig. 5. q-probability contour lines for H_s and T_p for a Northern North Sea location

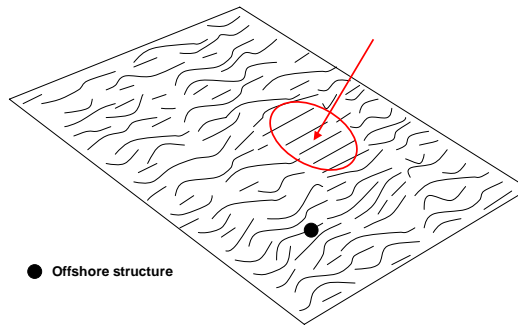


Fig. 6. Illustration of a short crested sea surface with a long crested sub-domain.

7 Conclusions

The discussions presented previously can be summarized as follows:

- Freak waves should be defined as a separate population well beyond the population used for design purposes.
- Freak waves are not likely to represent a problem for offshore structures if their frequency of occurrence experienced for the sea states observed so far is generally valid.
- There is some concern that traditional ships may experience considerable damages in extreme wave conditions, even if the waves are well within the classical extreme wave population.
- Freak waves may be of some concern if their conditional occurrence probability is increasing as we enter into the range of non-observed sea state severities.

- A first step to gain some robustness against unknown freak wave extremes, could be to involve an accidental wave event (10^{-4} – probability wave event) into the design process.

8 Acknowledgement

Statoil ASA is acknowledged for the permission to publish this paper. It should be pointed out the views presented herein are those of the author and should not be construed as necessarily reflecting the views of Statoil.

9 References

Forrinstall, G.Z. (2000): “Wave Crest Distribution: Observations and Second-Order Theory”, *Journal of Physical Oceanography*, Vol. 30, August 2000.

Olagnon, M. and Athanassoulis, G.A. (2001) (Editors): “Rogue Waves 2000”, *Proceedings of a Workshop organized by Ifremer, November 29-30, Brest France.*

Haver, S. and Andersen, O.J. (2000): “Freak Waves: Rare Realizations of a Typical Population or Typical Realizations of a Rare Population?”, *ISOPE-2000, May 2000, Seattle, USA.*

Haver, S. (2000): “Evidences on the Existence of Freak waves”, *Rogue Waves 2000, November 2000, Brest France.*

Haver, S., Vestbøstad, T. M., Andersen, O. J. and Jakobsen, J.B. (2004): “Freak Waves and Their Conditional Probability Problem”, *ISOPE 2004, May 2004, Toulon, France.*

Krogstad, H., Liu, J., Socquet-Jugland, H., Dysthe, K.B. and Trulsen, K. (2004): “Spatial extreme value analysis of nonlinear simulations of random surface waves”, *OMAE-2004, Vancouver, June 2004.*

Marthinsen, T. and Winterstein, S.R. (1992): “On the skewness of random surfaces”, *ISOPE 1992, San Francisco, 1992.*

Norsok(1999): “Norsok Standard – Action and Action Effects”, N-003, Oslo, 1999.

NPD (2001): “Regulations Relating to Design and Outfitting of Facilities etc in the Petroleum Activities (The Facilities Regulation)”, *Norwegian Petroleum Directorate, Stavanger, September 2001.*

WAVE IMPACTS DUE TO STEEP FRONTED WAVES

Bas Buchner and Arjan Voogt

Maritime Research Institute Netherlands (MARIN)

b.buchner@MARIN.NL, a.j.voogt@MARIN.NL

INTRODUCTION

It is the question whether 'Rogue waves' can only be identified and characterized by their extreme heights. The results presented in this abstract and related papers [1,2,4,5,6] show for instance that an extreme wave front steepness can induce large impact pressures on the hull of a moored ship-type offshore structure. As part of the 'SAFE-FLOW' Joint Industry Project these loads were investigated with a dedicated series of model tests.

PROBLEM

Wave impact damage has been experienced by both the Foinaven and Schiehallion FPSOs. During the night of the 9th November 1998, in a sea state estimated as $H_b = 14$ m, $T_p = 15-16$ seconds, an area of forecastle plating on Schiehallion above the main deck, between 15 and 20 m above notional mean water level was pushed in by 0.25 m.



Figure 1: Damage to the Schiehallion bow

There was some associated minor plating deformation inside the fore peak (see Figure 1), below the main deck but there was no damage to the flare supports (which are mounted on top of the forecastle) or any process equipment. The damage occurred at the time in the storm at which the measured wind gust speeds were strongest but at the time the wind sensors on the vessel recorded a 10-minute gust speed of 59 knots compared with a one-year-return-period design value of 69 knots. By contrast, the most severe vessel motion, due to heave and pitch, occurred between 2 and 6 hours later. Wave records from a vessel some 12 km distant from Schiehallion showed a rapid increase in wave height in the period leading up to the damage event. A mean zero crossing period of 11 s, coupled with a significant wave height of 14 m indicates a severe sea state steepness estimated as 1/13, but there are no corresponding records of individual waves.

EXPERIMENTS

As part of the SAFE-FLOW project MARIN performed 2 series of model tests at scale 1:60 in deep water. First tests were carried out on a free floating Schiehallion FPSO model (Figure 2).

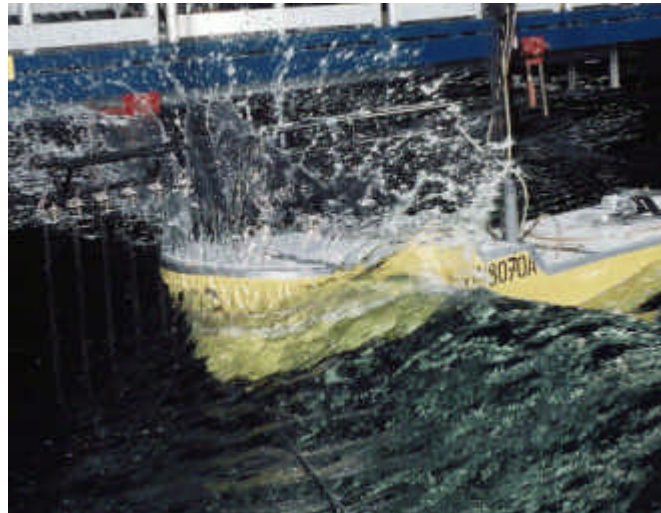


Figure 2: Bow impact event on free floating model

In these tests in irregular seas the incident wave data, vessel motions and resulting relative motions, bow pressures and structural response were measured. The tests showed that more detailed load measurements were necessary and that an investigation was needed into the relation between the incoming waves and these loads. This resulted in the second model test series on a highly instrumented fixed simplified bow, see Figure 3. The simplified bow was instrumented with a large array of pressure transducers and 3 force panels. The test program, also making use of extensive video recordings, was designed such that it was possible to determine the correlation between undisturbed wave shape and the impact pressure time traces. From these tests irregular sea incident wave data and bow pressure results are available on a fixed schematic bow structure with varying rake and plan angles.

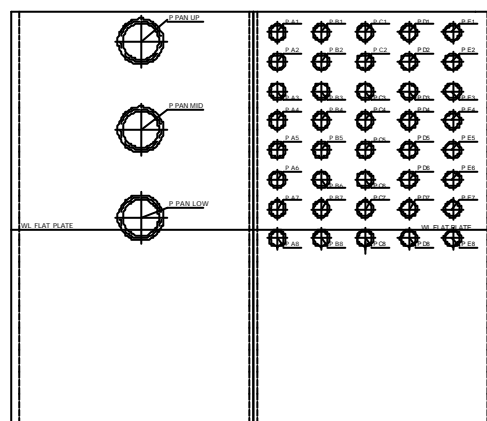


Figure 3: Instrumented plate-like fixed bow with force panels (left) and pressure cells (right)

OBSERVATIONS

It was found that the magnitude of the wave impacts at the front of the bow is dominated by the wave characteristics (namely the local wave steepness), rather than by the motions of the ship relative to the waves (relative wave motions). Further the maximum pressures are measured close to the crest of the incoming waves. An example of a steep wave front reaching the bow structure is shown in Figure 4.

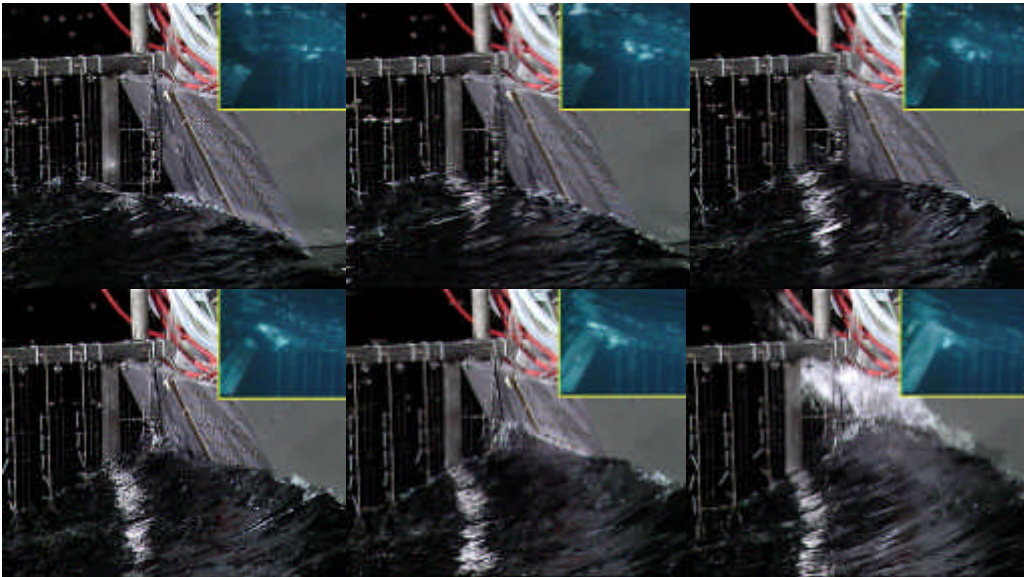


Figure 4: Typical stages during a bow impact

The local wave steepness ($d\eta/dx$) could be determined from measurements of the wave elevations in an array of probes. An example is shown in Figure 5, which shows the spatial wave profile for successive steps in time. The time step between the different lines is 0.31 seconds and the distance between the probes 6 meter allowing for an accurate derivation of the local wave steepness.

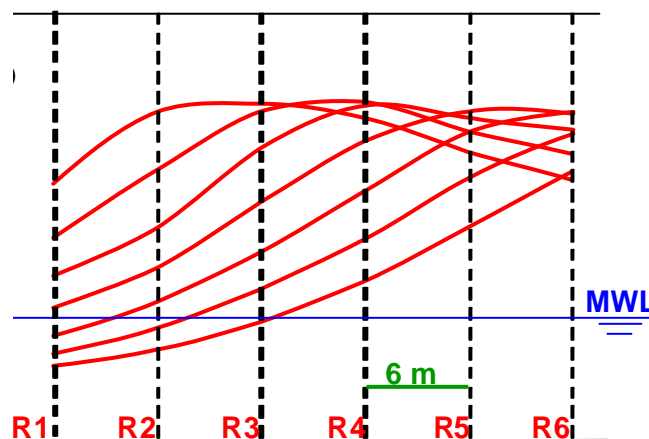


Figure 5: Visualisation of the local wave steepness ($d\eta/dx$) based on the measurements of the wave elevations in an array of probes

It was found that wave impacts on the bow could always be related to an exceedance of a certain wave front steepness. Typically wave front steepnesses above 30 degrees (with the horizontal) resulted in wave impacts, see Figure 6.

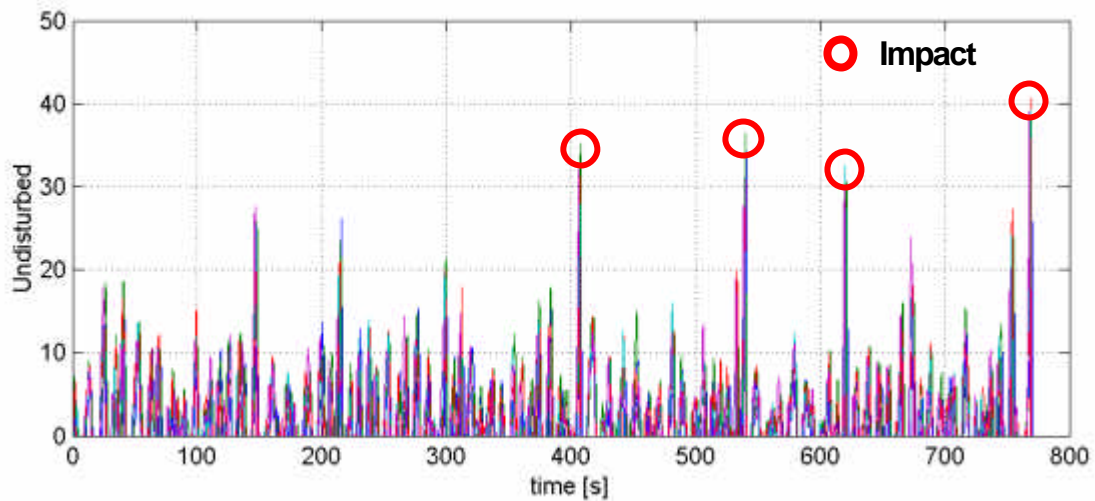


Figure 6: Relation between the local wave steepness ($d\eta/dx$ in degrees) and occurrences of wave impacts on the fixed bow

The combined spatial and temporal information of the sea state needed to derive the local wave steepness is not generally available (in full scale data and model tests). Therefore the vertical free surface velocity ($d\eta/dt$) is preferred as input to a prediction model.

The local free surface steepness is linearly related to the free surface vertical velocity ($d\eta/dt$) through the wave celerity. Though this is strictly true only for linear waves and on a wave to wave basis, given free surface continuity and according to Cauchy's intermediate value theorem, there are values of c and η such that the relationship is verified for a wave that results from a sum of elementary components.

The relationship between the maxima in the vertical free surface velocity ($d\eta/dt$) and the impacts is shown in Figure 7. It shows the traced impacts (circles) versus the time traces of the vertical surface velocity. The impacts occur at the same moment as the maxima in the vertical free surface velocity.

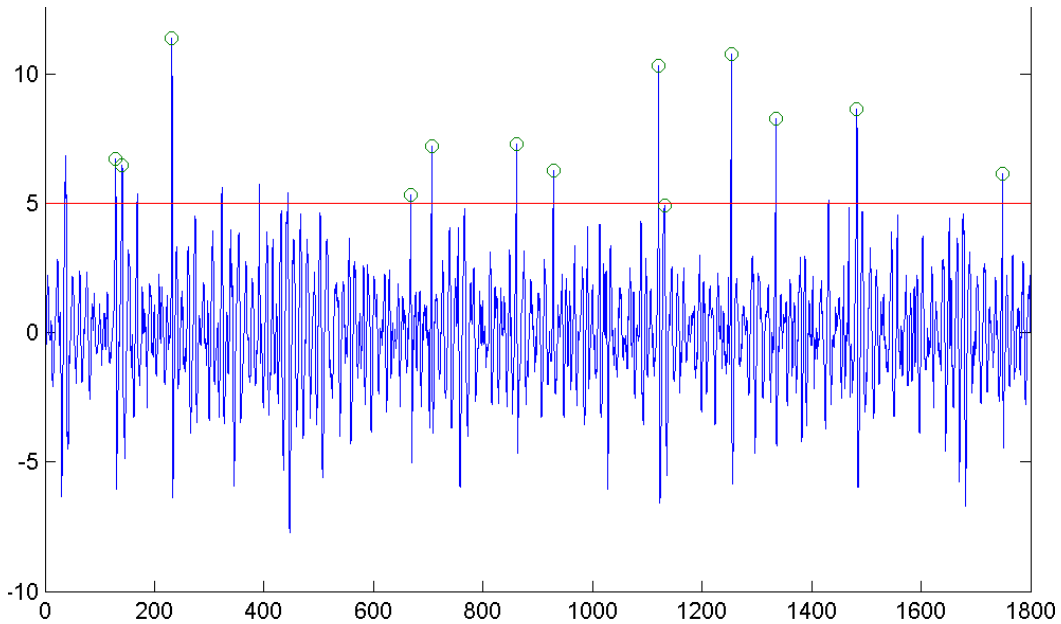


Figure 7: The traced impacts (circles) versus the time traces of the vertical free surface velocity

In steep waves that cause the bow impact, linear theory clearly under predicts the wave steepness. The most suitable method of simulating the water surface to give a reasonable probability of vertical free surface velocity was found to be second order wave theory, as described by Sharma and Dean (1981) for instance. Applying second order wave theory results in an improved prediction of $d\eta/dt$, as shown in Figures 8 and 9 for the basin waves applied.

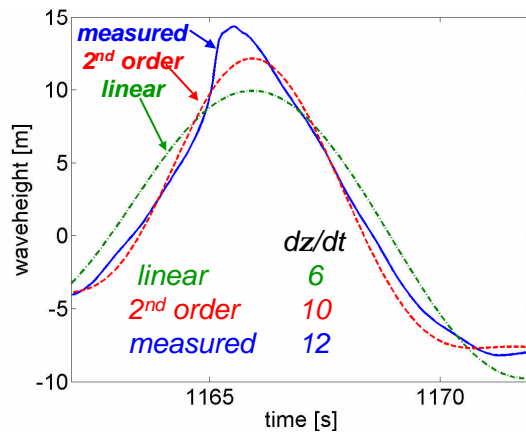


Figure 8: Measured, first order and second order wave time trace

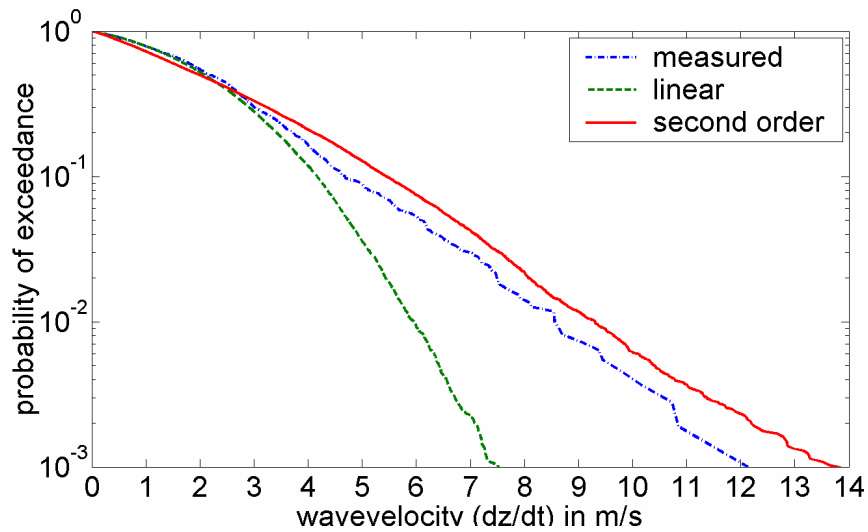


Figure 9: Probability of exceedance of a vertical free surface velocity (measured, linear and second order)

It is clear that the second order theory is not capable to describe the asymmetry in the measured non-linear wave. However, within the accuracy of the present design methodology this is not considered a critical aspect and the distribution of the vertical free surface velocities do match the measured non-linear distribution reasonably well.

Beside the slam probability, the slam magnitude is of vital importance. After analysis of all data, it was decided to relate the slam impulse (I), the area under the load time trace, to vertical free surface velocity ($d\eta/dt$).

Figure 10 shows the measured impulses versus the corresponding vertical free surface velocities. For different velocity bins the mean and standard deviation of the occurring impulses is added to the figure, resulting in straight lines.

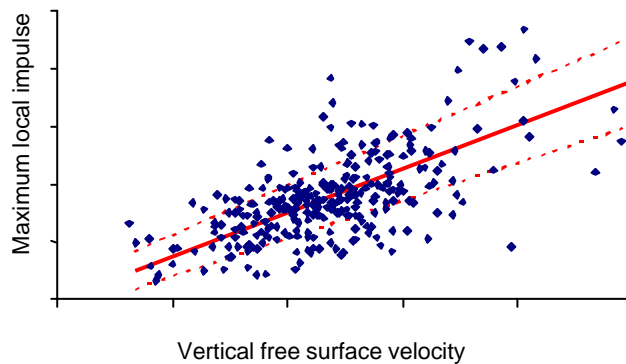


Figure 10: The measured impulses versus the corresponding vertical free surface velocities

The relation is independent of the sea state and holds for a schematic flat plate bow. Within the design method the mean fit is used as a maximum that can occur. For more realistic curved bow shapes the loads are reduced. The spreading around this mean can be used as input to the derivation of the load factors in a first principles reliability approach.

Other wave impact characteristics, such as rise time, decay time, spatial extent and the effect of the bow shape are later applied to this local impulse on a flat plate to determine the resulting structural response. More details can be found in [1,2,4,5,6].

ACKNOWLEDGMENTS

The SAFE-FLOW project (SAFE-FLOating offshore structures under impact loading of shipped green water and Waves) is funded by the European Community under the 'Competitive and Sustainable Growth' Programme (EU Project No.: GRD1-2000-25656) and a group of 26 industrial participants (oil companies, shipyards, engineering companies, regulating bodies). The participants are acknowledged for their interesting discussion of the results during the project and the permission to publish the present abstract. The authors are solely responsible for the present paper and it does not represent the opinion of the European Community.

REFERENCES

1. Buchner, B., Hodgson T., Voogt, A.J. (editors), Ballard, E., Barltrop, N., Falkenberg, E., Fyfe, S., Guedes Soares, C., Iwanowski, B., Kleefsman, T., 2004, "Summary report on design guidance and assessment methodologies for wave slam and green water impact loading", MARIN Report No. 15874-1-OE, Wageningen, The Netherlands.
2. Guedes Soares, C., Pascoal, R., Antão, E.M, Voogt, A.J. and Buchner B. 2004, "An approach to calculate the probability of wave impact on an FPSO bow", Proceedings of the 23st OMAE Conference, ASME, New York, paper OMAE2004-51575.
3. Sharma, J. N. and Dean, R. G., 1981, "Second-Order Directional Seas and Associated Wave Forces", J. Soc. Petroleum Engineering, 4, pp 129-140.
4. Voogt, A.J., 2001, "Discussion Problem Identification, SAFE-FLOW project", MARIN Report No. 15874-1-OB, Wageningen, The Netherlands.
5. Voogt, A.J. and B.Buchner, 2004, "Prediction of Wave Impact Loads on Ship-type Offshore Structures in Steep Fronted Waves", Proceedings of the ISOPE2004, paper no. 2004-JSC-343
6. Voogt, A.J. and B.Buchner, 2004, "Wave Impacts Excitation On Ship-Type Offshore Structures In Steep Fronted Waves", Proceedings of the OMAE Speciality Symposium on FPSO Integrity, Houston, 2004

Extreme Vertical Wave Impact on the Deck of a Gravity-Based Structure (GBS) Platform

Rolf Baarholm¹, and Carl Trygve Stansberg¹

¹ MARINTEK, P.O. Box 4125 Valentinlyst, 7450 Trondheim, Norway,
N-7450 Trondheim, Norway
(Rolf.Baarholm@marintek.sintef.no)
(CarlTrygve.Stansberg@marintek.sintef.no)

Abstract. A simple method for solving water impact loads on decks of offshore structures is developed. In the present paper the emphasis is on vertical wave-in-deck loads. The suggested method is three-dimensional and valid for general deck geometries and arbitrary incident wave direction. First and second order wave amplification due to the large-volume structure is included in the analysis. The method is implemented into a numerical simulation program. This tool uses the results from an a priori second order diffraction analysis of the platform hull as input. In particular the wave-in-deck simulation program applies computed linear and quadratic transfer functions from the diffraction analysis as input. The method is validated against experiments. Results from scaled model tests of a gravity-based structure (GBS) are compared to numerical results. The platform was subjected to extreme waves causing water impact on the deck structure. In the present work, only impact from regular waves is considered. Satisfactory results are obtained from the numerical simulations. The theoretical results compare well with the experiment. The vertical loads on the deck are well reproduced both during the water entry phase and the water exit phase. Moreover, the duration of the wave-in-deck event is satisfactorily predicted.

1 Introduction

It is common practice to design the lower deck of offshore platforms to be above the maximum predicted wave level. Knowledge regarding wave heights and the variability of environmental conditions has increased over the years, and existing platforms may have been built with lower deck clearance than today's requirements would dictate. Moreover, bottom-mounted platforms initially installed with sufficient deck height may experience that this decreases with time. This reduction can be caused either by settlements of the platform due to its own weight, or by reservoir compaction. Owing to these uncertainties in the safety level, it is important to obtain predic-

tions of the expected hydrodynamic loads on the structure induced by wave impact underneath the decks of existing platforms

In the present paper, a simple method for estimating wave-in-deck impact forces on column-based structures is described. A case study with a fixed GBS structure is used as an example, based on a model test experiment on the Statfjord A platform presented previously in [1]. For such structures, horizontal forces are usually considered to be most critical for platform safety, but the vertical loads may also contribute to the critical responses. According to [1], examples of the critical responses for the Statfjord A GBS are the capacity of the steel plates of the deck to transfer the combined vertical and horizontal slamming load into the shafts, the capacity of the deck to shaft connection and the capacity of the concrete shafts and the shafts to caisson connection. In the actual model tests, possible deck impact forces on the Statfjord A platform in a future late life production scenario were investigated, with focus on the horizontal forces. This subsequently led to the conclusion that the platform can sustain an expected future bottom subsidence and wave conditions. For a broader description of the actual Statfjord A case we refer to [1]. In the following, the focus will be limited to vertical force modelling only, using selected data from the model tests as a validation test case. The present method can also be generalized to study horizontal forces.

For wave impact on floaters, also vertical forces may be critical. Baarholm et. al. [2] showed that impact forces may influence the vertical platform motion significantly.

For jacket type platforms, simple wave impact prediction models exist. A review of some of them is given in [4]. No simple method is available for solving global wave impact loads on large-volume structures where wave diffraction due to the hull is important. So far one has been dependent on model test results exclusively when assessing such impact loads. Simple methods for assessing wave-in-deck loads are welcomed by the industry. The objective of the present work is to make a simple theoretical model to compute the vertical hydrodynamic loads on the deck of a large-volume platform due to impact from extreme waves. Published literature on the subject has limitations. Baarholm and Faltinsen [3] presented a fully non-linear boundary element method for simulating the wave-in-deck event. Good results were obtained for both the water entry phase, i.e. when the wetted area of the platform deck increases, and the water exit phase when the water detaches from the deck. The method is, however, two-dimensional and can thus not be applied to large volume structures. Kaplan [5] presented a mathematical model for determining time histories of impact forces on flat deck structures of offshore platforms. He applied the usual slamming assumption where gravity is neglected: An expression for the vertical wave-in-deck force is found from the principle of conservation of fluid momentum and the impact force can be found without solving the boundary value problem associated with the impact. Kaplan's method is limited to two-dimensional flow and undisturbed flow.

In this work, a method based on a combination of Kaplan's approach and a second-order three-dimensional diffraction analysis of the free-surface elevation and kinematics is proposed. Second-order effects have been observed to add significantly to

the maximum crest elevation (see e.g. [6] and [7]) and must therefore be accounted for in the analysis. The method is limited to provide integrated global loads. Pressure distributions are not available from the proposed method.

2 Theory

Exact Boundary Value Problem

In the theoretical description of the wave-in-deck problem, an incompressible fluid in three-dimensional, irrotational flow is assumed. Accordingly, potential flow is applied and viscous effects are disregarded. Moreover, effects of hydroelasticity and surface tension are neglected. A boundary value problem for the total velocity potential Φ can be set up. The three-dimensional Laplace equation $\nabla^2\Phi = 0$ becomes the governing equation in the fluid domain. Boundary conditions are required to solve the problem. The fully non-linear boundary conditions for the two-dimensional wave-in-deck problem are described by Baarholm and Faltinsen [3]. The exact boundary conditions are imposed in the instantaneous position of the boundaries. They also argue that it is necessary to include a Kutta type condition when the fluid flow reaches the downwave edge of the deck. This condition ensures that the fluid flow leaves the deck tangentially at the downstream end of the deck. For a three-dimensional impact problem, the formulation of the Kutta condition will be more complicated than in the two-dimensional case.

The boundary value problem must be solved as an initial value problem, e.g. with the fluid at rest as an initial condition. A wavemaker (or similar) must be included on the inflow boundary to generate the waves and a numerical beach must be included on the free surface near the downwave boundary. The boundary value problem must be solved at each time step by applying Green's second identity, and a robust time stepping procedure must be used to evolve the solution. When the boundary value problem is solved the force acting on the deck can be found either by direct integration of the hydrodynamic pressure on the wetted part of the deck, which can be found from Bernoulli's equation or by imposing conservation of fluid momentum. If the boundary value problem is properly solved, the resulting force found from these two alternative methods will converge towards each other. This is demonstrated in [3] for a two-dimensional wave-in-deck problem.

To solve the exact boundary value problem of a three-dimensional body in waves with impact included is an extremely cumbersome task that has not been solved yet. Both high temporal and spatial resolution of the numerical scheme would be needed. This will yield extremely computer demanding solutions. It is not within the scope of the present work to solve this problem. On the contrary, we aim to develop a simple method to assess wave-in-deck loads to rogue waves that can easily be used in design of new structures and in re-assessment of existing installations.

Simplified Boundary Value Problem

In the following, some assumptions will be made, and a method to evaluate the water impact loads based on a simple von Karman approach is established. Firstly, we let the total velocity potential be written as $\Phi = \phi_{slam} + \phi_{waves}$, where ϕ_{slam} and ϕ_{wave} are the perturbation velocity potential due to the water impact and the velocity potential of the wave, respectively. The latter comprises the undisturbed incident wave potential and the diffraction velocity potential due to the presence of the platform hull. ϕ_{wave} to second order is assumed to be known a priori. A standard second order frequency-domain diffraction program can be used to evaluate this. The computational results are given in terms of linear and quadratic transfer functions that can be used in a time domain simulation of e.g. the free surface elevation and the fluid particle kinematics. The use of the pre-computed quantities in the slamming analysis is described later.

A boundary value problem (BVP) for the unknown slamming potential ϕ_{slam} can be set up. The Laplace equation becomes the governing equation in the fluid domain. A typical assumption for slamming problems is that impact occurs over a small period of time, meaning that the acceleration of gravity g is negligible relative to the impact induced accelerations of the fluid particles, and that the rate of change of ϕ_{slam} with time is generally larger than the rate of change with respect to the spatial coordinates. Moreover, instead of imposing the free surface condition on the exact free surface, it can be simplified further by applying it on the horizontal plane $z=0$, i.e. the dynamic free surface condition becomes

$$\phi_{slam} = 0 \quad \text{on} \quad z = 0 \quad (1)$$

This condition implies that no waves are generated by the wave-in-deck event. This dynamic free surface condition is widely used for impact problems, e.g. in the classic works by von Karman [9] and Wagner [9], although they solved two-dimensional problems. Similarly, the instantaneous wetted area of the deck is collapsed onto the plane $z=0$ and the body boundary condition is imposed on this. The resulting boundary value problem is depicted in Fig. 1. S_B denotes an arbitrarily shaped wetted area, and S_F denotes the free surface. Both these surfaces are collapsed onto the plane $z=0$. The body boundary condition is described in terms of the temporally and spatially dependent relative impact velocities, $V_R(x,y,t)$. V_R is a combination of the fluid particle kinematics and the platform motions. In the two-dimensional case, the boundary value problem can be solved analytically for simple body boundary conditions. In case of spatially constant impact velocity, $V_R(x,t) = V_R(t)$, the solution is given in e.g. [9]. An analytical solution for a linearly varying impact velocity, $V_R(x,t) = V_0(t) + V_1(t)x$, is given by Zhao and Faltinsen [13]. They used this body boundary condition when studying slamming loads on high-speed vessels. Baarholm and Faltinsen, [15], used the same condition for solving two-dimensional wave-in-deck loads. In the three-dimensional case, an analytical solution is available for water entry of axisymmetric bodies (see [14]), but analytical solutions are not available for arbitrarily shaped wetted deck areas. In general, the simplified three-dimensional boundary value problem depicted in Fig. 1 must be solved numerically through use of Green's second identity.

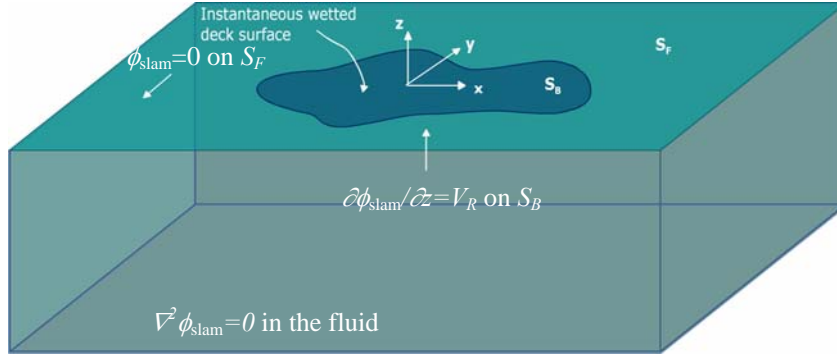


Fig. 1. Simplified hydrodynamic boundary value problem of the wave-in-deck event. ϕ_{slam} is the impact induced velocity potential and V_R is the averaged relative impact velocity over the wetted deck area.

Force computations

The main reasons why one needs to solve the boundary value problem is to be able to determine how the wetted area evolves in time and to compute the pressure distribution and the integrated force acting on the platform deck. In this work, the main objective has been to compute the integrated force acting on the deck and the mean pressure, but not the pressure distribution as such. If one assumes a constant impact velocity across the entire wetted area, the boundary value problem yields following simple expression for the vertical impact force

$$F_3 = \frac{d}{dt}(A_{33}V_R) = \frac{dA_{33}}{dt}V_R + A_{33}\dot{V}_R \quad (2)$$

where $A_{33}=A_{33}(t)$ is the high frequency added mass of the instantaneous wetted deck area and $V_R=V_R(t)$ is the average value over the wetted deck area of the relative impact velocity. The first term on the right hand side of Eq. (2) is denoted as the slamming force and the latter is an inertia force. This formula is well known and used for a large number water entry problems. In addition to the force from the rate of change of momentum, the total deck force will get contributions from hydrostatics and from the dynamic pressure in the diffracted wave field. Here the term diffracted wave field refers to the wave field that is unaffected by the deck impact, but diffraction due to the mean submerged platform hull is included. The latter force is here approximated by a modified Froude-Kriloff force term. The total vertical force acting underneath the deck structure is written as

$$F_3 = \frac{dA_{33}}{dt}V_R + A_{33}\dot{V}_R + \rho\Omega(g + \bar{a}_3) \quad (3)$$

where ρ is the water density and $\Omega = \Omega(t)$ is the instantaneous volume of fluid in the diffracted wave that is above the lower deck. For simplicity, \bar{a}_3 is taken as the average vertical fluid acceleration in the diffracted wave at the instantaneous wetted area. Thus, $\bar{a}_3 = \dot{V}_R$ for a stationary platform. The same type for formulation was used to Baarholm and Faltinsen [15] for two-dimensional wave-in-deck impact. The slamming term is set equal to zero during water exit. This treatment is based on the consideration of vertical momentum transfer only upon water entry and not during conditions associated with water exit. Such treatment is used in ship slamming analysis (see [11]) and is carried over to the present case. The same approach is used by e.g. [5] and [8].

Equation (3) shows that the vertical force due wave impact underneath a platform deck is governed by the kinematics in the wave crest in combination with the platform motions and the evolution of the high frequency limit of the added mass of the wetted deck area. An exact solution for the evolution of the wetted area cannot be found without solving the boundary value problem. Here, however, assume that the instantaneous wetted deck area can be approximated by a von Karman approach. This means that the wetted area is found from the intersection between the diffracted wave field, excluding diffraction effects from the impact potential, and the deck. When the wetted area is known, one can compute the added mass of this. Kaplan used a formula similar to (3) to compute the vertical wave-in-deck force on jacket platforms. In addition to the terms in the above expression, Kaplan also included a drag term in the force expression. He limited his analyses to long-crested head or beam sea waves relative to the rectangular deck. This means that the wetted deck area is rectangular at all times, and that he could solve the problem by a two-dimensional analysis. Moreover, he applied a von Karman type approach when evaluating the wetted deck area, i.e. the wetted area was found as the geometrical intersection between the deck and the undisturbed free surface. Since the wetted area was rectangular, the added mass could be found by analytical expressions. Consequently, the impact loads could be assessed without solving the boundary value problem as such.

The idea here is to generalize Kaplan's approach so that it can be applied for three-dimensional impact problems for which diffraction effects from the presence of a large-volume structure are accounted for. For such a case the wetted area due to impact may have a more general shape, and analytical expressions for the added mass cannot be found. In principle, the added mass must be evaluated numerically for each time step. This can be achieved by a three-dimensional panel method. To omit having to solve such a problem, an approximate approach is proposed. Analytical expressions for the added mass exist for thin rectangular plates and thin elliptical disks. The general idea is to approximate the wet area by one of these basic geometries. This enables us to estimate the added mass with explicit analytical expressions. The feasibility of using the added mass of elliptical disks or rectangular plates has been studied. An extract of the study is presented in [16]. The general conclusion was that one can get good estimates of the added mass of arbitrarily shaped thin plates by applying the added mass of a representative elliptical or rectangular plate. When fitting the

general shaped plate to one of the basic geometries it is important to keep the area of the model plate the same as the real wetted area and to use a representative aspect ratio.

Relative impact velocity and acceleration

The vertical fluid velocity and acceleration at the deck level are found to second order. In the following the velocity potential ϕ_{wave} is split into a first and second order part so that

$$\phi_{wave} = \phi^{(1)} + \phi^{(2)} + O(\zeta_a^3) \quad (4)$$

where ζ_a is the amplitude of the first order incident wave. $\phi^{(1)}(x,y,z,t)$ and $\phi^{(2)}(x,y,z,t)$ are the first and second order wave potentials (incident wave + diffracted wave due to the mean submerged part of the hull). By use of Taylor expansion to $O(\zeta_a^2)$, the relative vertical fluid velocity at the deck can be expressed as

$$w = \frac{\partial \phi^{(1)}}{\partial z} + \frac{\partial \phi^{(2)}}{\partial z} + \eta_{deck} \frac{\partial^2 \phi^{(1)}}{\partial z^2} - \dot{\eta}_{deck} \quad (5)$$

where the quantities $\partial \phi^{(1)} / \partial z$, $\partial \phi^{(2)} / \partial z$ and $\partial^2 \phi^{(1)} / \partial z^2$ are to be evaluated on $z=0$. $\dot{\eta}_{deck} = \dot{\eta}_{deck}(x,y,t)$ is the vertical velocity of the deck. This quantity vanishes for a stationary platform. V_R is taken as the average value of w over the wetted area. Similarly, \dot{V}_R is taken as the average value of \dot{w} .

Validity of second order diffraction analysis

The free-surface wave elevation and kinematics is disturbed due to the presence of the large-volume structure. The structure in case study below consists of three columns and a large caisson. This is an important factor in the wave-in-deck problem, leading to the input condition of the impact model described above. The prediction of elevation around vertical columns in steep waves, by use of linear as well as second-order numerical diffraction models, has been validated in [6,7]. From these works, it is found that while the use of linear theory can lead to significant under-estimation, second-order models can in many cases work fairly well even in steep waves. The largest discrepancies are observed for high column-to-wavelength ratios ($k\zeta_a > 0.4$), particularly due to over-predictions of the sum-frequency terms. For low $k\zeta_a$ -values, the agreement is better, while there are still some discrepancies due to effects beyond second order. Generally speaking, this can lead to under-prediction in the vicinity of the columns, and some over-prediction further away.

3 Present Implementation

The theory described above is implemented into a computer program. Below, the main steps in the numerical simulation are described in brief. A priori diffraction

analysis of the submerged part of the hull must be performed. In the present work second order frequency-domain diffraction analysis is performed by applying WAMIT (see [12]). Linear and quadratic transfer functions of wave kinematics and free surface elevation at a large number of field points below the deck is evaluated. The computed hydrodynamics are used as input to the simulation program. The field points are distributed in two horizontal layers. One layer is located at the mean free surface with the second layer just below. Two layers are needed to evaluate the z -derivative of the computed hydrodynamic quantities. These are needed to extrapolate the wave kinematics above the mean free surface.

In the case of regular waves, the diffracted wave field underneath the deck structure is evaluated for each time step by use of

$$\zeta(x, y, t) = \text{Re}\left(\zeta_a \tilde{\eta}^{(1)} \exp(i\omega t) + \zeta_a^2 \tilde{\eta}^{(2+)} \exp(i2\omega t)\right) + \zeta_a^2 \tilde{\eta}^{(2-)} \quad (6)$$

where ω is the oscillation frequency of the incident wave. The $\tilde{\eta}$'s are complex linear and quadratic transfer function values from WAMIT, all dependent upon spatial position although this is not explicitly stated in the expression. Note that the term $\tilde{\eta}^{(2-)}$ is real while the other terms are complex. The superscripts (2+) and (2-) denote second order sum- and difference frequency contributions, respectively. $\tilde{\eta}^{(1)}$ gives the linear contribution. When knowing the diffracted wave field, approximate values of the instantaneous wetted area, A_{33} and wave kinematics can be evaluated. The impact event is stepped forward in time until the wave has completely detached from the deck. Consequently, the vertical force on the deck can be evaluated from Eq. (3).

4 Validation case: Wave-in-deck loads on the Statfjord A GBS

A model test program on the Statfjord A GBS was undertaken in the Ocean Basin at Marintek to assess wave-in-deck loads (see [1]). The main objective was to determine hydrodynamic loads from extreme waves on the platform deck at various water depths, to study the effect of estimated future seabed subsidence. Two depths were tested: 150.1m (as-is today) and 151.6m, measured from still water level to the sea bottom. These water depths leave 23.2m and 21.7m air-gap, respectively; from the cellar deck (see Fig. 2). The GBS has 3 columns.

The deck on the Statfjord A platform is 83.60m long and 54.24m wide. In addition it has two extensions protruding from each of the decks long side. The dimensions of these are 13.20m by 16.00m. The measurements covered horizontal and vertical wave loads on the deck structure, air gap at critical locations, local slamming loads and measurements of wave amplification due to the large volume structure. Model tests were run with both regular waves and extreme wave packages. Two wave headings were tested (see Fig. 2). With the coordinate system used here, the wave headings are 240deg and 270deg.

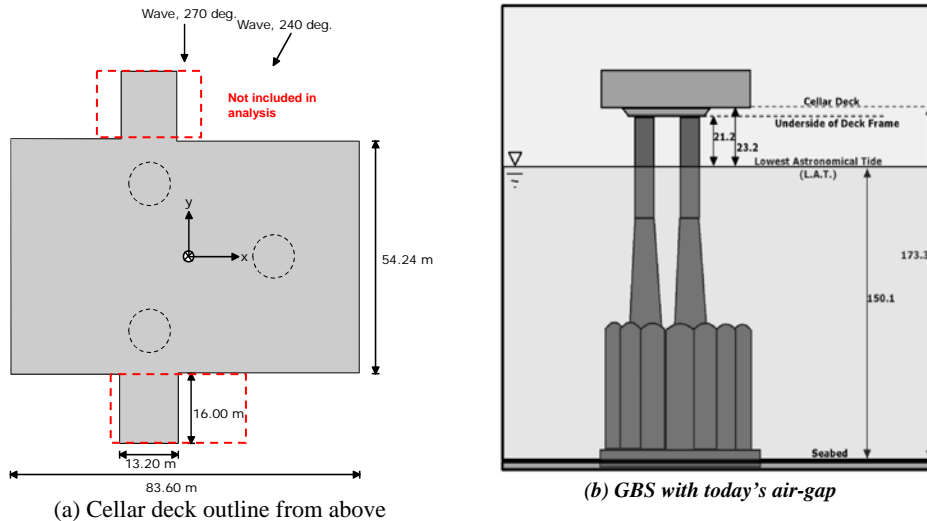


Fig. 2. GBS model with simplified topside (from [1])

Further information about the model tests can be found in [1].

Numerical model

WAMIT was used to perform a priori second order diffraction analysis. The panel model applied in the computations comprised of 5060 panels on the body and 6060 panels on the free surface. A total of 9800 field points were specified for the WAMIT analysis. Note that the field points, which are used when determining the instantaneous wetted area, cover a rectangular area equal to 83.60m by 54.24m. This means that the extensions on each of the long sides of the deck are not accounted for in the analysis.

Results

The maximum crest elevation obtained by use of the second-order WAMIT model has been validated by comparison to model test measurement. In Fig.3 this is shown for a wave condition $H=30\text{m}$, $T=15.5\text{s}$, 270deg heading. (The actual wave-in-deck load study included higher waves, up to 40m, but they are not included in the elevation study due to the deck interaction effects). Note that the coordinate system is rotated relative to Fig. 2. Results from linear theory, second-order theory and measurements at various locations are shown. Notice that in the present case, the scattering parameter ka is as low as approximately 0.1, which means that we are in the range where the second-order theory is found to work reasonably well [7]. Further results from this and other case studies analysis are presented in [7, 17].

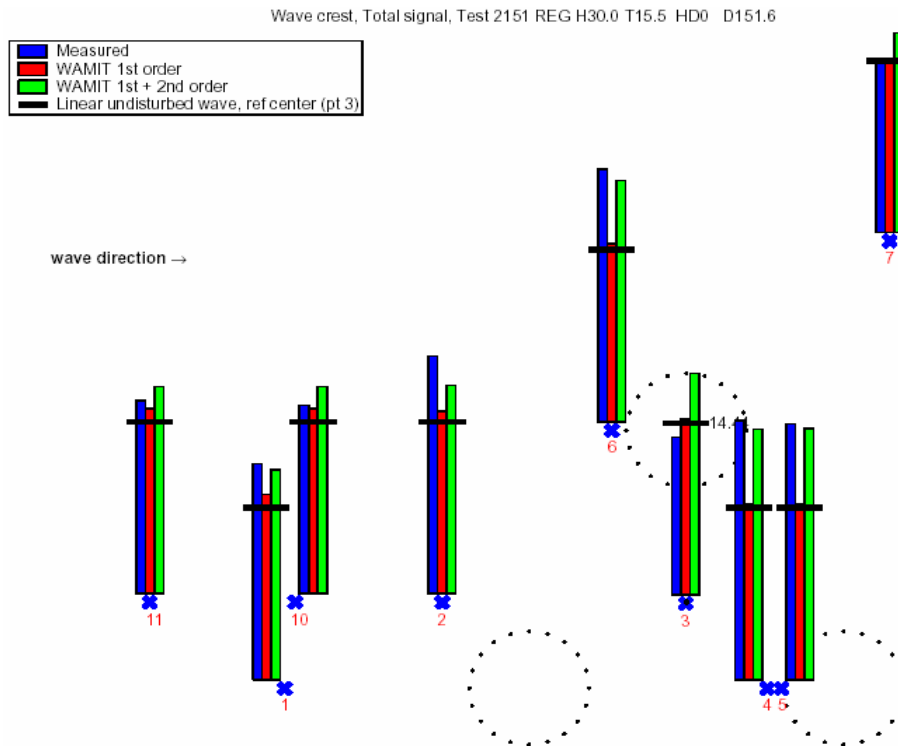


Fig. 3. Comparison of maximum crest elevation in wave field under the platform

The numerical load simulation program has been used to reproduce the wave-in-deck events. The analysis is limited to the regular wave tests. In this paper, results are reported for the tests with heading 270deg and with a deck height corresponding to a seabed subsidence of 1.5m. This adds up to altogether 7 test cases. Results from oblique sea computations are presented in [16]. Table 1 presents the main results. Both the maximum water entry force and the maximum magnitude of the negative water exit force from the experiments and the numerical simulations are listed in the table. However, not only the maximum and minimum force were found, the entire time history of the impact force has been simulated for each of the 7 test cases. Example plots of the simulated time series compared to the measured forces records are given in Fig. 4. Plots showing the wetness of the deck at the time instants of maximum and minimum force for case 2 are given in Fig. 5.

Table 1. Results from numerical computation of wave-in-deck impact due to regular incident waves. H and T are wave height and period, respectively. Maximum upward directed force (F_{max}) and maximum downward directed force (F_{min}) are reported. Corresponding experimental results are included.

Case No.	H (m)	T (s)	Measurements		Numerical results	
			F_{max} (MN)	F_{min} (MN)	F_{max} (MN)	F_{min} (MN)
1	34.0	17.0	7.8	-23.9	7.4	-12.3
2	40.0	17.0	166.4	-131.9	140.2	-153.6
3	37.0	15.5	51.0	-91.2	53.4	-95.3
4	34.0	15.5	15.2	-23.7	16.7	-23.0
5	37.0	16.25	70.8	-78.8	67.3	-84.2
6	34.0	16.25	7.5	-18.7	9.3	-17.0
7	33.0	14.0	45.3	-30.1	8.3	-23.1

5 Discussion and Conclusions

The diffracted elevation of the second-order model compares reasonably well to measurements in this case. Furthermore, it can be concluded that use of linear elevation theory may lead to significant under-prediction of both the occurrence and severity of wave-in-deck events. Linear waves would not give impact for any of the 7 cases analyzed.

In general, good agreement is also obtained between the numerical method and the experiments for the loads of hardest water impacts. Both the magnitude of the water entry force and the water exit force as well as the duration of the wave-in-deck event is satisfactory predicted. For the softer impacts, when the wave is barely reaching the deck structure, the relative difference between the measured force and the computed force is greater. This is as expected and in accordance with the experience presented in [8]. When the wave is just reaching the deck, great accuracy in both the wave elevation and the fluid particle kinematics are required to get good correspondence between measurements and computations. Case no. 1 in Table 1 is an example of such a soft impact event. The resulting force for such mild impacts is however small, and the absolute errors in the computed force is therefore also moderate. On the other hand, slight inaccuracies in the generated waves or in the numerical solution of the free surface elevation and fluid particle kinematics will give smaller relative errors for severe impacts. The absolute errors may be significant but the computed results always indicate the magnitude of the impact force.

The experience from [8] would indicate that a von Karman method should underestimate the magnitude of the upwards-directed slamming force. This is also the case here, but perhaps to a lesser extent than expected. The reason why a simple von Karman approach would under-estimate the slamming force is that diffraction due to the deck is omitted and dA_{33}/dt is thus underestimated. Karman approach would under-estimate the slamming force is that diffraction due to the deck is omitted and dA_{33}/dt is thus underestimated. The von Karman approach performs well here, but it is

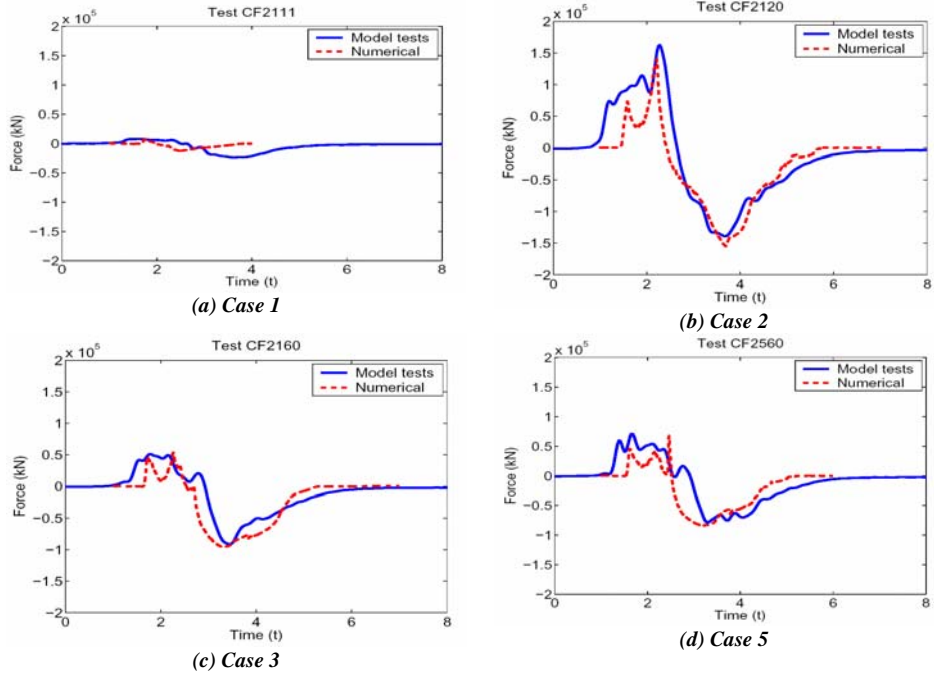


Fig. 4. Vertical impact force time series: comparisons between numerical results (dashed lines) and experimental results (solid lines).

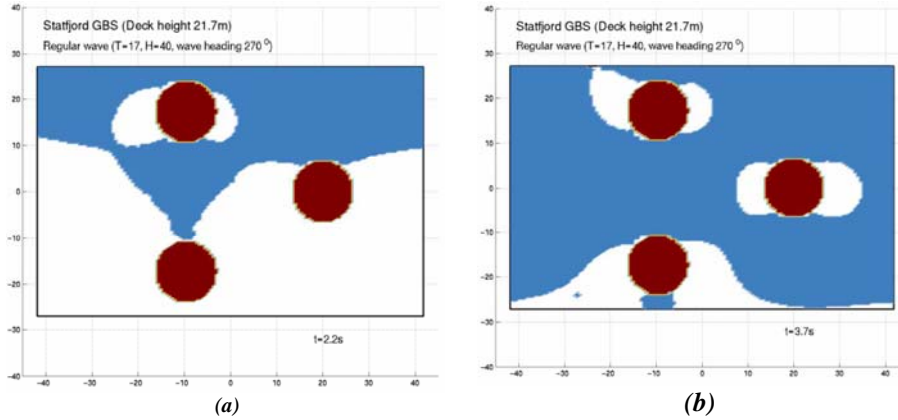


Fig. 5. Deck wetness at time instant of maximum upward directed force (a), and at the time instant of maximum downward directed force (b) for case 2 in Table 1.

probably helped by the geometry on the underside of the deck. Large beams protrude from the deck plates. These restrict the jet formation and propagation of the water along the deck, and the wetting process of the deck is probably slower than it would

have been for a flat deck. The downwards-directed water exit force is dominated by the added mass of the wetted area. During the wetted area diminishes, the slamming term is set equal to zero. Also the water exit force is in most cases satisfactorily predicted. This indicates that the maximum wetted area is fairly well predicted by the simulations, and, moreover, since the duration is well predicted, this means that the water detaches from the deck similarly in the simulations and in the experiments.

In the present work only impact on a stationary structure is studied. The main reason for this is that the data for the Staffjord A tests was readily available. It is, however, reasons to believe that the method also will be able to predict the vertical water impact loads on a floating structure such as a semisubmersible or a TLP. There are three main differences between impact on a floater and on a bottom-mounted platform. These are: 1) the platform motion contributes to the relative impact velocity and acceleration, 2) the deck height varies in time and space and 3) the impact will to some extent influence the motion of the platform. All these three items should in principle be accounted for. Accounting for first order and sum-frequency platform motion in the relative fluid kinematics and the deck elevation is straightforward. The slow-drift motion of the platform is not an issue in case of regular waves. If the water impact loads are significant in magnitude and duration, they may introduce rigid body motions that cannot be disregarded in the computation of the wave-in-deck load. The impact-induced motion contributes to the relative velocity and acceleration, and it also affects the instantaneous deck height. To solve such a problem properly, one has to solve the impact forces and the impact-induced motions simultaneously (see [2]).

In principle the present method can be used to solve both vertical and horizontal loads on the deck structure, though, it is believed that horizontal forces will be less precisely predicted than vertical forces. One reason is, as discussed above, that one does not take into account for hydrodynamic forces on beams protruding down below the deck structure. This can, however, be accounted for. Kaplan used a component-based model, contrary to the global model used in this work, where he computed drag forces from beams. More critical perhaps is the load from the wave impact on the side of the deck. A von Karman approach will at least for hard impacts, severely underestimate the wetted area and its rate of change. The reason for this is that the foremost contribution to the increase in wetted area is due to diffraction from the impact itself rather than from the diffracted wave field. For the wetting underneath the horizontal deck, the propagation velocity of the wave contributes significantly and the wetting due to the jet flow of the impact velocity potential is relatively of less importance than in the case of impact on a vertical wall.

Acknowledgements

The study presented in this work is performed within the WaveLand Phase II project. The Staffjord Late Life Project has kindly allowed the WaveLand JIP to use the data from the abovementioned model tests. The authors also wish to thank Frøydis Solaas,

Trygve Kristiansen and Vibeke Moe for valuable contributions to the numerical modeling and data analysis.

References

1. Stansberg C.T., Baarholm R., Fokk T., Gudmestad O.T. and Haver S. : Wave amplification and possible wave impact on gravity based structure in 10^{-4} probability extreme crest heights, OMAE 2004-51506. Proc. 23rd OMAE Conf., Vancouver, Canada (2004)
2. Baarholm, R, O.M. Faltinsen and K. Herfjord : Water impact on decks of floating platforms. Proc. 8th Int. Symp. on Practical Design of Ships and other Floating Structures (PRADS2001). Elsevier, Oxford. (2001).
3. Baarholm, R and O. Faltinsen: Wave impact underneath horizontal decks. J. Mar Sci Technol, 9, (2004) 1-13.
4. Health & Safety Executive: Review of wave in deck load assessment procedure. Offshore Technology Report – OTO 97 073, (1998).
5. Kaplan P.: Wave impact on offshore structures: re-examination and new interpretations. Proc. 24th Offshore Technology Conference, Houston, USA. (1992)
6. Kristiansen T, Baarholm R. and Stansberg C.T.: Validation of Second-Order Analysis in Predicting Diffracted Wave Elevation around a Vertical Circular Cylinder. Proc. 14th ISOPE, Toulon, France. (2004).
7. Stansberg C.T. and Kristiansen T.: Non-linear scattering of steep waves around vertical columns. Submitted for publication (2005).
8. Baarholm R.: Theoretical and experimental studies of wave impact underneath decks of offshore platforms. PhD Thesis, Norwegian University of Science and Technology (NTNU), Trondheim, Norway. (2001)
9. Von Karman T.: The impact on seaplane floats during landing. In National Advisory Committee for Aeronautics, NACA, (1929) 309-313.
10. Wagner H.: Über Stoß- und Gleitvorgänge an der Oberfläche von Flüssigkeiten, ZAMM, 12, (1932) 192-126
11. Kaplan P.: Analysis and Prediction of Flat Bottom Slamming Impact of Advanced Marine Vehicles in Waves. Int. Shipbuilding Progress, March (1987).
12. Lee C.-H.: WAMIT Theory Manual, Report No. 95-2, Dept. of Ocean Engineering, Massachusetts Institute of Technology (MIT), Cambridge, Mass., USA. (1995)
13. Zhao R. and Faltinsen O.M.: Slamming Loads on High-Speed Vessels. In W. D. C. National Academy Press (Ed.), Proc. of the 19th ONR Conference, Seoul, South Korea (1992).
14. Faltinsen O.M. and Zhao R.: Water entry of ship sections and axisymmetric bodies. Advisory Group for Aerospace Research and Development, AGARD REPORT R-827 (1998).
15. Baarholm R and Faltinsen O.M.: Experimental and theoretical studies of wave impact on an idealized platform deck. Proc. of the 4th Int. Conf. on Hydrodynamics (ICHHD 2000), Yokohama, Japan. (2000)
16. Baarholm R.: A Simple Numerical Method for Evaluation of Water Impact Loads on Decks of Large-Volume Offshore Platforms. In Proc. OMAE 2005, Paper no. OMAE2005-67097, Halkidiki, Greece (2005).
17. Stansberg, C.T., Baarholm, R., Kristiansen, T., Hansen, E.W.M and Rørtveit, G.: Extreme Wave Amplification and Impact Loads on Offshore Structures. In Proc. OTC 2005, Paper No. 17487, Houston, TX, USA (2005).

Violent water wave impacts on a wall

Howell Peregrine, Henrik Bredmose, *Mathematics, University of Bristol, U.K.*

d.h.peregrine@bris.ac.uk, h.bredmose@bris.ac.uk,

Geoffrey Bullock, Charlotte Obhrai, *Civil & Structural Engineering, University of Plymouth, U.K.*

g.bullock@plymouth.ac.uk, c.obhrai@plymouth.ac.uk

Gerald Müller*, Guido Wolters *Civil Engineering, Queen's University, Belfast, U.K.*

g.muller@qub.ac.uk, g.wolters@qub.ac.uk

Violent impact of an extreme wave onto a structure can be the criterion that determines a number of design parameters. Within the BWIMCOST (Breaking Wave IMPacts on COastal STRuctures) project such impacts have been measured in the field and the laboratory for waves breaking onto a sea wall or breakwater, see Bullock et al. (2003). The time and space scales of impact are sufficiently small that the hydrodynamics of impact is unlikely to differ for waves in deep water which hit fixed or floating structures. In practical situations when pressures exceed a few atmospheres, it is appreciated that compressibility of air becomes important. This is particularly so for air that is entrained into or trapped by water, so special efforts have been made to measure the air-fraction in the water. Peregrine (2003) is a recent review: work subsequent to that review is reported here.

The overturning jet of the breaker may trap a 'pocket' of air, and/or the water may have already entrained a multitude of air bubbles. Both types of air distribution influence the effect of wave impact, due to their greater compressibility compared with pure water. The compressibility, evident in the very low velocity of sound in the air-water mixtures that occur as and after waves break, is a primary concern when small-scale laboratory data is being used to estimate large-scale prototype impacts, since the usual Froude scaling is unlikely to be correct.

The three main strands of data are from prototype:

- 1) the Admiralty breakwater, Alderney, which is exposed to waves from the Atlantic Ocean.
- 2) 1:4 scale: in the big wave channel (Grosser Wellenkanal, GWK) Hanover.
- 3) 1:25 scale: laboratory experiments in Plymouth with both fresh and sea water.

Few examples of violent impacts have been obtained from Alderney, the most severe impact occurred on an otherwise quiet day and may be described as a rogue wave. On the other hand the GWK measurements have yielded exceptionally violent impacts with pressures up to 3 MPa. These impacts vary in character, some details will be presented.

The theoretical studies include

- a) careful analysis of the data for waves approaching the breakwater, and for the impacts.
- b) development of simple mathematical models.
- c) development and study of detailed numerical models.

Here attention is focussed on the detailed modelling.



Figure 1. Wave impact on a wall sloping at 27° to the vertical. Spray caused by air escaping from a trapped air pocket at high pressure can be seen. The exposure time is 1/125 second, and the width of the flume (GWK) is 5 metres.

* at Southampton University from January 2005.

Waves approaching the wall are approximated with irrotational flow for which a boundary-integral computation is used Tanaka et al. (1987). This computation stops when the wave hits the wall or the flow becomes too violent, rough, or a jet extends too far.

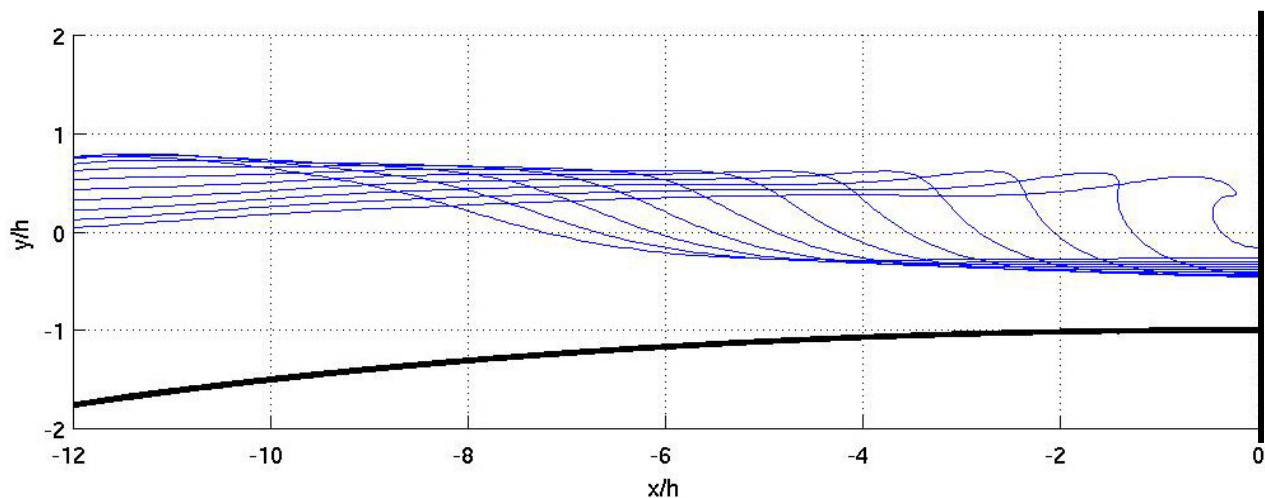


Figure 2 Wave profiles from a boundary-integral computation of a wave propagating over a berm towards a wall.

The compressible model. is the simplest possible, essentially the two-dimensional unsteady Euler equations for an air-water mixture with variable air volume fraction. It assumes adiabatic compression of the air and no relative movement between the phases. There are numerical problems with such a model when shock waves pass from light medium to a denser one, but, so far, they do not seem to be of importance in the first few wave impact examples that have been run at the time of writing.

The initial conditions for the compressible flow computations are taken for a region near the wall from the boundary-integral computation: for example, from a profile which is intermediate between the last two in figure 2. The computations provide a complete time history for the flow field and pressure on and near the structure. The analysis of these computations is in progress.

Support from EPSRC; E.U. Access to Research Infrastructures action; the co-operation of Joachim Grüne (GWK) and the breakwater maintenance staff on Alderney are gratefully recognised.

Bullock, G., Obhrai, C., Müller, G., Wolters, G., Peregrine, H. & Bredmose, H., (2003) Field and laboratory measurements of wave impacts. *Proc. Int. Conf. Coastal Structures 2003*. ASCE, to appear

Peregrine, D.H. 2003 Water wave impact on walls, *Ann. Rev. Fluid Mech.* **35**, pp.23-43.

Tanaka, M., Dold, J.W., Lewy, M. & Peregrine, D.H. (1987) Instability and breaking of a solitary wave, *Jour. Fluid Mech.* **185**, pp.235-248.

Bow Impact Forces in Steep Waves

Nigel Barltrop & Li Xu

Universities of Glasgow and Strathclyde

Following the 1998 damage to the Floating Storage and Offloading barge 'Schiehallion' work was undertaken for BP, the HSE and the UK research funding council EPSRC in a project which ran in parallel with and provided data to the SAFEFLOW project (reported by Buchner and Voogt at this conference).

The Glasgow work involved 1:80 scale wave tank testing of heavily instrumented models of Schiehallion and a tanker with a more conventional bow shape – the Loch Rannoch (Figures 1 and 2).

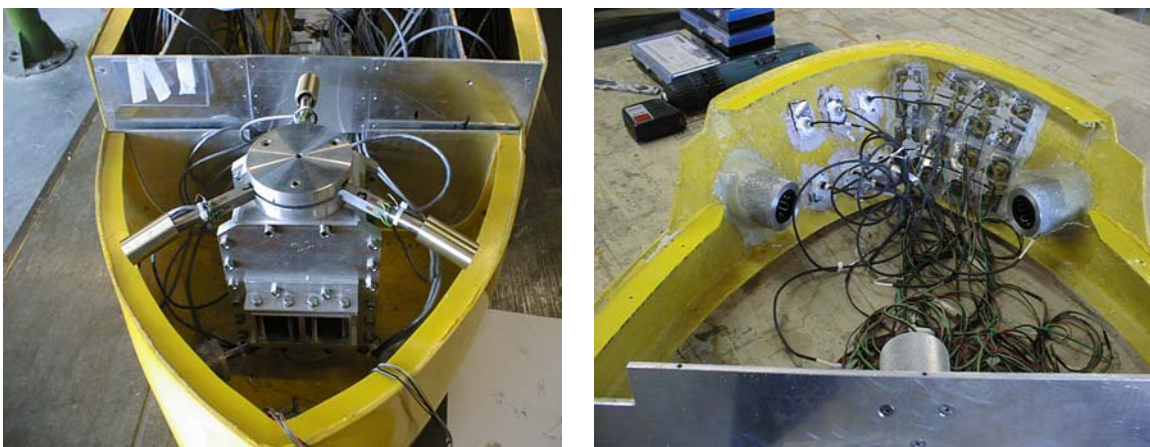


Figure 1 The Loch Rannoch Model showing the bow force, pressure panel and local pressure transducers

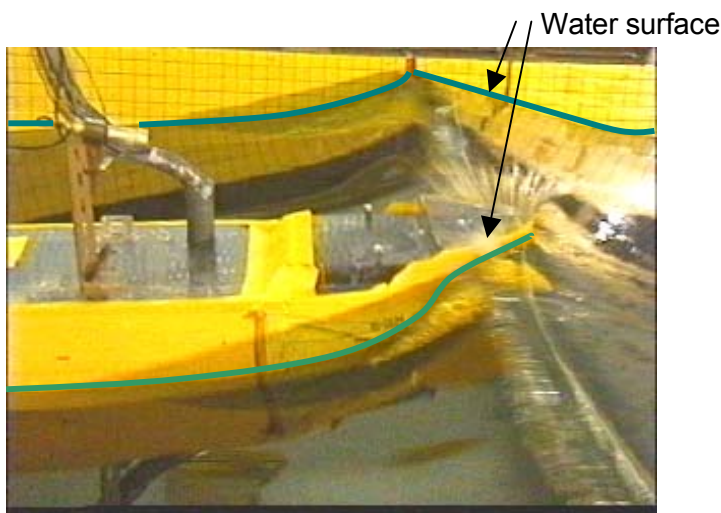


Figure 2 The Loch Rannoch model subject to a wave impact

The work identified the typical wave shapes that caused the highest pressure loads and proposes a simple method (based on the linear wave particle kinematics) (Figure 3) of estimating the change in surface slope and hence the non-linear slope and impact pressure statistics in a sea state or the time history of water surface shape for time history modelling of wave impact pressures. (Note there is a dependence on the time step which is not shown in Figure 3)

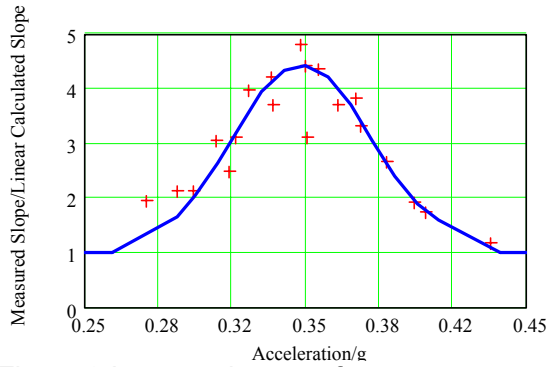


Figure 3 Increase in wave front steepness relative to a linear random model of the water surface

The bow forces may be calculated using a rate of change of added mass calculation in conjunction with the wave shape data (Figure 4). Alternatively pressures may be calculated using a slam force equation with additional terms to account for the size of the panel (non dimensionalized by bow width and wave height) for which the pressure is required.

$$P = \frac{1}{g} CE(S)F(W)G(Z)V_s^2 DAF$$

Where P is the estimated pressure in m head water

C is a constant

$E(S)$ is dependent on sea state steepness (S)

$F(W)$ is dependent on panel width (W)

$G(Z)$ is dependent on panel height (Z)

V_s is the slam velocity ($\sqrt{\text{celerity} \times \text{particle velocity}}$)

DAF is the dynamic amplification factor

The results were input to a reliability analysis (performed with other SAFEFLOW partners) to estimate combinations of sea state return periods and safety factors that should be used for structural design. As a result of the larger uncertainties in impact loads than in ordinary wave loading, slightly larger safety factors are recommended.

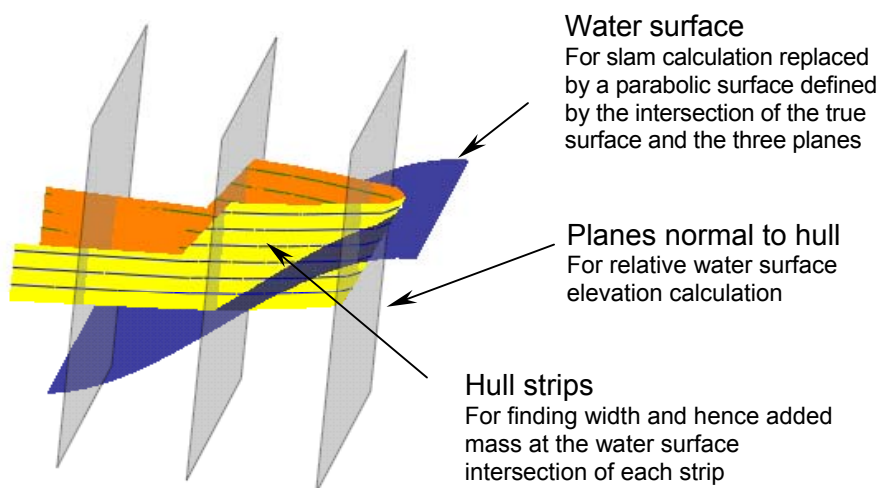


Figure 4 Visualisation of mathematical model used in conjunction with a rate of change of added mass calculation of slam force

Enhanced wave effects on the weather side of reflective structures

B. Molin, F. Remy, O. Kimmoun, E. Jamois

École généraliste d'ingénieurs de Marseille, 13 451 Marseille cedex 20

Strong wave effects are often observed on the weather side of marine or coastal structures. An example is wave runup, experienced by ships in beam waves and some offshore structures. These runup effects are sometimes far above design values, suggesting some "anomaly" of the incoming waves.

It is advocated that the incoming wave system can actually be modified through its non-linear interaction with the reflected wave system from the structure. This statement is based on extensive model tests, performed at BGO-First in la Seyne sur mer, and on theoretical and numerical analyses.

The experimental model consisted in a vertical plate, projected from one of the side-walls of the basin. It was submitted to regular waves of varying wavelengths and steepnesses, in deep water conditions ($kh > 3$). At wavelengths comparable with the width of the plate, strong runups are observed at the plate-wall intersection, increasing with the wave steepness. These runups take many wave cycles to develop, with no steady-state being reached in some cases. Free surface elevations as high as 5 times the amplitude of the incoming waves have been measured in some cases, far above calculated values with numerical models based on linearized potential flow theory.

A simple theoretical model is proposed, based on tertiary (third-order) wave interaction, as first given by Longuet-Higgins & Phillips (1962). A parabolic equation is derived, that describes the space evolution of the amplitude of the incoming waves through their tertiary interaction with the reflected waves (locally idealized as plane waves). A steady-state solution is obtained through iterations, where the incoming and reflected wave systems are successively updated. Details can be found in Molin *et al.* (2005). The figure shows the incoming wave system on the weather side of the plate, obtained at the end of this process, for a steepness H/L of 4 % and a wavelength equal to the length of the plate (1.2 m): the incoming wave amplitude has nearly doubled as it reaches the plate (in $x = 0$).

The numerical model is based on the enhanced Boussinesq equations as first proposed by Agnon *et al.* (1999) and Madsen *et al.*, and further developed by Fuhrman & Bingham (2004).

It is noteworthy that these nonlinear (tertiary) interactions between the incoming and reflected waves have some similarity with shoaling: the incoming waves are "slowed down", the wavelength decreases, the crest-lines bend and the wave energy gets focused toward the plate-wall intersection. As a matter of fact our parabolic equation resembles the parabolic

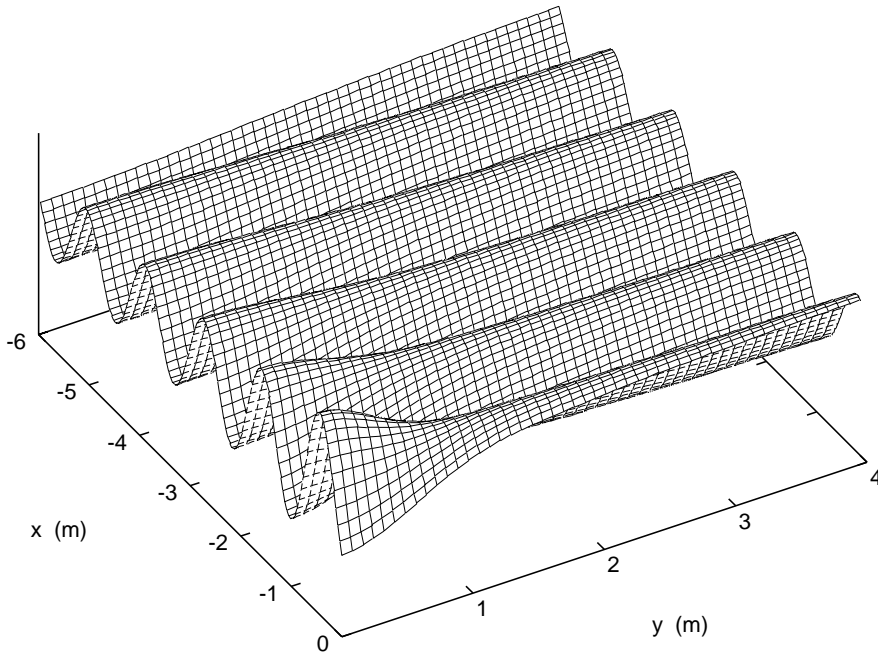


Figure 1: Three-dimensional view of the incoming waves by the plate.

approximation of the mild slope equation.

Numerical investigations have shown that the effective interaction area, between the incoming and reflected waves, can extend many wavelengths upwave. Contrary to intuition, the interaction area increases when the wavelength decreases, meaning that the incoming wave amplitude is being affected further and further from the plate.

Similar effects are expected to occur for other reflective bodies, such as multi-legged platforms or coastal structures.

References

- AGNON Y., MADSEN P.A. & SCHÄFFER H.A. 1999 A new approach to high-order Boussinesq models, *J. Fluid Mech.*, **399**, 319-333.
- FUHRMAN D.R. & BINGHAM H.B. 2004 Numerical solutions of fully non-linear and highly dispersive Boussinesq equations in two horizontal dimensions, *Int. J. Numer. Meth. Fluids*, **44**, 231-255.
- LONGUET-HIGGINS M.S. & PHILLIPS O.M. 1962 Phase velocity effects in tertiary wave interactions, *J. Fluid Mechanics*, **12**, 333-336.
- MADSEN P.A., BINGHAM H.B. & LIU H. 2002 A new Boussinesq method for fully nonlinear waves from shallow to deep water, *J. Fluid Mech.*, **462**, 1-30.
- MOLIN B., REMY F., KIMMOUN O. & JAMOIS E. 2005 The role of tertiary wave interactions in wave-body problems, *J. Fluid Mech.*, **528**, 323-354.

ROGUE WAVES 2004

ABSTRACT

On the shape of large waves in the central and southern North Sea

Anne Karin Magnusson

a.k.magnusson@met.no

Norwegian Meteorological Institute

Allégaten 70, 5007, Bergen, Norway

Alessandro Toffoli

alessandro.toffoli@bwk.kuleuven.ac.be

Hydraulics Laboratory, K. U. Leuven

Kasteelpark Arenberg 40, B-3001, Heverlee, Belgium

Jaak Monbaliu

jaak.monbaliu@bwk.kuleuven.ac.be

Hydraulics Laboratory, K. U. Leuven

Kasteelpark Arenberg 40, B-3001, Heverlee, Belgium

Elzbieta Bitner-Gregersen

Elzbieta.Bitner-Gregersen@dnv.com

Det Norske Veritas AS

N-1322 Høvik, Norway

Within the past two decades, a large amount of super carriers have been lost at sea. In some cases the losses are likely to be related to severe weather conditions. "Freak" or "rogue" waves are sometimes mentioned as probable cause. These terms are used to point at individual waves of exceptional wave height or abnormal shape. And it is, in particular, their shape that is of great importance for the design and operation of ships and offshore structures, as it can lead to significant impact damages. The present paper provides results of deterministic analysis concerning wave front steepness and horizontal asymmetry that was carried out on data collected at the Ekofisk field, central North Sea (operated by ConocoPhillips) and at several locations off the Belgian coast during a period of 6 months.

The Belgian data are collected from different locations and water depth off the Belgian coast, using non-directional buoys, operated by the Ministry of the Flemish Community. Wave records have been recorded continuously at the sample frequency of 2 Hz since January 2003. The Ekofisk data analysed here consist of one-dimensional time series of wave profile, also collected at a sampling frequency of 2 Hz. Data from a Waverider buoy and two down looking lasers are used.

Time domain parameters are calculated using a zero down-crossing analysis over a time period of 20 minutes. Concern is taken on the quality control of the data, since shape parameters are quite dependent on how small variations on larger waves are handled. Shape parameters during extreme conditions are compared to average values, and variations from finite to infinite water depth are demonstrated. Recent work (i.e. Olagnon and Magnusson, 2004) indicate that extremes occur due to changes on smaller time scales than 20 minutes, so variations of shape parameters over smaller time scales are also analysed here. Results on i.e. horizontal asymmetry are compared to literature (Olagnon and Krogstad, 1998, Myrhaug and Kjeldsen, 1986, Stansell et al., 2003).

Myrhaug D., Kjeldsen S.P, 1986: "Steepness and symmetry of extreme waves and the highest wave in deep water". Ocean Eng 1986; 13(6), pp549-86

....

Olagnon, M., and H.E.Krogstad, 1998: "Observed short- and long-term distributions of wave steepness". Proc. Int. Offshore and Polar Engineering Conf., Vol. 3, Montreal, pp. 63-70.

Olagnon, M., and A.K.Magnusson, 2004: "Sensitivity Study of Sea State Parameters in Correlation to Extreme Wave Occurrences". Proc. of ISOPE'2004, Toulon, May 23.-27.

Stansell P., Wolfram J., Zachary S., 2003: "Horizontal asymmetry and steepness distribution for wind-driven ocean waves from severe storms". Applied Ocean Research 2003; 25, pp137-55

Exploring Rogue Waves from Observations in South Indian Ocean

Paul C. Liu¹, Keith R. MacHuchon², and Chin H. Wu³

¹ NOAA Great Lakes Environmental Research Laboratory
Ann Arbor, Michigan 48105, U.S.A.
(email: paul.c.liu@noaa.gov)

² Liebenberg & Stander International (Pty) Ltd
Cape Town, 8000 South Africa
(email: lsi@liebstan.co.za)

³ University of Wisconsin-Madison,
Madison, Wisconsin 53706, U.S.A.
(email: chinwu@engr.wisc.edu)

Abstract. Amidst all the enticing advancements on rogue waves in recent years, the conspicuous scarcity of actual, in situ, rogue wave measurements still represents an inevitable hindrance shadowing over the horizon of rogue wave studies. In this paper we wish to present an exploratory observational study of rogue waves based on wave measurement made in South Indian Ocean. As there have been significant theoretical advancements in numerical simulation of rogue waves, the need for actual field observations of rogue waves should certainly be commensurably supplemented. We hope our efforts in this study can be ventured toward further understanding of rogue waves in reality.

1 Introduction

Amidst all the enticing advancements on rogue waves in recent years, the conspicuous scarcity of actual, in situ, rogue wave measurements still represents an inevitable hindrance shadowing over the horizon of rogue wave studies. From the meager observational rogue wave studies based on available wave measurements, on the other hand, the results usually provide objective outcomes that tend to refute rather than confirm some of the familiar conceptualizations of rogue waves. For instance, rogue waves have always been considered to be rare occurrences, but a radar satellite study (e.g. <http://195.173.17.24/news/pr2003/2.php>) carried out by the German Aerospace Centre recently found 10 monster waves around the world, ranging from 26 m to 30 m in height. They concluded that “it looks as if freak waves occur in the deep ocean far more frequently than the traditional linear model would predict.” Another recent study by Liu and Pinho (2004) based on wave measurements made from Campos

Basin outside Brazil coast in South Atlantic Ocean also concluded that freak waves are more frequent than rare.

In this paper we wish to present an exploratory observational study of rogue waves based on wave measurement made in South Indian Ocean. As there have been significant theoretical advancements in numerical simulation of rogue waves, the need for actual field observations of rogue waves should certainly be commensurably supplemented. We hope our efforts in this study can be ventured toward further understanding of rogue waves in reality.

2 The Measurement

The measurement used in this study is made from a gas-drilling FA Platform in South Indian Ocean, offshore from Mossel Bay, South Africa, located at 22.17°E and 37.97°S, alongside the Agulhas current in 100 m of water depth. (Figs. 1 and 2.) Waves are measured hourly from a Marex Radar Wave Monitor based on 20 minutes data sampled at 2 Hz frequencies. The wave sensor, as shown in Fig. 3., has a 7 to 50 m of minimum to maximum sensing range, respectively, for a possible upper limit for maximum wave height of 43 m. Wave parameters, consisting of significant wave height, maximum wave height, and average zero-crossing wave period, were processed and stored along with meteorological parameters, such as wind speed, wind gust, wind direction, air temperature, and barometric pressure among others. Presently, time series wave data is unfortunately discarded after wave parameters are processed. Nevertheless the availability of maximum wave height jointly with wind speed and wind gust has provided a unique opportunity for us to explore rogue waves as well as their potential meteorological connections in this renowned region of colossal waves.



Fig. 1. A map showing the location of the FA Platform in the red spot.



Fig. 2. A snapshot of the FA Platform.

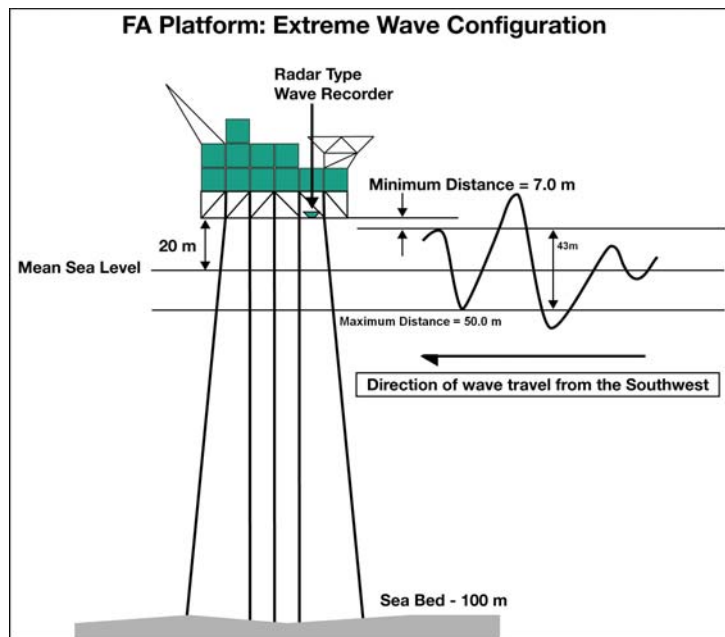


Fig. 3. Schematic illustration of the platform wave measurement.

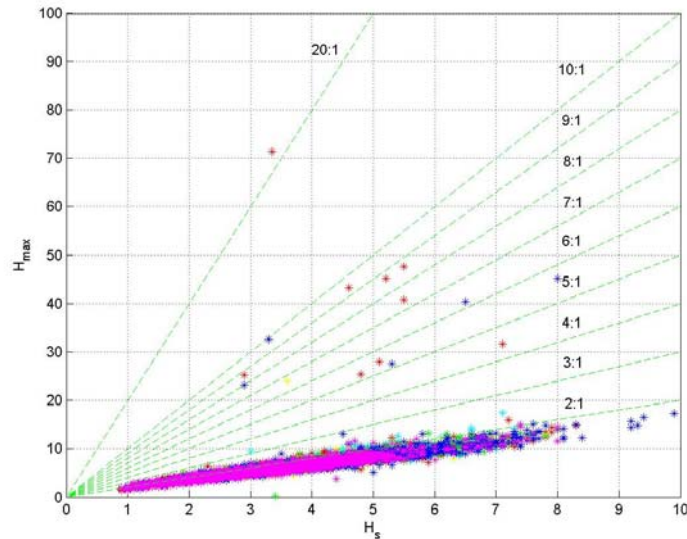


Fig. 4. Correlation plot of H_{\max} vs, H_s .

3 Data and Analysis

From an examination of the most recent 6 years data that covered the turn of the millennium, 1998 – 2003, we have found some interesting results, which may or may not be immediately intuitive. Based on the customary criterion of defining rogue waves as $H_{\max}/H_{\text{sig}} > 2$, there are 1563 potential rogue wave cases contained in a total record of 50359 hours over the 6 years. A general occurrence rate of 3.1 percent, which is less than, but reasonably close to, the 3.7 percent Liu and Pinho (2004) found from South Atlantic Ocean. These presumably rogue wave cases we examined generally conform to the expectable configurations as shown in Fig. 4 with H_{\max}/H_{sig} lying mostly between 2 and 3. However our primary interest have unwittingly engrossed by a number of isolated cases occurred during 1999, 2000, and 2002 where the data appeared to be entirely out of line with the bulk of general conglomeration of the data. These cases show that H_{\max} hiked up to between 23.2 and 71.4 m and with H_{\max}/H_{sig} accordingly varying between 4.5 and 21.3. Are they just simple outliers?

Our initial inclination tends to respond affirmatively to the above question. It is usually non-disputive to implicate that the recording can somehow be temporarily in malfunction, so the outliers can be summarily discarded. However, after further deliberation, and considering the fact that the wave recorder is positioned 20.0 m above mean sea level and most of the outliers are around the wave height sensing limit, we now believe that some of the anomalies may very well be real recordings of waves,

including taking tides and surface spray into account. In these cases the maximum wave heights could reasonably be expected to be within the sensing range of 43.0 m or more and thus it generally accounts for all the very high H_{\max} cases shown in Fig. 4 except the one case with $H_{\max} = 71.4$ m which is obviously not justifiable. Since we kept an open mind on outliers, we included all the data in for now. Without the benefit of time series data the aforementioned inference is certainly not unreasonable, especially given that the recording operated flawlessly both immediately before and after those instances and throughout the years.

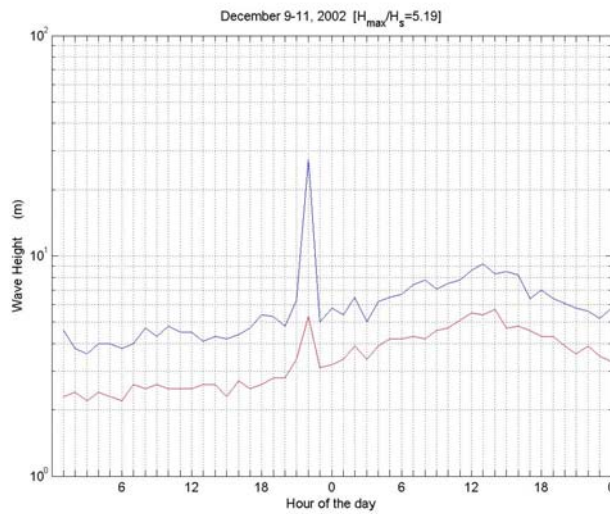


Fig. 5. Hourly data plot of maximum wave heights shown as the upper blue curve and significant wave heights as the lower red curve for the Dec. 9-11, 2002 case.

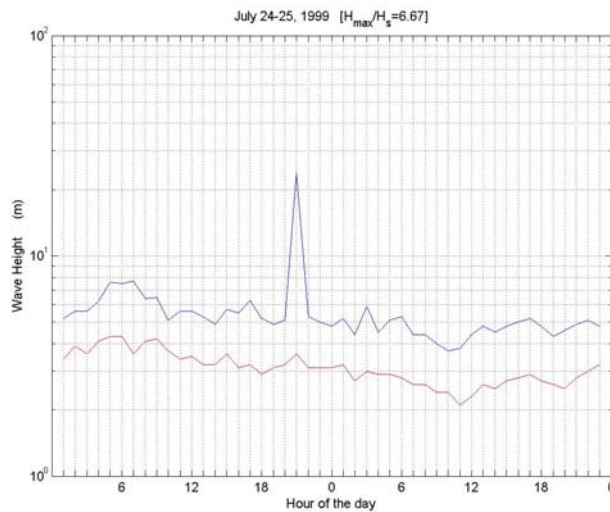


Fig. 6. Same as Fig. 5 for July 24-25, 1999 case.

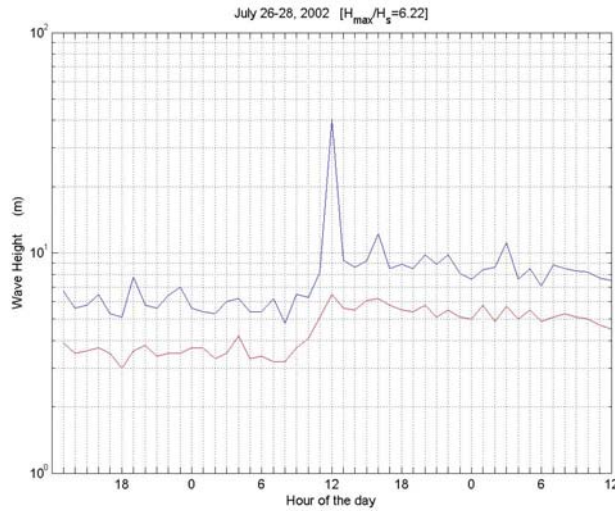


Fig. 7. Same as **Fig. 5** for July 26-28, 2002 case.

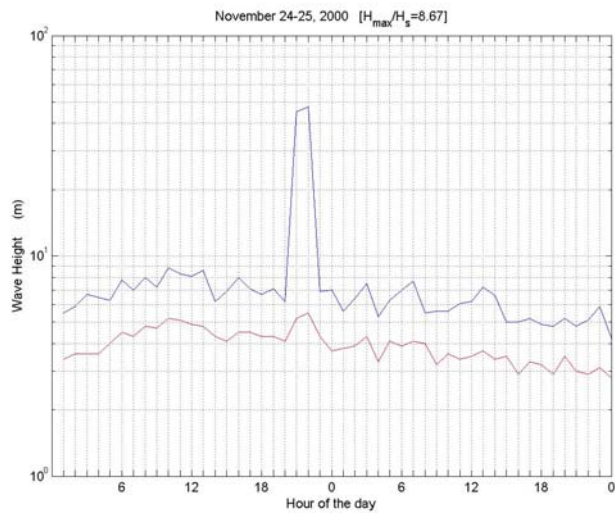


Fig. 8. Same as **Fig. 5** for Nov. 24-25, 2000 case.

As shown in the plots of sample cases presented in Figs. 5 – 8, these cases were in relatively fully-developed seas, and wind fields were generally quite steady in all cases, there is really no discernable physical reason for these anomalies. One plausible reason for these exceptionally high maximum wave height records could be that the wave monitor was momentarily under water during the over passing of these waves and we are not certain if the wave monitor can still accurately sense the water surface under these circumstances. In any event, the actual wave amplitudes would

certainly have been far beyond 20 m. In the end we are inclined to postulate that these cases are actually indicative of the presence of the real rogue waves this area is famed for. If this is true, we can only be thankful that their occurrences did not cause any disastrous damage. [Recall the lost of passenger liner SS *Waratah* in this area in late July, 1909. See, e.g., <http://www.numa.co.za/sswaratah.htm> .]

4 Discussion

One of the consequences of the presence of these large rogue waves shown in the previous section is that they led to unprecedented large ratios of H_{\max}/H_s . What do these large ratios signify? Are they for real or are they outliers?

The central concept of the Rayleigh distribution clearly does not overtly preclude large ratios of H_{\max}/H_s . One of the well-known equations correlates H_{\max}/H_s with the number of waves needs for it to occur as

$$H_{\max} / H_s = [\ln(N) / 2]^{1/2} .$$

So based on Rayleigh distribution, to have ratios of H_{\max}/H_s to be 3, 4, 5, 6, for instance, it simply requires 6.5×10^7 , 7.9×10^{13} , 7.9×10^{21} , and 1.9×10^{31} number of waves to occur. As these are extremely large numbers that can translate into millions of years for it to occur. This is rather unrealistic as well impractical. Basically the Rayleigh approach would consider large ratio of H_{\max}/H_s case extremely rare occurrences.

Conceivably plausible indications can also come from laboratory experiments such as the one conducted by Wu and Yao (2004). While H_{\max}/H_s was not included in the publication, the ratio of H_{\max}/H_s was nevertheless available. They varied from 2.947 to 8.731 along with 6 cases of H_{\max}/H_s in the 3 to 4 range and 4 cases in the 4 to over 5 range. This is very encouraging. In order for us to be able to directly compare the field data with laboratory data. We have to first normalize the available data with the length parameter gT^2 , where T is the corresponding mean wave period for each available data set. This is effectively converted the process of correlation of H_{\max} versus H_s to the correlation of corresponding wave steepnesses between the average conditions versus the extreme cases. Of course the field data do not have the wave period when the extreme cases occurred. The results are shown in Fig. 9 that presents a rather more coherent appearance than the H_{\max} versus H_s results. The laboratory results appropriately situated at the extreme boundary of all the data cases at the low end of the steepness scale. But it is also clearly corresponds to the lower boundary of large wave cases, that provides some indication that the large wave cases may not be simply outliers.

Further rationales may also come from the local complicated and perplexing physical environment surroundings where the data were measured. As shown in Fig. 10 this

area is dynamically dominated by the Agulhas current from the northeast and from the

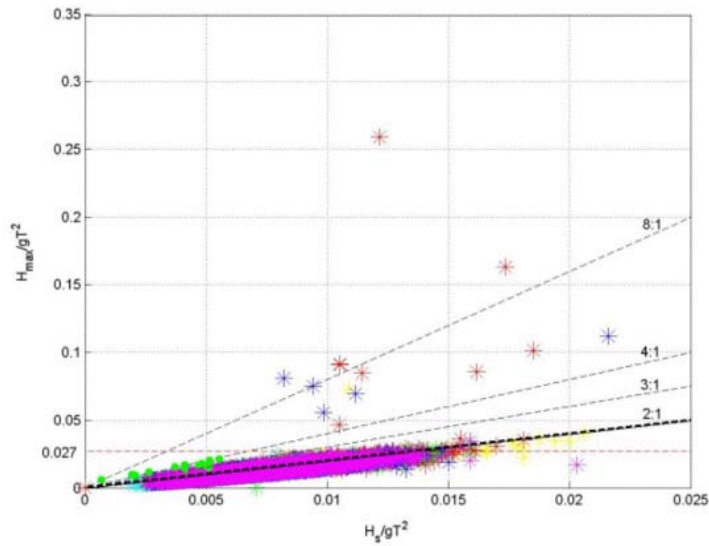


Fig. 9. Comparing wave measurement from FA platform in stars with laboratory measurements in closed green circles.

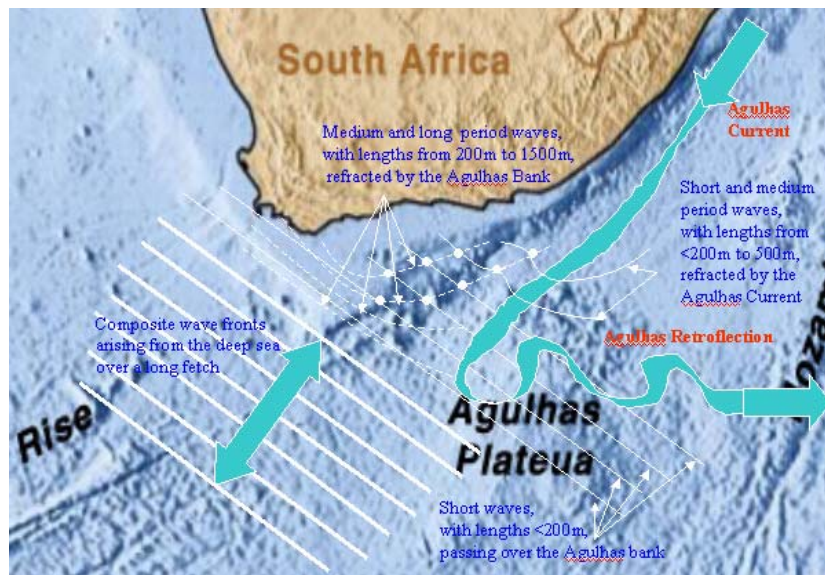


Fig. 10. Physical environment of South Indian Ocean area where the wave measurements were made.

southeast there are composite wavefronts arising from the the deep sea over long fetches. As medium and long period waves with lengths from 200 m to 1500 m refracted by the Agulhas plateau, short waves with wave length of 200 m or less passing across the Agulhas bank and meeting the Agulhas retroflection. At the same time short and medium period waves with length in the range of 200 – 500 m further refracted by the oncoming strong Agulhas current. Surrounded by such an varied assortment of dynamical interactions, it should not be surprised that very large rogue waves can appear from time to time. That's what makes the exploration invigorating and an envision of these unusual cases as simply outliers would be frivolous.

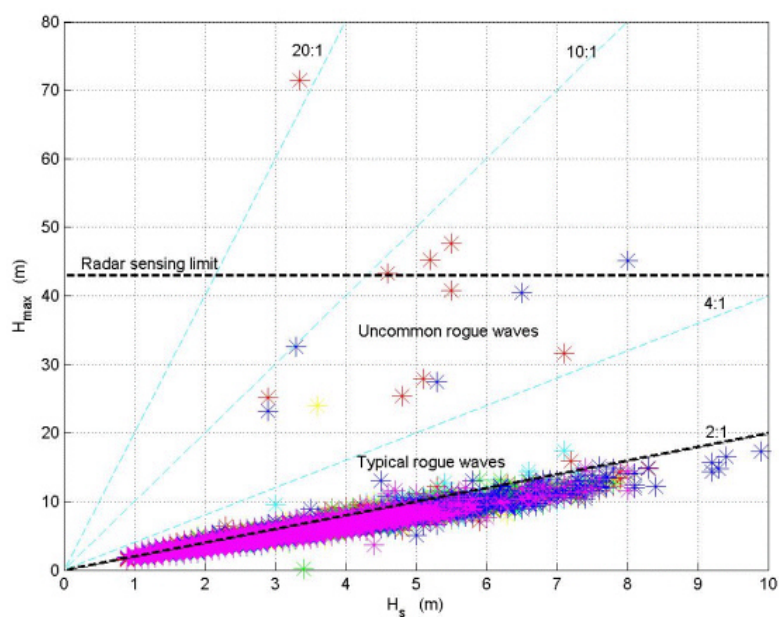


Fig. 11. Proposing a new classification of rogue waves

5 Concluding Remarks

While Liu and Pinho (2004) did not consider a 3.7 percent occurrence rate of $H_{\max}/H_s > 2$ cases to be of rare occurrence, the 15 recorded anomalous cases with much higher ratios for H_{\max}/H_s which we discovered from among the 50359 hours of measure-

ments in 6 years, with an occurrence rate of 0.03 percent, would certainly befit the pertinent nature of rareness by which rogue waves have been customarily known. So would it be possible that there can be different kind of rogue waves? Upon deliberation, we are hereby to propose that may be a new classification for rogue waves can be considered. As shown in Fig. 11, for the cases of ratio range of $2 < H_{\max}/H_s < 4$, which embodies most of currently known and available data and analysis, we call them the “*typical* rogue waves.” For the cases of H_{\max}/H_s ratios of 4 or higher, we propose to call them the “*uncommon* rogue waves.” This action will not interfere with the current ongoing rogue wave studies. But this does provide a new realm for the past, present and future seemingly outlier cases to reside. Though these may merely be our speculations, we do feel strongly that the existence of these cases further emphasizes the crucial need for long-term wave time series measurements for studying rogue waves. Without tangible measurements, no amount of theoretical simulations can truly divulge the reality of the phenomenon so long as we still do not have the slightest notion as to whatever is really happening out there.

Acknowledgements

The authors gratefully acknowledge Petro SA, the owners of the Platform, and the CSIR of South Africa, who generously made the information used in this paper available to us.

References

1. Liu and Pinho, 2004, Freak waves - more frequent than rare! *Annales Geophysicae*, Vol. 22, 1839-1842.
2. Wu, C.H. and Yao, A., 2004 Laboratory measurements of limiting freak waves on currents, *J. Geophysical Research-Oceans*, 109, C12, C12002, 1-18.

Development of Operational Guidance Criteria for Small Craft Operating in Dangerous Seas

Bruce Johnson, *US Naval Academy, Annapolis., MD 21402, USA*
Tel: +1-410-295-9393; Fax +1-410-293-2219; e-mail: aronj@bellatlantic.net
Stefan Grochowalski, *Ottawa, Canada*

The most dangerous seas to small craft operation are those which produce groups of extreme, steep waves (relative to the size of the vessel) and those that involve breaking waves impacting from the beam or astern quartering directions. Rogue waves of twice the significant wave height are certainly dangerous to vessel operation, but groups of steep waves which are large relative to the vessel size are far more likely to be encountered and are equally dangerous.

The paper presents additional analysis of the comprehensive model tests of fishing vessel capsizing carried out by the National Research Council of Canada in the 1980s. The analysis is focused on those dangerous elements of ship behavior in large, steep waves which indicate the possibility of ship capsize. The symptoms of danger of capsize can include: water shipping on deck, large amplitude of motions with hesitant return, riding on the wave crest, tendency to surfing, difficulty to maintain course control, bulwark immergence, and others. The occurrence of these phenomena is related to ship loading conditions, **wave parameters**, ship speed and course direction relative to waves.

Special attention is paid to the frequency of occurrence and intensity of the phenomena in the test runs in which the model eventually capsized. Certain parameters of these phenomena are considered as the pre-capsize symptoms. They should be an important part of the operational guidance in the future.

The paper will also address the problem of using the results of model tests in steep regular waves to predict the probability of encountering the same type of vessel motions in irregular waves. One correlation being investigated is to use the probability of encountering large amplitude wave groups with an equivalent regular wave height and mean period found in various irregular wave spectra formulations. This approach is based on work by Dawson and Kriebel using Markov theory for wave group statistics combined with Longuet-Higgins analysis for narrow band frequency spectra. In the case of the JONSWAP spectral formulation, fetch length, wind speed and duration will be systematically varied in order to find a range of significant wave heights, periods and resulting probabilities of encountering irregular wave groups roughly equivalent to the vessel motions found from regular wave tests. The goal of this analysis is to develop a performance-based approach to capsize risk assessment for various loadings of fishing vessels in typical operational sea states based on model tests in regular waves. Limited validation of this concept is available from the irregular wave tests done as part of the NRC model test series.

MEASUREMENTS OF FREAK WAVES IN NORWAY

AND RELATED SHIP ACCIDENTS.

by

Søren Peter Kjeldsen.

Trondheim Maritime Academy.

Ladehammerveien 6. – 7004 Trondheim. NORWAY.

E-mail: peter.kjeldsen@c2i.net

Abstract. This paper describes establishment of a world data bank related to ship and platform accidents caused by freak waves and rogue waves. It was found that many of these accidents follow a certain pattern. It was not the highest waves but violent breaking waves that gave the largest responses on the structures. Force models that predict drag- lift- and impact forces on superstructures of ships and platforms are developed. Some of the coefficients used in the force models are obtained from measurements on platforms at sea. Here impact forces were measured in asymmetric wind waves.

Others are obtained from laboratory experiments some of them performed in a wind-wave flume with asymmetric wind waves. Thus a large data bank was established, and valuable information might be available for future designs. Accidents related to freak waves are not randomly distributed but are concentrated in 21 specific sea areas worldwide. Further a forecast of freak waves were established in one of these exposed areas.

1. Introduction.

When the first gravity platforms were installed on the Norwegian Continental Shelf nearly no knowledge was available, regarding the frequencies, durations and peak values of slamming wave loads caused by deep water gravity waves in interaction with fixed and floating structures during gales. Some rough non-mandatory guidelines were made in order to take such extreme wave loads into account in design. However in order to obtain a better documentation that could be of value for future designs a large research programme was initiated by the offshore industry.

30 pressure transducers were installed dedicated for full scale measurements of wave loads on a concrete gravity platform during full gale conditions. Because very little was known about the shape in space of 3-dimensional extreme waves a stereo-photogrammetric data acquisition was initiated.. Thus the frequencies of breaking of extreme waves, the type of breaking that occurred and the associated water wave kinematics in the free surface zone could be analysed in addition to the measured wave loads. The research programme contained also an extensive series of model experiments some of them performed in a wind-wave flume with a model of the concrete platform. Here slamming pressures were measured in asymmetric wind waves. Thus a large data bank was established, thus valuable information is available for future designs.

Motivation for the investigation on this topic was the loss of the semi-submersible “ OCEAN RANGER “ near New-Foundland in Canada. The reason for the loss of this platform was that a breaking wave crushed several windows in the control room and then the ballast control panel failed. The platform then lost watertight integrity and was gradually filled with sea water. After several hours the platform heeled nearly 30 degrees towards one of the corners and was evacuated.. The platform finally lost stability and capsized. All 84 people onboard were lost. The rescue operations that were attempted failed in very severe waves.

Hence new research on wave impact forces was carried out in full scale combined with stereo-photogrammetric data acquisition of severe breaking waves. The severe waves were found to be asymmetric in the wind direction with steep fronts and less steep rear sides. Numerical simulations were made to predict both wave crest kinematics in breaking waves and associated wave impact forces. These numerical simulations were calibrated against full scale measurements. The results show that the wave impact from non-breaking waves on structures increase with wave height, however it was not the highest waves but the breaking waves that produced the most severe wave impacts.

Experiments were also performed in a wind-wave flume in order to study the effects of asymmetric wind waves and their influence on wave impact forces. The results have been used to establish mathematical force models which can be useful for future designs of superstructures of ships and offshore platforms. In particular FPSO-ships in the offshore industry recently has been exposed to broken windows in the superstructures and severe bow damages. Thus it has become clear that at advanced sea states, breaking waves exert by far the largest unitized forces against ships and interfacial structures, with all their implications to ship design, maneuvering and operation.

2. Ship accidents.

Loss of a large Norwegian ship with the entire crew in the middle of the North Atlantic is not a common event. However at a special occasion two large Norwegian bulk ships M/S "NORSE VARIANT" and M/S "ANITA" disappeared at the same time at the same location. Both ships passed Cape Henry with only one hour interval in time on voyages from the U.S.A. to Europe. Both ships came right into the center of a very extreme weather event with a strong low pressure giving 15 m significant wave heights and mean wave periods close to 10 seconds and strong northerly winds with wind velocities near 60 knots. "NORSE VARIANT" had deck cargo that was damaged and moved by water on deck with the result that a hatch cover was broken and left open. The ship took in large amounts of water and sank before an organised evacuation was completed.. Only one member of the crew was rescued on a float.

"ANITA" disappeared completely at sea with the whole crew and no emergency call was ever given. The Court of Inquiry then concluded that the loss can be explained by an event in which a very large wave suddenly broke several hatch covers on deck, and the ship was filled with water and sank before any emergency call was given. The wave that caused the loss of "ANITA" was probably a freak wave.

3. Establishment of a data bank.

In our research we have defined a freak wave as a wave with a zero-downcross wave height that exceed 2 times the significant wave height. Crucial questions are then:

1. - Will a freak wave that hits a ship be a breaking wave ?
2. - Is it possible to analyse measured freak waves in order to determine if they are breaking waves or non-breaking waves ?

Therefore considerable work has been made to analyse the observed freak waves in the established data bank and divide them into the following 3 groups shown in Table 1.:

Table 1. Classification of freak waves.

NON-BREAKING FREAK WAVES
2 dimensional FREAK WAVES breaking as " PLUNGING BREAKERS " – Longcrested waves.
3 dimensional FREAK WAVES breaking as " PYRAMIDAL BREAKERS " Shortcrested waves.

It is not possible to characterise the severeness of a particular sea state containing large random waves some of them even breaking using only traditional parameters height and period of the individual waves. Experiences show that accidents occur if there is a quite unique exceedance of critical threshold values for several parameters simultaneously. Wave steepness seems to be a parameter at least as important as wave height, under some special circumstances even more important. Traditionally wave steepness of a random wave has been introduced as a ratio between total wave height and total wave length.

However, in a random sea many waves can occur with the same total steepness but different asymmetry, and thus some of them will be breaking others not. The random waves in a severe directional wind generated sea are clearly asymmetric both in the wind direction and in the vertical direction. In order to obtain a better

description of freak waves and rogue waves, and in particular to distinguish if they are breaking or not a DATUM and 4 important wave parameters were introduced. Then the mean water level is taken as reference DATUM and crest height, crest front steepness, crest rear steepness and horizontal and vertical wave asymmetries are introduced see Kjeldsen & Myrhaug (1979) and I.A.H.R./P.I.A.N.C. (1986). The parameters relevant for analyse of freak waves are shown in Fig 1. Kjeldsen & Myrhaug (1979) found that inception of wave breaking in deep water took place for the following values of wave asymmetry parameters measured in space from high speed films:

0.32 < Crest front steepness < 0.78

0.84 < Vertical asymmetry factor < 0.95

Examples of severe damages to platforms and ships are given by Kjeldsen (1984) , and (1997). Haver (2000) has reported a very significant freak wave event on the Norwegian Continental shelf. Here a large freak wave occurred at the “ DRAUPNER “ platform.

Accidents including a large number of severe heavy weather damages on ships and offshore structures were collected in a WORLD DATA BANK from several sources:

1. – **Cargo ships and passenger liners.**
2. – **Fishing vessels.**
3. - **Experiences from the offshore industry with FPSO ships, steel jackets and semisubmersibel platforms.**

Ship capsizings caused by freak waves were mapped, one of them was the loss of the british trawler “GAUL”. The performed research showed that freak waves occur typically in some specific areas of the world, see Fig. 2.. Here 21 specific areas are identified where freak waves have been observed and related ship accidents have been reported. In cases with ship capsizings the actual waves that caused the accidents were normally not measured However in a few rare occasions freak waves with a particular capsizing potential were measured, see an example from Area No 5 in Fig. 3.

A joint probability density distribution is computed for this case. It is remarkable that this particular wave has not only an abnormal wave height but at the same time an abnormal crest front steepness. This gives this particular wave a large capsizing potential. Based on the above it is reasonable to expect that this wave developed further with a breaking mode as a plunging breaker occurring in deep water.

Only in a few unique cases photos of such freak waves have been taken. Fig 3 shows such a scenario with a large norwegian bulk ship heading into an abnormal wave in the Bay of Biscay, Area No 8.

Even more rare is the opportunity to have a ship with recording instruments running into a freak wave. Such a case happened unexpected in Area No 20 the Mediterranean Sea. A 100 m long monohull high speed vessel was running with 40 knots in a sea state with significant wave height 3.5 – 4 m and was suddenly struck by a freak wave. Fig 4 shows the recorded bow acceleration 1.5 g (2.17 times the 10th value), and the recorded strain in the longitudinal beam that was 80 Mpa. (5.28 times the 10th value.)

4. Learning from ship accidents.

If a freak wave occur it often happens that it comes from a direction that deviate significantly from the main wind direction. It thus suddenly strikes on the ship with another direction than the other waves and this makes the situation particular dangerous during storm conditions if the ship is in a head sea and suddenly goes into an abnormal roll, because the freak wave strikes 40 degrees off the wind direction.

Many ship officers claim that several of the real difficult situations at sea rarely are tested in laboratory experiments, in particular crossing seas with a wind sea and a swell from different directions and sometimes confused pyramidal breakers striking on the ship.

Good seakeeping has been a forgotten factor in many cases. For the ship officers there is a need for further education in particular in the following items:

1. – **How to avoid hot spots in the sea when freak waves is expected to occur ?**
2. – **How to handle a damaged ship in severe waves ?**
3. – **What is the right time to evacuate a damaged ship ?**

For naval architects and designers the following items should be considered:

1. – Ship displacement and mass moment of inertia should be taken into account in criteria for dynamic stability.
2. – High impact forces caused by extreme waves breaking on the superstructure should be considered. In particular large windows are weak points.
3. – Pressure from large amounts of water on deck should be considered.
4. – Hatch covers on bulk ships are weak points and should have the same strength as the ship hull.
5. – Extreme freak weather events caused by change of climate, might lead to an increasing number of scenarios containing extreme waves and freak waves in the future.

5. The reversed tsunami model.

Laboratory experiments have been performed in several large wave flumes, one of them is a wind wave flume. A freak wave event is modelled with a Dirac-function, and wave dispersion is controlled by a non-linear term depending on wave amplitude. With such a technique it is possible to focus a number of waves in such a way that a single elevated wave suddenly occurs at one prescribed time and position in the middle of the flume, see Kjeldsen (1982). Thus a 3-dimensional breaking freak waves were generated as shown in Fig 5.

With wind superimposed all the waves in the generated sea spectrum developed asymmetry. Wave kinematics have been measured in the wave crests above mean water level using a wave follower technique and platforms and ships have been installed at the dangerous position where wave focusing occur.

Also an axisymmetric counterpart of this wave generation technique was investigated experimentally. When a “ **tsunami-wave** “ is generated from a point source all waves spread out isotropically and their propagation depend on their group velocities and the distance from the point source. The energy in the different wave components is determined by the initial disturbance. Thus modelling and forecasting “ **tsunami-waves** “ using a Dirac-function at the epicenter is possible, and such a technique has also been used in the Pacific Ocean for several years.

In the laboratory experiments large 3-dimensional breaking freak waves were generated with a reversed version of the “ **tsunami wave model** “. See Fig 5. Only wave components with wave lengths corresponding to wind generated waves were used. However the generated waves that finally focused in one point had a directional spreading of 60 degrees, corresponding to the directional spreading in the actual sea spectrum.

6. Forecasting of Freak Waves.

A forecast of freak waves is made for Area No 5 along the Norwegian coast. Here non-linear effects are present in a combination of wave depth and wave current refraction. 8 capsizings has occurred in this particular area.

The ship officers have been very satisfied with this forecast and have suggested that a similar forecast is prepared for other of the sea areas shown in Fig 2.

7. CONCLUSIONS.

- There is a need to increase survivability of modern ships, in such away that a damaged ship with a heeling angel can sustain impacts from large waves and still maintain a marginal dynamic stability.
- The rules and requirements of ship dynamic stability is clearly insufficient. Not only the area below the GZ-curve should be taken into account but also the displacement of the ship and the mass moment of inertia given as the radius of gyration. This applies both to intact stability criteria and to criteria for damaged stability.
- High impact forces caused by extreme waves breaking on the superstructure of ships and should be considered. In particular large windows are weak points.
- Dynamic pressures from large amounts of water on deck should be considered. Hatch covers on bulk ships are weak points and should have the same strength as the ship hull.
- A better education of ship officers is needed. In particular we need a better education in ship handling of intact and damaged ships in severe weather conditions. Better guidelines should be given to ship officers regarding the choice of the right time to evacuate a damaged ship, and the time needed to evacuate in severe wave conditions.
- The “ **tsunami wave model** “ reversed in the time domain was found to be a successful mathematical technique for modeling of a 3-dimensional freak wave.

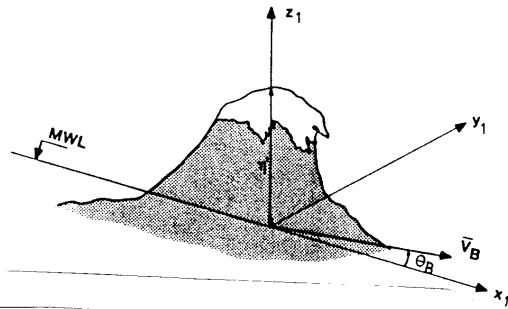
- A risk management model with the scope to avoid capsizing in freak waves in a given sea area can be established as a joint probability model for encounter of a wave with an abnormal wave height and at the same time an abnormal crest front steepness. A successful forecasting of freak waves is already established.
- An international standard is needed for hydrodynamic laboratories performing capsizing experiments with ships and platforms in breaking waves and extreme non-breaking waves. This standard should be based on laboratory measurements of wave kinematics.

6. ACKNOWLEDGMENTS.

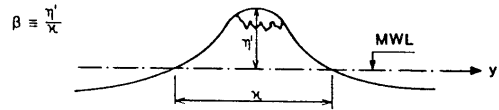
We will express our gratitude to Dr. Pierre Bonmarin, Dr. Michel Huther, Dr Michael Skafel, Dr William Drennan, Dr. Hiroshi Tomita, and Professor Bruce Johnson. They all contributed in a significant way to this study.

7. REFERENCES.

- Haver S. 2000:” On the Existence of Freak Waves.” Proc. The Rogue Waves Symposium , Brest France. December 2000.
- I.A.H.R./P.I.A.N.C. 1986: ”List of Sea State Parameters. Supplement to Bulletin No 52.”
- Kjeldsen S.P., Myrhaug D. 1979:» Breaking Waves in Deep Waters and Resulting Wave Forces.» Paper No. 3646.Proc. 11th Offshore Technology Conference. Houston, Texas.
- Kjeldsen S.P., Vinje T., Myrhaug D., Brevig P. 1980:» Kinematics of Deep water Breaking Waves.» Paper No 3714. Proc. 12th Offshore Technology Conference. Houston, Texas, U.S.A.
- Kjeldsen S.P. 1982:» 2- and 3-dimensional Deterministic Freak Waves.» Proc. 18th Int. Conf. on Coastal Engineering . Cape Town, South Africa.
- Kjeldsen S.P. 1984: « Dangerous Wave Groups.» Norwegian Maritime Research, Vol 12, No 2 pp 4-16.
- Kjeldsen S.P. 1997:” Examples of Heavy Weather Damages caused by Giant Waves.” SNAJ. Bulletin of the Society of Naval Architects of Japan. Vol 828 1997/10 pp 744-748.
- Kjeldsen S.P., Bonmarin P., Skafel M.G., Drennan W.M. 1998: ” Lagrangian Measurements of Accelerations in the Crest of Breaking and Broken Waves.” Proc. 26th International Conference on Coastal Engineering. Copenhagen. Denmark. 22-26 June 1998.
- Kjeldsen S.P., Drennan W.M.,Skafel M.G. 2000:” Modelling of Velocities in Giant Waves.” The ISOPE-Journal. Volume 10. No 3. September. 2000. pp 170-172.

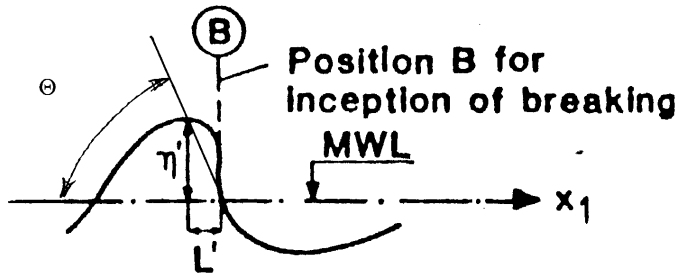


DEFINITION OF CREST LENGTH λ AND 3-D CREST SHAPE FACTOR β IN SYNOPTIC DOMAIN :



DEFINITION OF CREST FRONT STEEPNESS ϵ_x IN SYNOPTIC DOMAIN :

$$\epsilon_{x,B} = \frac{\eta'}{L'}$$



VERTICAL ASYMMETRY FACTOR
 $\lambda = \frac{\epsilon}{\delta} = \frac{L'}{L''}$

HORIZONTAL ASYMMETRY FACTOR
 $\mu = \frac{\eta'}{H}$

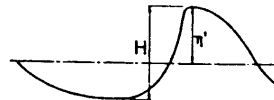
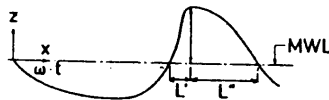
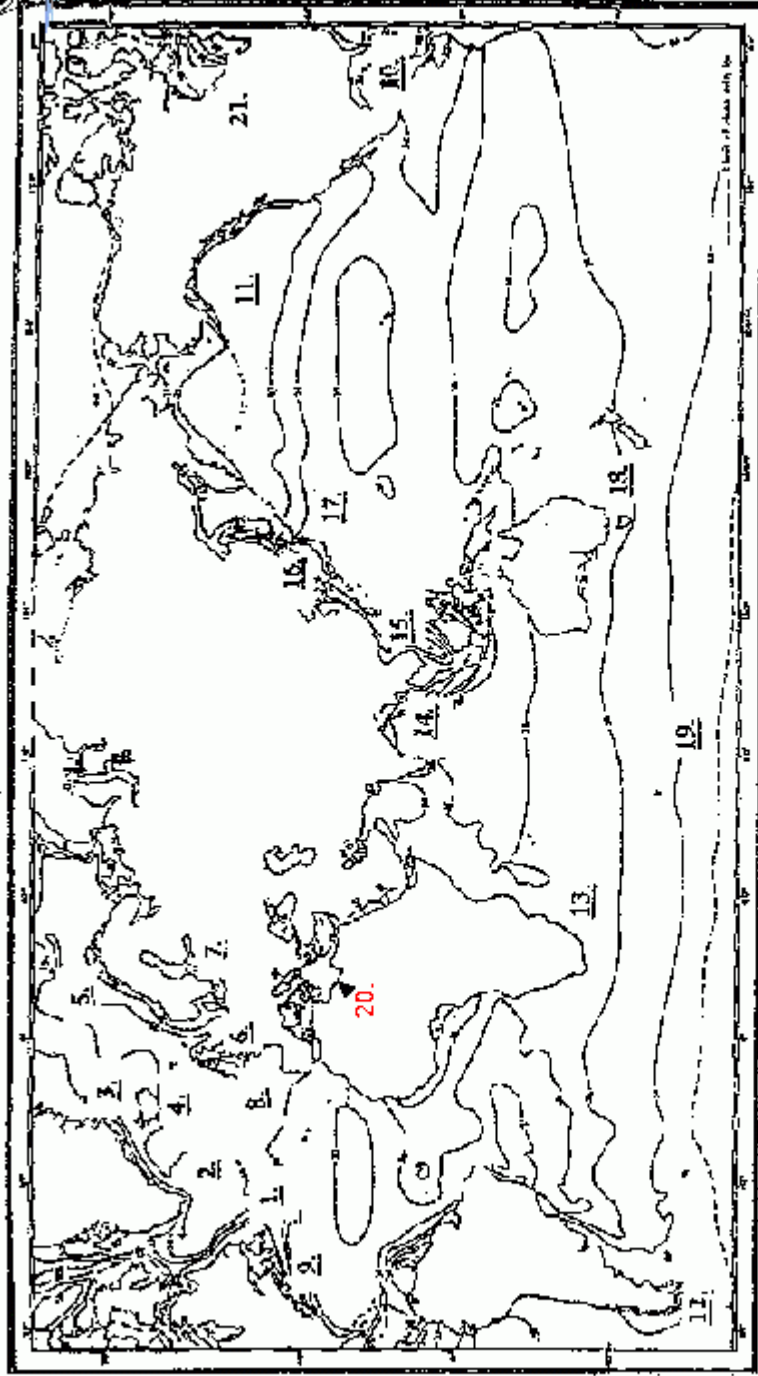
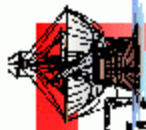


Fig. 1. Photo by Fukumi Kuriyama of a 3-dimensional freak wave and basic definitions for the same wave.



Contours Areas that contain Fish Waves under certain Meteorological Condition

1	New Foundland Banks	8	The Biscay Bay	15	The South China Sea
2	The Sea south of Greenland	9	Gulf Stream on the east coast of USA.	16	The Japan Sea
3	Coastal areas near Iceland	10	The Mexican Gulf	17	The Pacific Sea east of Japan
4	Coastal areas near Farø Islands	11	The Sea west of British Columbia.	18	Coastal areas near Australia
5	Coastal areas on the Norwegian coast	12	The Sea near Cap Horn	19	Areas south of 40 degr. South
6	The North sea	13	Agulhas current east of South Africa	20	Mediterranean Sea
7	The Baltic Sea	14	The Bengal Sea	21	Great Lakes

Fig. 2.

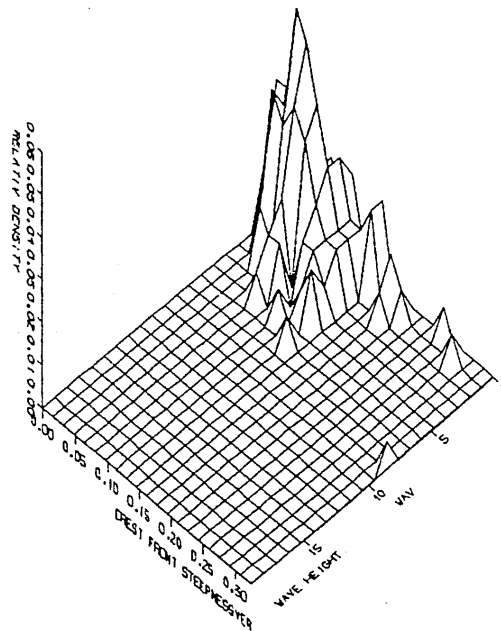
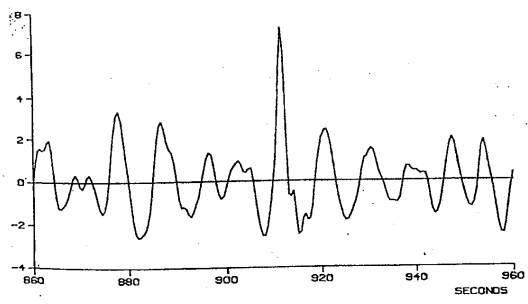
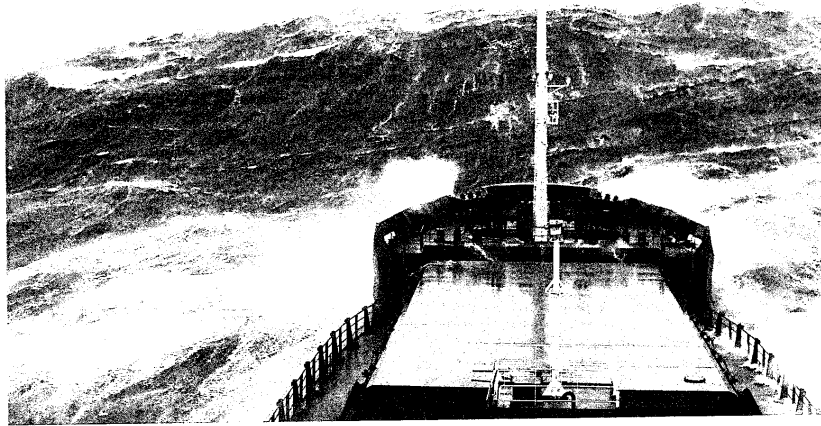
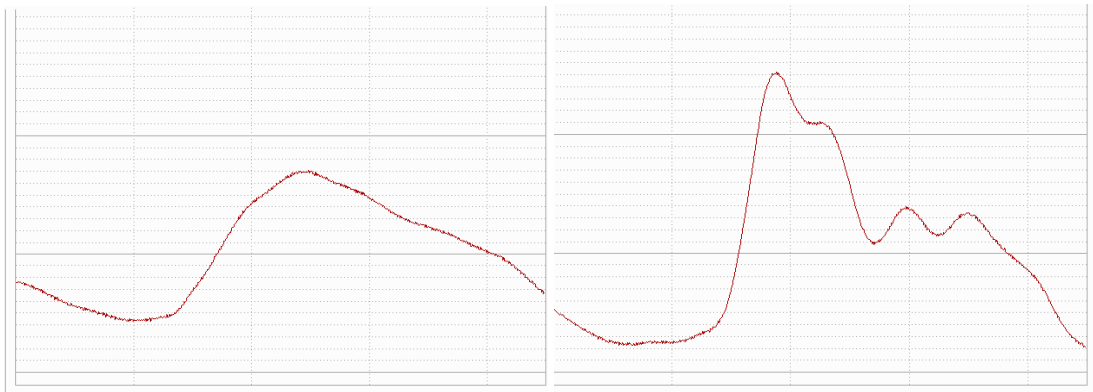


Fig. 3. Above: A Norwegian bulk ship heading into an abnormal wave in area No 8. Below: Exampel of a freak wave and the corresponding joint probability distribution of wave height and crest front steepness measured in area No 5.

Time history of the bow acceleration



The same at a larger time scale



Stress time history on a bottom longitudinal stiffener



Fig. 4. Example of extreme bow acceleration and stress measured on a high speed ship in Area No 20. The significant wave height was 3.5 – 4 m.

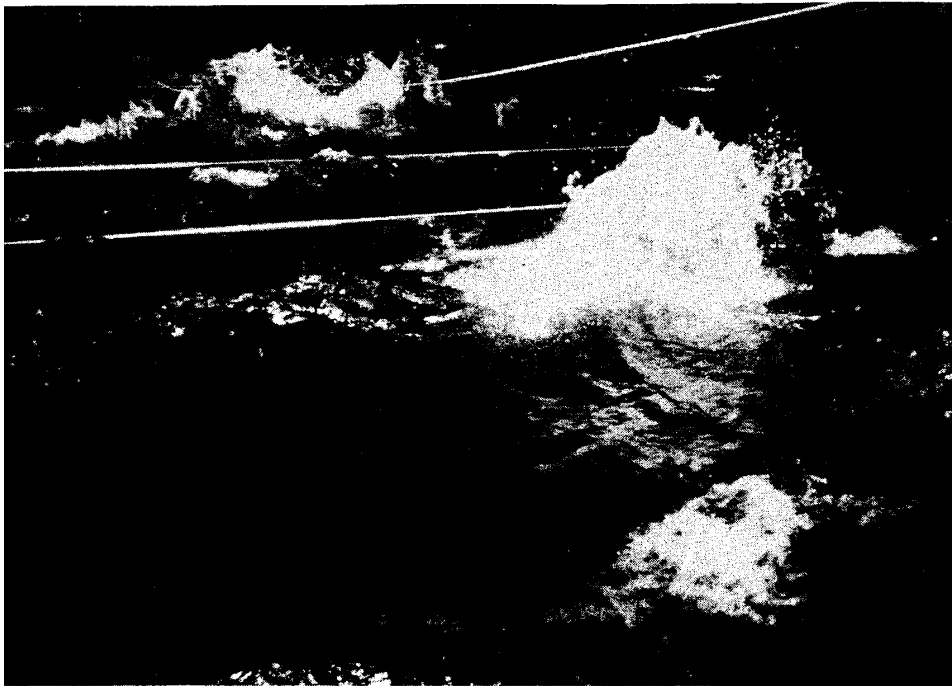
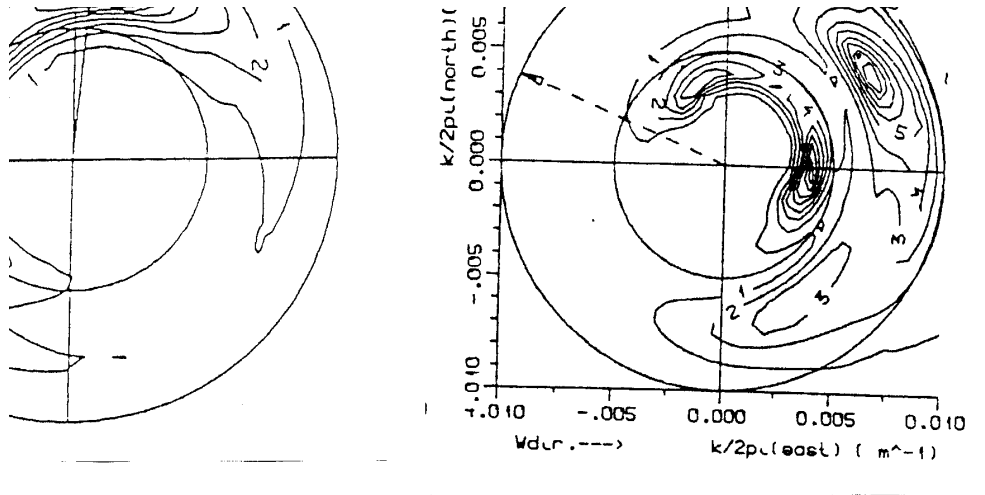


Fig. 5. Above left: A bimodal directional wave number spectrum. Right: A directional wave number spectrum showing wave-current refraction in the Gulf Stream. Freak waves have been measured in such directional seas. Below: A 3-dimensional shortcrested freak wave generated in laboratory experiments in order to simulate the wave shown in Fig. 1.

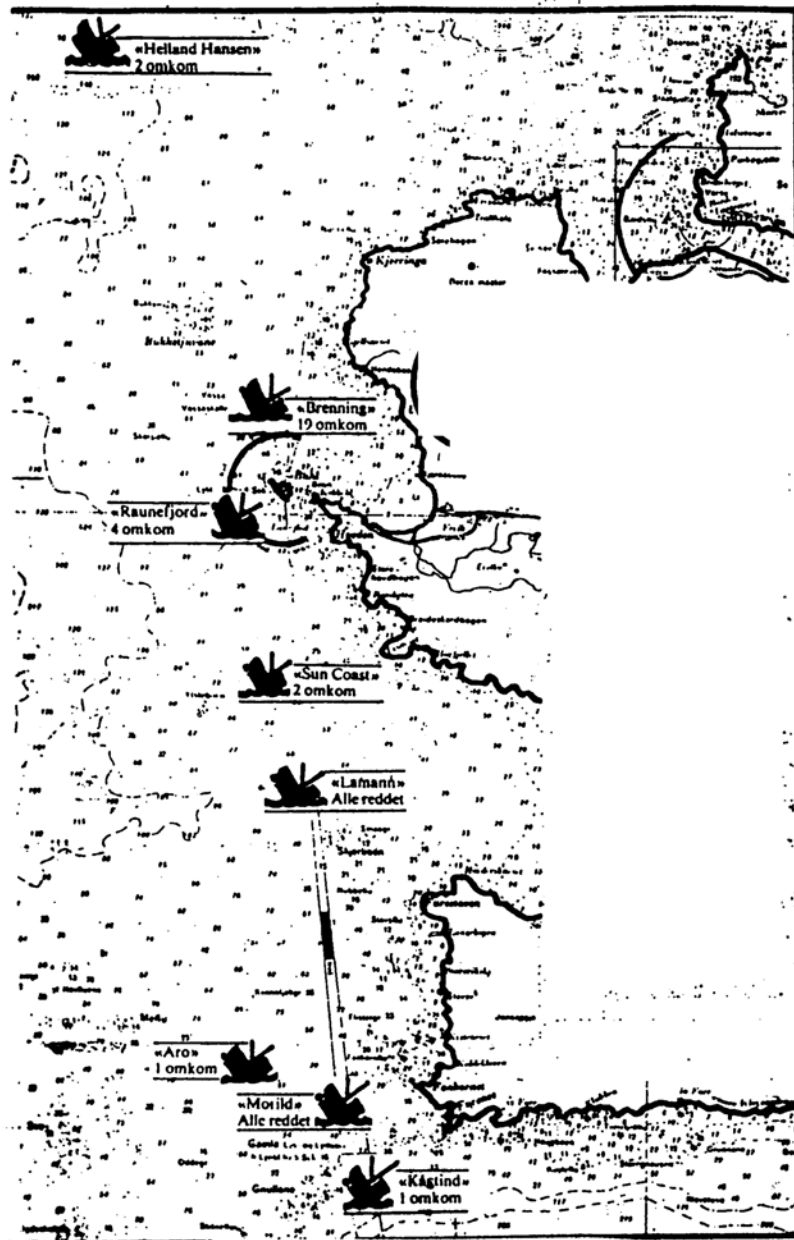


Fig. 6. Altogether 8 capsizings has occurred in Area no 5 along the Norwegian coast and 29 people have lost their lives in these accidents. In this Area a warning for freak waves is initiated with success. Pyramidal waves of the kind shown in Fig 1 and Fig 5 can be observed here in severe weather conditions.

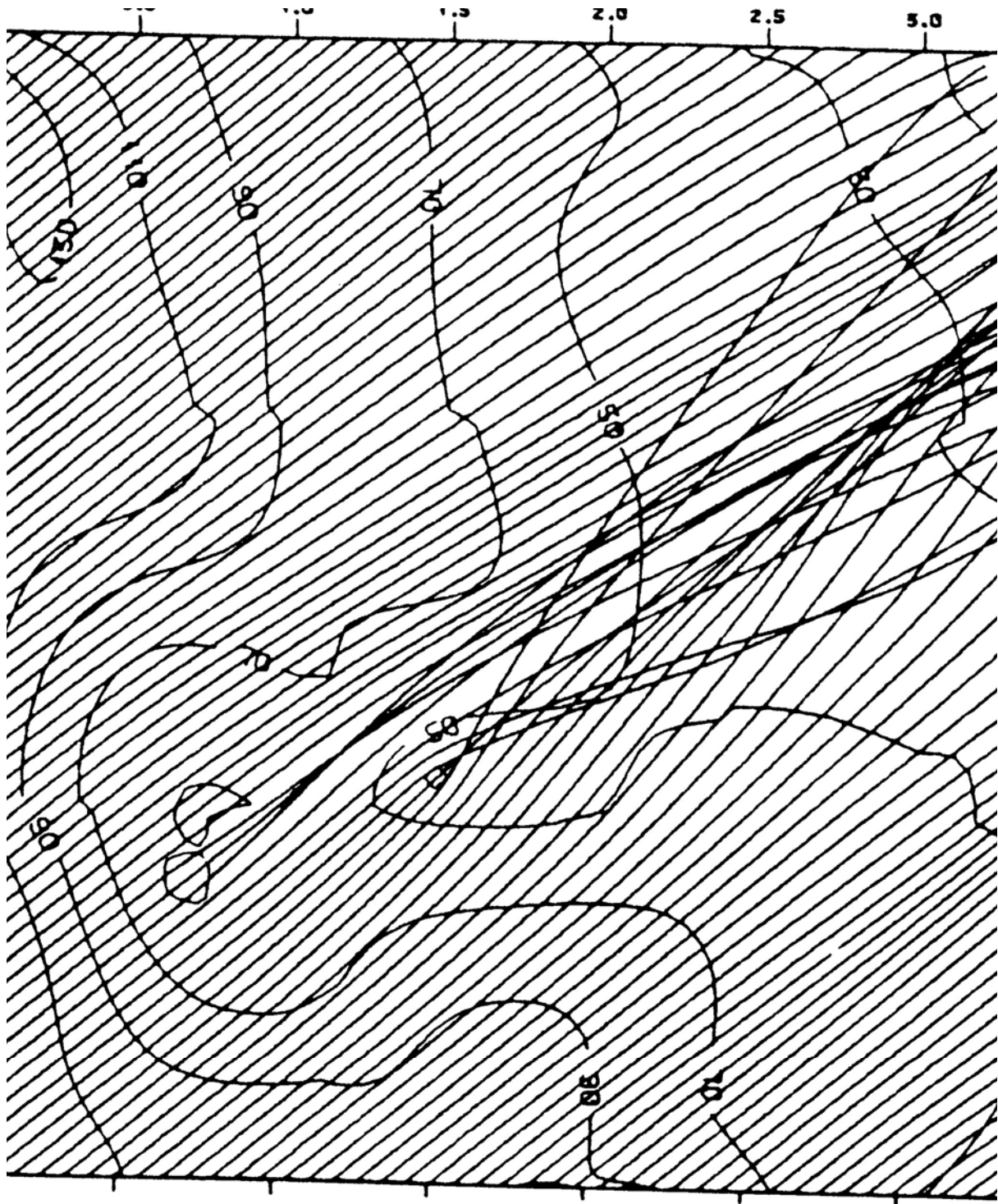


Fig. 7. Wave rays in severe weather conditions in the Area shown in Fig 6. A non-linear wave depth and wave current refraction takes place here. Depth contours are also shown.

Rogue waves and wave focusing – speculations on theory, numerical results and observations

Paul H Taylor

Department of Engineering Science
University of Oxford
Oxford OX1 3PJ U.K.
paul.taylor@eng.ox.ac.uk

This review will discuss recent work on the question of rogue waves on the open ocean. Observations of waves on the open sea are consistent with weakly non-linear modifications to a linear random process, at least most of the time even in violent storms¹. The occurrence of large waves might then be attributable to the random alignment of many small independent components. Extracted from a random background, this process would then look like the linear focusing of an initially dispersed wave group.

The focusing of uni-directional groups can produce dramatic extra surface elevation consistent with contraction of the group in the direction of motion. Simulations with the numerical scheme of Bateman² with significant directional spreading show that much of the extra elevation is lost. However, considerable elongation of the group structure along the wave crests can occur. 2-D and 1-D evolution is also different in that, although the non-linear dynamics occur over a much shorter period in 2-D and require steeper waves for much to happen, the spectral content well after focus in 2-D is markedly different to that before even in the absence of wave breaking. For this type of focusing event, simple models based on the nonlinear Schrodinger equation reveal the importance of the Benjamin-Feir index in 1-D and suggest that directional spreading should be incorporated into the index.

Recent work by Segur³ shows that the Benjamin-Feir instability is significantly affected by small amounts of dissipation. The review will end by pointing out that most work with phase resolved wave models neglects both energy input and dissipation. Does this invalidate our conclusions?

References

1. Taylor, P.H. & Williams B.A. Wave statistics for intermediate depth water – NewWaves and symmetry. *Journal of Offshore Mech. and Arctic Eng* 126, 54. (2004)
2. Bateman, W.J.D., Swan, C. & Taylor, P.H. On the efficient numerical simulation of directionally spread surface water waves. *Journal of Computational Physics*, 174, 277 (2001).
3. Segur, H. Stabilizing the Benjamin-Feir Instability. Talk at Workshop on Free Surface Water Waves, held at the Fields Institute, Toronto, June 2004

The role of resonant wave interactions in the evolution of extreme wave events

Richard Gibson & Chris Swan

Department of Civil and Environmental Engineering
Imperial College London
SW7 2AZ
United Kingdom
r.gibson@imperial.ac.uk, c.swan@imperial.ac.uk

Abstract. This paper is concerned with the formation of large waves in a realistic, directionally-spread, wave-field. In particular, the role of *resonant* interactions, capable of rapidly altering the underlying wave-spectrum, is ascertained. This is investigated through the use of a fully-nonlinear numerical wave-model and Zakharov's evolution-equation. The former allows the full-nonlinearity of the wave-field to be considered, whilst the latter enables the physical mechanisms responsible for the formation of the largest waves to be determined. The paper shows that in unidirectional sea-states the *resonant* interactions enable the formation of waves that are very much larger than would be predicted by a second-order *bound* wave solution. However, it is also shown that in broad-banded directionally-spread sea-states the effect of these interactions is linked to the phase relationship between the wave components; with significant spectral evolution only occurring when the wave components do not fully focus at one point in space and time. This suggests that the focussing of wave components is not a mechanism by which so-called *freak*, or *rogue*, waves can form in a broad-banded directional wave-field. However, large increases in crest elevation are obtained in a more narrow-banded directionally-spread sea-state, characterised by a Gaussian spectrum, and representative of swell wave conditions. The present results suggest that it is in these conditions that *freak* waves are most likely to occur.

1 Introduction

The water surface elevations arising in a realistic ocean environment are commonly modelled by the sum of wave components, of different frequency, travelling in different directions. The constructive interference, or focussing, of these components at one point in space and time results in a large wave-event that is often higher and steeper than linear, or second-order, *bound* wave theory would predict. This is the result of the rapid evolution of the wave spectrum due to *resonant* interactions. As a result, the coupling of linear dispersion with nonlinear *resonant* interactions offers a possible explanation for the formation of *freak*

or *rogue* waves in deep water. This paper is concerned with the evolution of realistic wave spectra. In particular, it is concerned with the relationship between the phasing of the wave components, the evolution of the wave spectrum and the resulting nonlinear crest elevation. This has been undertaken by applying two nonlinear wave-models: Bateman *et al.* (2001) and Zakharov (1968). This paper begins in §2 by describing the two wave-models. It continues in §3 by investigating the evolution of both unidirectional and directional sea-states. Concluding remarks can be found in §4.

2 Wave Models

Two wave-models have been applied in order to model, and understand, the evolution of realistic directionally spread sea-states. The first is the fully-nonlinear numerical wave-model of Bateman *et al.* (2001). The second is the evolution-equation of Zakharov (1968). Whilst the former solves the exact fully-nonlinear boundary conditions it gives very little direct indication as to the physical mechanisms that govern the evolution of a sea-state. In contrast, Zakharov (1968) enables the interactions at each order to be separated and the dominant physical processes to be determined.

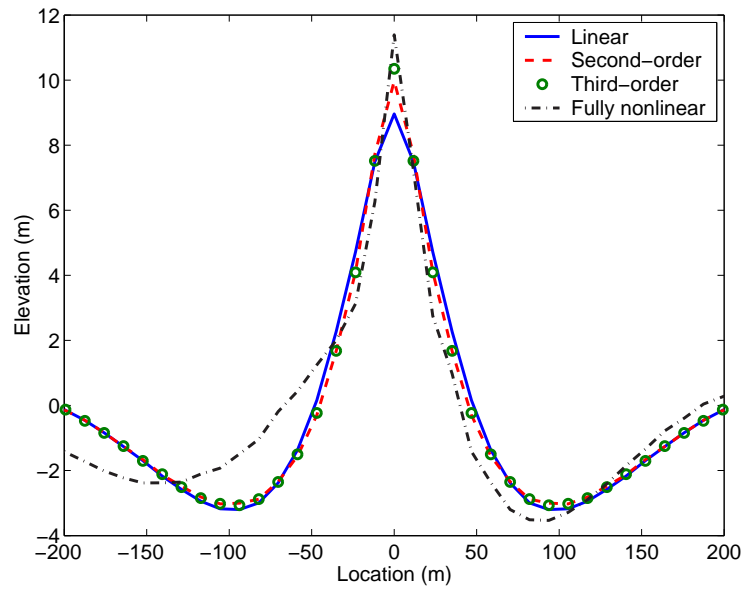
Bateman *et al.* (2001) is an extension to three-dimensions of the unidirectional wave-model of Craig & Sulem (1993). It is applied by time-marching the surface profile, $\eta(x, y)$, and the velocity potential on that surface, $\varphi(x, y)$, as first suggested by Zakharov (1968). At each time-step the horizontal derivatives of the surface, and of the velocity potential, can be rapidly calculated using fast Fourier transform techniques. However, the calculation of the vertical derivative requires the application of a Dirichlet-Neumann operator that transforms values of the potential on the surface into its vertical gradient. This is achieved by evaluating a high-order Taylor series. This last step is the reason for the efficiency of the Bateman *et al.* (2001) model; allowing realistic directional spectra, with a large range of frequencies, to be successfully modelled. In contrast, the wave-model of Johannessen & Swan (2003), itself an extension of the unidirectional wave-model of Fenton & Rienecker (1982), solved for the unknown coefficients using large matrix inversion. This is computationally intensive, leading to an inefficient model incapable of describing realistic directional spectra.

In contrast, Zakharov (1968) is an integro-differential equation that has been derived to fourth-order by Krasitskii (1994). At each order it is possible to isolate the *bound* and *resonant* interactions that occur, and hence, it is an excellent tool for understanding the physical mechanisms that govern the evolution of a wave-field. In this model the wave spectrum is time-marched according to which interactions are desired; making it possible to model the evolution of a wave-field including only the *bound* terms, only the *resonant* terms, or a mix of terms at different orders. This allows the dominant physical processes to be isolated. A detailed account of how it can be applied numerically is given by Annenkov & Shrira (2001), and a comparison with laboratory data is discussed in Shemer *et al.* (2001).

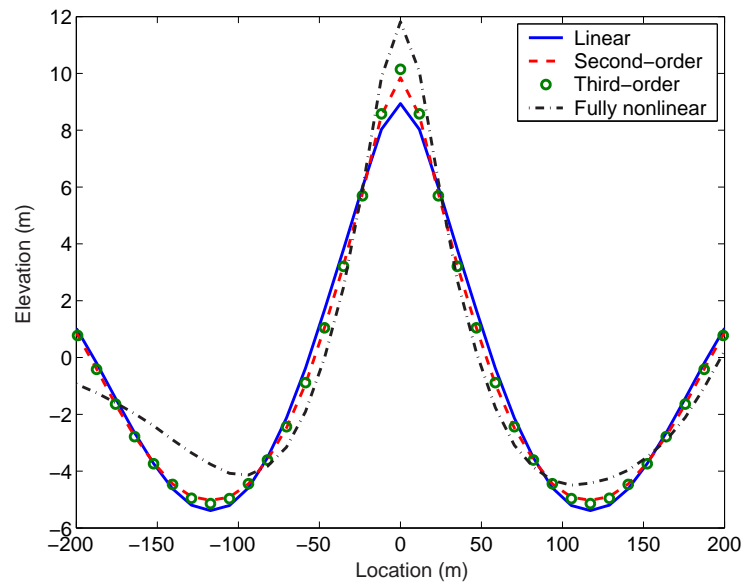
In order to investigate the evolution of large focussed wave-events the wave-models have been initiated with a specified wave spectrum at one point in time, $t = t_0$, when the sea-state is dispersed. The phasing of the wave components has been determined on the basis of the linear dispersion relationship such that a perfectly focussed wave-event will occur at $t = 0s$. The wave-models are then time-marched up to and beyond the largest crest elevation and the changes to the wave profile and the wave spectrum ascertained. In the Zakharov (1968) model the spectrum at each time-step is given in terms of the underlying linear wave components. In contrast, the Bateman *et al.* (2001) model gives the spectrum of the surface profile, which inevitably includes *bound* terms. However, it is possible to remove some of these *bound* terms by running the same cases so that a focussed wave trough occurs rather than a focussed wave crest. The trough focussed wave profile is then subtracted from the crest focussed profile and the Fourier transform of this result is a wave spectrum from which all the even-order (for example, second- and fourth-order) terms have been removed. However, odd-order terms are still present, and, although small, can potentially contaminate the results.

3 Results

The fully-nonlinear model of Bateman *et al.* (2001) has been used to model the evolution of two unidirectional sea-states; both of which are characterised by a JONSWAP spectrum of peak period $T_p = 12.8s$. However, the two spectra differ in their degree of broad-bandedness: the first has a peak enhancement factor $\gamma = 1$ (case J1D0) and the second a peak enhancement factor $\gamma = 5$ (case J5D0). Figure 1 shows that in both cases the fully-nonlinear wave profile of the extreme wave-event has a crest elevation much larger than that predicted by the solution of Zakharov (1968) that includes only the *bound* terms. Therefore, the formation of a large wave in a unidirectional sea-state cannot be modelled without taking into account the evolution of the wave spectrum. Figure 2 shows the rapid evolution of the freely propagating wave components of cases J1D0 and J5D0. In both sea-states this analysis shows that the underlying linear spectrum broadens considerably during the evolution of an extreme wave-event. This broadening is associated with an increase in the amplitude sum of the wave spectrum (Figure 3), and hence, the broadening is responsible for the large increases in maximum crest elevation. The physical mechanisms responsible for this evolution can be determined by applying Zakharov (1968). Indeed, figure 4 shows that an excellent agreement between the two models can be found by including only the third-order *resonant* terms. Furthermore, the evolution of these spectra is occurring much more rapidly than is predicted in random sea-states by Hasselmann (1962). The strong correlation between the phase of the wave components allows the third-order *resonant* interactions to broaden the wave spectrum over the time-scale of tens of wave periods rather than hundreds. Whilst this is true for unidirectional sea-states, in more realistic directionally spread wave-fields these conclusions need revising.

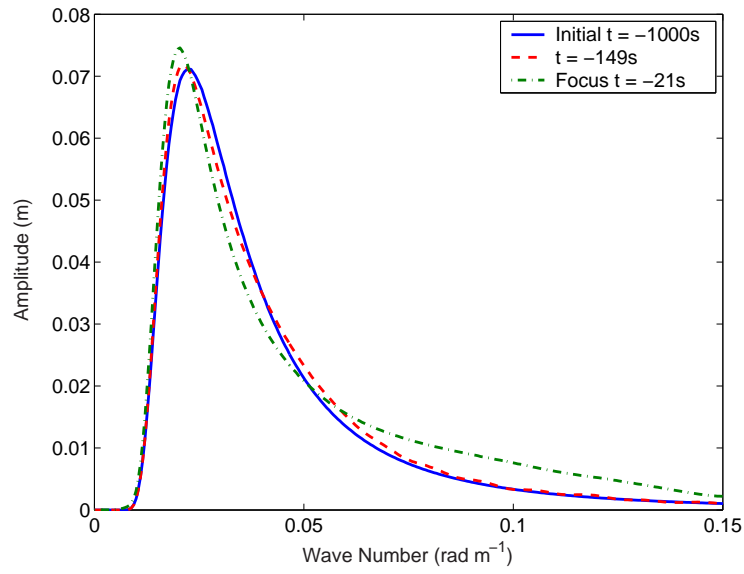


(a) J1D0

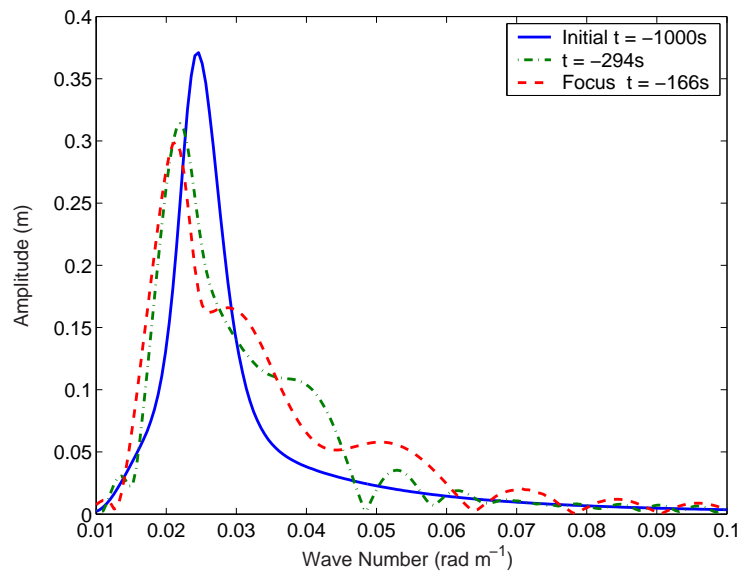


(b) J5D0

Fig. 1: Surface profile of extreme wave-events modelled using only the first-, second- and third-order *bound* terms of Zakharov (1968), and fully-nonlinearly using Bateman *et al.* (2001).



(a) J1D0



(b) J5D0

Fig. 2: The evolution of the underlying linear spectrum calculated using Bateman *et al.* (2001).

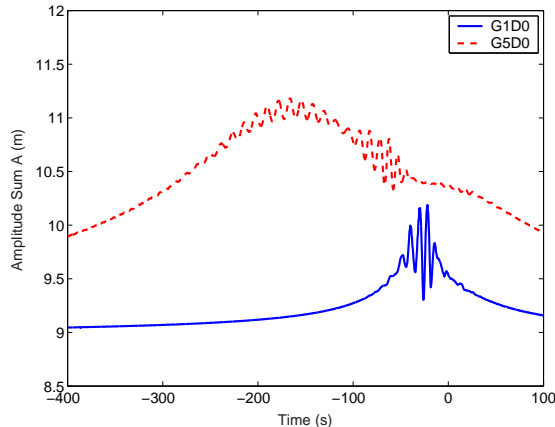
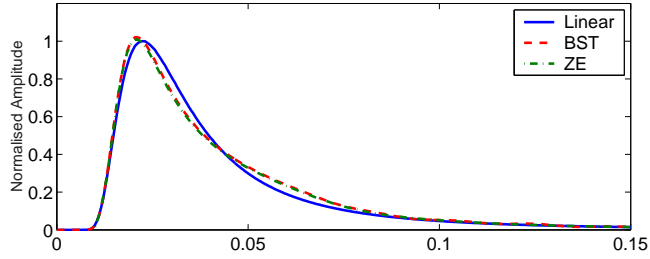


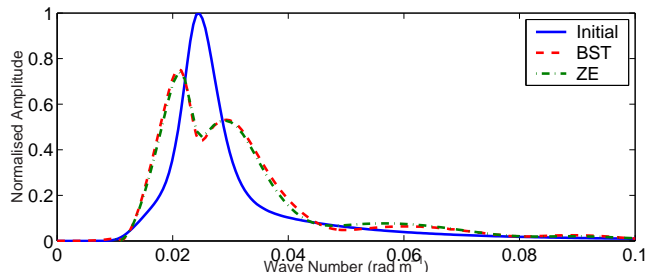
Fig. 3: The amplitude sum of the underlying linear spectrum. The high frequency oscillations represent third-order nonlinearities.

The fully-nonlinear model of Bateman *et al.* (2001) has also been used to model the evolution of two directional sea-states; both of which are characterised by a JONSWAP spectrum of peak period $T_p = 12.8s$ and peak-enhancement factor $\gamma = 5$. However, the two spectra differ in their degree of directional spreading: the first corresponds to a wrapped normal distribution with a standard deviation of $\sigma_\theta = 5^\circ$ (case J5D5), while the second has a standard deviation $\sigma_\theta = 30^\circ$ (case J5D30). Figure 5 shows that in both cases the crest elevation associated with the extreme wave profile is actually *lower* than that predicted by second-order theory. An analysis of the amplitude sum of the spectra (figure 6) indicates that the evolution of the amplitude spectra does not directly explain the reduction in crest elevation: in case J5D5 the amplitude sum increases from 9m to 11.6m; whilst, in case J5D30 it decreases from 9m to 8.7m. These changes to the amplitude sum are directly related to changes in the bandwidth of the two spectra, with a broadening of case J5D5 and a narrowing of J5D30. The actual changes to the spectral shape are considered in more detail in Gibson & Swan (2005). However, it is clear that there is a further factor to consider in determining the maximum crest elevation.

The maximum crest elevation associated with an extreme wave-event at any point in time, t_e , is the product of four inter-related factors. The first is the amplitude sum of the underlying linear wave spectrum at the initial time, $A_0 = A|_{t=t_0} = \sum_i^N a_i|_{t=t_0}$, where a_i are the amplitudes of the wave components. The second is the change to this amplitude sum due to *resonant* interactions ΔA . The third is the nonlinear correction due to *bound* interactions. Finally, the fourth is the phase relationship between the wave components. These factors are not independent; for example, the *bound* correction depends upon the amplitude sum of the wave components and their phasing. Despite this, it can be informative to investigate these factors in terms of a number of ratios:



(a) J1D0



(b) J5D0

Fig. 4: Comparison between the evolution of the underlying linear spectrum calculated using Bateman *et al.* (2001) with that calculated using Zakharov (1968). All the results are from $t = -100s$.

$$\begin{aligned}
 \eta_{actual} &= FA|_{t_0} = F_0 F_1 F_2 A|_{t_0}, \text{ where,} & (1) \\
 F_0 &= (\Delta A + A_0)/A_0, \\
 F_1 &= \eta_{bound}/(\Delta A + A_0), \\
 F_2 &= \eta_{actual}/\eta_{bound},
 \end{aligned}$$

and η_{bound} defines the crest elevation, including the effect of *bound* interactions, if a perfectly focussed wave-event occurred, and η_{actual} is the actual crest elevation. Taking each in turn: F_0 is the increase in the amplitude sum of the underlying linear wave components; F_1 is the increase in the crest elevation due to *bound* interactions, if the wave components are perfectly focussed; and F_2 defines the focal quality of the event.

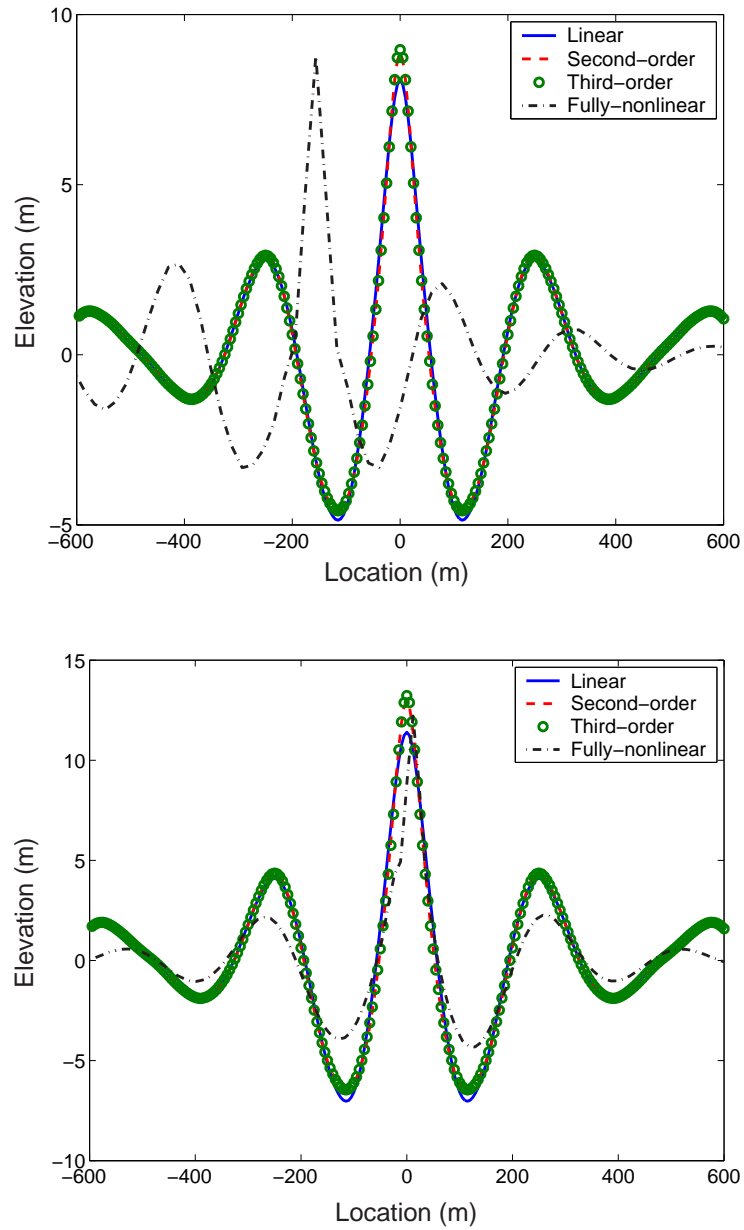


Fig. 5: Surface profile of extreme wave-events modelled using only the first-, second- and third-order *bound* terms of Zakharov (1968), and fully-nonlinearly using Bateman *et al.* (2001).

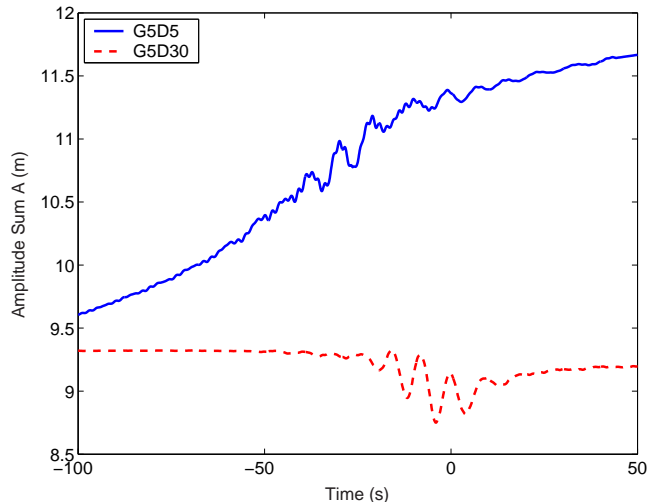


Fig.6: The amplitude sum of the underlying linear spectrum. The high-frequency oscillations represent third-order nonlinearities, and hence, represent rapid changes to the steepness of the wave profile and should be ignored.

For example, if linear theory is considered then $F_0 = F_1 = F_2 = 1.0$ as there is no change to the amplitude sum of the spectrum, there are no *bound* interactions and the wave-event focusses perfectly. However, if second-order theory is considered then $F_0 = F_2 = 1.0$ as again there is no change to the amplitude sum, nor to the phasing; and, $F_1 = 1.12$ as the second-order *bound* interactions increase the crest elevation by 12% in case J5D0. Figure 7 shows the change in these factors as the initial amplitude sum of a unidirectional sea-state is increased. In all of the cases the initial phasing has been determined on the basis of the linear dispersion relationship and the *resonant* interactions have altered this phasing so that the event does not focus perfectly. However, the reduction in focal quality, F_2 , is more than compensated by the increase in the amplitude sum of the wave spectrum, F_0 .

In contrast, in directional sea-states, the focal quality is inversely correlated with increases in the amplitude sum of the spectrum, so that if $F_0 > 1$, $F_2 < 1$ (figure 8). Hence, the two balance and, for all but the most long-crested sea-states, the final crest elevation is less than that predicted by second-order theory. This highlights the fact that the result of the *resonant* interactions is critically dependent upon the phase relationship between the wave components: if the event focusses perfectly then the spectrum narrows and the amplitude sum of the underlying linear wave components reduces; however, if the event is imperfectly focussed then the spectrum can broaden, the amplitude sum increase, but the resulting crest elevation is limited by its poor focal quality. Therefore, in broad-banded directionally-spread sea-states it is not possible to obtain the large increases in crest elevation observed in similar unidirectional sea-states.

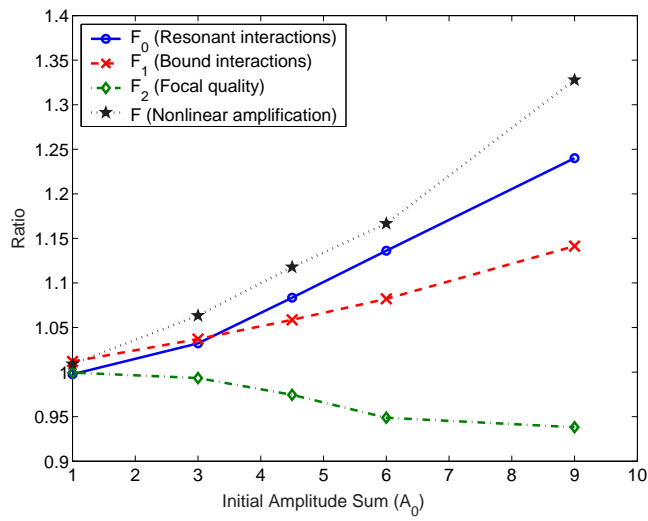


Fig. 7: The factors that effect the crest elevation of an extreme wave-event in a unidirectional sea-state.

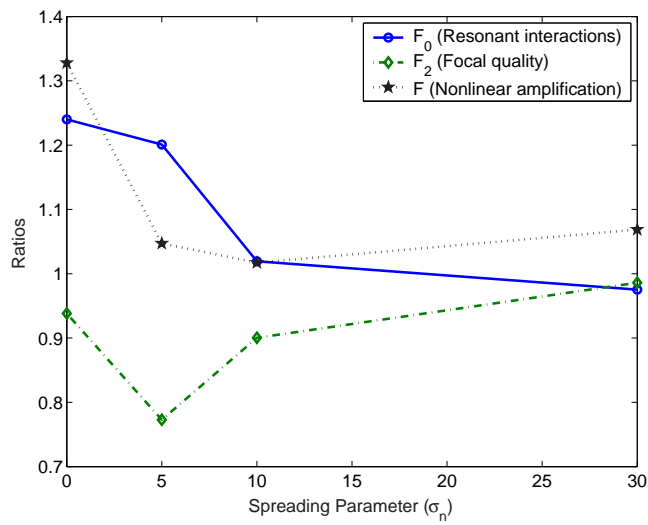


Fig. 8: The factors that effect the crest elevation of an extreme wave-event in a multi-directional sea-state characterised by a JONSWAP spectrum with a peak-enhancement factor $\gamma = 5.0$.

However, whilst it is not possible to obtain large increases in crest elevation if the spectrum is broad-banded, it is possible in more narrow-banded sea-states. Bateman *et al.* (2001) has been used to model the evolution of a Gaussian sea-state with a small directional spread of $\sigma_n = 5^\circ$, characteristic of swell waves. In this case the sea-state disperses slowly, and the balance between changes to the spectral bandwidth due to *resonant* interactions and the focal quality of the extreme-event is balanced towards the former. Figure 9 shows that the maximum crest elevation is much larger than that predicted by a *bound* wave solution. It therefore follows that, swell-dominated sea-states are perhaps those in which *rogue* waves are intrinsically more likely to occur.

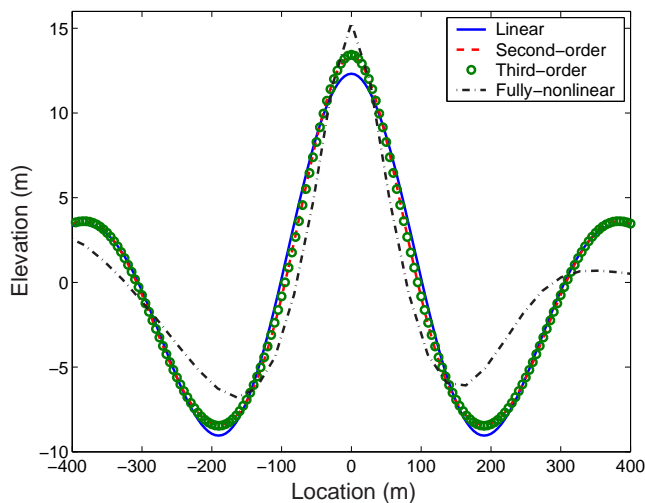


Fig. 9: Surface profile of an extreme wave-event in a swell-dominated sea-state, characterised by a Gaussian spectrum with a spreading parameter $\sigma_n = 5^\circ$.

4 Concluding Remarks

The fully-nonlinear evolution of both unidirectional and directional sea-states has been investigated. It has been shown that in the former third-order *resonant* interactions lead to the rapid evolution of the wave spectrum, and to an increase in the crest elevation of an extreme wave-event. Whereas, in the latter the extreme crest-elevation is less than that predicted by second-order theory. This reduction is due to the balance between the phasing of the wave components and the spectral changes that occur during the formation of a large event. This suggests that the focussing of wave components is not a possible mechanism by which *rogue* waves can form in broad-banded sea-states. However, in more narrow-banded Gaussian spectra, characteristic of swell-dominated sea-states,

large waves are slow to disperse. Hence, the balance is now in favour of the *resonant* interactions and large increases in crest elevation can be obtained.

Acknowledgement

The early stages of this work were undertaken within the project 'Reliability Based Structural Design of FPSO Systems', which involves Shell International, Instituto Superior Tcnico, DHI, Det Norske Veritas, Imperial College, Noble Denton and Oxford University. The project is partially funded by the European Union through the Energy Programme under contract ENK6-2000-00107. The later stages of the work were completed with support from the UK Engineering and Physical Sciences Research Council under grant number GR/R64971.

Bibliography

- ANNENKOV, S. & SHRIRA, V. 2001 Numerical modelling of water-wave evolution based upon the zakharov equation. *Journal of Fluid Mechanics* **449**, 341–371.
- BATEMAN, W. J. D., SWAN, C. & TAYLOR, P. H. 2001 On the efficient numerical simulation of directionally-spread surface water waves. *Journal of Computational Physics* **174**, 277–305.
- CRAIG, W. & SULEM, C. 1993 Numerical simulation of gravity waves. *Journal of Computational Physics* **108**, 73–83.
- FENTON, J. D. & RIENECKER, M. M. 1982 A fourier method for solving nonlinear water-wave problems: application to solitary-wave interactions. *Journal of Fluid Mechanics* **118**, 411–443.
- GIBSON, R. S. & SWAN, C. 2005 The evolution of large ocean waves: the role of local and rapid spectral changes.. *Submitted to the Royal Society* .
- HASSELMANN, K. 1962 On the nonlinear energy transfer in a gravity wave system. Part 1. *Journal of Fluid Mechanics* **12**, 481–500.
- JOHANNESSEN, T. B. & SWAN, C. 2003 On the nonlinear dynamics of focused wave groups in two and three dimensions. *Proc. Roy. Soc. Lond. A* **459**, 1021–1052.
- KRASITSKII, V. P. 1994 On reduced equations in the hamiltonian theory of weakly nonlinear surface waves. *Journal of Fluid Mechanics* **272**, 1–20.
- SHEMER, L., JIAO, H., KIT, E. & AGNON, Y. 2001 Evolution of a nonlinear wave field along a tank: experiments and numerical simulations based upon the spatial zakharov equation. *Journal of Fluid Mechanics* **427**, 107–129.
- ZAKHAROV, V. E. 1968 Stability of periodic waves of finite amplitude on the surface of a deep fluid. *Journal of Applied Mechanics and Technical Physics* **9**, 190–194, english Translation.

Experimental study of the wind effect on the focusing of transient wave groups

J.P. Giovanangeli¹⁾, C. Kharif¹⁾ and E. Pelinovsky^{1,2)}

¹⁾Institut de Recherche sur les Phénomènes Hors Equilibre, Laboratoire IRPHE/IOA, Marseille, France. Email: giovanangeli@irphe.univ-mrs.fr

²⁾Laboratory of Hydrophysics and Nonlinear Acoustics, Institute of Applied Physics, Nizhny Novgorod, Russia. Email: Pelinovsky@hydro.appl.sci-nnov.ru

One of the popular mechanisms of the freak waves phenomenon is the dispersive focusing of transient wave groups. In all published theoretical and experimental papers the surface gravity waves are considered as an ensemble of free waves. This paper reports on a series of experiments conducted in the large wind-wave tank of IRPHE (Marseille – Luminy) to study the wind effect on the generation of freak waves. A suitable theory is presented to explain and discuss the experimental results.

1. Introduction

Freak wave phenomenon is now explained by many physical theories: dispersive and geometrical focusing, nonlinear modulational instability (Benjamin – Feir instability), wave-current and wave-bottom interactions; see, for instance (Olagnon and Athanassoulis, 2001; Rogue Waves, 2003; Kharif and Pelinovsky, 2003). In all published theoretical and experimental papers the gravity waves on sea surface are assumed to be an ensemble of free waves. In early stages the wind flow is considered as the source of the spatial and temporal inhomogeneity of the wind wave field or as the factor of wave amplification. The present paper reports on a series of experiments with transient wave groups under wind action up to 10 m/s conducted in the large wind-wave tank of IRPHE (Marseille – Luminy). Theoretical model to explain the experimental results is developed. It includes the sub-surface current induced by wind. The theoretical predictions are in good agreement with experimental results.

2. Set-up and experimental conditions

The experiments have been conducted in the large wind-wave tank of IRPHE at Marseille - Luminy (Figure 1). It is constituted of a closed loop wind tunnel located over a water tank 40m long, 1 m deep and 2.6 m wide. The wind tunnel over the water flow is 40 m long, 3.2 m wide and 1.6 m high. The blower allows to produce wind speeds up to 14 m/s and a computer-controlled wave maker submerged under the upstream beach can generate regular or random

waves in a frequency range from 0.5 Hz to 2 Hz. Particular attention has been taken to simulate pure logarithmic mean wind profile with constant shear layer over the water surface. A trolley installed in the test section allows to locate probes at different fetches all along the facility. The water surface displacements were determined by using three capacitive wave gauges of 0.3 mm outer diameter with DANTEC model 55E capacitance measuring units. Two wave gauges were located at fixed fetches of 1 m and 3 m from the upstream beach. A third wave gauge was installed on the trolley in order to determine the water surface deflections η at various distances from the upstream beach. The typical sensitivity of the wave probes was of order of 0.6 V/cm.

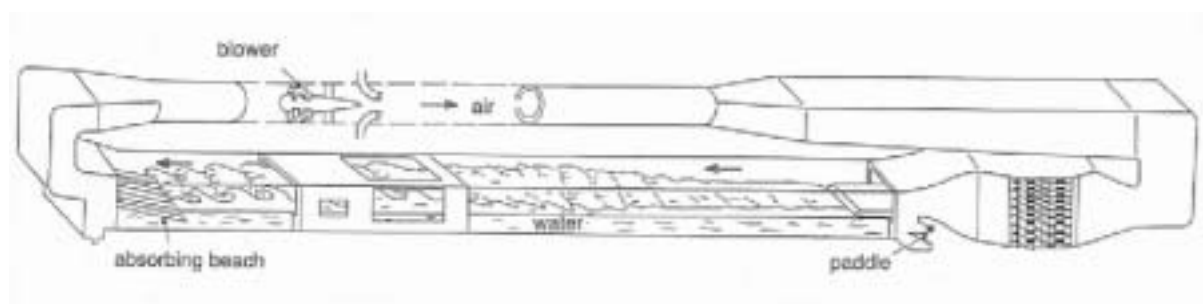


Figure 1: A schematic representation of the Large Air-Sea Interactions Facility.

For each value of the mean wind speed, W equals to 0, 4, 5, 6, 8 and 10 m/s, the water surface deflections η was measured at 1 m fetch and at different fetches between 5m and 35 m. The wave maker was driven by an analog electronic signal varying linearly with time from 1.3 Hz to 0.8 Hz in 10 seconds with constant amplitude of displacements corresponding to nearly constant amplitude of the initial wave group. The fetch values are taken from the entrance of the wave-tank, where the airflow meets the water surface i.e. at the end of the upstream beach. Typical value of σ equal to the rms of the water deflections η determined at the distance 1 m for different wind speeds is 1.87-1.88 cm.

3. Experimental Results

Figure 2 demonstrates the focusing of the free transient wave groups when there is no wind flow above waves. Initial wave packet has the step-wise amplitude modulation and linearly frequency modulation. As predicted by the linear theory of the free deep-water waves, the waves focused at a precise distance, leading to the occurrence of a high amplitude freak wave. Downstream of the point of focusing, the amplitude of the group decreases rapidly (defocusing). The influence of the wind flow with speed 6 m/s on the wave focusing process is shown in Figure 3. The characteristics (frequencies and amplitude) of the initial mechanically generated waves are kept the same. As it can be seen, the scales of spatial -

temporal evolution of the group are changed with wind. For each value of the wind speed, the amplification ratio $A(X,W)$ can be defined as $A = \eta_{max}/\sigma$, where η_{max} is the maximum amplitude of the wave packet on fixed distance. Figure 4 gives the amplification ratio as a function of the distance from the upstream probe located at 1 m fetch and for different values of the wind speed. This figure shows that in presence of wind, we observed a freak wave of a larger amplitude, occurring at a longer distance than observed without wind. Moreover, contrarily to the case without wind, the freak waves maintains its coherency and its amplitude as it propagates downstream the previous focusing point. The effects of wind on the location of the focusing point, on the amplitude and the coherency of the freak wave increases as the wind velocity increases.

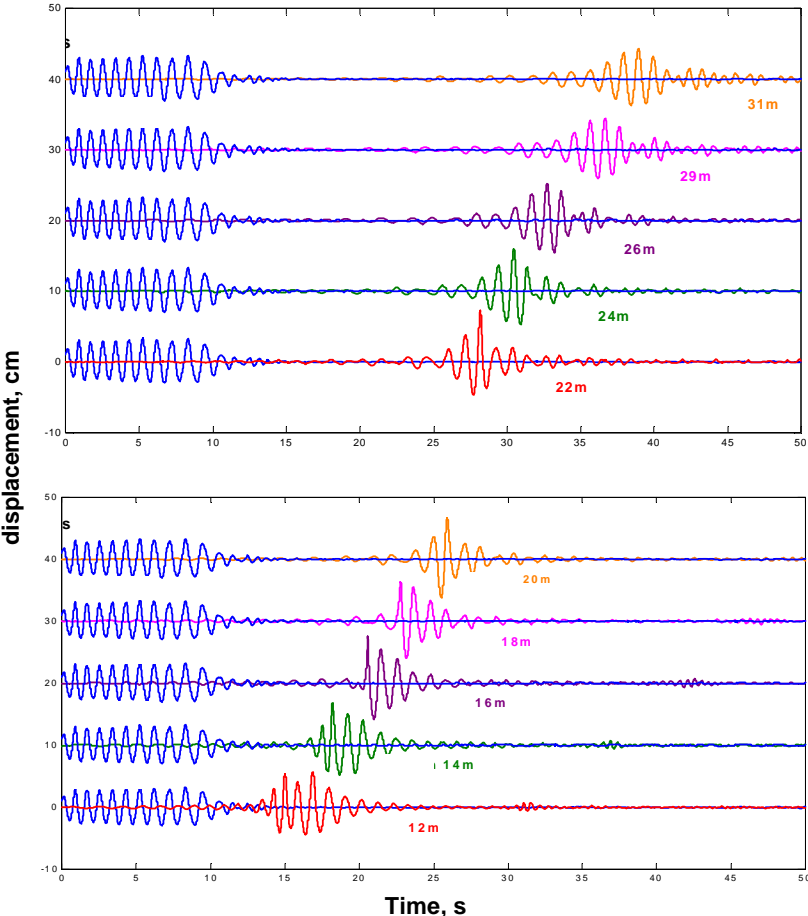


Figure 2: Time series of the water surface displacement, η on various distances from the wave paddle (no wind); initial packet is shown on the left

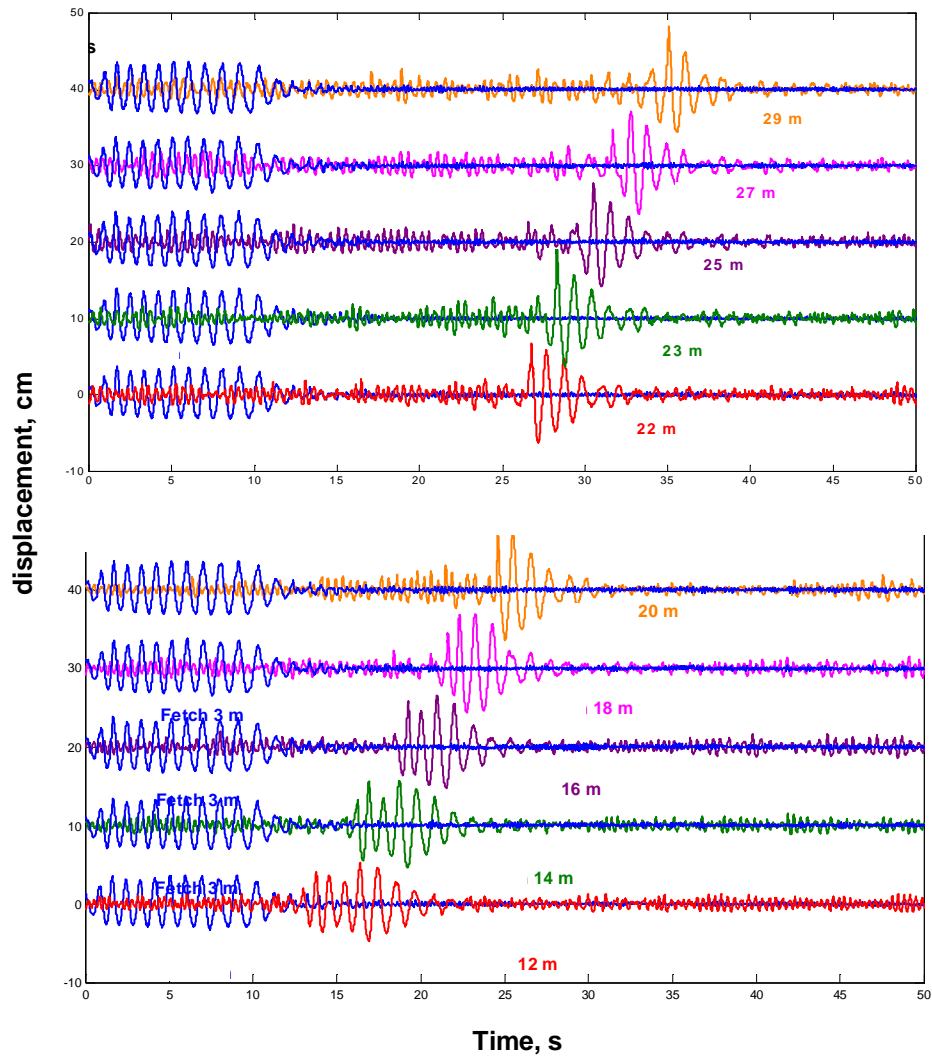


Figure 3: Time series of the water surface displacement, η on various distances from the wave paddle, wind speed 6 m/s; initial packet is shown on the left

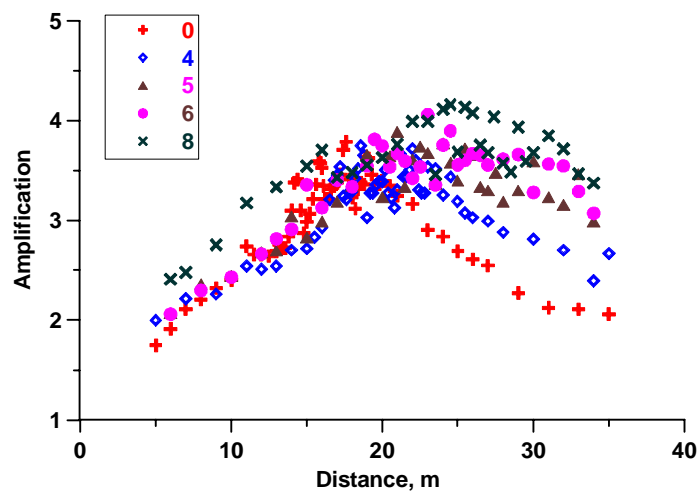


Figure 4: Amplification ratio versus the distance from the wave paddle for various wind speed

Results of the wavelet analysis of time series of the surface elevation at 3 m and 25 m for wind speed 8 m/s are presented in Figure 5. These figures show the time frequency evolution of the group as it propagates downstream along the wave tank. As it can be seen, the wind generated ripples have other frequencies than the transient group.

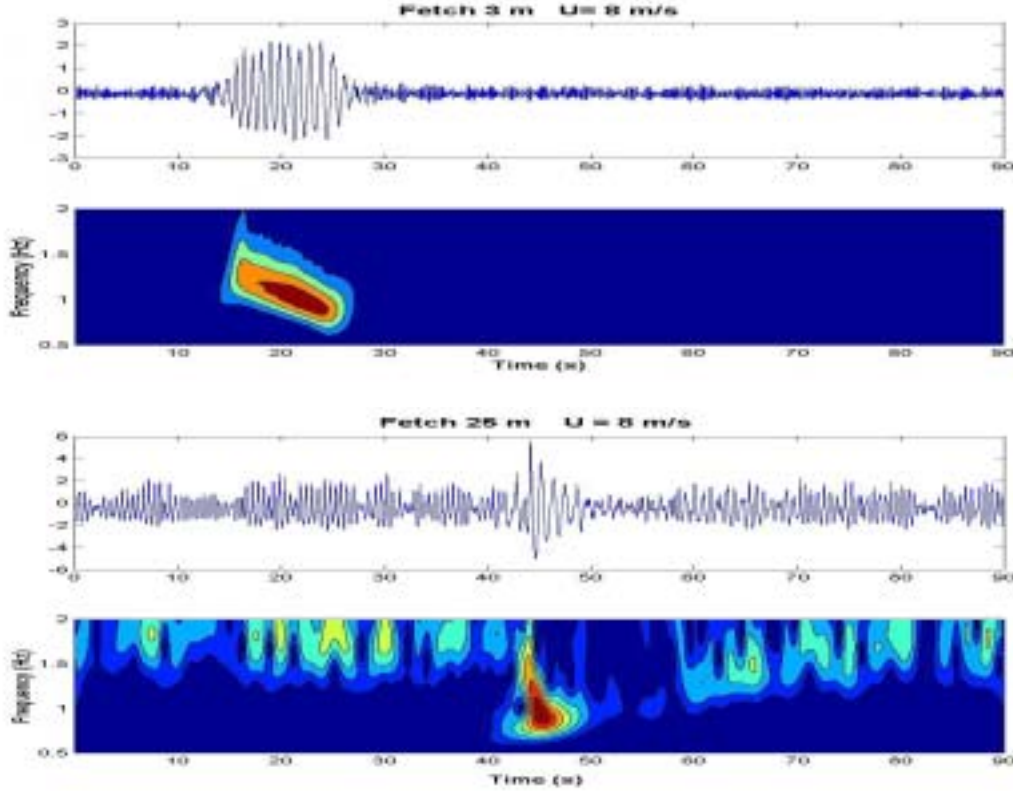


Figure 5: Wavelet analysis of the time records for wind speed 6 m/s

Clearly Figure 5 shows the wind waves are damped by the freak wave. This result is of the first importance for remote sensing.

4. Focusing of narrow-banded wave groups

The dynamics of narrow-banded linear wave packets can be described by the parabolic equation for wave amplitude

$$i \left(\frac{\partial A}{\partial t} + c_{gr} \frac{\partial A}{\partial x} \right) = \frac{\omega_0}{8k_0^2} \frac{\partial^2 A}{\partial x^2}, \quad (1)$$

where k_0 and ω_0 are the wave number and frequency of the carrier wave, $c_{gr} = d\omega/dk$ is the group velocity. The wave amplitude, A , is a slowly varying function of x and t .

Let us consider first the wave transformation of the wave packets with no wind. Transforming the variables into dimensionless form

$$\tau = \omega_0(t - x/c_{gr}), \quad y = k_0x, \quad a = k_0A, \quad (2)$$

equation (1) can be re-written as spatial parabolic equation

$$i \frac{\partial a}{\partial y} = \frac{\partial^2 a}{\partial \tau^2}, \quad (3)$$

which should be completed by the boundary condition on the paddle

$$a(\tau, y=0) = f(\tau). \quad (4)$$

Equation (1) or (3) are widely used to demonstrate the effect of the wave focusing of the linear transient groups (Clauss and Bergmann, 1986; Pelinovsky & Kharif, 2000; Brown & Jansen, 2001). In particular, if the boundary condition (4) corresponds to the packet with amplitude modulation of gaussian shape

$$a(\tau, 0) = A_0 \exp(-\Omega_0^2 \tau^2), \quad (5)$$

in the process of the wave evolution its complex envelope is described by

$$a(\tau, y) = \frac{A_0}{\sqrt{1 - 4i\Omega_0^2 y}} \exp\left(-\frac{\Omega_0^2 \tau^2}{1 - 4i\Omega_0^2 y}\right), \quad (6)$$

and, as a result, the wave has a variable amplitude and phase (frequency) modulation. The variation of the amplitude of the wave packet is

$$|a(\tau, y)| = \frac{A_0}{[1 + 16\Omega_0^4 y^2]^{1/4}} \exp\left(-\frac{\Omega_0^2 \tau^2}{1 + 16\Omega_0^4 y^2}\right). \quad (7)$$

At each point the amplitude modulation presents a gaussian profile in time, and its peak value decreases on large distance as $y^{-1/2}$

$$|a|_{\max} = \frac{A_0}{[1 + 16\Omega_0^4 y^2]^{1/4}}. \quad (8)$$

The characteristic width of the amplitude modulation is

$$T(y) = \frac{\sqrt{1 + 16\Omega_0^4 y^2}}{\Omega_0} \quad (9)$$

and it increases on large distances as y . The imaginary part of the complex amplitude gives the phase correction variable in time and space

$$\arg[a(\tau, y)] = \frac{\text{atan}(4\Omega_0^2 y)}{2} - \frac{4\Omega_0^4 \tau^2 y}{1 + 16\Omega_0^4 y^2}. \quad (10)$$

At each point the frequency correction is

$$\Omega(\tau, y) = \frac{\partial \arg(a)}{\partial \tau} = -\frac{8\Omega_0^4 \tau y}{1 + 16\Omega_0^4 y^2}. \quad (11)$$

It corresponds to the linear variation of the frequency with time in the wave packet. Adding the carrier frequency, it means that the wave packet has low frequency oscillations on the front because they have large values of speed propagation (usual action of the frequency dispersion).

If this wave packet is inverted in space ($y \rightarrow -y$), it will represent a wave packet with high frequency waves on the front, which propagate slowly. Let the paddle generate such a wave packet, it means that the boundary condition (4) for complex amplitude, $a(\tau, 0)$ is

$$a(\tau, 0) = A_{in} \exp[-\Omega_{in}^2 \tau^2 + iq\Omega_{in}^2 \tau^2] \quad (12)$$

with three independent parameters: peak value, A_{in} , characteristic spectral width, Ω_{in} , and phase index, q ; formally these parameters can be obtained from (7) and (11) using $y = -L$. It means that the amplitude modulation in the process of the wave evolution from the paddle will describe by

$$|a(\tau, y)| = A_{in} \left[\frac{1 + q^2}{1 + q^2(y/L - 1)^2} \right]^{1/4} \exp\left(-\Omega_{in}^2 \tau^2 \frac{1 + q^2}{1 + q^2(y/L - 1)^2}\right), \quad (13)$$

where the focus distance is

$$L = \frac{q}{4\Omega_{in}^2(1 + q^2)}. \quad (14)$$

At the focal point, $y = L$ the complex envelope has the real part only of the gaussian profile and it will correspond to the amplitude modulated pulse

$$a(\tau, L) = A_f \exp(-\Omega_f^2 \tau^2), \quad A_f = A_{in} [1 + q^2]^{1/4}, \quad \Omega_f = \Omega_{in} [1 + q^2]^{1/2}. \quad (15)$$

The solution given above describes the evolution of a free transient group with the formation of a freak wave. Results of the comparison with experimental data are presented in Figure 6. We used the following parameters: $A_f = 3.8$ m, $f_0 = 1$ Hz and $\Omega_0 = 0.062$. In the case of no wind the agreement between theoretical and numerical results is quite good.

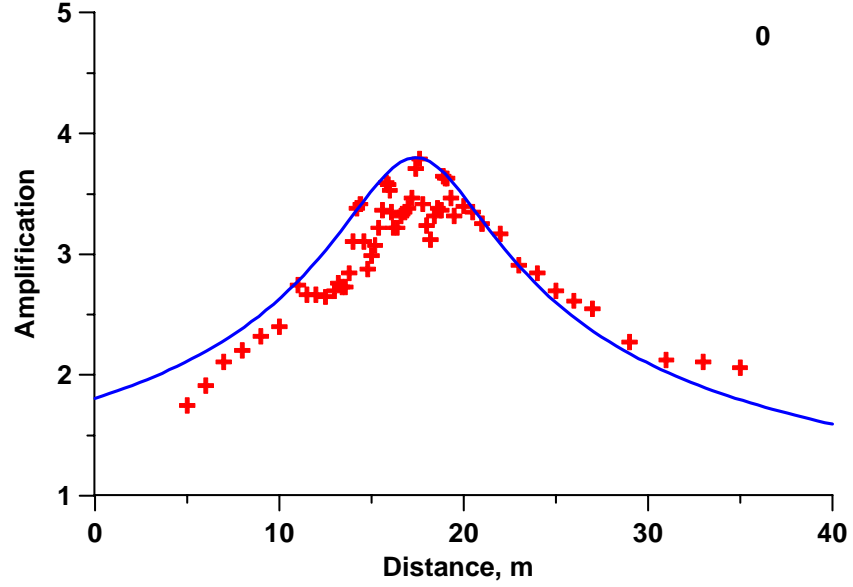


Figure 6: Comparison between experimental points and solution of the parabolic equation

The next step is to include the wind effect. The wind leads to the wind increment and also the induced flow. As it is known, the linear part of the any evolution equation is the inverse Fourier transformation of the linear dispersion relation. The induced flow modifies the dispersion relation which can be written as follows

$$k = \frac{g}{4u^2} \left[\sqrt{1 + \frac{4u\omega}{g}} - 1 \right]^2. \quad (166)$$

Then, the wave number should be developed by using Taylor series in the vicinity of the carrier frequency, ω_0

$$k = k_0 + \frac{dk}{d\omega} \Big|_{\omega_0} (\omega - \omega_0) + \frac{1}{2} \frac{d^2k}{d\omega^2} \Big|_{\omega_0} (\omega - \omega_0)^2 + \dots, \quad (17)$$

where k_0 and ω_0 satisfy the dispersion relation (16), and two important coefficients in (17) equal to

$$\left. \frac{dk}{d\omega} \right|_{\omega_0} = \frac{1}{u} \left[1 - \frac{1}{\sqrt{1 + \frac{4u\omega_0}{g}}} \right], \quad \left. \frac{d^2k}{d\omega^2} \right|_{\omega_0} = \frac{2}{g} \left(1 + \frac{4u\omega_0}{g} \right)^{-3/2} \quad (18)$$

When the flow is absent, these coefficients transform into known formulas

$$\left. \frac{dk}{d\omega} \right|_{\omega_0} = \frac{2\omega_0}{g}, \quad \left. \frac{d^2k}{d\omega^2} \right|_{\omega_0} = \frac{2}{g}, \quad (19)$$

which are the inverse group velocity and inverse dispersion parameter. The evolution equation can be easily obtained from (17) considering $i(k - k_0)$ and $-i(\omega - \omega_0)$ as the differential operators $\partial/\partial x$ and $\partial/\partial t$ (in fact, coordinate and time are slow variables of the wave envelope)

$$i \frac{\partial A}{\partial x} = \frac{1}{2} \left. \frac{d^2k}{d\omega^2} \right|_{\omega_0} \frac{\partial^2 A}{\partial \tau^2}, \quad (20)$$

where $\tau = t - x/c_{gr}$. Equation (20) reduces to (3) when the current vanishes. The wind increment can be introduced by adding a linear term

$$i \frac{\partial A}{\partial x} = \frac{1}{2} \left. \frac{d^2k}{d\omega^2} \right|_{\omega_0} \frac{\partial^2 A}{\partial \tau^2} + isA. \quad (21)$$

This latter term responsible of the wind generation can be eliminated by

$$A(\tau, x) = B(\tau, x) \exp(sx), \quad (22)$$

and finally we obtain again a parabolic equation

$$i \frac{\partial B}{\partial x} = \frac{1}{2} \left. \frac{d^2k}{d\omega^2} \right|_{\omega_0} \frac{\partial^2 B}{\partial \tau^2}. \quad (23)$$

Equation (23) was investigated earlier and we may use the previous gaussian solution (by replacing the coefficients) to study the wind effect. First of all, some conclusions can be done before any procedures. As it is evident, the wind increment modifies the wave amplitude providing additional growth of the wave field, but really this effect is not important; see Figure 5. The second one is that the group velocity ($d\omega/dk$) increases with the current and, therefore, the focal point will be shifted on large distance from the paddle. The third one is

that the dispersion parameter ($d^2k/d\omega^2$) decreases with the current and, therefore, the wave amplitude will change more slowly with distance. All these conclusions correspond to the experimental data and may be illustrated by the gaussian solution again. If the wave envelope in the focal point is the gaussian pulse

$$a(\tau,0) = A_0 \exp(-\Omega^2 \tau^2) \quad (24)$$

(now we use dimensional variables), the maximal amplitude will vary with distance as

$$|a|_{\max} = \frac{A_0}{[1 + 4(d^2k/d\omega^2)^2 \Omega^4 (x-L)^2]^{1/4}}. \quad (25)$$

Figure 7 shows the comparison with observed data for wind speed value 4 m/s. Here we used experimental values for envelope in the focal point: $A_0 = 3.8$ m, $\Omega = 0.98$ Hz. The comparison is quite good.

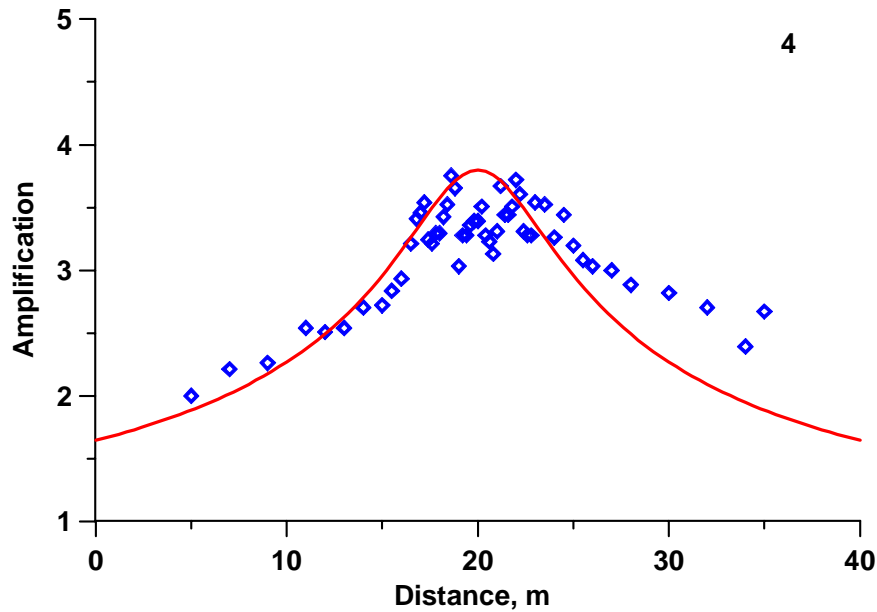


Figure 7: Comparison between predictions of linear parabolic equation and experimental data for wind speed 4 m/s

However, in presence of wind, the assymetry observed on the curve is not found by the model. Reul et al , 1999 have shown that over a steep wave, air flow separation process can occur inducing large local enhancement of the momentum flux from wind to the wave. We therefore could suggest that this process could occur in the same manner over the rogue wave at and downstream the focusing point. This could maintain the freak as it propagates after the focusing point.

5. Conclusion

The focusing of the transient wave groups under a wind flow action has been investigated experimentally and theoretically. It is shown that focal distance is increased as well as the maximum wave amplitude in this point. This effect is explained by the kinematic (Doppler) effect in the dispersion relation in the framework of the parabolic equation.

This research is supported by CNRS and for EP by FRBR (05-05-64265) and INTAS (03-514286).

References

- Brown M.G., Jensen A.** Experiments on focusing unidirectional water waves. *J. Geophys. Research*, 2001, vol. 106, N. C8, 16917 – 16928.
- Clauss G., Bergmann J.** Gaussian wave packets: a new approach to seakeeping tests of ocean structures. *Applied Ocean Research*, 1986, vol. 8, 190-206.
- Kharif C., Pelinovsky E.** Physical mechanisms of the rogue wave phenomenon. *European Journal Mechanics / B – Fluid*, 2003, **22**, 603-634.
- Olagnon M., Athanassoulis G.A.** (Eds.), *Rogue Waves 2000*. France: Ifremer, 2001.
- Pelinovsky E., Talipova T., Kharif, C.** Nonlinear dispersive mechanism of the freak wave formation in shallow water. *Physica D*, 2000, vol. 147, N. 1-2, 83-94.
- Rogue Waves: Forecast and Impact on Marine Structures.** GKSS Research Center, Geesthacht, Germany, 2003.
- Reul N., H. Branger and Giovanangeli J.P.** Air flow separation over unsteady breaking waves. *Physics of Fluids*, 1999, Vol 11, N.7, 1959-1961

A rapid fully nonlinear method in three dimensions with simulations of steep wave event.

D. Fructus and J. Grue

Mechanics Divison, Department of Mathematics, University of Oslo, Norway

Introduction

An efficient numerical scheme for simulations of fully nonlinear non-breaking surface water waves is presented. The water depth is either finite or infinite and the bottom is allowed to be varying in time and space. The method is based on a fast, rapidly converging, iterative algorithm to compute the Dirichlet to Neumann operator. This is evaluated by expanding the operator as a sum of global convolution terms and local integrals with kernels that decay quickly in space. The global terms are computed very quickly via FFT. The local terms are evaluated by numerical integration. Analytical integration of the linear part of the prognostic equations is combined with a special step size control technique. This yields a very stable and accurate time marching procedure. Zeros-padding in the spectral space represents the anti-aliasing strategy. The method requires no smoothing. The scheme is stable and accurate, even for very long time simulations of very steep wave events. The scheme is easily parallizable. Illustration through examples are considered. In a first simulation, the bottom is varying in time. In a second one, where the water depth is infinite, the focus is put upon long time evolution of wave group leading to the generation of rogue wave.

Fully nonlinear numerical model

We consider three-dimensional irrotational wave motion at the surface of a homogeneous incompressible fluid over a horizontal impermeable bottom.

$\mathbf{x} = (x, y)$, z , denotes horizontal and vertical coordinates. $z = 0$, $z = -h$ and $z = \eta(\mathbf{x}, t)$ are, respectively, the equations of the still level, of the impermeable bottom and of the free surface. Let also $\vec{v} = (\mathbf{u}, w)$ be the velocity field, where $\mathbf{u} = (u, v)$ and w are the horizontal and vertical velocities, so that $\vec{v} = \text{grad } \phi$. $\mathbf{u} = \nabla \phi$ and $w = \phi_z$; ϕ being the velocity potential and ∇ being the horizontal gradient. We denote with ‘tildes’ the quantities at the free surface, e.g. $\tilde{\phi}(\mathbf{x}, t) = \phi(\mathbf{x}, z = \eta(\mathbf{x}, t), t)$. At the free surface, $\tilde{\mathbf{u}}$ and \tilde{w} are expressed by,

$$\tilde{\mathbf{u}} = \frac{\nabla \tilde{\phi} - V \nabla \eta + (\nabla \eta \times \nabla \tilde{\phi}) \times \nabla \eta}{1 + |\nabla \eta|^2}, \quad \tilde{w} = \frac{V + \nabla \eta \cdot \nabla \tilde{\phi}}{1 + |\nabla \eta|^2},$$

$$V = \phi_n \sqrt{1 + |\nabla \eta|^2}$$

The kinematic and dynamic conditions give at the surface

$$\eta_t - V = 0, \quad \tilde{\phi}_t + g\eta + \tilde{\mathbf{u}} \cdot \nabla \tilde{\phi} - \tilde{w}V = 0.$$

The Laplace equation (resulting from incompressibility and irrotationality), together with the bottom impermeability, is solved exactly by means of a Green function and the method of images. For simplicity, we present here the deep water case only ($h = \text{const.} =$

∞). The generalization to an arbitrary bottom (allowed to be varying in time and space) will be as well presented.

The Fourier transform of V , $\mathcal{F}(V) = \hat{V}$ is then decomposed into

$$\hat{V} = \hat{V}_1 + \hat{V}_2 + \hat{V}_3 + \hat{V}_4.$$

The equation is inverted to give (in deep water):

$$\begin{aligned} \hat{V}_1 &= k \hat{\phi}, \\ \hat{V}_2 &= -k \mathcal{F} \{ \eta V_1 \} - i \mathbf{k} \cdot \mathcal{F} \{ \eta \nabla \tilde{\phi} \}, \\ 2\pi \hat{V}_3 &= k \mathcal{F} \left\{ \int \tilde{\phi}' \left[1 - (1 + D^2)^{-\frac{3}{2}} \right] \nabla' \cdot [(\eta' - \eta) \nabla' R^{-1}] d\mathbf{x}' \right\}, \\ 2\pi \hat{V}_4 &= -\pi k \mathcal{F} \{ \eta^2 \mathcal{F}^{-1} \{ k \mathcal{F} \{ V \} \} \} - 2\eta \mathcal{F}^{-1} \{ k \mathcal{F} \{ \eta V \} \} + \mathcal{F}^{-1} \{ k \mathcal{F} \{ \eta^2 V \} \} \\ &\quad + k \mathcal{F} \left\{ \int V' R^{-1} \left[1 - D^2 - (1 + D^2)^{-\frac{1}{2}} \right] d\mathbf{x}' \right\}. \end{aligned}$$

Where $R = |\mathbf{x}' - \mathbf{x}|$ and $D = (\eta(\mathbf{x}', t) - \eta(\mathbf{x}, t))/R = (\eta' - \eta)/R$. The kernels of the inner integrals of \hat{V}_3 and \hat{V}_4 decay like R^{-4} and R^{-5} , respectively. These integrals are evaluated over a very limited region of the \mathbf{x} -plane. V_4 is determined implicitly and hence computed iteratively, for practical computations one iteration is sufficient. The method is shown to be very fast, accurate and stable without requiring any smoothing.

Applications

We present two examples of application of the method. The first simulation illustrates the method with an arbitrary bottom which is varying in time and space. A sudden collapse of the bottom generates waves that propagates at the surface of the fluid, this is illustrated in figure 1-a. A second simulation presents the evolution in infinite depth of a modulated wave. Modulational instability build up to generate a rogue wave. This is exemplified in figure 1-b.

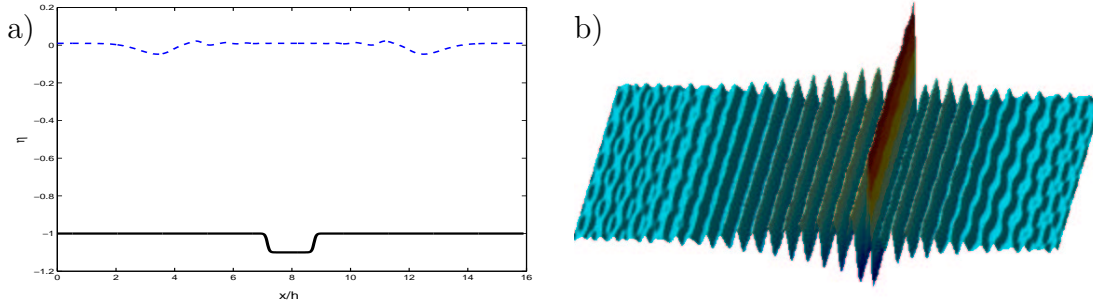


Figure 1: a): Wave elevation (- -) resulting from a sudden collapse of the bottom (-).
b): Fully nonlinear simulation of a rogue wave event with the present model.

References

- Clamond and J. Grue, *J. Fluid Mech.*, 2001, **447**, 337.
- J. Grue, *Applied Ocean Res.*, 2002, **24**, 261-274.
- D. Fructus, D., Clamond, J., Grue & Ø. Kristiansen, 2004, sub. to *J. Comp. Phys.*

On the role of downshifting in formation of large wave events

John Grue¹, Marc Francius², Didier Clamond¹ and Christian Kharif²

¹Mechanics Division, Department of Mathematics, Univeristy of Oslo, Norway

² Institut de Recherche sur les Phénomènes Hors Equilibre, Marseille, France

Fully nonlinear modeling: The long time evolution of long wave packets which split into a number of envelope solitons is studied. The split-up process is highly nonlinear, with locally very high steep waves being formed, even if the initial wave slope is rather small. The initial state of the wave field is specified in two steps. First an exact steady Stokes wave, with wavenumber k_0 and amplitude a_0 (half the total wave height) is computed. Secondly, the surface elevation and the tangential velocity at the surface are multiplied by the ‘bell’ function $\text{sech} \left[\epsilon_0 \sqrt{2} a_0 k_0^2 (x - x_0) \right]$ where the parameter ϵ_0 determines the length of the wave packet. An exact soliton solution of the nonlinear Schrödinger equation (NLS) is obtained with $\epsilon_0 = 1$. An initial condition with $a_0 k_0 = 0.09$ and $\epsilon_0 = 0.26$ is input to a fully nonlinear model (Clamond and Grue, 2001).

The computational domain involves 128 wavelengths and the carrier wave is discretized over 32 nodes per wavelength. This means that all harmonics up to the 15th are resolved, and that 128 Fourier modes are included in the spectral band $[k_0 - \frac{1}{2}k_0; k_0 + \frac{1}{2}k_0]$. The fully nonlinear simulations show that three large wave events occur during the 3000 wave periods of simulation: number one at $t/T_0 = 155$ wave periods ($k_0 \eta_m = 0.2866$, $k \eta_m = 0.34$ - k the local wavenumber - which is the maximal wave elevation observed during the computations), number two at $t/T_0 = 410$ wave periods ($k_0 \eta_m = 0.2545$), number three at $t/T_0 = 627$ wave periods ($k_0 \eta_m = 0.2704$).

The simulations show that a number of three solitons is formed within the wave envelope, that the ongoing interaction between the two leading solitons form large wave events, and that the smallest soliton in the end of the wave group is the first to detach from the group. (From about $t/T_0 \approx 1200$ the wave field consists of three separated solitary wave groups with ordered heights, the steepest being ahead.)

The spectral content of the wave group may be illustrated by the Fourier transform $\mathcal{F}(\eta)$ (figure 1) and the wavelet transform of the surface elevation η . The spectrum is initially relatively narrow, but widens during the evolution. It is evident that growth of sidebands is an inherent feature in the formation of the large wave events. The spectrum is characterized by substantial portions of energy being transferred to subharmonic and superharmonic wavenumbers. The energy content at the central wavenumber is reduced accordingly. Comparison between runs of different wave slope indicates that the sidebands recur with time scale proportional to $(a_0 k_0)^{-2}$. We note that the theoretically most unstable sidebands appear at symmetric wavenumbers with $\Delta k/k_0 = 2a_0 k_0 = 0.18$ which is obtained during the initial growth of the instabilities. This is observed in the fully nonlinear computations as well as using the NLS equation.

The role of downshifting in the large wave events: The present numerical experiment confirm what is evident from the wave tank experiments by Su (1982), namely that the formation of a downshift in long wave groups is associated with formation of envelope-solitons (within the group). While in the experiments by Su a permanent downshift was observed (including potential breaking of the waves with associated loss of mechanical energy) we find in our numerical experiments that the downshift is temporary. This downshift is responsible for the interaction taking place

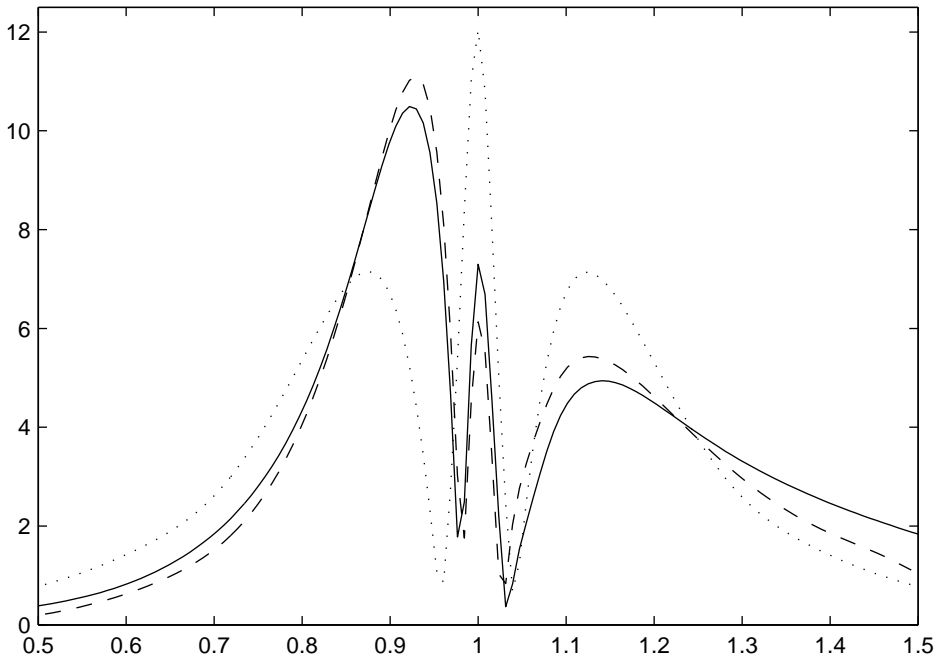


Figure 1: $|\mathcal{F}(\eta)|$ where \mathcal{F} denotes Fourier transform and η the surface elevation, $t/T_0 = 155$. Fully nonlinear model (solid line), extended Dysthe equation (dashed line), NLS (dots).

between the two leading wave groups in our simulation. This wave group interaction results in the formation of the three large wave events in the simulation.

From our experiment we can generalize the result obtained by Su who found a systematic downshift for wave slopes exceeding $ak = 0.1$. We find here that the same mechanism occurs when the initial wave slope is less than 0.1 ($a_0k_0 = 0.09$). The initial wave group is very long and shows a subsequent evolution that is highly nonlinear. We have also investigated longer wave groups with smaller slope ($a_0k_0 = 0.046$), finding similar temporary downshifting, corresponding formation of envelope solitons and thereby formation of large wave events. Fully nonlinear simulations predict multiple interactions between envelope solitons for small wave slope. Localized and temporary downshifting of the spectrum accompanies the formation of large waves.

References

- CLAMOND, D. AND GRUE, J. 2001 A fast method for fully nonlinear water-wave computations. *J. Fluid Mech.* **447**, 337–355.
- SU, M. Y. 1982 Evolution of groups of gravity waves with moderate to high steepness. *Phys. Fluids* **25**, **12**, 2167–2174.

Extreme elevations and slopes of interacting Kadomtsev-Petviashvili solitons in shallow water

Tarmo Soomere & Jüri Engelbrecht

Institute of Cybernetics, Tallinn University of Technology
Akadeemia tee 21, 12618 Tallinn, Estonia
soomere@cs.ioc.ee, je@ioc.ee

Abstract. We analyse certain geometrical features of interaction of long-crested waves in the framework of two-soliton solution of the Kadomtsev-Petviashvili equation. Such interactions may be responsible for the existence of high-amplitude wave humps. Shown is that the area of extreme elevations is very narrow whereas the extreme slope of the front of the resulting structure may be eight times as high as the maximum slope of the interacting solitons. Analytical expressions for extreme slopes of interacting solitons of arbitrary amplitude are derived. Interactions of solitons of greatly different heights do not cause extreme elevations but may result in extensive bending of the crests of the counterparts.

Introduction

Many authors have suggested that an appropriate nonlinear mechanism could be responsible for extreme waves [1]. We concentrate on a specific source for considerable changes in the wave amplitudes, namely, nonlinear superposition of solitary waves in shallow water. A suitable mathematical model for the description of the interaction of soliton-like shallow water waves travelling under slightly different directions is the Kadomtsev-Petviashvili (KP) equation [2]. It is actually weakly dependent on the transverse coordinate and has been frequently stated to apply to one and one-half dimensions. This equation admits explicit formulae for multi-soliton solutions and offers a possibility to study interaction and resonance of several solitons. A well-known feature of such interactions is that they may lead to spatially localised extreme surface elevations [3–5].

Although known for a long time, this mechanism has been only recently proposed for a possible mechanism of long-living rogue wave formation in shallow water [1,6]. The reason is that it is suitable (i) provided long-crested shallow water waves can be associated with solitons and (ii) provided the KP equation is a valid model for such waves. These conditions may be uncommon for storm waves; however, they may be satisfied when two or more systems of swell approach a certain shelf sea area from different directions. Since a moving pressure disturbance can generate solitary waves also in open sea areas [7,8], unexpected wave humps may occur in areas hosting intense fast ferry traffic [9,10] owing to interaction of wake wash from different ships.

Geometry of interacting waves

The spatial extension of the high hump in the framework of soliton interactions is frequently associated with the area where the interacting waves have a common crest [6]. For equal amplitude incoming solitons the area where elevation exceeds the sum of amplitudes of the counterparts may considerably exceed the estimates based on the geometry of the wave crests [11]. The limits of the amplitude, the spatial occupancy of the high elevation and the slope of the front of the interaction pattern were analysed in some detail for interactions of solitons of equal amplitude [6,7] that are equivalent to the Mach reflection [12,13] of a single soliton and have specific symmetry properties. A pronounced feature of freak waves is that they are particularly steep. Nonlinear interaction in the framework of the KP equation substantially modifies the profile of the two-soliton solution [11]. The slope of the high wave hump may be 8 times as large as the slope of the incoming waves. Thus in this case the nonlinear interaction leads to an extraordinarily high and narrow structure. Such wave hump might easily break before it reaches its theoretically maximum height. The possibility of breaking of the high and nonlinear wave hump makes a hit by a near-resonant structure exceptionally dangerous.

However, nonlinear interactions of solitons of unequal amplitudes are important in many applications [4,14,15]. A part of the analysis of the geometry of high elevations is extended to the case of interacting solitons with unequal amplitudes in [16]. The location and the height of the global maximum of the two-soliton solution as well as its symmetry properties are established in [16] for the case when the maximum amplitude exceeds the sum of amplitudes of the interacting solitons. The relative increase of the amplitude (compared to the sum of amplitudes of the incoming solitons) is largest when the counterparts are equal whereas elevations greatly exceeding the sum of amplitudes of the counterparts only occur when the amplitudes of the intersecting solitons are comparable.

In this paper, we extend a part of the analysis of extremely large slopes of the nonlinear interaction pattern to incoming solitons with unequal amplitudes. The maximum slope of the two-soliton solution in the principal propagation direction is established for the case when its amplitude exceeds the sum of amplitudes of the incoming solitons. The maximum increase of the slope of the interaction pattern occurs in the case of equal amplitude solitons and decreases if the amplitudes of the counterparts become different.

Counterparts of the two-soliton solution

The standard KP equation in normalised variables (η, x, y, t) reads

$$(\eta_t + 6\eta\eta_x + \eta_{xxx})_x + 3\eta_{yy} = 0, \quad (1)$$

where $\eta = \eta(x, y, t)$ describes a certain disturbance, e.g., the elevation of the water surface. A two-soliton solution of Eq. (1) is $\eta = 2\partial^2 \ln(1 + e^{\vartheta_1} + e^{\vartheta_2} + A_{12}e^{\vartheta_1 + \vartheta_2}) / \partial x^2$,

where $\varphi_i = k_i x + l_i y + \omega_i t$ are phase variables, $\kappa_i = (k_i, l_i)$, $i = 1, 2$ are the wave vectors, the frequencies ω_i satisfy the dispersion relation $P(k_i, l_i, \omega_i) = k_i \omega_i + k_i^4 + 3l_i^2 = 0$ of the linearised KP equation, $A_{12} = -P(2k_-, 2l_-, \omega_1 - \omega_2)P^{-1}(2k_+, 2l_+, \omega_1 + \omega_2)$ is the phase shift parameter, $k_{\pm} = \frac{1}{2}(k_1 \pm k_2)$ and $l_{\pm} = \frac{1}{2}(l_1 \pm l_2)$ [15,17,18]. In the following we take $t = 0$ without loss of generality. Doing so is equivalent to introducing of a proper coordinate frame moving in a certain direction. This solution can be decomposed into a sum $\eta = s_1 + s_2 + s_{12}$ of two incoming solitons s_1, s_2 and an interaction soliton s_{12} [18]:

$$s_{1,2} = A_{12}^{1/2} k_{1,2}^2 \Theta^{-2} \cosh(\varphi_{2,1} + \ln A_{12}^{1/2}), s_{12} = \frac{1}{2} B \Theta^{-2}, \quad B = 4A_{12} k_+^2 + 4k_-^2, \quad (2)$$

$$\Theta = \cosh[(\varphi_1 - \varphi_2)/2] + A_{12}^{1/2} \cosh[(\varphi_1 + \varphi_2 + \ln A_{12})/2],$$

The solution $\eta(x, y)$ is symmetric with respect to rotations by 180° around the point $x_0 = l_-(k_1 l_2 - k_2 l_1)^{-1} \ln A_{12}$, $y_0 = -k_- l_-^{-1} x_0$ corresponding to $\varphi_1 = \varphi_2 = -\ln A_{12}^{1/2}$ and called the interaction centre. The maximum heights (amplitudes) $a_{1,2} = \frac{1}{2} k_{1,2}^2$ of the counterparts $s_{1,2}$ occur infinitely far from the interaction centre. The phase shift $\Delta_{12} = -\ln A_{12}$ of the counterparts may be either positive or negative. In what follows we consider the negative phase shift case $\Delta_{12} < 0$, $A_{12} > 1$ when $\max \eta \geq a_1 + a_2$. In the case of equal amplitude solitons $k_1 = k_2$ with $l_1 = -l_2 = l$ the interaction soliton s_{12} has two axes of symmetry: the x -axis and the line $k_+ x = -\ln A_{12}^{1/2}$. The incoming solitons s_1, s_2 are the mirror images of each other with respect to these axes. The solution $\eta(x, y)$ is symmetric with respect to these axes. This symmetry is lost in interactions of solitons of unequal amplitudes; however, the interaction soliton is symmetric with respect to both the coordinate axes in the (φ_-, φ_+) -plane, where

$$\varphi_- = \frac{\varphi_1 - \varphi_2}{2}, \quad \varphi_+ = \frac{\varphi_1 + \varphi_2}{2} + \ln A_{12}^{1/2} \quad (3)$$

and expressions for s_1, s_2 and Θ have the particularly simple form [16]:

$$s_1 = A_{12}^{1/2} k_1^2 \Theta^{-2} \cosh(\varphi_+ - \varphi_-), \quad s_2 = A_{12}^{1/2} k_2^2 \Theta^{-2} \cosh(\varphi_+ + \varphi_-), \quad (4)$$

$$\Theta = \cosh \varphi_- + A_{12}^{1/2} \cosh \varphi_+$$

Equations (3) define a regular linear affine transformation (unless the wave vectors κ_1, κ_2 are collinear) that maps lines of the (x, y) -plane to lines of the (φ_+, φ_-) -plane. In particular, the lines $k_+ x + l_+ y + \ln A_{12} = 0$ and $k_- x + l_- y = 0$ correspond to the φ_+ - and the φ_- -axes, respectively. These lines are rectangular on the (x, y) -plane and serve as the pair of axes of symmetry of the interaction soliton only provided $|\kappa_1| = |\kappa_2|$ [16].

Crests and lines of steepest descent of the two-soliton solution

The two-soliton solution is stationary in the coordinate system moving in the direction bisecting the angle between κ_1 and κ_2 , that is, in the φ_+ -direction on the (φ_+, φ_-) -plane. Usually, wave crests are defined as sets of points corresponding to the maximum of the wave profile in the direction of its propagation. Since the counterparts of the two-soliton solution of the KP equation propagate at only slightly different directions, it is natural to consider the crest(s) of the whole structure in the principal propagation direction [11,16]. For two-dimensional structures this definition is sometimes ambiguous, because its counterparts may propagate in different directions. If this direction is not known (e.g. there exist only a snapshot of the water surface), crests of a smooth surface $\eta(x, y)$ could be defined as lines of curvature corresponding to the minimum normal curvature of the surface and going through a maximum (minimum) of the surface [19].

A complementary problem to determining of wave crests is to estimate of the slope of the (water) surface. The lines of minimum normal curvature of a single soliton are always parallel with its crest. This feature suggests that the steepest descent of an interaction pattern may be (at least, roughly) perpendicular to the direction of wave crests. Therefore, the problem of the maximum slope has something in common with the problem of finding the lines of curvature corresponding to the maximum normal curvature. In the process of soliton interaction, the formal crests of the incoming solitons form quite a complex pattern [11,12]; however, to a large extent, the crests of the whole pattern are nearly perpendicular to the principal direction of propagation. Therefore, the steepest descent apparently exists roughly along the φ_+ -direction. This property has been used heuristically by [11]. The largest slope found based on this assumption for the interaction pattern of equal amplitude solitons is eight times as large as the slope of single solitons.

We use the same heuristic argument, and look for the maximum slope of the solution containing unequal amplitude solitons (interpreted as, e.g., the water surface) along the φ_+ -axis. The slopes of the counterparts in the φ_+ -direction are

$$\frac{\partial s_{1,2}}{\partial \varphi_+} = -A_{12}^{1/2} B \Theta^{-3} \sinh \varphi_+, \quad (5)$$

$$\frac{\partial s_{1,2}}{\partial \varphi_+} = A_{12}^{1/2} k_{1,2}^2 \Theta^{-3} \left[\Theta \sinh(\varphi_+ \mp \varphi_-) - 2 \cosh(\varphi_+ \mp \varphi_-) A_{12}^{1/2} \sinh \varphi_+ \right],$$

where the upper sign corresponds to s_1 and the lower sign to s_2 . The slope of the surface is

$$S = \frac{A_{12}^{1/2}}{\Theta^3} \left\{ -B \sinh \varphi_+ + k_1^2 \left[\Theta \sinh(\varphi_+ - \varphi_-) - 2 A_{12}^{1/2} \cosh(\varphi_+ - \varphi_-) \sinh \varphi_+ \right] + \right. \\ \left. + k_2^2 \left[\Theta \sinh(\varphi_+ + \varphi_-) - 2 A_{12}^{1/2} \cosh(\varphi_+ + \varphi_-) \sinh \varphi_+ \right] \right\}. \quad (6)$$

Since the global maximum of the interaction pattern for the negative phase shift case is at the interaction centre [12] and since the whole structure is most shrunk in the vicinity of this centre, the largest slope apparently exists near this point. For that

reason, we only consider the slope along the φ_+ -axis ($\varphi_- = 0$). Expression (6) can be simplified as follows:

$$\tilde{S} = \frac{A_{12}^{1/2}}{\Theta_0^3} \left[-B + (k_1^2 + k_2^2)(1 - A_{12}^{1/2} \cosh \varphi_+) \right] \sinh \varphi_+, \quad \Theta_0 = 1 + A_{12}^{1/2} \cosh \varphi_+. \quad (7)$$

The slope obviously is zero at $\varphi_+ = 0$. For any other φ_+ where $\tilde{S} = 0$ we have

$$A_{12}^{1/2} \cosh \varphi_+ = 1 - \frac{B}{k_1^2 + k_2^2}. \quad (8)$$

For the negative phase shift case $A_{12} > 1$ this condition cannot be satisfied. However, for the positive phase shift Eq. (9) may have real solutions. If this happens, there exists exactly one additional point of zero slope at each side of the axis of the interaction pattern. For example, for equal amplitude solitons $k_1 = k_2$, condition (8) can be reduced to $A_{12}^{1/2} \cosh \varphi_+ = 1 - 2A_{12}$ and may have real solutions if $A_{12}^{1/2} < 1 - 2A_{12}$, or $A_{12} < 1/4$ [11,12].

The location of the maximum slope in the φ_+ -direction can be found from the condition $\partial S / \partial \varphi_+ = 0$. From expressions (5) we have that

$$\begin{aligned} \frac{\partial^2 s_{12}}{\partial \varphi_+^2} &= \frac{A_{12}^{1/2} B}{\Theta^4} (3A_{12}^{1/2} \sinh^2 \varphi_+ - \Theta \cosh \varphi_+), \\ \frac{\partial^2 s_{12}}{\partial \varphi_+^2} &= \frac{A_{12}^{1/2} k_{1,2}^2}{\Theta_4} \left[-4\Theta A_{12}^{1/2} \sinh(\varphi_+ \mp \varphi_-) \sinh \varphi_+ - 2A_{12}^{1/2} \Theta \cosh(\varphi_+ \mp \varphi_-) \cosh \varphi_+ \right] \\ &\quad + \frac{6A_{12}^{1/2} A_{12}^{1/2} \cosh(\varphi_+ \mp \varphi_-) \sinh^2 \varphi_+ + \Theta^2 \cosh(\varphi_+ \mp \varphi_-)}{\Theta_4}. \end{aligned} \quad (9)$$

At the φ_+ -axis, $\Theta = \Theta_0 = 1 + A_{12}^{1/2} \cosh \varphi_+$ and the condition $\partial S / \partial \varphi_+ = 0$ at this axis can be written as

$$\begin{aligned} A_{12} (k_1^2 + k_2^2) \cosh^3 \varphi_+ + 2A_{12}^{1/2} [B - 2(k_1^2 + k_2^2)] \cosh^2 \varphi_+ + \\ + [(1 - 2A_{12})(k_1^2 + k_2^2) - B] \cosh \varphi_+ + A_{12}^{1/2} [4(k_1^2 + k_2^2) - 3B] = 0. \end{aligned} \quad (10)$$

This is a cubic equation with respect to $\cosh \varphi_+$ and serves as a generalisation of Eq. (29) in [11]. Certain differences between these equations are caused by different coordinate systems. The sum of all the coefficients of Eq. (10) is $(1 - 3A_{12}^{1/2} - A_{12})(k_1^2 + k_2^2) - A_{12}^{1/2} B - B$. It is negative for the negative phase shift case $A_{12} > 1$, and may become positive only for very small A_{12} . Therefore, there exists always at least one solution $\cosh \varphi_+ \geq 1$ corresponding to the maximum slope provided $A_{12} > 1$. Physically, the existence of such a solution is obvious, because the slope of the surface is zero at the interaction centre, becomes negative in the positive direction of the x -axis, and approaches zero at infinity.

In the particular case $A_{12}=1$, $B=2(k_1^2+k_2^2)$ Eq. (10) has the form $\cosh^3 \varphi_+ - 3 \cosh \varphi_+ - 2 = 0$ and has an obvious solution $\cosh_1 \varphi_+ = 2$, $\sinh_1 \varphi_+ = \sqrt{3}$ (cf. [11]). This case is similar to the linear superposition of waves, because neither phase shift nor changes in the resulting wave amplitude occur; however, this is possible only if one of the incoming waves is infinitesimally small [15]. The maximum slope in this case is

$$\tilde{S}_1 = \frac{1}{3\sqrt{3}}(k_1^2 + k_2^2). \quad (11)$$

For near-resonant case $A_{12} \rightarrow \infty$ Eq. (10) has an asymptotic solution $\cosh_\infty \varphi_+ = \sqrt{3/2}$, $\sinh_\infty \varphi_+ = \sqrt{1/2}$. In [11] the corresponding point at the x -axis is located at the distance $\sim \ln A_{12}^{1/2}$ from the origin. This location tends to infinity when $A_{12} \rightarrow \infty$ and the maximum slope calculated in [11] is, strictly speaking, correct only asymptotically. In the coordinate system used in the current paper the point of the maximum slope is located at a finite distance from the origin. The slope at this point at the resonance case $A_{12} \rightarrow \infty$ and the corresponding slope amplification factor are

$$\tilde{S}_\infty = \frac{2(k_1+k_2)^2}{3\sqrt{3}}, \quad m_s = \frac{\tilde{S}_\infty}{\tilde{S}_0} = \frac{2(k_1+k_2)^2}{(k_1^2+k_2^2)}, \quad (12)$$

respectively. The latter expression is the generalisation of an analogous result for equal amplitude solitons [11]. This factor is exactly twice the analogous amplitude amplification factor [12]. In the case of equal amplitude solitons $m_s = 4$, and it decreases to 1 for solitons of greatly different amplitudes.

Extent of the area of nonlinear effects of the two-soliton solution

The spatial extent of the extreme slopes apparently follows the extent of the extreme elevations and the area where extensive deformation of the crests of the incoming solitons occur and where the whole structure has a single crest. This extent for the special case of equal amplitude solitons is studied in [11]. To the first approximation, the area where the two-soliton solution exceeds the amplitude occurring in the process of linear superposition of s_1 and s_2 can be well described with the use of the (geometric) length of the idealised common part L_{12} (Fig. 1) of the crests of the incoming soliton [6,11].

Since the interaction pattern of the two-soliton solution of the KP equation only depends on the amplitudes of the incoming solitons and the angle between their crests (that define the parameter λ), the coordinate system for description of the instantaneous interaction pattern can be always chosen so that $l_1 = -l_2 = l$. The whole pattern is not necessarily steady in such coordinates.

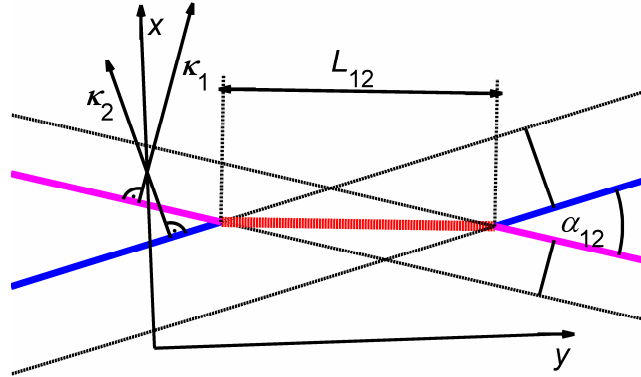


Fig. 1. Idealised patterns of crests of incoming solitons (blue and magenta lines), their position in the absence of interaction (dashed lines) and the interaction soliton (bold-dashed red line) corresponding to the negative phase shift case.

However, in this particular case the geometric length $L_{12} = l^{-1} \ln A_{12}$ [6] only depends on the l -component of the wave vectors and the phase shift parameter $\ln A_{12}$, and shows no explicit dependence on the amplitudes of the incoming solitons. Therefore, the spatial extent of appearance of nonlinear effects for interactions of solitons with drastically different amplitudes in terms of the geometric length is as large as if the amplitudes were equal (Fig. 2).

This feature of interaction of solitary waves of unequal height may be particularly important in applications where the function $\eta(x, y)$ has the meaning of surface elevation [1,6,12,20] and the extent and orientation of the near-resonant structure are equally important [15,18]. For example, in shallow sea areas near-resonant interaction of solitonic surface wave systems with radically different amplitudes apparently become evident in the form of bending of crests of the waves [15,16,20,21] rather than in the form of extreme elevations. This feature can be frequently observed in very shallow water (Fig. 3). In open sea conditions it apparently cannot be recognize in isolated form but its effect may drastically increase the probability of encountering a hit by a high wave possibly with a particularly large slope [7] and arriving from an unexpected direction.

Apart from wind-generated rogue waves, the presented mechanism may have an intriguing application in the analysis of abnormally high waves in shallow coastal areas hosting intense high speed ship traffic. The sequences of long-crested soliton-like waves are frequently excited by contemporary ships if they sail at speeds roughly equal with the maximum phase speed of gravity waves [8,10,22,23]. Groups of solitonic waves intersecting at a small angle may appear if wakes from two ships meet each other. Their interaction may be responsible for dangerous waves along shorelines.

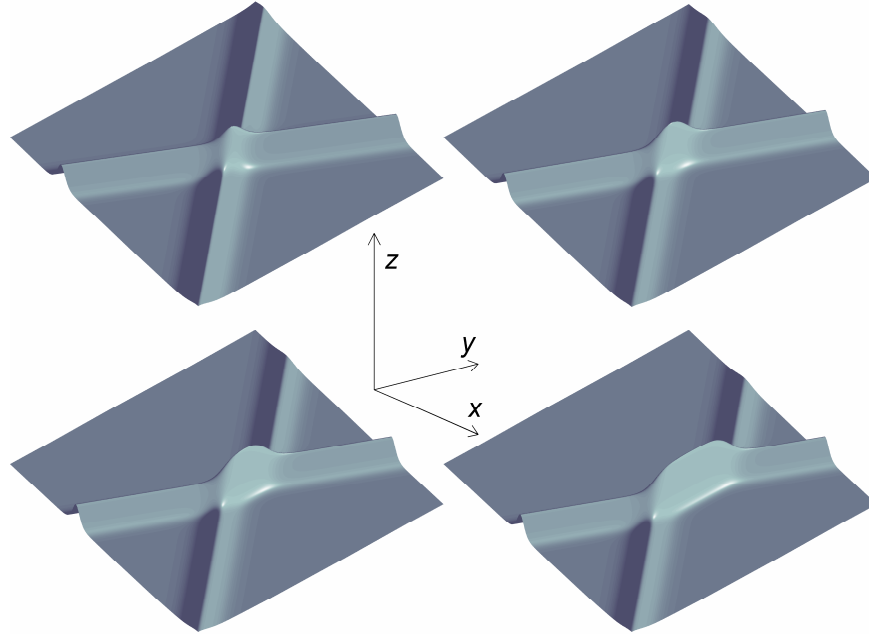


Fig. 2. Surface elevation in the vicinity of the interaction area, corresponding to incoming solitons with unequal amplitudes: $k_2 = 0.3$, $l = -l_1 = 0.2$, $k_{res} = 2/3$ and $k_1 = 0.9k_{res}$ (upper left panel), $k_1 = 0.99k_{res}$ (upper right), $k_1 = 0.999k_{res}$ (lower left), $k_1 = 0.9999k_{res}$ (lower right) in normalised coordinates (x, y) . Area $|x| \leq 60$, $|y| \leq 90$ is shown at each panel.

The fraction of sea surface occupied by extreme elevations or waves propagating in an unexpected direction apparently is small as compared with the area of a wave storm, because extensive areas of appearance of nonlinear effects may occur only if the heights of the incoming waves and their intersection angle are specifically balanced. An important difference should be underlined between specific waves possibly excited by the described mechanism and those arising owing to focusing of transient and directionally spread waves. In the latter case a number waves with different frequencies and propagation directions are focused at one point at a specific time instant to produce a time-varying transient wave group that normally does not propagate far from the focussing area. A wave hump from nonlinear interaction, theoretically, has unlimited life-time and may cross large sea areas in favourable conditions. Thus, one should account for the expected life-time of nonlinear wave humps (additionally to the sea area covered by extreme elevation at a certain time instant) when estimating the probability of occurrence of abnormally high waves.



Fig. 3. Interaction patterns of soliton-like surface waves in very shallow water near Kauksi resort on Lake Peipsi, Estonia (Photo by Lauri Ilison, July 2003).

Acknowledgements

This work has been partially supported by the Estonian Science Foundation, grant No 5762.

References

1. **Kharif, G. & Pelinovsky, E.** "Physical mechanisms of the rogue wave phenomenon", *Eur. J. Mech. B Fluids*, Vol.22, (2003), pp. 603–634.
2. **Kadomtsev, B.B & Petviashvili, V.I.** "The stability of solitary waves in weakly dispersive media", *Dokl. Akad. Nauk SSSR (Soviet Phys. Dokl.)*, Vol.192, (1970), pp. 532–541.
3. **Miles, J.W.** "Obliquely interacting solitary waves", *J. Fluid Mech.*, Vol.79, (1977), pp. 157–169.
4. **Miles, J.W.** "Resonantly interacting solitary waves", *J. Fluid Mech.*, Vol.79, (1977), pp. 171–179.
5. **Maxworthy, T.** "Formation of non-linear internal waves from the gravitational collapse of mixed regions in 2 and 3 dimensions", *J. Fluid Mech.*, Vol.96, (1980), pp. 47–64.

6. **Peterson, P., Soomere, T., Engelbrecht, J. & van Groesen, E.** "Interaction soliton as a possible model for extreme waves in shallow water", *Nonlinear Process. Geophys.*, Vol.10, (2003), pp. 503.
7. **Haragus-Courcelle, M & Pego, R.L.** "Spatial wave dynamics of steady oblique wave interactions", *Physica D*, Vol.145, (2000), pp. 207–232.
8. **Li, Y & Sclavounos, P.D.** "Three-dimensional nonlinear solitary waves in shallow water generated by an advancing disturbance", *J. Fluid Mech.*, Vol.470, (2002), pp. 383–410.
9. **Soomere, T., Rannat, K., Elken, J. & Myrberg, K.** "Natural and anthropogenic wave forcing in Tallinn Bay", Baltic Sea, in *Coastal Engineering VI*, (Brebbia, C.A., Almorza, D. & López-Aguayo, F., Eds.), WIT Press, Southampton, Boston 2003, pp. 273–282.
10. **Soomere, T., Elken, J., Kask, J., Keevallik, S., Kõuts, T., Metsaveer, J. & Peterson, P.** "Fast ferries as a new key forcing factor in Tallinn Bay", *Proc. Estonian Acad. Sci. Eng.*, Vol.9, (2003), pp. 220–242.
11. **Soomere, T. & Engelbrecht, J.** "Extreme elevations and slopes of interacting solitons in shallow water", *Wave Motion*, Vol.41, (2005), pp. 179–192.
12. **Melville, W.K.** "On the Mach reflection of solitary waves", *J. Fluid Mech.*, Vol.98, (1980), pp. 285–297.
13. **Mase, H., Memita, T., Yuhi, M. & Kitano, T.** "Stem waves along vertical wall due to random wave incidence", *Coast. Eng.*, Vol.44, (2002), pp. 339–350.
14. **Gabl, E.F. & Lonngren, K.E.** "On the oblique collision of unequal amplitude ion-acoustic solitons in a field-free plasma", *Phys. Lett. A*, Vol.100, (1984), pp. 153–155.
15. **Peterson, P. & van Groesen, E.** "A direct and inverse problem for wave crests modelled by interactions of two solitons", *Physica D*, Vol.141, (2000), pp. 316–332.
16. **Soomere, T.** "Interaction of Kadomtsev-Petviashvili solitons with unequal amplitudes", *Phys. Lett A*, Vol.332, (2004), pp. 74–81.
17. **Segur, H. & Finkel, A.** "An analytical model of periodic waves in shallow water", *Stud. Appl. Math.*, Vol.73, (1985), pp. 183–220.
18. **Peterson, P. & van Groesen, E.** "Sensitivity of the inverse wave crest problem", *Wave Motion*, Vol.34, (2001), 391–399.
19. **Gray, A.** "*Modern Differential Geometry of Curves and Surfaces with Mathematica*", CRC Press, Boca Raton, FL, 1997, pp. 14, 140, 222.
20. **Hammack, J. Scheffner, N. & Segur, H.** "Two-dimensional periodic waves in shallow water", *J. Fluid Mech.*, Vol.209, (1989), 567–589.
21. **Duan, W.-S., Shi, Y.-R. & Hong, X.-R.** "Theoretical study of resonance of the Kadomtsev-Petviashvili equation", *Phys. Lett. A*, Vol.323, (2004), pp. 89–94.
22. **Parnell, K.E. & Kofoed-Hansen, H.** "Wakes from large high-speed ferries in confined coastal waters: Management approaches with examples from New Zealand and Denmark", *Coastal Manage.*, Vol.29, (2001), pp. 217–237.
23. **Soomere, T., Pöder, R., Rannat, K. & Kask, A.** "Profiles of waves from high-speed ferries in the coastal area", *Proc. Estonian Acad. Sci. Eng.*, Vol.11, (2005), submitted.

Distribution of extreme waves by simulations.

Hervé Socquet-Juglard and Kristian Dysthe, University of Bergen

Karsten Trulsen, University of Oslo

Harald E.Krogstad and Jingdong Liu, NTNU, Trondheim

Abstract

Several ideas for physical mechanisms that can produce large waves have been suggested as reasons for rogue- or freak waves (see e.g. Dysthe 2000, Kharif & Pelinovsky 2004). It seems, however, that these mechanisms need special preparations or coherence to work. It is therefore difficult to see how they can occur spontaneously during a storm on the open ocean.

To investigate the possibility that nonlinear wave interactions may influence the spontaneous occurrence of extreme waves, we have done fairly large scale 3D simulations using higher order NLS type equations (Dysthe 1979). Our "numerical" ocean contains approximately 10^4 waves at any time, and has a time horizon of 150 typical wave periods $2\pi/\omega_p$. As has been reported elsewhere (Dysthe et.al. 2003) a characteristic evolution is seen where the initial wave spectrum "relaxes" towards a more steady form. This process is most prominent for very narrow spectra, and takes place on the Benjamin-Feir timescale $(\omega_p s^2)^{-1}$ where s is a typical steepness. Such spectral change due to the Benjamin-Feir type instability has been linked to increased occurrence of extreme waves (Onorato et.al. 2000, Mori & Yasuda 2000, Janssen 2003). This connection is investigated using our simulations.

We are concerned with the distributions of surface elevation and crest height. For relatively short crested waves the mentioned spectral evolution does not seem to influence these distributions significantly. We find that up to 5 standard deviations the theoretical distributions found by Tayfun (1980) seems to fit the simulated data very well. For a very narrow initial angular distribution, however, we see a significant increase in the occurrence of extreme waves during the spectral relaxation, in qualitative agreement with laboratory experiments done by Onorato et.al. (2004).

Acknowledgements

This research has been supported by the BeMatA programme of the Research Council of Norway, and also by Statoil and Hydro.

References

- DYSTHE, K.B. 2000 Modelling a "rogue wave"-speculations or a realistic possibility? *Proceedings of the workshop Rogue Waves 2000 IFREMER*, pp. 255-264 .
- KHARIF, C. & PELINOVSKY, E. 2004 Physical mechanisms of the rogue wave phenomenon. *European Journal of mechanics B/Fluids*. **22**, pp. 603-634.
- DYSTHE, K.B. 1979 Note on a modification to the nonlinear Schrödinger equation for application to deep water waves *Proc. R. Soc. Lond. A* **369**, pp. 105–114.
- DYSTHE K.B., TRULSEN, K., KROGSTAD, H.E. & SOCQUET-JUGLARD, H. 2003 Evolution of a narrow-band spectrum of random surface gravity waves. *J. Fluid Mech.* **478**, pp. 1-10.
- MORI, N and YASUDA, T. 2000 Effects of high-order nonlinear wave-wave interactions on gravity waves. *Proceedings of the workshop Rogue Waves 2000 IFREMER* pp. 229-244.
- ONORATO, M., OSBORNE, A.R., SERIO, M. and DAMIANI, T. 2000 Occurrence of freak waves from envelope equations in random ocean wave simulations. *Proceedings of the workshop Rogue Waves 2000 IFREMER*. pp. 181-191.
- JANSSEN, P.A.E.M. 2003 Nonlinear four wave interaction and freak waves. *J.Phys.Oceanogr.* **33**, pp. 863-884.
- TAYFUN, M.A. 1980 Narrow-band nonlinear sea waves. *J. Geophys. Res.* **85**, pp. 1548-1552.
- ONORATO, M., OSBORNE, A.R., SERIO, M., CAVALERI, L., BRANDINI, C. and STANSBERG, C.T. 2004 Extreme waves and modulational instability: wave flume experiments on irregular waves. *Submitted to J. Fluid Mech.*

Numerical and Physical Experiments of Wave Focusing in Short-Crested Seas

Félicien Bonnefoy, Pierre Roux de Reilhac, David Le Touzé & Pierre Ferrant

Équipe Hydrodynamique et Génie Océanique
École Centrale de Nantes
B.P. 92101, F-44321 Nantes, France
`pierre.ferrant@ec-nantes.fr`

Abstract. This paper aims at determining the wave generator motion required to deterministically reproduce a prescribed wave packet in a wave basin. In two dimensions, a partial model at third order is proposed, which accounts for the nonlinear phase velocities during the propagation from the wavemaker to the focusing point. Advantage is being taken of knowing these nonlinear velocities to build a command law of the wave generator that notably enhances the quality of the target reproduction, both in numerics and in experiments. In three dimensions where directionality adds significant complexity to the reproduction process, a linear decomposition of the target wave packet is developed, one frequency per direction, starting from a set of five wave probe measurements.

Introduction

The evolution of extreme waves due to the focusing of several wave components is studied both in laboratory experiments and simulation. Our main concern here is to deterministically reproduce in a wave basin a large wave event that could have been measured in the open ocean or in our case generated preliminary in the wave basin. The unknown is the wavemaker motion.

Whereas the classical use of linear backward propagation and transfer function of the wavemaker leads to good results in small amplitude waves, this approach obviously fails at larger amplitudes and hence needs further improvement. The estimation of the nonlinear phase velocity is the key point for accurate reproduction of deterministic wave trains, see *e.g.* the iterative technique of Clauss *et al.* [4]. In two dimensions, the direct iterative corrections of the wavemaker motion frequency components [3] have furnished a first attempt to improve the reproduction both for experiments and numerical simulations using a fast and accurate fully nonlinear spectral model [8, 2]. This original model reproduces the complete 3D wave basin with perfectly reflecting sidewalls, damping at one end to simulate the physical beach and generation process by imposing an inlet flux condition on the opposite boundary of the domain. A novel approach is considered here where the nonlinear phase speed is evaluated from the generation of the wave packets with the determined input (crest focusing η) and the π radians out of phase input (trough focusing η_π). The correction of the wavemaker motion

with this adjusted phase velocity shows considerable improvement of the reproduced wave field. In three dimensions, arrays of probes are generally too coarse to produce reliable results from a spatial Fourier Transform so an alternative approach is investigated to deduce the wavemaker motion.

1 Wave basins

The methods of deterministic reproduction studied here have been tested in both numerical and physical basins that we briefly describe in the following sections.

1.1 Fully nonlinear numerical model

We consider a three-dimensional wave tank of length L_x , width L_y and constant water depth h , filled with water assumed to be an inviscid fluid (see Fig. 1). Under

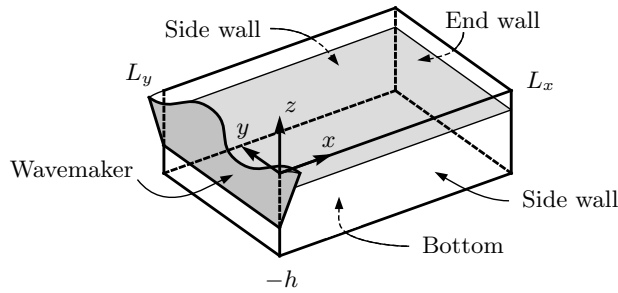


Fig. 1. Sketch of the wave basin

the potential-flow theory assumption, the unknown velocity potential $\phi(\mathbf{x}, z, t)$ satisfies Laplace's equation in the whole fluid domain D . Side and end walls are reflecting waves perfectly, and are modeled by no-flux conditions $\partial\phi/\partial n = 0$. The wave generation is taken into account on the wavemaker boundary through a linear flux condition $\partial\phi/\partial x = \partial X/\partial t$ on $x = 0$ where $X(y, z, t)$ is the wavemaker motion [2]. An additional potential ϕ_a (Agnon and Bingham [1]) is introduced by separating the potential in two $\phi = \phi_w + \phi_a$. The additional potential satisfies Laplace equation in the domain, homogeneous Neumann conditions on the walls, no condition on the free surface and the flux condition on $x = 0$. It is solved in an extended basin, in the time domain to deal with elaborated wavemaker motion $X = G(z)F(y, t)$ with G the vertical geometry (flap or piston) and F the control law to generate oblique waves. The second potential ϕ_w needs to satisfy the Laplace equation, the free surface boundary conditions (FSBCs) and homogeneous Neumann conditions on the walls, including the wavemaker $x = 0$.

The free surface potential $\phi^s(\mathbf{x}, t) = \phi_w(\mathbf{x}, z = \eta, t)$ is introduced and the fully nonlinear FSBCs are rewritten as follows

$$\frac{\partial \eta}{\partial t} = (1 + |\nabla \eta|^2) W + \frac{\partial \phi^{add}}{\partial z} - \nabla(\phi^s + \phi_a) \cdot \nabla \eta \quad \text{for } z = \eta, \quad (1a)$$

$$\begin{aligned} \frac{\partial \phi^s}{\partial t} = & -g\eta - \frac{1}{2} |\nabla \phi^s|^2 + \frac{1}{2} (1 + |\nabla \eta|^2) W^2 - \nu \frac{\partial \eta}{\partial t} \\ & - \nabla \phi^s \cdot \nabla \phi_a - \frac{\partial \phi_a}{\partial t} - \frac{1}{2} |\tilde{\nabla} \phi_a|^2 \quad \text{for } z = \eta, \end{aligned} \quad (1b)$$

with $W = \frac{\partial \phi_w}{\partial z}(\mathbf{x}, z = \eta, t)$. Here the additional potential acts in the form of forcing terms on the RHS of the FSBCs. The damping pressure $-\nu \frac{\partial \eta}{\partial t}$ added on the dynamic FSBC (1b) provides an efficient model for the absorbing beach at the opposite of the basin, the coefficient $\nu(\mathbf{x})$ being non-zero only in a region close to the end wall (no term is added in the kinematic FSBC (1a) to ensure mass conservation). The High-Order Spectral approach (HOS) of Dommermuth and Yue [5] is used to approximate the vertical velocity W through a double series expansion (Taylor series around $z = 0$ and powers of η). To obtain a consistent development in powers of η in the two terms $(1 + |\nabla \eta|^2) W$ and $(1 + |\nabla \eta|^2) W^2$ of Eqn. (1), we adopt the formulation of West *et al.* [11] for these terms.

Both the additional and the wave potential are solved with a spectral method combined with adequate dealiasing procedures, thus providing fast and accurate computations.

1.2 Physical model

In parallel to the numerical simulations presented above, wave experiments are conducted in the 50 x 30 x 5 m wave basin in ECN. The segmented wavemaker consists of 48 paddles (0.6 m width, hinged at mid depth), allowing directional wave generation. Wave elevations are measured at several locations with 1 m resistive wave probes.

The wavemaker is controlled in the frequency domain by a set of wave components (frequency, amplitude, phase plus angle in 3D wave fields). The motion is deduced by applying the linear transfer function of the wavemaker. The same frequency components are used to derive the numerical flux at the wavemaker wall with the same transfer function so that the two generation processes correspond. Dalrymple's method is used for directional wave fields to take advantage of the reflective side walls and correctly generate the large wave angles.

1.3 Comparisons

Comparisons were carried out between the numerical and physical wave basins to validate our numerical approach. Simulations of regular waves show the ability of the numerical model to reproduce the effects of high order nonlinearities such as the increase of the wave velocity due to finite amplitude and the presence of return current in the basin (not shown here for brevity, see [8, 2]). The case

of long time irregular wave fields has been investigated. Figure 2 presents an example of 900 s long 2D experiment of a modified two parameters Pierson-Moskowitz spectrum ($H_s = 16$ cm and $T_Z = 1.4$ s, that is a characteristic steepness $\varepsilon_c = H_s/\lambda_p = 3$ % with λ_p the wavelength at the peak frequency). The time window in Fig. 2 isolates a large wave event at $t = 488$ s among the 640 generated waves and shows a very good agreement between the experimental data and the fully nonlinear model (HOS). For comparison, results obtained from a second order model [9] previously developed are also plotted in Fig. 2 and show inadequacy of second order theory to accurately model the large event.

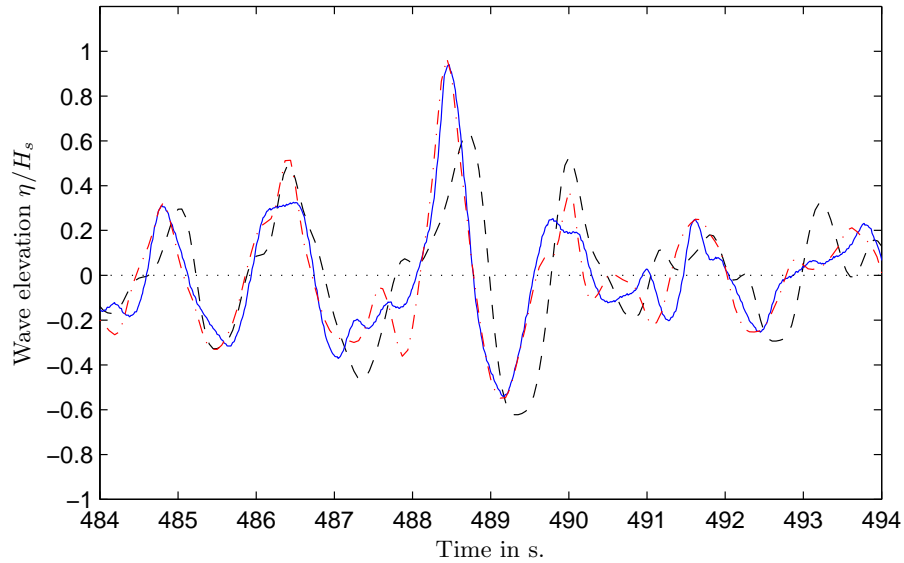


Fig. 2. Wave elevation: experimental (—), second order simulation (--) and HOS simulation (-.-)

The more specific case of a focused wave packet is shown in Fig. 3 (40 cm amplitude and peak wavelength $\lambda_p=9$ m). The fully nonlinear model compares satisfactorily to the experiments. Especially phases are correctly solved so the main peak is well described. In the following, we use alternatively the numerical or the physical experiments.

2 Deterministic reproduction in two dimensions

2.1 Principle

Basic linear and second order decompositions (see appendices A and B) yield satisfactory results only when the packet steepness is small. Their application to higher steepness reveals differences between the wave packet generated from

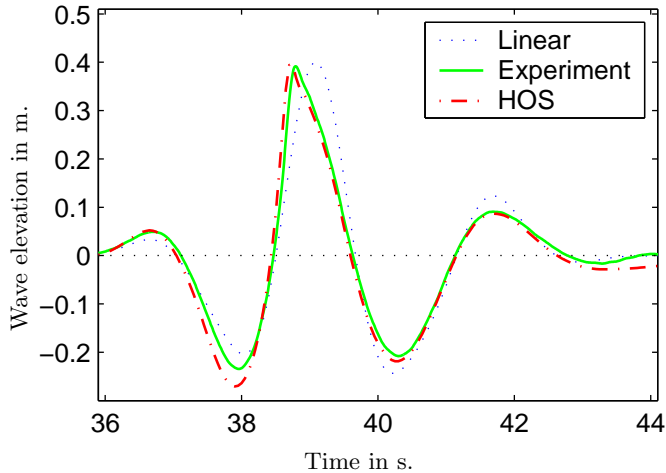


Fig. 3. Comparisons between experimental and numerical elevations

the linear or second order decomposition input and the target event. Those differences are believed here to be due mainly to the nonlinear increase of phase velocity by four wave resonant interactions as predicted in [10]. Iterative corrections of the wavemaker motion [3] show improvement for frequencies around the peak of the spectrum whereas uncorrect control of the high frequency range is observed. We thus developed a two-steps method to directly estimate the modification of the phase velocity due to nonlinear interactions. The first step is the double generation of the wave packet, one with amplitudes determined by a simple decomposition technique either linear or second order (crest focusing) and one with 180° out of phase amplitudes (trough focusing). The second step is the even/odd decomposition of the nonlinear effects (*e.g.* [7]):

$$\eta_{even} = (\eta + \eta_\pi)/2, \quad (2a)$$

$$\eta_{odd} = (\eta - \eta_\pi)/2. \quad (2b)$$

2.2 Validation

This decomposition is first validated with a low amplitude wave packet in which the nonlinear effects are reduced to second order. Figure 4 (left) shows a very good agreement between the odd elevation given by Eqn. (2b) and the linear theoretical elevation calculated from the wavemaker frequency components. On the same figure (right), the even elevation given by Eqn. (2a) is correctly modeled by a second order elevation build with an expression similar to (6).

For larger wave steepness, the odd surface elevation is interpreted as the superposition of components with the linear input amplitudes and phases but modified phase velocity (or wavenumbers k'_n):

$$\eta_{odd} \simeq \sum_n a_n e^{i(\omega_n t - k'_n x)}. \quad (3)$$

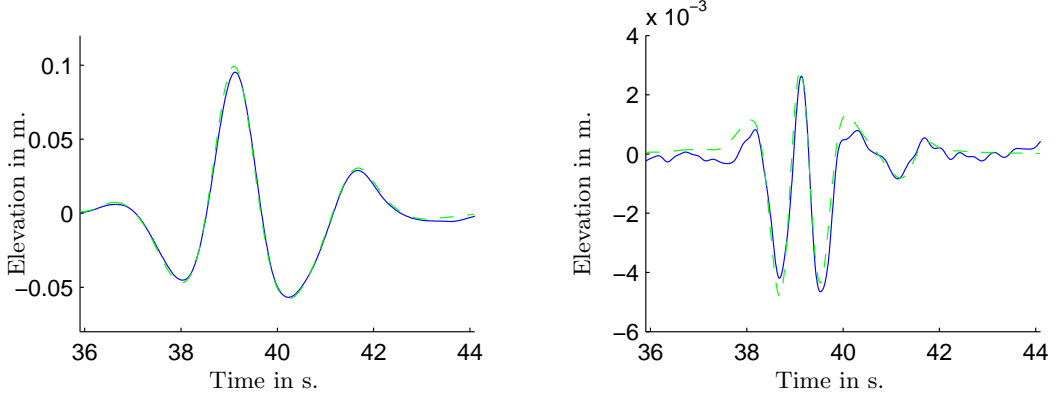


Fig. 4. Odd/even decompositions and analytical solutions (amplitude $A=10$ cm: left η_{odd} (—), linear (---), right η_{even} (—) and second order (---))

After a Fourier Transform of the odd elevation, the modified wavenumber k'_n is determined from Eqn. (3) and from the complex amplitude a_n known from a linear or second order theory. This provides a simple evaluation of the nonlinear phase velocity. Figure 5 (left) shows a comparison between the measured odd elevation and two linear elevations calculated from the wavemaker components either with the linear phase velocity or the estimated nonlinear phase velocity (named *corrected* in the legend). The correction of the linear elevation leads to satisfactory results as expected. A stronger validation is given at second order in Fig. 5 (right). The corrected second order elevation calculated with Eqn. (6) but with estimated nonlinear phase velocity is in good agreement with the measured even elevation, whereas the classical second order elevation (Eqn. (6)) fails to describe the even elevation.

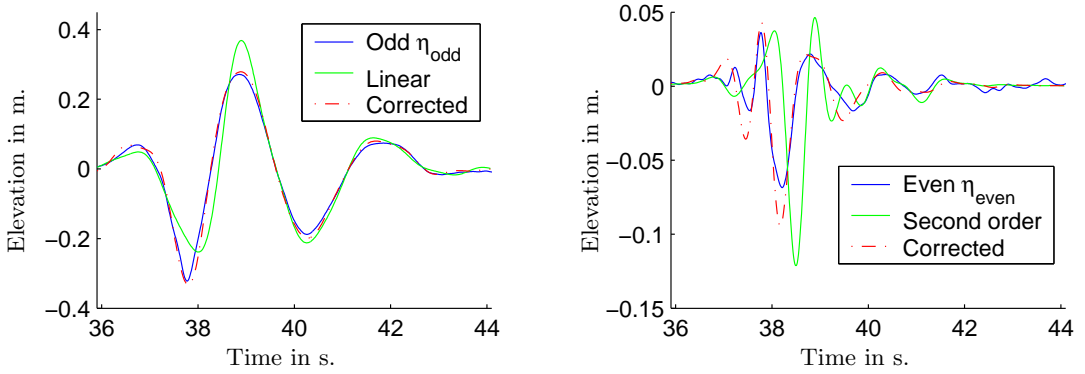


Fig. 5. Odd/even decomposition and analytical elevations with linear or nonlinear phase velocity (amplitude $A=40$ cm)

2.3 Application

After having evaluated the nonlinear phase velocity occurring during the focusing of the generated wave packet, we correct the wavemaker motion with the corresponding phase shift $\exp -i(k'_n - k_n)x$. Figure 6 presents the measured surface elevation at the focusing location for the reproduced wave packets, from both the initial input and the nonlinear phase velocity corrected input. Comparison with the target elevation shows the better agreement obtained with the nonlinear correction. The main features of the focused target wave packet are well reproduced with one correction of the wavemaker motion (non iteration required). The main crest and the lateral trough are close to the target in both amplitudes and phases. The main crest amplitude is correctly estimated showing a better control of the high-frequency range than in the previous iterative scheme [3].

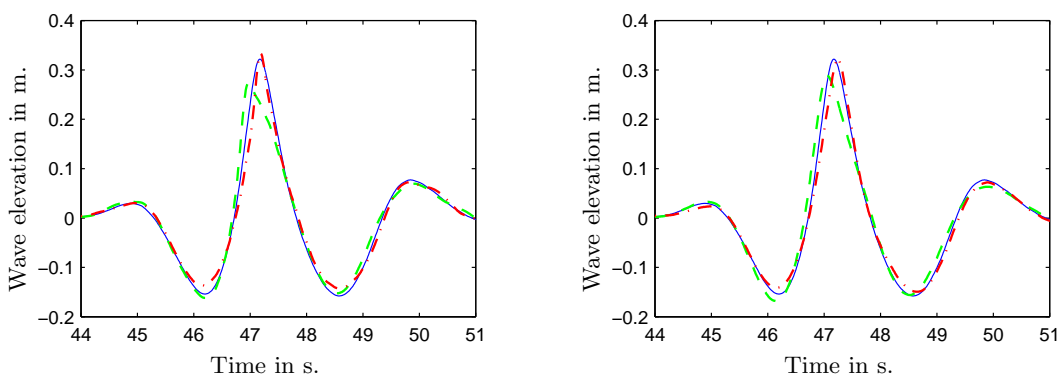


Fig. 6. Wave elevation: target (—), initial input(---) and corrected input (-.-) (left: linear input, right: second order input)

3 Deterministic reproduction in three dimensions

A first step towards directional deterministic reproduction is achieved. The target wave field is a directional wave packet, measured in a wave basin with five probes, set in a truncated pentagon shape commonly used for laboratory irregular directional wave analysis. This target is seen as the linear superimposition of directional waves, with a single direction per frequency. The Fourier Transforms of the five recorded surface elevations form the RHS of a set of nonlinear equations

$$a e^{-ik(x_p \cos \theta + y_p \sin \theta) + \phi} = TF(\eta_p) \text{ for } p = 1 \text{ to } 5, \quad (4)$$

where the unknowns are the amplitude a , the direction θ and phase ϕ . This system is solved with a nonlinear least squares method where initial guess for the

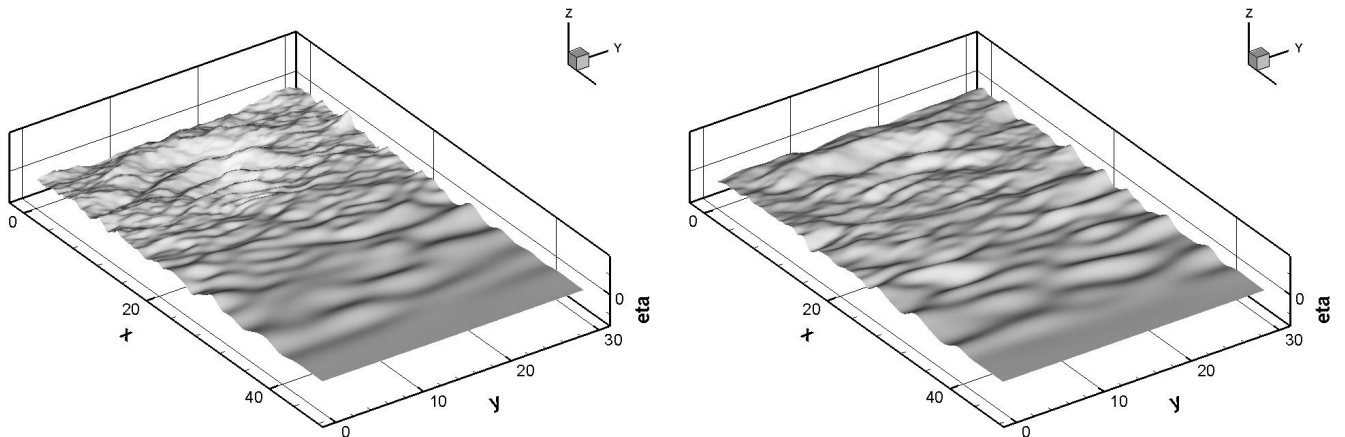


Fig. 7. View of the target wave field (left) and the reproduced one (right) at $t = 33$ s

three unknowns is provided respectively by the mean of the probe Fourier modulus, a gaussian random angle with estimated mean direction and spreading and a random phase. Local minima are expected so several solutions are computed with different initial guess and the solution is selected for the reproduction as the one that minimises the time integral squared errors between target surface height and linearly reconstructed elevation on the five probes. We finally obtain a set of directional components that is linearly propagated backwards to the wavemaker to calculate its motion. In case the requested direction of the wave is too high regarding the dimensions of the basin, the wavelength and the capabilities of the serpent-type wavemaker Dalrymple's method is used to control the motion and avoid spurious reflection on the sidewalls. Figures 7 and 8 show views of the target and reproduced wave fields at $t = 33$ s and $t = 45$ s, respectively before and at the focusing event. The main features of the focusing packet are correctly estimated by the described method although the high frequency range is underestimated. At the focusing time (Fig. 8), the reproduced wave packet is larger than the target one and its amplitude lower.

4 Conclusion

Two approaches of deterministic reproduction in 2D and 3D wave basin have been tested. The wavemaker motions are tested indifferently in the HOS fully nonlinear numerical basin or the physical basin at ECN. In 2D, the separation of odd and even nonlinear effects up to the third order leads to an estimation of the nonlinear phase velocity. Used to deduce the wavemaker motion required for the generation of a target wave packets, this nonlinear velocity yields satisfactory results for highly nonlinear targets.

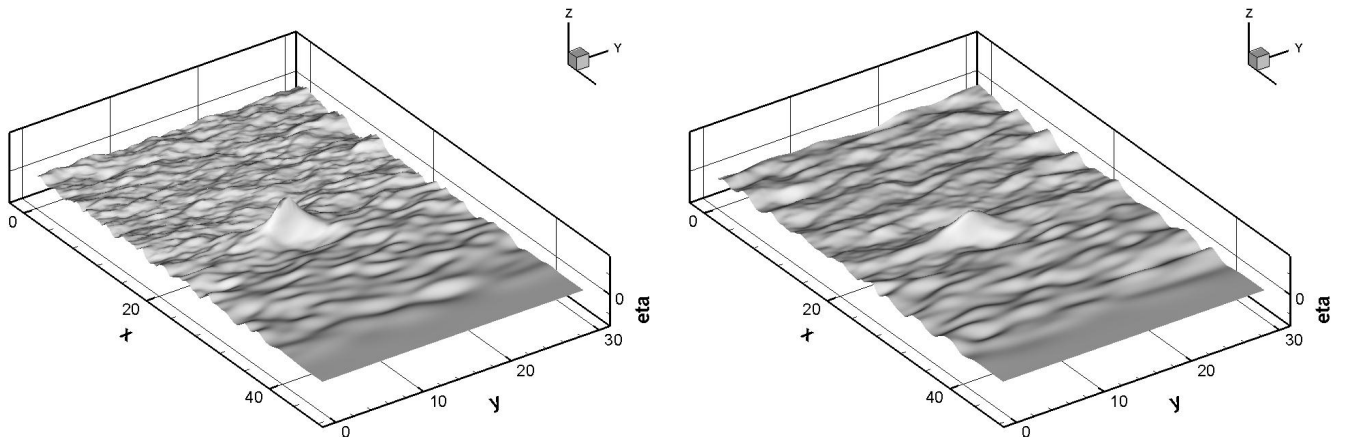


Fig. 8. View of the target wave field (left) and the reproduced one (right) at $t = 45$ s

In 3D, a basic approach is build for the reproduction of focused directional wave packets. Assuming that each frequency components has a single direction, this approach gives encouraging first results, although a better control of the high-frequency range and a study of the nonlinear effects are required.

A Appendix: Linear decomposition

In two dimensions, the wavemaker motion can be easily derived by linear theory, provided the wave packet steepness is sufficiently small. In such a case the target elevation η_c required at a distance x_c from the wavemaker is seen as the superimposition of frequency components whose complex amplitudes \underline{c}_n are given by Fourier Transform of η_c .

$$\eta_c(t) = \sum_n \underline{c}_n e^{i\omega_n t} = \eta^{(1)}(x_c, t) = \sum_n \underline{\widehat{a}}_n e^{i(\omega_n t - k_n x_c)}. \quad (5)$$

Knowing from the dispersion relation the phase speed $v_n = \omega_n/k_n$ of each component, the wave amplitudes $\underline{\widehat{a}}_n$ at the wavemaker are simply $\underline{\widehat{a}}_n = \underline{c}_n \exp(ik_n x_c)$. The transfer function of the wavemaker is then applied to get the required motion.

B Appendix: Second order decomposition

The iterative technique of Duncan et Drake [6] describes the target elevation as the superimposition of a linear elevation plus its bound second order elevation,

that is $\eta_c = \eta^{(1)} + \eta^{(2)}$. The linear part may be written as in (5) and the second order component as

$$\eta^{(2)} = \sum_{m \geq n} \widehat{a}_m \widehat{a}_n^\pm G_{mn}^\pm e^{i((\omega_m \pm \omega_n)t - (k_m \pm k_n)x)}, \quad (6)$$

with $\widehat{a}_n^+ = \widehat{a}_n$ and \widehat{a}_n^- its conjugate. The linear amplitudes at the wavemaker location $x = 0$ are then used to build the required wavemaker motion.

References

1. Y. Agnon and H. B. Bingham. A non-periodic spectral method with applications to nonlinear water waves. *Eur. J. Mech. /B Fluids*, 18:527–534, 1999.
2. F. Bonnefoy. Modélisation expérimentale et numérique des états de mer complexes. *Ph-D Thesis*, École Centrale de Nantes, 2005.
3. F. Bonnefoy, D. Le Touzé, and P. Ferrant. Generation of fully-nonlinear prescribed wave fields using a high-order spectral method. In *Proc. ISOPE*, 2004.
4. G. F. Clauss *et al.* Non-linear calculation of tailored wave trains for experimental investigations of extreme structure behaviour. In *Proc. OMAE*, 2004.
5. D. G. Dommermuth and D. K. Yue. A high-order spectral method for the study of nonlinear gravity waves. *J. Fluid Mech.*, 184:267–288, 1987.
6. P. E. Duncan and K. R. Drake. A note on the simulation and analysis of irregular non-linear waves. *App. Ocean Res.*, 17:1–8, 1995.
7. T. Johannessen and C. Swan. A laboratory study of the focusing of transient and directionally spread surface water waves. *Proc. R. Soc. of Lond.*, 457:971–1006, 2001.
8. D. Le Touzé. Méthodes spectrales pour la modélisation non-linéaire d'écoulements à surface libre instationnaire. *Ph-D Thesis*, École Centrale de Nantes, France, 2003.
9. D. Le Touzé, F. Bonnefoy and P. Ferrant. Second-Order Spectral Simulation of Directional Wave Generation and Propagation in a 3D Tank. In *Proc. ISOPE*, 2002.
10. M. S. Longuet-Higgins and O. M. Phillips. Phase velocity effects in tertiary wave interactions. *J. Fluid Mech.*, 12:333–336, 1962.
11. B. J. West *et al.* . A new numerical method for surface hydrodynamics. *J. Geoph. Res.*, 92(C11):11,803–11,824, 1987.

Wave energy focusing in a three-dimensional numerical wave tank

Christophe Fochesato, Frédéric Dias, and Stephan Grilli

¹ MAB, Université de Bordeaux,
351 Cours de la Libération, 33405 Talence cedex, France
`Christophe.Fochesato@math.u-bordeaux1.fr`

² CMLA, ENS Cachan,
61, avenue du Président Wilson, 94235 Cachan cedex, France
`Frederic.Dias@cmla.ens-cachan.fr`

³ Department of Ocean Engineering,
University of Rhode Island, Narragansett, RI 02882, USA
`grilli@oce.uri.edu`

Abstract. Extreme waves are obtained from the motion of a snake wavemaker in a numerical wave tank. Spatial focusing is one of the mechanisms which may take part in the generation of a rogue wave. In particular, directional focusing is only a three-dimensional phenomenon, that we want to isolate in this study. The numerical model solves incompressible free-surface Euler equations for potential flow, with a Boundary Element Method and a mixed Eulerian-Lagrangian time updating. Its more recent improvement has consisted in the insertion of the Fast Multipole Algorithm in order to reduce the computational complexity of the spatial solver. A typical case of a near breaking rogue wave is presented. A description of the particular geometry of such a wave is discussed, as well as the kinematics at the surface.

Introduction

The general framework is the study of the rare but important phenomenon that are the freak waves. Indeed, in spite of their low probability of occurrence, these waves can cause severe damages and the off-shore and naval communities must take into account such events for their design rules. Besides their low probability, freak waves are characterized by the fact that they are localized in time as well as in space. They come from energy focusing, which may be due to multiple factors. Spatial focusing is one of the commonly proposed mechanisms to explain the appearance of a rogue wave. More generally, linear theory suggests that different wave components can have different phases and directions, so that they superimpose in a small region of space and time. Actually, energy focusing may come from another factor. It can result from the bottom topography in shallow water, or from wave-current interactions. In deep water and without the presence of a current, a more recent proposed mechanism is the modulational instability (Benjamin-Feir instability). Other wave-wave interactions or interactions with

atmospheric conditions may also play a role in the phenomenon. These mechanisms are summed up in the recent review article by Kharif and Pelinovsky [10].

If most work on rogue waves deals with deep water, it has been remarked that it can occur for any water depth. In the present study, we consider finite depth, but specify a flat bottom in order to concentrate only on one focusing mechanism. Spatial focusing is the natural mechanism to generate extreme waves in laboratory. It is a controlled phenomenon which represents the superposition of several sinusoidal wave components. The first possibility is frequential focusing which occurs when faster waves catch slower ones, generated earlier. This is how two-dimensional studies have been carried out. Directional focusing is a pure three-dimensional phenomenon. In order to generate it, a snake wavemaker can be used to give several swells which cross at one point of the basin. She *et al.* [11] made such laboratory experiments and studied the kinematics of breaking waves using the PIV technique. Brandini and Grilli [3, 2] adapted the Boundary Element code of [8] by inserting a snake wavemaker, and started a numerical study on spatial focusing. More recently, Bonnefoy *et al.* [1] developed a numerical tool based on a spectral solver of Euler's equations with a free surface and compared with experiments. Their method allows to consider more wave components in a larger basin, such as a random wave field with the wave components propagating as wave packets. Then, they can reproduce a focusing wave event, close to one coming from a sea state. Nevertheless, from the numerical point of view, their calculations are limited by the nature of the method used, and they cannot pursue until wave overturning. The present study arises in a slightly different context. Indeed, the aim consists in isolating the phenomenon of directional focusing which leads to breaking waves in order to study their kinematics. It follows the work of Grilli and Brandini [3] on the use of a Boundary Element Method to solve Euler equations with a free surface. The main drawback of this kind of discretization is its computational cost, which is quadratic with the number of nodes used to discretize the whole boundary of the domain. This obstacle has been removed by inserting the Fast Multipole Algorithm (FMA) in order to speed up all the matrix-vector products in the spatial solver [6]. The next section presents the numerical method and its more recent improvements. Then the configuration of the tank is described. Finally, the results are discussed in section four.

Numerical model

We consider the equations for a potential flow of a perfect, incompressible fluid, with a free surface. Inside the domain, they reduce to Laplace's equation

$$\Delta\phi = 0$$

for the velocity potential ϕ , defined from the velocity $\mathbf{u} = \nabla\phi$. Green's second identity transforms this equation into a Boundary Integral Equation (BIE) on

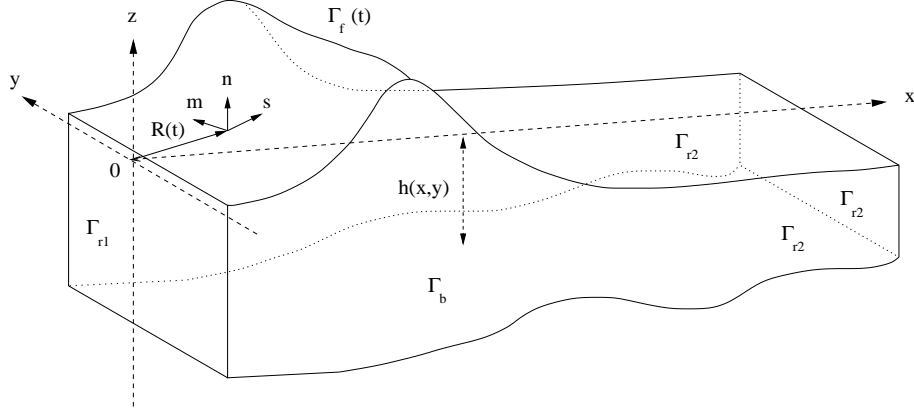


Fig. 1. Domain of computation. The free surface $\Gamma_f(t)$ is defined at each time step by the position vector $\mathbf{R}(t)$. Lateral boundaries are denoted by Γ_{r1} and Γ_{r2} . The bottom Γ_b is defined by $z = h(x, y)$. Use is made of the Cartesian coordinate system (x, y, z) and of the local curvilinear coordinate system (s, m, n) , defined at the point $\mathbf{R}(t)$ of the boundary.

the boundary

$$\alpha(\mathbf{x}_l) \phi(\mathbf{x}_l) = \int_{\Gamma(t)} \left\{ \frac{\partial \phi}{\partial n}(\mathbf{x}) G(\mathbf{x}, \mathbf{x}_l) - \phi(\mathbf{x}) \frac{\partial G}{\partial n}(\mathbf{x}, \mathbf{x}_l) \right\} d\Gamma, \quad (1)$$

where $G(\mathbf{x}, \mathbf{x}_l) = 1/4\pi|\mathbf{x} - \mathbf{x}_l|$ is the Green's function for the 3D free space, \mathbf{n} is the normal vector exterior to the boundary and $\alpha(\mathbf{x}_l)$ is proportional to the solid exterior angle made by the boundary at the collocation point \mathbf{x}_l . On the free surface, the potential ϕ satisfies the nonlinear kinematic and dynamic boundary conditions

$$\frac{D \mathbf{R}}{D t} = \nabla \phi, \quad (2)$$

$$\frac{D \phi}{D t} = -gz + \frac{1}{2} \nabla \phi \cdot \nabla \phi, \quad (3)$$

where \mathbf{R} is the position vector of a fluid particle on the free surface, g the acceleration due to gravity and D/Dt the material derivative. Lateral boundaries are either fixed or moving boundaries. In the first case, the potential is specified on the free surface in order to determine the initial perturbation. In the second case, waves are generated by a wavemaker at the open boundary, $\Gamma_{r1}(t)$, the motion \mathbf{x}_p and velocity \mathbf{u}_p being specified as

$$\bar{\mathbf{x}} = \mathbf{x}_p \quad \text{and} \quad \overline{\frac{\partial \phi}{\partial n}} = \mathbf{u}_p \cdot \mathbf{n}$$

where overlines denote specified values. Along the fixed parts of the boundary, the no-flow condition is prescribed:

$$\overline{\frac{\partial \phi}{\partial n}} = 0.$$

The domain represents a closed basin such as a wave tank, whose bottom can be defined with arbitrary shape. The numerical model is presented in detail in Grilli *et al.* [8]. The time scheme consists in updating the position vector and the velocity potential on the free surface based on second order Taylor expansions. At each time step, The BIE is solved through the use of a Boundary Element Method. The boundary is divided into elements for which a local interpolation is defined, both for the geometry and field variables. Polynomial shape functions are introduced, that also define a change of variables which brings the integrations on a cartesian reference element. The numerical computation of these integrals by a Gauss-Legendre quadrature and appropriate techniques for singularities of the Green's functions compose the assembling phase of the discretization matrix. This one is modified by taking into account the rigid mode technique which allows to directly compute the solid angles and thus avoid the singular integrations of the normal derivative of the Green's function. The insertion of the multiple node technique in order to deal with the edges also leads to a modification of the matrix. The velocity potential, or its normal derivative depending on the boundary, is obtained by solving the resulting linear system. Since the matrix is full, the method has a N^2 computational complexity, where N is the number of nodes, by using the iterative algorithm GMRES. thus the solving phase is of the same complexity as the assembling phase. In order to reduce this complexity, the Fast Multipole Algorithm is inserted. The idea is to replace every matrix-vector product coming from the discretization of the BIE by a call to this algorithm.

The FMA lies on the fact that the Green's function can be expanded in separate variables when the source point and the evaluation point are far enough from each other. It can then be written for a point O (origin of the expansion) close to \boldsymbol{x} and far from \boldsymbol{x}_l

$$G(\boldsymbol{x}, \boldsymbol{x}_l) \approx \frac{1}{4\pi} \sum_{k=0}^p \sum_{m=-k}^k \rho^k Y_k^{-m}(\alpha, \beta) \frac{Y_k^m(\theta, \varphi)}{r^{k+1}}, \quad (4)$$

where $O\boldsymbol{x} = (\rho, \alpha, \beta)$ and $O\boldsymbol{x}_l = (r, \theta, \varphi)$ in spherical coordinates. The functions $Y_k^{\pm m}$ are the spherical harmonics defined from the Legendre polynomials. In order to determine in what cases this new approximation can be used, a hierarchical subdivision of space is defined, whose regular partitioning automatically gives distance criteria. Then, close interactions are obtained by direct computation with Green's functions, whereas far interactions can be approximated by successive local operations based on the subdivision into cells and expansions of the Green' functions into spherical harmonics. The underlying theory to this

approximation is well established in the case of Laplace's equation. In particular, error and complexity analysis are given in the monograph by Greengard [7].

In our case, Laplace's equation has been transformed into an integral equation and a specific discretization has been used. Thus, the fast algorithm must be adapted in order to be part of the surface wave model, but the expansions remain the same. The integral equation can be written as

$$\alpha(\mathbf{x}_l) \phi(\mathbf{x}_l) \approx \frac{1}{4\pi} \sum_{k=0}^p \sum_{m=-k}^k M_k^m(O) \frac{Y_k^m(\theta, \varphi)}{r^{k+1}}, \quad (5)$$

where $M_k^m(O)$ is the moment at the origin O :

$$M_k^m(O) = \int_{\Gamma} \left\{ \frac{\partial \phi}{\partial n}(\mathbf{x}) \rho^k Y_k^{-m}(\alpha, \beta) - \phi(\mathbf{x}) \frac{\partial}{\partial n} \left(\rho^k Y_k^{-m}(\alpha, \beta) \right) \right\} d\Gamma. \quad (6)$$

Instead of considering mutual interactions between two points, we need to look at the contribution of an element of the discretization to a collocation point. The local computation of several elements grouped together into a multipole relies on a boundary element analysis with the spherical harmonics instead of the Green's function. The integration of the normal derivative of the spherical harmonics is done by taking care of avoiding an apparent singularity which could generate numerical errors. The discretization by boundary elements only takes place in the computation of the moments. So the rest of the Fast Multipole Algorithm is unchanged, especially for translation and conversion formulas which allow to pass the information through the hierarchical subdivision, from the multipole contributions to the evaluation at every collocation point. From the surface wave model point of view, we had to adapt all the aspects depending on the existence of the matrix in the former model. The storage of the coefficients that we want to use several times for each time step is now done inside the cells of the hierarchical subdivision. The rigid mode and multiple nodes techniques modified the matrix *a priori* before the computation of the matrix-vector products. They are now considered as correction terms to the result of such products, so that the linear system to be solved keeps the same properties.

The accelerated model only benefits from a faster solver for Laplace's equation at each time step. It has been tested by comparing with the former model the results of a three-dimensional application which requires a great accuracy. It is the propagation of a solitary wave on a sloping bottom with a transverse modulation which leads to a plunging jet. The consistency of the new approximation has been checked. But, what is important is that the accuracy and stability are not distorted. By adjusting the parameters of the Fast Multipole Algorithm, it is possible to get the same results as with the former model. In this case, the computing times evolve nearly linearly with the number of nodes, above roughly 4000 nodes.

Description of the tank

A rectangular basin with a flat bottom is defined. It is limited by fixed and moving boundaries. At one extremity, a snake wavemaker has been implemented [3]. It is a rotating wavemaker whose axis is located at the bottom, at depth h_0 . It is composed of several vertical parts which can move independently. The position $\mathbf{x}_p = (x_p, y_p, z_p)$ of each vertical part is defined by

$$\mathbf{x}_p = \mathbf{x}_o - \rho \mathbf{m} \quad , \text{ with } \quad \mathbf{x}_o = y_p \mathbf{j} - h_0 \mathbf{k} \quad (7)$$

the coordinates of the paddle axis rotation, where the angular velocity $\dot{\Omega} \mathbf{j}$ is applied. We denote ρ the distance from the axis of rotation, measured on the wavemaker in vertical planes. Hence,

$$\rho = \sqrt{x_p^2 + (h_0 + z_p)^2} \quad , \text{ and } \quad \Omega = \arctan \frac{S_o}{h_0} \quad (8)$$

where $S_o(y, t)$ corresponds to the horizontal stroke specified at $z = 0$. From these definitions, we find the velocity and acceleration vectors

$$\begin{aligned} \mathbf{u}_p &= -\dot{\rho} \mathbf{m} - \rho \dot{\Omega} \mathbf{n} \\ \frac{d\mathbf{u}_p}{dt} &= (\rho \ddot{\Omega} - \dot{\rho}^2) \mathbf{m} - (2\dot{\rho} \dot{\Omega} + \rho \ddot{\Omega}) \mathbf{n}. \end{aligned} \quad (9)$$

Following Dalrymple [5], we specify the wavemaker stroke S_o as the linear superposition of N_θ sinusoidal components of amplitude a_n and direction θ_n , as

$$S_o(y, t) = \sum_{n=1}^{N_\theta} a_n \cos \{k_n (y \sin \theta_n - x_f \cos \theta_n) - \omega_n t\} \quad (10)$$

where k_n and ω_n denote components' wavenumber and wave frequency, related by the linear dispersion relationship

$$\omega_n^2 = g k_n \tanh(k_n h_0) \quad (11)$$

and x_f is the focusing distance for the waves in front of the wavemaker. Angles θ_n are uniformly distributed in the range $[-\theta_{\max}, \theta_{\max}]$. Only directional focusing is studied here, hence $\omega_n = \omega$. Frequential focusing could be added by adjusting the frequency as a function of the angle θ_n . Moreover, we restrict ourselves to the case where the amplitudes are the same, but different values could be chosen.

The first objective of this work has consisted in looking for a parameter set such that a breaking wave is generated. We consider the superposition of eight components having identical properties but with directions between -45 and 45 degrees. The variables being non-dimensionalized (length by the water depth h_0 , and time by $\sqrt{h_0/g}$), every component is determined by a frequency 1.2816 which gives a wavelength 3.725 from (11) and a linear velocity $c = 0.7599$. The shared amplitude of each individual component is fixed to 0.04, leading to a

steepness of 0.0675. The focusing point is specified at the distance 7.5 from the wavemaker. Once the features of the wave field are defined, the dimensions of the tank are adapted. We choose 10 for the length and 20 for the width. The discretization uses 50 elements in the longitudinal direction, what corresponds to roughly 20 nodes per wavelength. The width of the domain is divided into 70 elements, and the depth into 4 elements. Note that all the boundaries are discretized. The present simulation has been obtained in 4min 30s per time step with an Intel Pentium 4 processor, for more than 300 time steps.

Figure 2 presents the kind of movement executed by the wavemaker. At the other extremity of the domain, an absorbing piston is used [4,9]. Though it is not perfectly suited for these three-dimensional waves, it delays the instant when reflection cannot be neglected any more. The implementation of a piston having the same kind of movement as the snake wavemker would improve this feature.

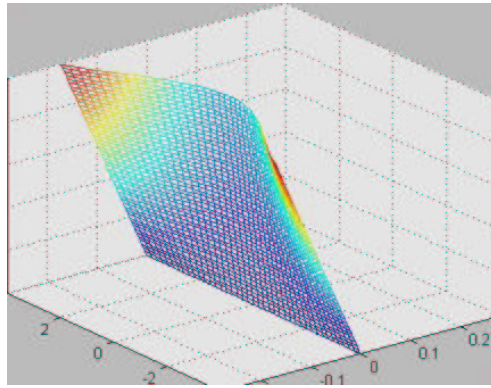


Fig. 2. Illustration of the snake movement of the wavemaker located at the left of the tank.

Results

Figures 4 and 5 present the time evolution of the wave field. Note that only the free surface is shown. The wavemaker progressively sets out in order to reduce the singularities at the interface between the free surface and the moving boundary [3]. We observe the flat free surface at rest which starts to move near the wavemaker and generates a first focused wave of moderate amplitude (Figure 4). Then, the wave amplitude diminishes before disappearing at the graph scale (Figure 5). The studied mechanism effectively produces some local focusing both in time and space. Behind this first wave, we can see a second one which clearly results from the superposition of the wave components with different directions (Figure 5(b),(c)). The amplitude of the wavemaker oscillations increases and

the sum of the wave components gives rise to an extreme wave in the middle of the tank (Figure 5(d),(e)). This one steepens before reaching the focus point, foreseen at $x = 7.5$. At the end time of the simulation, the crest is located at $x = 4.4$ (Figure 5(f)). Behind, we remark that the phenomenon was starting to be repeated with a new curved crest line converging to the center of the basin.

The observation of the free surface shape for this three-dimensional application leads to the following comments. First of all, we see a circular trough located just in front of the wave. Behind it, a deeper trough has formed, separating the main wave from the curved crest line which follows it. This trough has a crescent shape. A strong asymmetry between the back and the front of the wave is observed. Its amplitude is significantly greater than that of the following waves which have not yet converged. This asymmetry increases with time and indicates that the wave is about to break. The wave itself appears like a curved front. In the present case where the directionality is important, the front is not so wide and three-dimensional effects are emphasized (though noting that axes are not at real scale). The observation of this extreme wave gives some geometrical properties found for freak waves. In particular, a vertical slice of the solution at $y = 0$ allows to bring out the shape observed in measured spectra as well as in 2D numerical studies, for instance those about the modulational instability of a wave packet [10]. The crest amplitude is greater than the trough amplitudes, the back trough being deeper (Figure 3). The crest is measured at 0.35, and the back and front troughs are respectively measured at 0.17 and 0.07. It is remarkable that we get such a 2D characteristic shape whereas the mechanism here is only due to the third dimension. This suggests some independence of the wave shape from the causes which generate it.

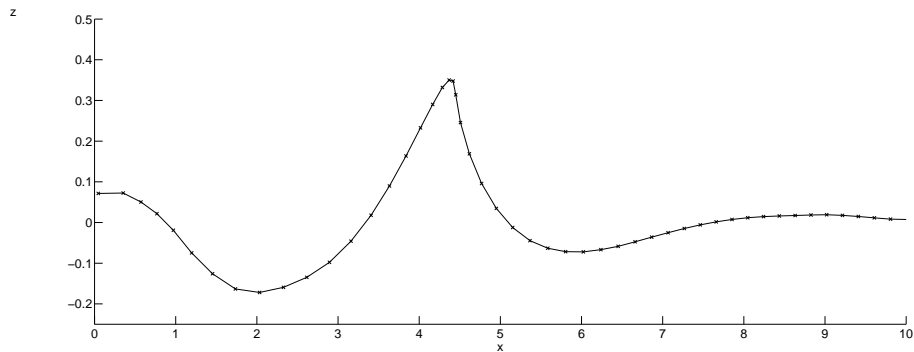


Fig. 3. Vertical slice of the free surface at $y = 0$ and $t = 18.308$.

The observation of the velocity and acceleration fields at the free surface shows two main steps in the evolution of this focused wave event. The first step

is a phase of approach where the different wave components form a crest line converging to a point. The kinematics simply presents the features of the propagation of this curved crest line. The second phase corresponds to the appearance of a unique wave, resulting from the superposition. The maximal value of the longitudinal component of the velocity field increases and the greatest values concentrate more and more at the crest. So this crest tends to go forward faster than the basic wave, thus leading to wave breaking. At the same time, the transverse component of the velocity and acceleration fields shows that three-dimensional effects are reduced on the front face of the wave. This way, the dynamics of the imminent wave breaking approaches an almost 2D configuration. This is in good agreement with some description of a “wall of water”, that we can find in stories about extreme wave events in the ocean.

Conclusion

This paper sums up the numerical method used to study the mechanism of directional focusing in a numerical wave tank. It is based on the solution of incompressible Euler’s equations with a free surface for a potential flow, by a Boundary Element Method [8]. Its more recent improvement is presented. It consists in using the Fast Multipole Algorithm in order to compute faster every matrix-vector product coming from the discretization [6]. This allows to overcome the main drawback of such numerical method, that is to say its computational complexity which is $O(N^2)$. The application consists in observing an extreme wave event generated by the movement of a snake wavemaker. Directional focusing is one of the mechanisms which may take part in the generation of a freak wave. This mechanism is only three-dimensional. Following Brandini and Grilli’s study [3], we define the conditions of the numerical tank which lead to a breaking extreme wave. The description of such a focused wave is done, but the overturning phase could not be obtained until now. We observe that a 2D vertical slice of the solution looks like the characteristic shape observed for freak waves. Its three-dimensional aspect appears as a curved front with a circular trough in front of the wave, followed by a deeper trough with a crescent shape. The kinematics shows two main phases. First, we observe the propagation of a curved crest line converging to one point. When the focused wave is generated, it steepens and the velocity and acceleration vectors on the front face of the wave have a weak transverse component. Therefore, after the focusing phase, the occurrence of wave breaking approaches some essentially two-dimensional dynamics. This corresponds to the aspect of a “wall of water” which appears in some stories of rogue waves in the ocean. The maximal value of the velocity on the crest just before breaking is $0.73\sqrt{gh_0}$, where g is the acceleration due to gravity and h_0 the depth of the tank at rest.

References

1. Bonnefoy F., Le Touze D., Ferrant P., Generation of fully-nonlinear prescribed wave fields using a high-order spectral method, Proc. 14th Offshore and Polar Engng. Conf. (ISOPE 2004), Toulon, France, vol. III, 257–263 (2004).
2. Brandini C., Nonlinear interaction processes in extreme wave dynamics, Ph.D. Dissertation, University of Firenze (2001).
3. Brandini C., Grilli S., Modeling of freak wave generation in a 3D-NWT, Proc. 11th Offshore and Polar Engng. Conf. (ISOPE 2001), Stavanger, Norway, Vol III, 124–131 (2001).
4. Clément A., Coupling of two absorbing boundary conditions for 2D time-domain simulations of free surface gravity waves, *J. Comp. Phys.* **26**, 139–151 (1996).
5. Dalrymple R.A., Directional wavemaker theory with sidewall reflection, *J. Hydraulic Res.* **27** (1), 23–34 (1989).
6. Fochesato C., Dias F., Numerical model using the Fast Multipole Algorithm for nonlinear three-dimensional free-surface waves, prépublication CMLA, 2004.
7. Greengard L., *The Rapid Evaluation of Potential Fields in Particle Systems*, MIT Press, Cambridge, MA, 1988.
8. Grilli S., Guyenne P., Dias F., A fully nonlinear model for three-dimensional overturning waves over arbitrary bottom, *Int. J. Num. Meth. Fluids* **35**, 829–867 (2001).
9. Grilli S.T., Horrillo J, Numerical Generation and Absorption of Fully Nonlinear Periodic Waves, *J. Engng. Mech.* **123** (10), 1060–1069 (1997).
10. Kharif C., Pelinovsky E., Physical mechanisms of the rogue wave phenomenon, *Eur. J. Mech. B-Fluids* **22** (6), 603–634 (2003).
11. She K., Greated C.A., Easson W.J., Experimental study of three-dimensional wave breaking, *J. of Am. Soc. C. E.* **120**, 20–36 (1994).

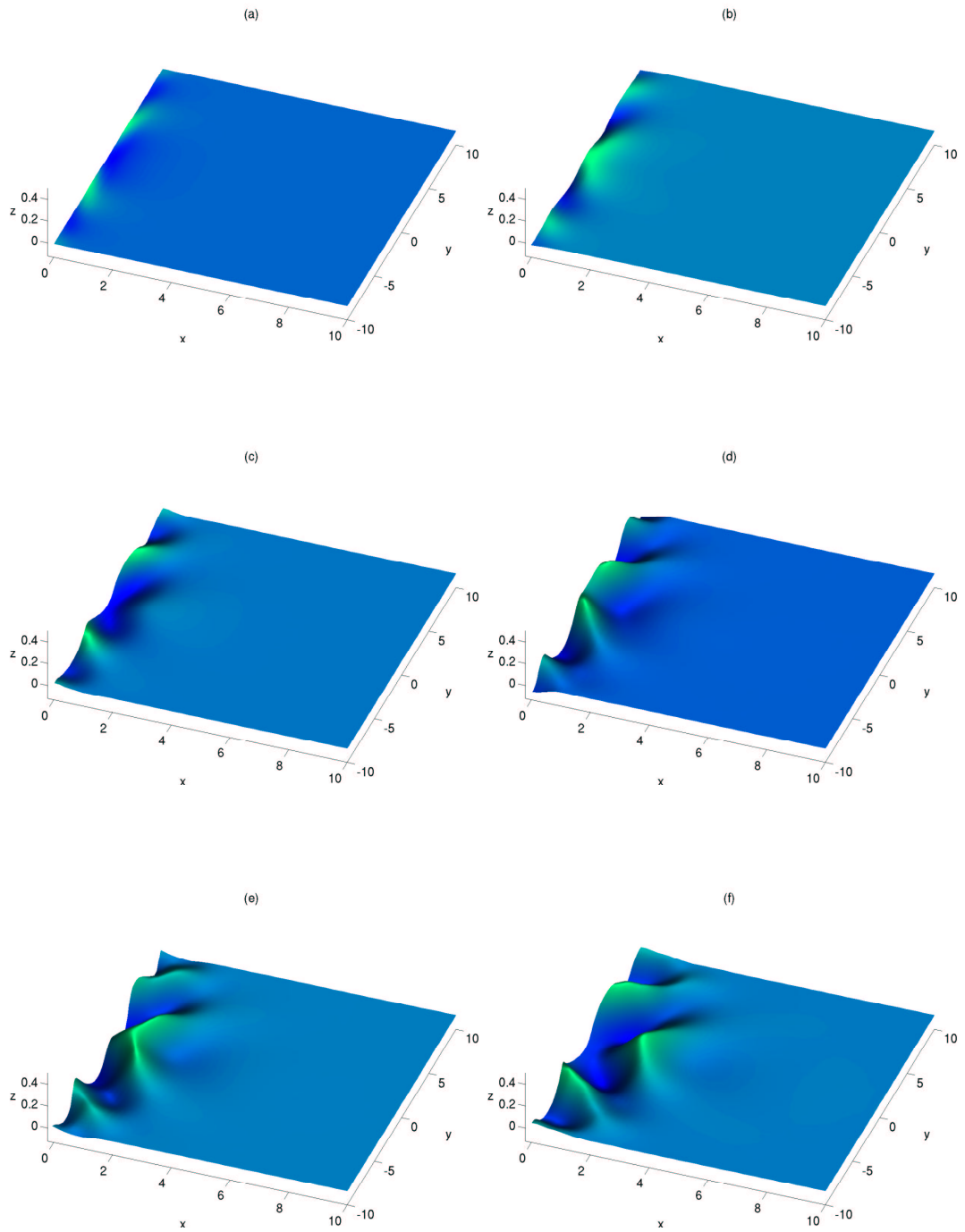


Fig. 4. Evolution of the free surface: (a) at $t = 2.143$, (b) at $t = 4.243$, (c) at $t = 6.231$, (d) at $t = 8.025$, (e) at $t = 9.465$, (f) at $t = 10.974$.

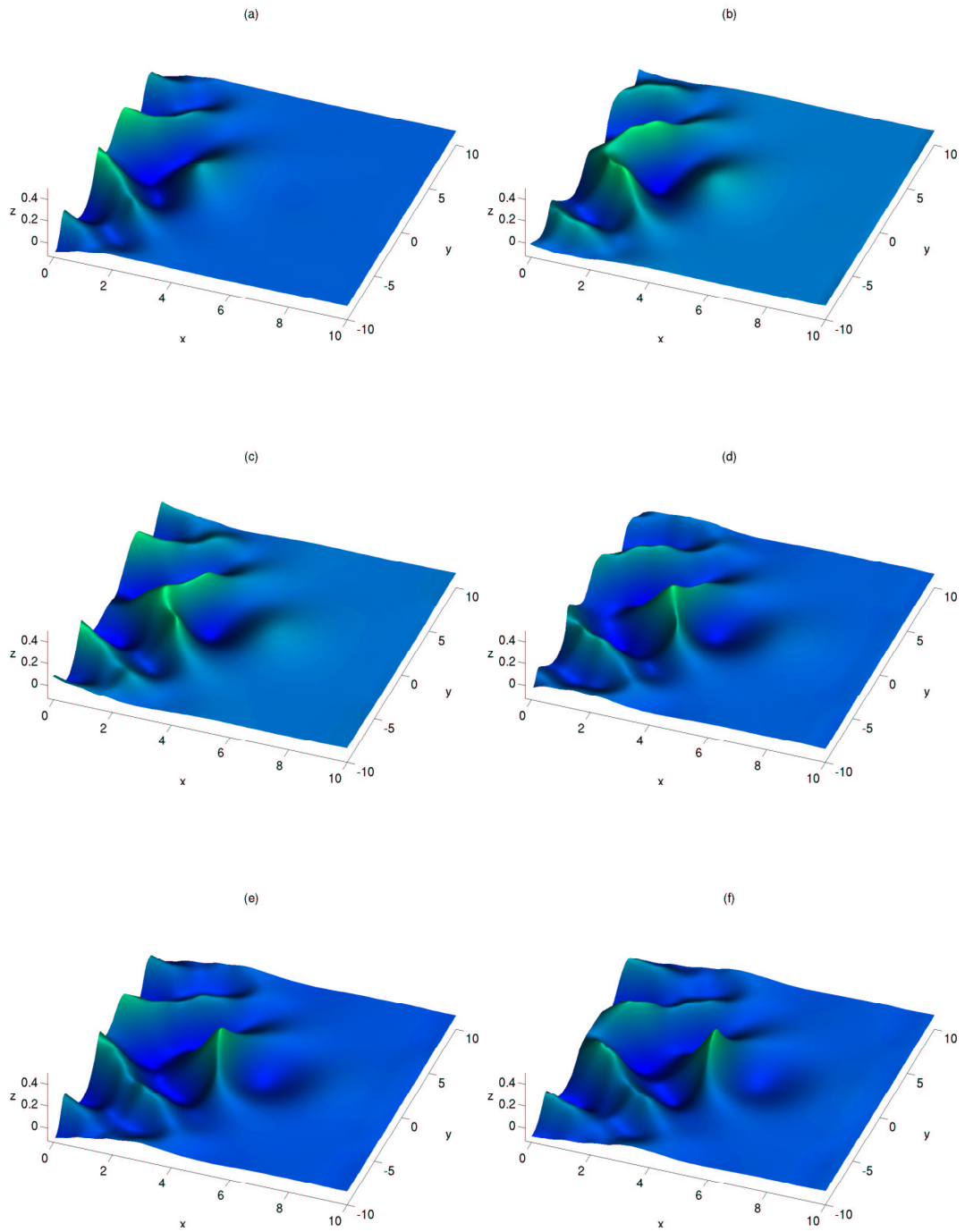


Fig. 5. end of the evolution of the free surface: (a) at $t = 12.639$, (b) at $t = 14.077$, (c) at $t = 15.431$, (d) at $t = 16.640$, (e) at $t = 17.650$, (f) at $t = 18.308$.

Quasi-Resonant Interactions and Non-Gaussian Statistics in long crested waves

Miguel Onorato¹, Alfred Osborne¹, Marina Serio¹, and
Luigi Cavaleri²

¹ Dip. di Fisica Generale, Università di Torino
10100, Torino, Italy

onorato@ph.unito.it, al.osborne@flashnet.it, serio@ph.unito.it

² ISMAR

S. Polo 1364, Venice, Italy
luigi.cavaleri@ismar.cnr.it

Abstract. We compare the statistical properties of long crested surface gravity waves recorded in a long wave tank with numerical results obtained from a modified kinetic equation derived from the Dysthe equation. We find experimentally and theoretically that the statistical properties of the surface elevation depend on the ratio between the steepness and the spectral band-width of the spectrum at the wave maker. We compare successfully the kurtosis computed from the experimental data with the one obtained by the statistical description of the Dysthe equation.

1 Introduction

In the standard weak turbulence theory for surface gravity waves an irreversible transfer of energy between free modes is known to be allowed only if the following resonant conditions are satisfied:

$$\mathbf{k}_1 + \mathbf{k}_2 - \mathbf{k}_3 - \mathbf{k}_4 = 0 \quad (1)$$

$$\omega_1 + \omega_2 - \omega_3 - \omega_4 = 0, \quad (2)$$

where \mathbf{k}_i are wave vectors and ω_i are angular frequencies related to wave number through the dispersion relation. For surface gravity waves in deep water this is a very fundamental result, obtained more than 35 years ago independently by Hasselmann [1] and Zakharov [2]. Starting from the fully nonlinear inviscid equations for surface gravity waves, under a number of assumptions, they were able to derive the so called *kinetic equation* that describes the evolution in time of the wave spectrum. The kinetic equation is of fundamental importance for applicative purposes because it is the base for operational wave models: in order to forecast waves, an approximate version of this kinetic equation is daily numerically solved in many research centers (it should be here mentioned that besides the nonlinear interactions, source terms such as wave breaking and wave forcing by the wind must be included in the energy balance equation).

More recently, it has been found that the modulational instability can be considered as an important mechanism for the formation of large amplitude waves [3],[4],[5]; for random waves the instability is particularly relevant for long crested wave packets, see [6], [7]. In spectral space, the modulational instability can be thought as a four wave interaction process which has the peculiarity of being *quasi-resonant*, i.e. equation (2) is not exactly satisfied, but $|\omega_1 + \omega_2 - \omega_3 - \omega_4| \leq O(\epsilon^2)$. Because of this, the standard kinetic equation cannot in principle describe the dynamics of the modulational instability. Nevertheless, P. Janssen in [8] derived a *kinetic equation* which includes *quasi-resonant interaction* and therefore it is capable of describing the statistical properties of groups of random waves that can become unstable. In [8] a formula for the kurtosis which depends on the wave spectrum of the free waves is also derived.

Here we test these ideas and compare the prediction of the just mentioned *quasi-resonant kinetic equation* with recent experiments performed in a 270 meters wave flume in Norway (Marintek facility) where different JONSWAP spectra, characterized by different steepness and spectral band-width, have been considered as boundary conditions at the wave-maker. Our analysis is concentrated on the evolution of the kurtosis along the tank. In order to compare our experimental results with the theory an evolution equation in space is needed. More in particular, we will build a kinetic equation including four wave quasi-resonant interactions starting from the Dysthe equation written as an evolution in space. The paper is organized as follows: in Section 2, following the approach in [8], we derive from the Dysthe equation the kinetic equation including the quasi-resonant interactions. In Section 3 experimental details are given. Finally experimental and numerical results will be compared in Section 4.

2 Evolution in space of the quasi resonant Kinetic equation

Our aim is here to estimate the kurtosis from the spectral properties of the Dysthe envelope equation (an extension of the nonlinear Schrodinger equation). The approach is the same as the one used by Janssen [8] to derive a kinetic equation from the Zakharov equation [9]; here the only complication is that we are dealing with a boundary-value problem, therefore the kinetic equation should be written as an evolution equation in space rather than in time. Moreover the hypothesis of homogeneity does not hold anymore (as we will see, the statistical properties of the surface elevation changes along the tank) and will be substituted by the hypothesis of stationarity. Here we will just give a short description of the procedure (the interested reader should read [8]).

In order to compare our experimental data with the theory we consider the Dysthe equation written as an evolution equation in space (see for example [10]):

$$\frac{\partial B}{\partial x} + i \frac{k_0}{\omega_0^2} \frac{\partial^2 B}{\partial t^2} + i k_0^3 |B|^2 B - \frac{8k_0^3}{\omega_0} |B|^2 \frac{\partial B}{\partial t} +$$

$$-\frac{2k_0^3}{\omega_0} B^2 \frac{\partial B^*}{\partial t} - i \frac{4k_0^3}{\omega_0^2} B \frac{\partial \bar{\phi}}{\partial t} \Big|_{z=0} = 0, \quad \text{at } z = 0 \quad (3)$$

$$\frac{\partial \bar{\phi}}{\partial z} = -k_0 \frac{\partial |B|^2}{\partial t}, \quad \text{at } z = 0 \quad (4)$$

$$\nabla^2 \bar{\phi} = 0, \quad \text{for } -\infty < z < 0, \quad (5)$$

$$\frac{\partial \bar{\phi}}{\partial z} = 0, \quad \text{at } z = -\infty \quad (6)$$

x is space, t is time, ω_0 and k_0 are respectively the dominant angular frequency and wave-number. B is the complex wave envelope related to the surface elevation η as follows:

$$\eta(x, t) = \bar{\eta} + \frac{1}{2} \left(B(x, t) e^{i(k_0 x - \omega_0 t)} + B^{(2)}(x, t) e^{i2(k_0 x - \omega_0 t)} + \dots + c.c. \right), \quad (7)$$

where $c.c.$ denotes complex conjugate; $\bar{\eta}$ and $B^{(2)}$ are functions of B . This implies that the higher harmonics (and the zero harmonic) are phase locked to the complex envelope B that describes the evolution of free waves. Their explicit forms are given for example in [10]. In order to relate the kurtosis to the spectral properties of the surface elevation, it is useful to write all the equations in frequency Fourier space. Applying the Fourier transform to the set of equations (3-6), we obtain, as expected, the following Dysthe equation:

$$\frac{\partial B_1}{\partial x} - ikB_1 = i \int D_{1,2,3,4} B_2^* B_3 B_4 \delta_{12}^{34} d\omega_{2,3,4}, \quad (8)$$

where $D_{1,2,3,4} = D(\omega_1, \omega_2, \omega_3, \omega_4)$ is the coupling coefficient (its analytical form is given in [11]), $B_i = B(\omega_i)$ and δ_{12}^{34} is just a short notation for $\delta(\omega_1 + \omega_2 - \omega_3 - \omega_4)$. We now consider the contribution to the kurtosis only from free waves (we do not consider the effect of B_2 and $\bar{\eta}$). Using (7), it is straightforward to obtain:

$$kurt = \frac{\langle \eta^4 \rangle}{\langle \eta^2 \rangle^2} = \frac{3}{8} \frac{\langle B_1 B_2 B_3^* B_4^* \rangle}{\langle \eta^2 \rangle^2} \int \delta_{12}^{34} d\omega_{1,2,3,4}, \quad (9)$$

where brackets $\langle \dots \rangle$ stand for ensemble averages. Now we assume that waves are weakly nonlinear (this is also an hypothesis needed for deriving the Dysthe equation) and we split the fourth order correlator as

$$\langle B_1 B_2 B_3^* B_4^* \rangle = \langle B_1 B_3^* \rangle \langle B_2 B_4^* \rangle + \langle B_1 B_4^* \rangle \langle B_2 B_3^* \rangle + C_{1,2,3,4} \quad (10)$$

where $C_{1,2,3,4}$ is the fourth order cumulant which is exactly zero for a Gaussian random process. Using equation (8), we can calculate the evolution of the cumulat $C_{1,2,3,4}$ by making the hypothesis of stationarity, $\langle B_i B_j^* \rangle = N_i \delta(i - j)$. Assuming that the process is Gaussian at $x = 0$ (this is the condition imposed by us at the wave maker), we obtain the following final form for the kurtosis:

$$kurt = 3 + \frac{6}{\langle \eta^2 \rangle^2} \int D_{1,2,3,4} N_1 N_2 N_3 \frac{1 - \text{Cos}(\Delta k x)}{\Delta k} \delta_{12}^{34} d\omega_{1,2,3,4} \quad (11)$$

where $\Delta k = k_3 + k_4 - k_1 - k_2$. An analogous equation for the evolution of the kurtosis in time has been obtained in [8]. In order to compute numerically the evolution of the kurtosis, the evolution of N is needed, therefore, using the standard procedure, we obtain from the deterministic Dysthe equation the following *quasi-resonant kinetic equation*:

$$\frac{\partial N_1}{\partial x} = 4 \int |D_{1,2,3,4}|^2 \frac{\text{Sin}(\Delta k x)}{\Delta k} (N_3 N_4 (N_1 + N_2) - N_1 N_2 (N_3 + N_4)) \delta_{12}^3 d\omega_{2,3,4}$$

Our goal is to verify experimentally the prediction from equation (11). Note that here we have only discussed the contribution to the kurtosis from the interaction of free modes. It should be mentioned that bound modes can also give a contribution that can be included in (11) by using the complete relation between the surface elevation η and the complex envelope B , see [11].

3 Experimental Set-up

The experiment was carried out in the long wave flume at Marintek (see [12] for details). The length of the tank is 270 m and its width is 10.5 m. The depth of the tank is 10 meters for the first 85 meters and then is reduced to 5 meters for the rest of the flume. The effect of the jump from 10 to 5 meters is insignificant for the 1.5 seconds waves considered here. A sloping beach is located at the far end of the tank opposite the wave maker. After half an hour of an irregular wave run with peak period of 1.5 seconds, the wave reflection was estimated to be less than 5%. The wave surface elevation was measured simultaneously by 19 probes placed at different locations along the flume (Figure 1). The sampling frequency for each probe was 40 Hz. JONSWAP random wave signals were synthesized as

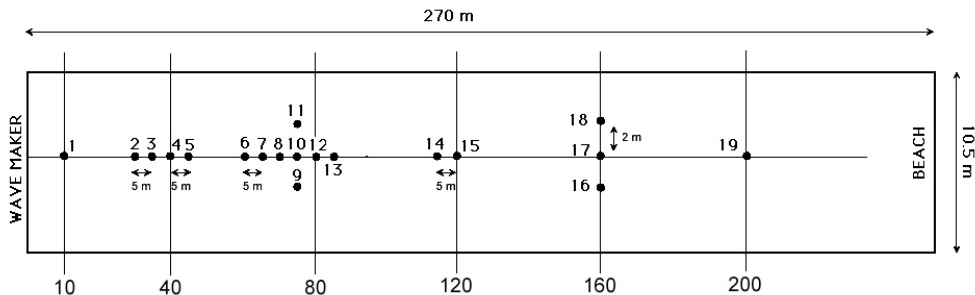


Fig. 1. Schematic of the wave tank facility at Marintek and location of wave probes.

sums of independent harmonic components, by means of the inverse Fast Fourier Transform of complex random Fourier amplitudes. Three different JONSWAP spectra with different values of α and γ have been investigated. All of them

were characterized by a peak period of 1.5 seconds. In Table below we report the parameters that characterized each JONSWAP spectrum. In order to have

<i>Experiment</i>	γ	$H_s(m)$	$\epsilon = k_p H_s / 2$	$\Delta f / f_p$	$\epsilon f_p / \Delta f$
I	6	0.16	0.15	0.08	1.87
II	3.3	0.14	0.13	0.09	1.44
III	1	0.11	0.1	0.28	0.36

Table 1. Parameters of the three different experiments performed at Marintek

sufficiently good statistics, a large number of waves was recorded. Note that the large amount of data is of fundamental importance for the convergence of higher order moments such as the kurtosis: for each type of spectrum, 5 different realizations with different sets of random phases have been performed. The duration of each realization was 32 minutes.

4 Results and conclusions

As mentioned before, we are mainly interested in the evolution of the kurtosis. We recall that for a Gaussian distribution the value of the kurtosis is 3, while

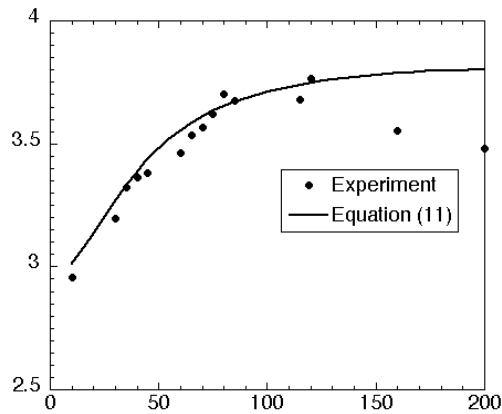


Fig. 2. Evolution of the kurtosis from filtered data for experiment I (see Table 1) and from equation (11).

larger values of kurtosis in a measured time series can give an indication of the presence of extreme events. Deviation from gaussian behaviour of the surface

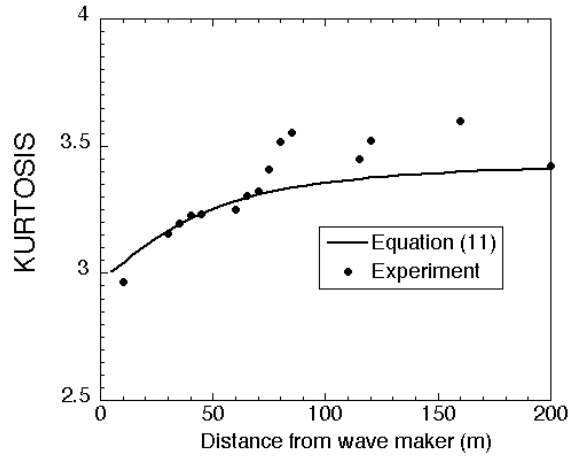


Fig. 3. Evolution of the kurtosis from filtered data for experiment II (see Table 1) and from equation (11).

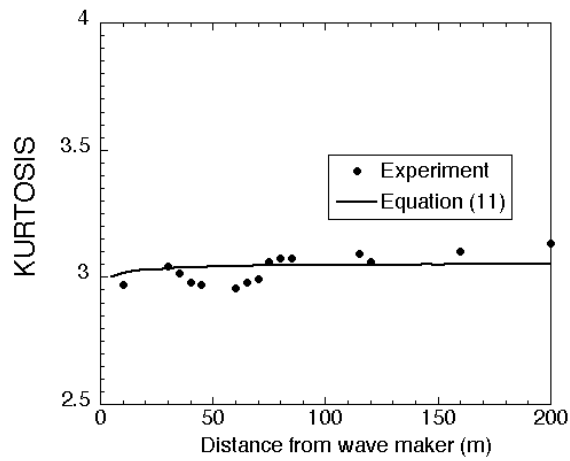


Fig. 4. Evolution of the kurtosis from filtered data for experiment III (see Table 1) and from equation (11).

elevation can possibly be associated to the Stokes contribution, i.e. waves that are phase locked to the peak of the wave spectrum: if ω_p is the dominant angular frequency in the spectrum, then we expect bound modes at $\omega = n\omega_p$ for $n = 2, 3, \dots$. On the other hand the modulational instability is a typical process that takes place between free modes mainly near the peak of the spectrum, therefore close to $\omega = \omega_p$. In order to compare the theory developed (equation 11 is obtained considering only free modes) with experimental data, the free waves should be extracted from the time series. This is not an easy task, therefore here we simply filter our data by excluding all the frequencies larger than 1.1 Hz . By doing this we are confident that our filtered data do not have any contribution from the phase locked second, third and so on harmonics. In other words we build new time series in which the Stokes contribution has been removed. The second step consists in calculating the kurtosis on the filtered data and in comparing it with the kurtosis of the original data. In Figures 2- 4 we show the evolution along the tank of the kurtosis for the three experiments compared with equation (11). For the first two experiments, kurtosis grows quite rapidly and reaches its maximum between 25 and 30 wave lengths from the wave maker. For the third experiment, the kurtosis remains very close to the gaussian value. The qualitative behaviour of all three experiment is well captured by the theory previously described. Our figure 4 is also consistent with preliminary results obtained for the unfiltered kurtosis for experiment I in [13]. The results suggests a significant dependence of the statistical properties of surface gravity waves on the spectral shape of the initial spectrum. In particular, as it has been discussed in other papers ([4], [8]), the so called Benjamin Feir Index, given by the ratio between the steepness and the spectral band-width, plays an important role for determining the statistical properties of long crested waves. Although the comparison between theory and experiment can be considered as quite successful, we are unable to reproduce “exactly” the experimental data (see figure 4 where at the last probe the theory overestimates substantially the value of the kurtosis). Nevertheless, it should be mentioned that the model contains only the weakly nonlinear interactions in one dimensions, therefore three dimensional instabilities or wave breaking are not considered. Here we recall that any second order theory would give a very small contribution to the kurtosis with respect to the observed experimental data, [11]. As a final conclusion, we may state with some confidence that the BFI plays an important role for determining the statistical properties of surface elevation for the present experiment. We should recall here that the Benjamin-Feir-Index has been derived for long crested, narrow banded waves in deep water [4],[8], therefore it should be used with care for any other physical condition.

Acknowledgments This research has been supported by the Improving Human Potential - Transnational Access to Research Infrastructures Programme of the European Commission under the contract HPRI-CT-2001-00176. M.O., A.R.O and M.S. acknowledge MIUR (PRIN project) for support. We thank C.T. Stansberg and C. Brandini for their help during experiments at Maritek.

P. Janssen is also acknowledged for discussions during the early stages of this work.

References

1. HASSELMANN, K. "On the non-linear energy transfer in a gravity wave spectrum, part 1: general theory" *J. Fluid Mech.* **12**, 481 (1962)
2. ZAKHAROV, V AND FILONENKO, N.N. 1966 "Energy spectrum for stochastic oscillations of the surface of a liquid" *Soviet Phys. Dokl.* **11**,881 (1967)
3. TRULSEN, K. AND DYSTHE, K.B. "Freak Waves - A three-dimensional wave simulation" *Proceedings of the 21st Symposium on Naval Hydrodynamics (National Academy Press, Washington, DC, 1997)*, 550-560 (1997)
4. ONORATO, M., OSBORNE, A.R., SERIO, BERTONE, S. "Freak waves in random oceanic sea states" *Phys. Rev. Letters* **86**, 5831 (2001) see also ONORATO, M., OSBORNE, A.R., SERIO, M., DAMIANI, T. "Occurrence of Freak Waves from Envelope Equations in Random Ocean Wave Simulations" *Rogue Wave 2000, (Ifremer, Brest 29,30 November 2000)*, eds. M. Olagnon and G.A. Athanassoulis 181 (2000)
5. YASUDA, T. AND MORI, N. "High order nonlinear effects on deep-water random wave trains" *International Symposium: Waves-Physical and Numerical Modelling* **2**, 823 Vancouver (1994).
6. ONORATO, M., OSBORNE, A.R., SERIO "Extreme wave events in directional, random oceanic sea states" *Phys. of Fluids* **14**, L25-L28, (2002).
7. SOCQUET-JUGLARD, H., DYSTHE K., TRULSEN, K. KROGSTAD, H., LIU, J. 2004 "Distribution of extreme waves by simulations" *Proceedings of Rogue Waves 2004, Brest, 20-22 October* (2004)
8. JANSSEN, P. A. E. M. "Nonlinear Four-Wave Interactions and Freak Waves" *J. Physical Ocean.* **33**, 863 (2003)
9. ZAKHAROV, V. "Stability of of periodic waves of finite amplitude on the surface of a deep fluid" *J. Appl. Mech. Techn. Phys.* **9** 190 (1968)
10. TRULSEN, K. AND STANSBERG, C.T. "Spatial Evolution of Water Surface Waves: Numerical Simulation and Experiment of Bichromatic Waves" *Proceedings of the Eleventh (2001) International Offshore and Polar Engineering Conference*, 72 (2001)
11. ONORATO, M. ET AL. 2005 *In preparation*
12. STANSBERG, C. T. " Propagation-dependent spatial variations observed in wave trains generated in a long wave tank". *Data Report 490030.01 Marintek, Sintef group, Trondheim* (1993)
13. JANSSEN, P. A. E. M. AND BIDLOT, J. "New wave parameters to characterize Freak Wave Conditions" *Memorandum Research Department, R60.9/PJ/0387, ECMWF* October (2003)

SPH: Towards the simulation of wave-body interactions in extreme seas

Guillaume Oger, Mathieu Doring, Bertrand Alessandrini, and Pierre Ferrant

Fluid Mechanics Laboratory (CNRS UMR6598)
Ecole Centrale de Nantes, FRANCE
guillaume.oger@ec-nantes.fr

Abstract Water entry of a solid through a free surface is of interest in ship hydrodynamics applications, namely to study ships behavior in slamming cases for instance. The present study deals with the introduction of an enhancement of SPH method, and aiming at an accurate numerical prediction of the free motion of a body in a free surface flow. The validation case exposed here is the water entry of a massive wedge, and comparisons with experimental data are provided.

INTRODUCTION

Recent advances in the field of free surface flows allowed the computation of breaking and reconnection of interface through the development of interface capturing methods such as Level Set or Volume Of Fluid. Nevertheless the inclusion of a free solid in this kind of approach remains rather complicated, due to the need of a specific treatment of the solid. "Smooth Particles Hydrodynamics" is a recent compressible Lagrangian method whose flexibility and robustness allow to solve complex free surface flows [1] [2] [3]. Concerning the computation of free solid motion, SPH avoids problems related to mesh managing but a numerical method to evaluate loads on solid boundaries had to be developed. This has been achieved through a new method consisting in calculating forces on the solid from fluid flow characteristic (Pressure, Velocity). To evaluate the accuracy of this new scheme, some results concerning a wedge water entry are provided, including comparison of dynamic condition (accelerations) with experimental data. A very good agreement is obtained, confirming the effectiveness and the accuracy of the proposed scheme. The next step consists in the simulation of steep waves interactions with a floating body. Preliminary simulations in such a situation shows a qualitatively satisfying behavior of the model, although a complete validation is still needed. As an illustration, the time evolution of a pierced box in interaction with waves is given at the end of this paper, proving the ability for this improved SPH scheme to handle some complex coupled interior-exterior fluid-solid computations such as a sinking vessel in waves.

SPH SOLVER

SPH methods are based on a set of interpolating points which are chosen in the medium. Using an interaction function (Kernel function), these points can

be used to discretise partial differential equations without any underlying mesh. For free surface flows, the equations we solved are Euler equations (1, 2) and an equation of state for the pressure which is called Tait's equation (3).

$$\frac{d\mathbf{v}}{dt} = \mathbf{g} - \frac{\nabla P}{\rho} \quad (1)$$

$$\frac{d\rho}{dt} = -\rho \cdot \nabla \cdot \mathbf{v} \quad (2)$$

$$P = \kappa \left(\left(\frac{\rho}{\rho_0} \right)^7 - 1 \right) \quad (3)$$

The use of this equation of state allows to avoid an expensive resolution of Poisson equation. Incompressible flows are obtained as weakly compressible flows: if the Mach number remains below 0.1 during the whole simulation, the flow can be regarded as incompressible.

The kernel function which approximates a Dirac distribution, is used to discretise previous equations through a convolution with the variables (velocity, pressure, density...).

$$W(q = \frac{|\mathbf{r}|}{h}) = C \begin{cases} \frac{2}{3} - q^2 + \frac{1}{2}q^3 & \text{if } 0 \leq q < 1 \\ \frac{1}{6}(2 - q)^3 & \text{if } 1 \leq q < 2 \\ 0 & \text{else} \end{cases} \quad (4)$$

Particles carry all informations concerning the flow (velocity, pressure, density ...). To enhance the numerical performance, such as conservation of linear momentum, the formulae are symmetrized [4] leading to the following scheme, where i -subscripted variables correspond to the i^{th} particle:

$$\frac{d\mathbf{x}_i}{dt} = \mathbf{v}_i \quad (5)$$

$$\frac{d\mathbf{v}_i}{dt} = \mathbf{g} - \sum_j m_j \left(\frac{P_i}{\rho_i^2} + \frac{P_j}{\rho_j^2} + \Pi_{ij} \right) \nabla W(\mathbf{r}_i - \mathbf{r}_j) \quad (6)$$

$$\frac{d\rho_i}{dt} = -\sum_j m_j (\mathbf{v}_i - \mathbf{v}_j) \cdot \nabla W(\mathbf{r}_i - \mathbf{r}_j) \quad (7)$$

In order to avoid a centered scheme which would lead to numerical instability, an artificial viscosity term Π_{ij} is added following Monaghan ([4]). This ordinary differential equation system can be integrated in time by schemes such as Runge-Kutta, Leap-Frog or Predictor-Corrector to ensure at least second order convergence in time. In this paper, a third order Runge-Kutta scheme was used.

To this point, a standard SPH scheme has been presented. This scheme has been enhanced to be able to deal with solids in free motion. It can be found in SPH related literature some applications of SPH scheme to the specific case of a wedge water entry [5].

However in this reference, the coupling between fluid and solid body motion is not solved: either the wedge is supposed to be deformable and is modeled by SPH particles with a specific equation of state which describes metal behavior, or the motion of the wedge is imposed. In the case of a deformable wedge, the computation of deformations of the body through the motion of solid particles leads to very small and restrictive time steps.

To evaluate efforts on an undeformable body, a numerical method had to be developed. This means :

1. evaluation of forces on the solid boundaries: the pressure is interpolated from the water particles which are located in the neighborhood of the solid. Indeed pressure at the boundary particles was found to be too oscillating to give satisfying results.
2. integration of the pressure effort along the solid boundaries: this is done through a low order trapezoidal rule. An increase in the order of accuracy of this quadrature formula would give better estimation of effort on the solid, this will be investigated in the near future.
3. updating of solid position and velocity: given accelerations on the solid, position and velocity are updated together with flow features using an ODE integrator (third order Runge-Kutta in this paper).

Since viscous terms are neglected in this paper, Euler equations are to be solved, and pressure loads only are evaluated.

WEDGE WATER ENTRY

These methods will be applied to the standard validation test case of a free-fall impact of a wedge. In this paper we chose the case of an asymmetric drop test of a light wedge given in [6].

At $t=0$ s, this free-falling wedge is dropped from 0.61 meters above the free surface with a five degrees clockwise initial heel angle and no initial velocity. Its two knuckle angles are both fitted with accelerometers dedicated to the measurement of angular and vertical accelerations. After a free fall in the air, the wedge enters the free surface. This impact generates a large deformation of the free surface and imposes a strong vertical deceleration as well as a transverse self-righting of the solid. Experiments are supposed to be realized so that no reflexion of pressure waves interacts with the wedge and the flow can be regarded as two-dimensional.

In the SPH simulation, the numerical set-up has been adapted : the tank size has been chosen to ensure no interaction between the wedge and the sound wave generated by the impact. Concerning numerical parameters, about 350,000 irregularly spaced water particles were used to achieve this computation. The smoothing length was about 14 millimeters. An adaptive time step based on

Courant condition (with a Courant number lower than 0.25), is implemented in order to reduce the computational time. The typical time step in the impact phase was of order 10^{-5} second. Since air is neglected in this SPH simulation, it was useless to simulate the whole free fall of the wedge. Thus, the initial conditions imposed in this computation are the dynamic features of the wedge at the experimental impact instant.

As can be seen in figure 1, the temporal evolution of the vertical acceleration of the wedge is well predicted in comparison with experimental data. More precisely, the maximum load at $t = 0.365$ s seems to be accurately evaluated in time as well as in amplitude in the SPH simulation. Nevertheless it should be noticed that in this SPH simulation, some features of the flow in the early stage of the impact are not well captured. Indeed, in this simulation we can see some differences at the very beginning of the impact: the slope of the temporal evolution of the vertical acceleration estimated using SPH is stiffer than in the experiment. Preliminary results of two-phase SPH simulations seem to confirm the origin of these differences to be due to air influence.

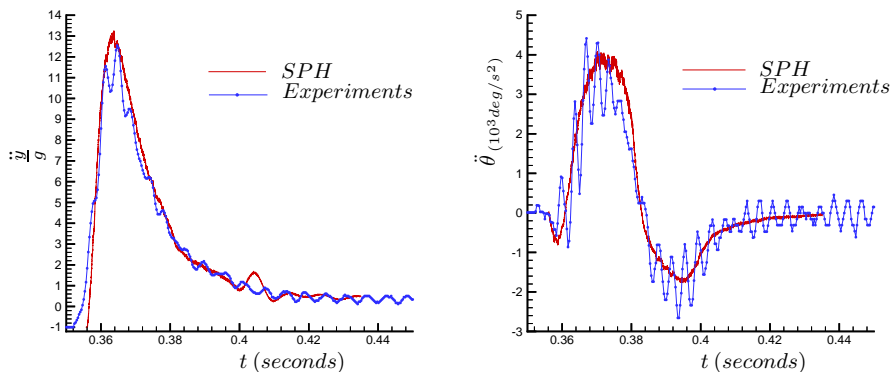


Figure 1: *Temporal evolution of the wedge vertical and angular accelerations*

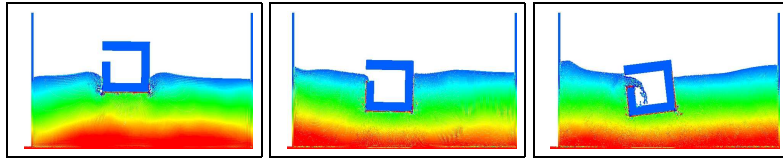
The global behavior of the solid in terms of angular acceleration is also well evaluated, despite the difficulty of comparison due to the noise on the experimental signal. Note that this noise is due to structural vibrations [6], that cannot be captured by our SPH simulation since we consider the numerical wedge as non deformable.

CONCLUSION

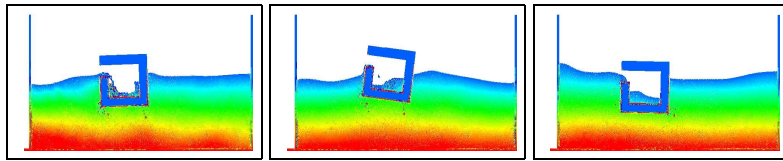
In this paper, a new method in the field of SPH has been briefly presented. The standard SPH scheme has been enhanced with a particles sampling method which makes it able to simulate the free motion of solids in interaction with complex free surface flows including jets for instance. In the standard test case of the wedge water entry, results obtained using this approach have been compared to experimental data showing promising agreement. The main effects that occur in this specific problem are captured with a good accuracy. Future works will focus on the development of a two-phase SPH solver, in order to take into account the air-cushion effects at the very beginning of the wedge impact for instance. Furthermore, validation of this load evaluation method on other test cases would be of interest, namely once applied to industrial cases.

References

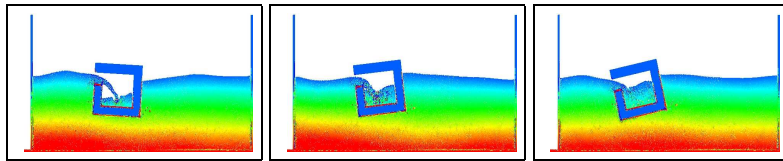
1. J. J. Monaghan. Simulating free surface flows with SPH. *Journal of Computational Physics*, 110:399–406, 1994.
2. Y. Andrillon, M. Doring, P. Ferrant, and B. Alessandrini. Simulation d'écoulement à surface libre complexe au moyen de méthodes SPH et VOF. In *Proceedings des 9^{èmes} Journées de l'Hydrodynamique*, Mars 2003.
3. M. Doring, Y. Andrillon, P. Ferrant, and B. Alessandrini. SPH free surface flow simulation. In *Proceedings of the 18th International Workshop on Water Waves and Floating Bodies*, April 2003.
4. J. J. Monaghan. Smoothed particle hydrodynamics. *Annu. Rev. Astron. Astrophys.*, 30:543–574, 1992.
5. J. P. Vila and A. Rompoteaux. Calcul du tossage avec Smart Fluids un code de calcul particulaire compressible. In *Proceedings des 7^{èmes} Journées de l'Hydrodynamique*, 1999.
6. R. Petterson L. Xu, A. W. Troesch. Asymmetric hydrodynamic impact and dynamic response of vessels. *Proceedings of 17th International Conference on OFFSHORE MECHANICS and ARCTIC ENGINEERING*, pages 98–320, 1998.



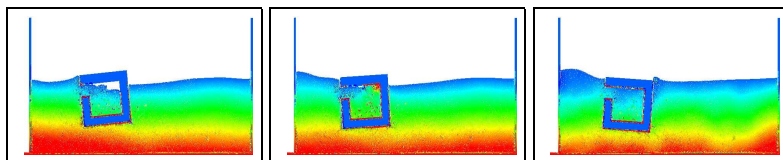
(a) $T = 0.45 \text{ s}$, $T = 0.95 \text{ s}$, and $T = 1.45 \text{ s}$



(b) $T = 1.95 \text{ s}$, $T = 2.45 \text{ s}$, and $T = 3.45 \text{ s}$



(c) $T = 3.95 \text{ s}$, $T = 4.45 \text{ s}$, and $T = 4.95 \text{ s}$



(d) $T = 5.45 \text{ s}$, $T = 5.70 \text{ s}$, and $T = 5.95 \text{ s}$

Figure2: *Time evolution of a crude sinking vessel*

Self-Similarity of Wind-Wave Spectra. Numerical and Theoretical Studies

Sergei I. Badulin¹, Andrei N. Pushkarev^{2,3}, Donald Resio⁴, and
Vladimir E. Zakharov^{2,5}

¹ P.P.Shirshov Institute of Oceanology, Moscow, Russia
`bsi@wave.sio.rssi.ru`

² Waves and Solitons LLC, Phoenix, Arizona, USA
`andrei@cox.net`

³ Landau Institute for Theoretical Physics, Moscow, Russia

⁴ Coastal and Hydraulics Laboratory, Massachusetts, USA
`Donald.T.Resio@erdc.usace.army.mil`

⁵ University of Arizona, Tucson, USA
`zakharov@math.arizona.edu`

Abstract. Results of theoretical and numerical studies of the Hasselmann kinetic equation for wind waves are presented. Approximate self-similar solutions for duration-limited and fetch-limited wind-wave growth are analyzed and related with the classic Kolmogorov spectra of the weak turbulence theory. It is shown that these solutions can be considered as non-stationary and non-homogeneous generalization of these spectra. The experimental parameterizations like JONSWAP spectrum, that have features of self-similarity, give a solid basis for comparison with the theoretical predictions. The comparison is detailed in extensive numerical studies of duration-limited growth of wind waves basing on the algorithm by Webb [20] first realized by Resio & Perrie [16]. Strong tendency of numerical solutions to self-similar behaviour is shown for rather wide range of conditions of wave generation and dissipation. A composite model of wind-wave balance is proposed for description of the self-similar fraction of wind-wave field: the shapes of the solutions are described by the “conservative” Hasselmann equation while the wave growth is determined by the balance equation for generation and dissipation in an integral form. The shapes of the self-similar spectra display perfect coincidence with the spectra measured in the JONSWAP and other major fetch-limited studies, while parameters of wave growth governed by the balance equation are consistent with experimental dependencies of total wave energy and mean frequency on time.

1 Introduction

The rogue waves in the ocean do not exist on their own. Their appearance and transformation is closely linked with environmental conditions and, first of all, with the wind-wave state.

Spectral description is widely used to describe the wind-wave field and its evolution in time and space. Experimental parameterizations of the spectra imply

self-similar and quasi-universal dependencies of the spectra on a set of non-dimensional parameters. E.g. the widely used modified JONSWAP spectrum [5, 4] has exactly the form of the so-called incomplete or the second type self-similar dependence

$$E(\omega) = \alpha_T g^2 \omega^{-4} \omega_p^{-1} \exp \left[\left(\frac{\omega}{\omega_p} \right)^{-4} \right] \gamma^{\exp[-\frac{(\omega-\omega_p)^2}{2\sigma_p^2 \omega_p^2}]} \quad (1)$$

where the spectrum shape depends on an “internal” parameter — non-dimensional frequency ω/ω_p , while the dependence of α_T on an “external” parameter — inverse wave age $U_{10}/C_p = \omega_p U_{10}/g$ is generally fitted by power-like approximation [21]

$$\alpha_T = \alpha_0 (U_{10} \omega_p / g)^{\kappa_\alpha} \quad (2)$$

Hereafter C_p and ω_p are phase speed and frequency of the peak component of wave spectra and wind speed U_h is taken at some reference height h . For α_0 we accept the estimate [1]:

$$\alpha_0 = 0.08 / (2\pi) \quad (3)$$

The standard set of shape parameters was proposed as a good fit for the JONSWAP data

$$\begin{aligned} \gamma &= 3.3; \\ \sigma &= \begin{cases} \sigma_a = 0.07 & \text{for } \omega \leq \omega_p; \\ \sigma_b = 0.09 & \text{for } \omega > \omega_p \end{cases} \end{aligned} \quad (4, 5)$$

Wave spectra at different stages of wave development can differ considerably from the “universal” parameterization (1) with fixed shape parameters (4, 5). Later basing on analysis of various wave data these parameters have been treated as functions of wind-wave conditions, first of all, of wave age.

Probability of rogue waves can show significant correlation with the spectral shapes variability, in particular, with the peakedness parameter γ [7, 12, 13]. Thus, more accurate description and forecasting of wind-wave spectra (not integral or mean characteristics of waves only) may be useful for prediction of rogue wave events.

In this paper we present recent results of theoretical and numerical studies of the Hasselmann kinetic equation that is a basis of many wave prediction models such as WAM and SWAN. This equation describes evolution of spectral densities of wave action $N(\mathbf{k})$ (or energy $E(\mathbf{k})$) as a result of nonlinear transfer due to four-wave resonant interactions and numerous mechanisms of wave generation and dissipation (wind impact, turbulence etc.)

$$\frac{\partial N_{\mathbf{k}}}{\partial t} + \nabla_{\mathbf{k}} \omega_{\mathbf{k}} \nabla_{\mathbf{r}} N_{\mathbf{k}} = S_{nl} + S_{in} + S_{diss} \quad (6)$$

While the nonlinear transfer term S_{nl} is known “from the first principles” the knowledge of wave input S_{in} and generation S_{diss} terms is based mainly on experimental parameterizations. The dispersion of wave input terms S_{in} given

by different authors is comparable in magnitude with the terms themselves. This raises the evident question: whether the models can provide a reliable wave forecasting when there is the uncertainty in source functions in (6)?

The message of the study:

The nonlinear transfer is a dominating mechanism of developing wind-wave spectra and, thus, basic features of the spectra evolution can be predicted quite well without knowledge of details of non-conservative terms S_{in} and S_{diss} .

In §2 the theoretical analysis of the asymptotic self-similar solutions of the Hasselmann equation is presented. We show that the self-similar behaviour of wind-wave spectra is a result of the dominating non-linear transfer as compared with wave input and dissipation.

In §3 we consider numerical solutions of the Hasselmann equation for different functions of wave input and find that the self-similar behaviour of these solutions shows universality features, i.e. spectral shapes depend very slightly on parameters of wave input.

In §4 we analyse variations of the numerical solutions from a universal shape and show that these solutions can be presented effectively as a self-similar “core” superimposed on a non-self-similar background. The evolution of the self-similar core depends rather slightly on the particular wave input function S_{in} and, thus, the parameters of the core — the peak frequency and the spectral peak magnitude can be predicted better than mean frequency and total wave energy contaminated by non-self-similar wave background.

In Discussion we propose a composite model of evolution of wind-wave spectra basing on the concept of self-similarity and universality of spectra of wind-driven waves.

2 Self-Similar Solutions for the Hasselmann Equation

The Hasselmann equation [8] is a subject of the theory of weak turbulence. The key point of the theory is investigation of the stationary kinetic equation

$$S_{nl} = 0 \quad (7)$$

The Rayleigh-Jeans solutions describe local balance of each resonant quadruplet of water wave harmonics, while the so-called Kolmogorov-Zakharov (KZ) solutions correspond to a dynamical equilibrium when input and output for each element of the nonlinear system are balanced, i.e. spectral fluxes of integrals of motion are constant. Two solutions of this type play a fundamental role: the direct cascade solution with a constant flux of energy from large to small wave scales [22] and the inverse cascade solution that describes a constant flux of wave action to long waves [23]. These solutions are usually considered as irrelevant to wind-wave problems because they are isotropic and non-localized in wave scales.

A generalization of the KZ solutions can be found for “conservative” non-stationary or non-homogeneous kinetic equations that model duration-limited

$$\frac{\partial N_{\mathbf{k}}}{\partial t} = S_{nl} \quad (8)$$

or fetch-limited growth [24] of wind-driven waves in x direction

$$\frac{\partial \omega}{\partial k_x} \frac{\partial N_{\mathbf{k}}}{\partial x} = S_{nl} \quad (9)$$

Further we shall discuss the duration-limited case only, the fetch-limited case can be analysed similarly. Details can be found in [2, 3]. The models (8, 9) do not contain terms or wave input or dissipation. In fact, sources and sinks are implied at infinitely small and at infinitely large wave scales quite similarly to the constant flux KZ solutions. The homogeneity property of the collision integral

$$S_{nl} \sim N^3 |\mathbf{k}|^{19/2} \quad (10)$$

allows for constructing non-stationary anisotropic self-similar solutions in the form (duration-limited case)

$$N(\boldsymbol{\xi}) = at^\alpha U_\beta(\boldsymbol{\xi}) \quad (11)$$

where the self-similar variable $\boldsymbol{\xi} = b\mathbf{k}t^\beta$ and the solution parameters obey

$$a = b^{19/4}, \quad \alpha = (19\beta - 2)/4 \quad (12)$$

The exponents α and β can be determined from the condition of power-like growth of total wave action

$$N_{tot} \sim \int N(\boldsymbol{\xi}, t) d\mathbf{k} \sim b^{11/4} t^r \quad (13)$$

As already noted, the self-similar solutions (11) with parameters defined by (12, 13) imply sources (sinks). The integral condition (13) replaces wave input and dissipation term in the generic Hasselmann equation (6). One has for the exponent of wave action growth

$$r = \alpha - 2\beta = (11\beta - 2)/4 = (11\alpha - 4)/19 \quad (14)$$

For the total wave energy $E_{tot} \sim t^p$ one gets

$$p = \alpha - 5\beta/2 = (11\beta - 4)/4 = (9\alpha - 5)/19 \quad (15)$$

The ‘‘shape’’ function $U_\beta(\boldsymbol{\xi})$ satisfies the equation in self-similar variables that resembles a stationary kinetic equation with a special source term

$$\alpha U_\beta + \beta \boldsymbol{\xi} \nabla_{\boldsymbol{\xi}} U_\beta = S_{nl}[U(\boldsymbol{\xi})] \quad (16)$$

In fact, we split the Hasselmann equation into two parts. The first one (16) gives a shape of the solutions, while the condition (13) describes an integral balance of wave action. This composite model of the wind-wave balance implies that the nonlinear transfer dominates as compared with wave input and, thus, the latter

can be taken into account in the integral form (13). A simple estimate of validity of such substitution gives for the duration-limited case

$$\alpha > 1; \quad r > 7/19 \quad (17)$$

— the solution should grow fast enough for the nonlinearity to be dominating over the wave input and dissipation terms. The result is physically transparent — the strong non-linear transfer requires strong non-stationarity. In fact, the effect of dominating collision integral S_{nl} in the kinetic equation can be justified correctly in numerical experiments only.

3 Quasi-Universality of Wind-Wave Spectra

Extensive numerical studies of the Hasselmann equation (6) for different wave input parameterizations [6, 11, 17, 14, 18] has been carried out recently basing on the Resio & Perrie approach [16] improved by Pushkarev [15]. The analysis of the numerical solutions was focused on features of self-similarity of wind-wave spectra. The form of the approximate self-similar solutions (11) allows for a time-independent presentation of the solution and, thus, for an analysis of dependencies in terms of non-dimensional wave frequencies. Using the freedom in scaling parameters a and b in (12) one can let

$$\xi = b|\mathbf{k}|t^\beta = (\omega/\omega_p)^2; \quad U_\beta(1) = 1 \quad (18)$$

Quite similarly to the parameterizations of wind-wave spectra (e.g. eq.1) one has a form of the second-type self-similar dependence in terms of non-dimensional frequency (“internal” variable) and an “external” combination of the scaling parameters a , b and the solution peak frequency — a straightforward analogue of wind-wave age. These dependencies can be analysed separately in order to check the idea of self-similarity of the numerical solutions.

Two large series of experiments were carried out. First, the “academic” experiments with special input functions in (6) have been targeted at obtaining the self-similarity properties “in pure” state in the wide range of the key parameter of self-similarity r — the exponent of total wave action growth. All the experiments showed very strong tendency of the numerical solutions to the asymptotic self-similar behaviour. Moreover, the “shape” functions $U_\beta(\xi)$ (18) for different β (or r) were found to be rather close to each other. In other words, the shapes of the asymptotic solutions turn out to be quasi-universal, independent of input function S_{in} .

The results of the “academic” series have been used as a reference for the second series of numerical experiments with realistic input functions given by experimental parameterizations [6, 11, 17, 14, 18]. The similar strong tendency to self-similar behaviour has been observed in this case and, quite like to the “academic” experiments, the shape functions $U_\beta(\xi)$ have been found to be quasi-universal. Fig.1 illustrates this result for parameterizations of input functions by Snyder et al. [17], Hsiao & Shemdin [11] and swell. The normalized dependence

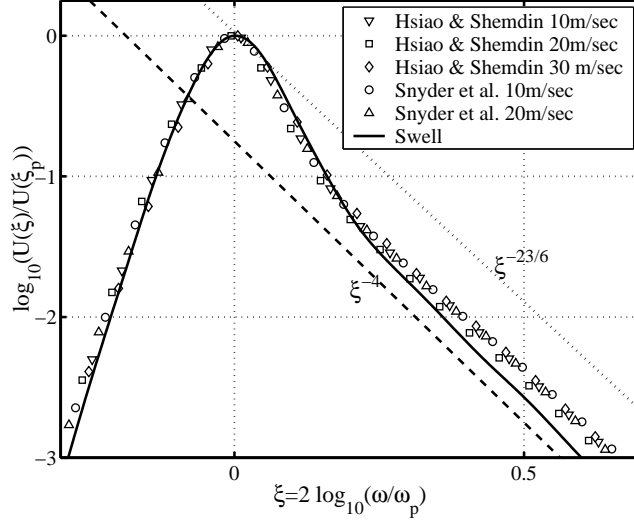


Fig. 1. Normalized spatial spectra of wave action $U_\beta(\xi)/U_\beta(\xi_p)$ for down-wind direction as functions of non-dimensional frequency ω/ω_p for different wave input parameterizations and wind speeds (shown in legend). The JONSWAP spectrum for the standard peakedness $\gamma = 3.3$ is shown by dashed curve. Power laws for stationary Kolmogorov's solutions are shown by dashed (ω^{-4} — direct cascade) and dotted lines ($\omega^{-23/6}$ — inverse cascade).

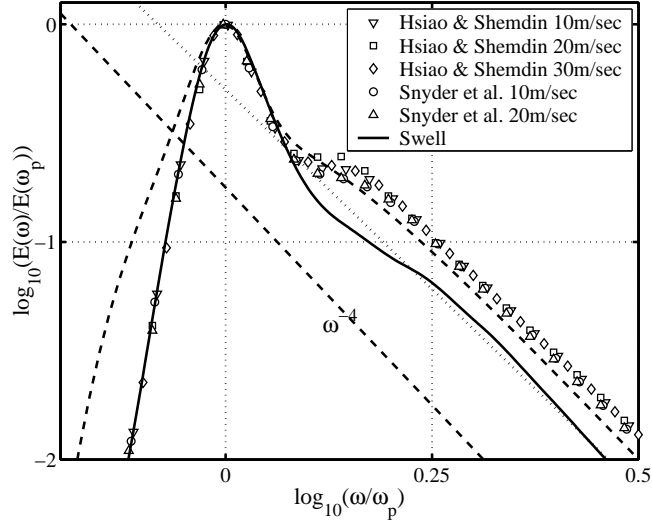


Fig. 2. Normalized frequency spectra $E(\omega)/E(\omega_p)$ as functions of non-dimensional frequency ω/ω_p for different wave input parameterizations and wind speeds (shown in legend). The JONSWAP spectrum for the standard peakedness $\gamma = 3.3$ is shown by dashed curve. Power laws for stationary Kolmogorov's solutions are shown by dashed (ω^{-4} — direct cascade) and dotted lines ($\omega^{-11/3}$ — inverse cascade).

$U_\beta(\xi)/U_\beta(\xi_p)$ is shown for down-wind direction where the wave input is maximal. In view of this fact and the results of the “academic” series the universality of the shapes of solutions in self-similar variables does not look surprising as far as the corresponding self-similarity parameter r varied very slightly: in all the experiments with realistic pumping $0.85 < r < 1.0$. The special case of swell ($r \approx 0$, solid curves in figs.1, 2) shows a visible difference as compared to other cases. The difference of numerical solutions for different wave inputs becomes prominent in terms of spectra averaged in direction. Fig.2 shows the normalized frequency spectra for the same set of numerical runs as fig.1. The spectral shapes are close to each other and to the standard JONSWAP dependence (dashed line) near the peak (approximately up to $1.3\omega_p$) and at high-frequency tails ($\omega > 2\omega_p$).

In the range $1.3 < \omega_p < 2\omega_p$ noticeable variations of spectra are observed depending on the wave input parameterization and on time. The relaxation of the solutions to an asymptotic form is very fast irrespectively to the wave input parameterization: generally, it takes less than 2 hours for a solution to fit its asymptotic with accuracy less than 5%. For the range $1.3 < \omega_p < 2\omega_p$ this time is substantially longer. Figs.3, 4 illustrates this result for approximately 2 and 8 hours of development of wave spectrum with the parameterization [6] and wind speed 10 m/s. A plateau is seen in the spectrum at 8 hours (fig.4). In some experiments a prominent peak was observed in the same frequency range. In all the cases the shape of the spectral peak is reproduced remarkably well irrespectively to the way of wave pumping while outside the narrow peak there is a variety of spectral forms that depends on wave pumping and the stage of wind-wave development.

Our analysis of self-similarity features allows to present (at the moment qualitatively) the wind-wave spectra as a combination of a self-similar “core” and a wave background. Evidently, the evolution of the core that does not depend on details of functions S_{in} and S_{diss} can be predicted quite well while the spectrum background depends on these details essentially and, thus, cannot be forecasted reliably.

4 Exponents of Wind-Wave Growth

The next part of our analysis of self-similarity features of the numerical wind-wave spectra concerns the evolution of global properties of wind-wave field such as characteristic frequencies (periods) and total energy (or significant wave height). In view of previous results the question can be formulated as follows:

What characteristics of wind-wave field are more adequate to the problem of wind-wave prediction? What predictions are more reliable?

The wind-wave growth can be characterized in different ways: first, in terms of mean (integral) quantities like dispersion of wave heights or mean frequency, second, in terms of characteristic quantities of spectral distribution, i.e. peak frequency and spectral peak magnitude. Certainly, the first way is easier to realize, while the latter method requires more keen data processing. In our numerical experiments one can calculate easily both sets of characteristics and the corre-

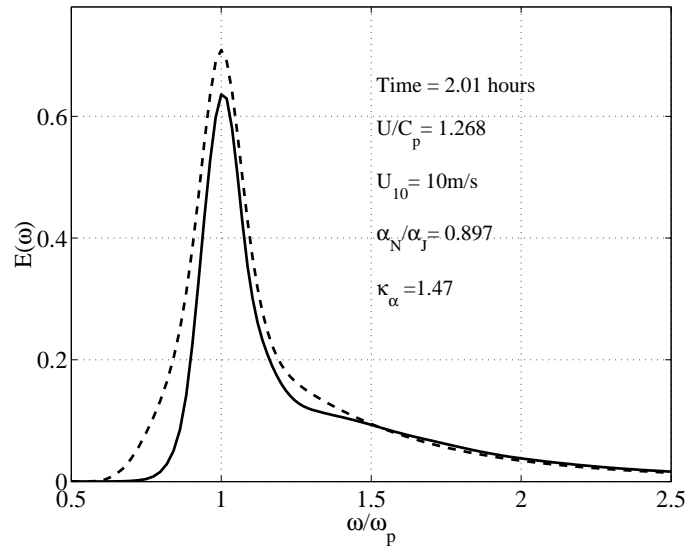


Fig. 3. Frequency spectra for numerical solution of the Hasselmann equation with Donelan et al. wave generation rate [5] (solid line) and modified JONSWAP spectrum (eq.1, dashed) for “young” waves. Wind speed $U_{10} = 10\text{m/s}$, time 2 hours

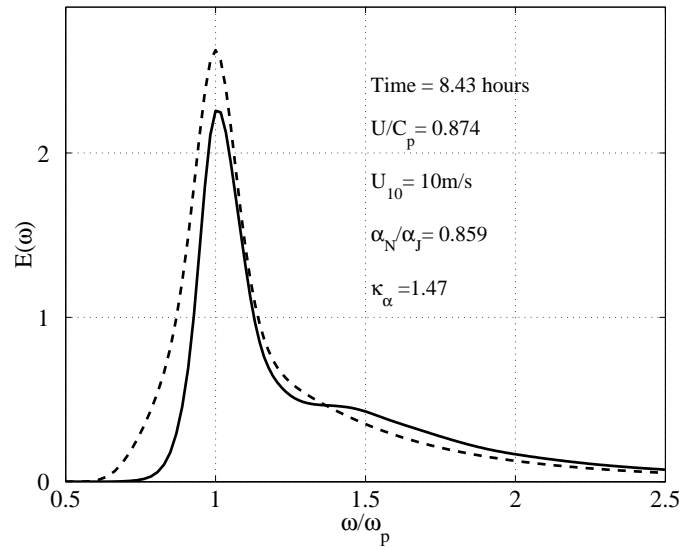


Fig. 4. The same as in previous figure for time approximately 8 hours

sponding exponents of power-like fits. For total energy and mean frequency one can define (see eq.15) these exponents as follows

$$E_{tot} = \int E(\mathbf{k})d\mathbf{k} \sim t^p; \quad \omega_{mean} = \frac{\int \omega E(\mathbf{k})d\mathbf{k}}{E_{tot}} \sim t^{-q} \quad (19)$$

These definitions take into account the wave spectrum globally, that is, in terms of the previous section, both self-similar core and non-self-similar fraction of the spectrum contribute into the exponents p and q .

Alternatively, one can try to extract parameters of the growth of self-similar core of the numerical solutions by tracing dependencies of peak frequency and the spectral peak magnitude. In terms of exponents α and β in (11) one can calculate easily the “self-similar counterparts” of p and q

$$p_{ss} = \alpha - 5\beta/2 = (11\beta - 4\alpha)/4 = (9\alpha - 5\beta)/19; \quad q_{ss} = \beta/2 = (2\alpha + 1)/19 \quad (20)$$

The parameter α is more useful for calculating p_{ss} and q_{ss} because of wider

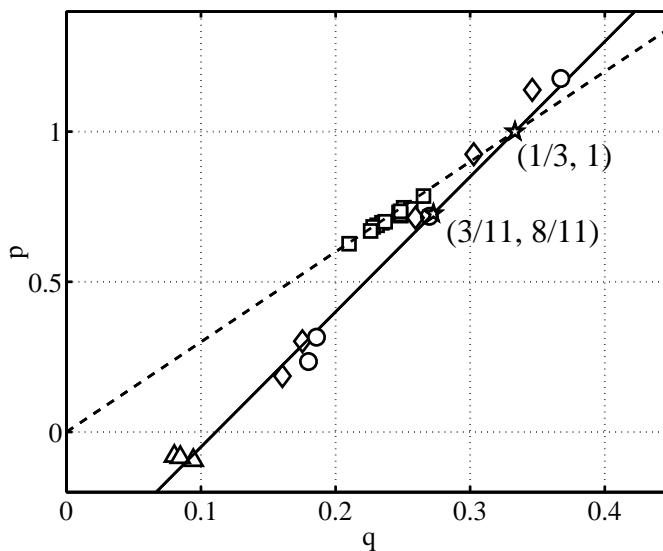


Fig. 5. Exponents p and q for power-like approximations of total energy and mean frequency of the kinetic equation solutions. \circ — Isotropic ‘academic’ runs; \diamond — Anisotropic ‘academic’ runs; \triangle — Swell; \square — ‘Real’ wave pumping. Exponents for constant wave action and wave energy inputs are given by stars. Hard line shows theoretical dependence of p on q , dashed line corresponds to Toba’s law.

range of change of the spectra magnitudes. The use of β is limited essentially by discrete frequency grid. Introduce the corresponding Toba’s parameter

$$T = p/(2q); \quad T_{ss} = p_{ss}/(2q_{ss}) = \frac{9\alpha - 5}{4\alpha + 2} \quad (21)$$

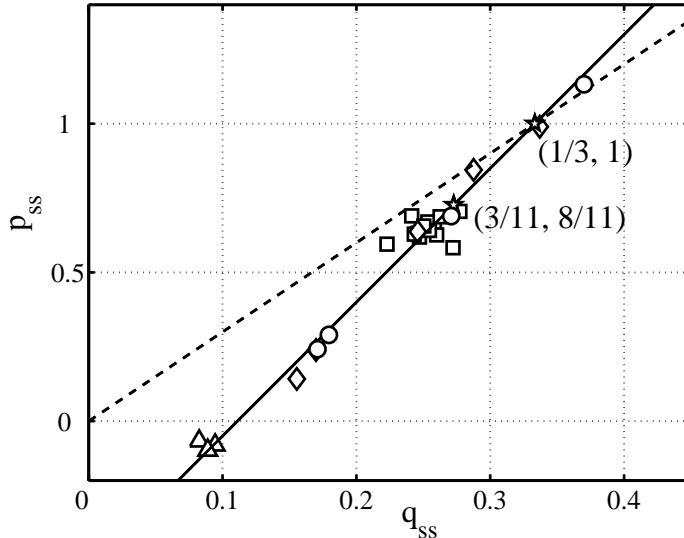


Fig. 6. The same as in previous figure for exponents p_{exp} and q_{exp} calculated for the parameters of solutions' peaks (exponents α and β of the self-similar solutions).

that describes the power-like dependence of significant wave height on wave period (frequency)

$$A \sim (1/\omega)^T$$

The empirical value of the exponent $T = 3/2$ has been obtained by Toba [19]. Fig.5 presents values of exponents of wave growth for different numerical experiments with both “academic” and “realistic” functions of wave input. One can see that “academic” series follow the self-similar relation (20) rather than Toba’s law $3/2$. At the same time the “realistic” series give the exponents that are closer to Toba’s exponent $3/2$ (dashed line). This divergence in “academic” and “realistic” dependencies becomes vanishing if we consider the wave growth exponents p_{ss} , q_{ss} for the self-similar core of wave spectra (fig.6). The peak frequency is growing faster than the mean frequency while the energy of the self-similar core is growing slower than the full wave energy, i.e. the non-self-similar fraction of wind-wave field can affect essentially wave growth features.

5 Discussion. A Composite Model of Wind-Wave Balance and Predictability of Wind-Wave Spectra

In this paper we showed that the self-similar solutions of the Hasselmann equation give a good approximation to the observed wind-wave spectra and parameters of wind-wave growth. These approximate solutions do not take into account details of wave input but depend on integral properties of this input. The asymptotic procedure that leads to these solutions implies a splitting of the wind-wave

balance into two parts. First, the “conservative” Hasselmann equation with no generation or dissipation terms describes a family of spectral shapes

$$\frac{dN_k}{dt} = S_{nl} \quad (22)$$

The parameters of the particular solution of the family is specified by the equation of integral balance of wave action (energy)

$$\left\langle \frac{dN_k}{dt} \right\rangle = \langle S_{in} + S_{diss} \rangle \quad (23)$$

In the consideration presented above these parameters are nothing but exponents of temporal growth of total wave action (energy). It should be stressed that the composite model is valid not for all waves but for those only which evolution is governed predominantly by non-linear transfer. Strictly speaking, the model is valid for a self-similar “core” of the solutions of the Hasselmann equation.

A key result of the present study is: the self-similar forms of wave spectra given by (22) depend very slightly on the integral balance (23). Thus, the quasi-universal spectra can be characterized effectively by their peak positions and magnitudes. This note becomes very important for non-self-similar background of wind-wave spectra. This background is beyond the composite model (22, 23). It depends on details of wind-wave balance and can affect essentially the integral energy and mean frequency. Thus, the prediction of the background behaviour is less reliable than one of the self-similar core. At the same time, the mean frequency and the total energy that characterize this background are easier to be measured in the ocean than the spectral peak properties.

As it was pointed out in Introduction, occurrence of rogue waves is likely associated with certain stages of wind-wave development. In our opinion, the analysis of wind-wave state in terms of the concept of self-similarity presented above can help in more adequate description of the wind-wave state in the context of rogue wave dynamics.

The research was conducted under US Army Corps of Engineers grants W912HZ-04-P-0172 and DACW42-03-C-0019, INTAS grant 01-234, ONR grant N00014-03-1-0648, Russian Foundation for Basic Research 02-05-6514, 04-05-64784 and the Russian Academy Program “Nonlinear Dynamics”. S.I. Badulin acknowledges support of NATO under the linkage grant EST.CLG.978941.

References

1. Babanin, A.N. & Soloviev, Yu.P: Field investigation of transformation of the wind wave frequency spectrum with fetch and the stage of development, *Journ.Phys. Oceanogr.* **28** (1998) 563–576
2. Badulin, S., Pushkarev, A., Resio, D., Zakharov, V.: Direct and inverse cascade of energy, momentum and wave action in wind-driven sea. 7th International workshop on wave hindcasting and forecasting. Banff, October 2002, (2002) 92–103

3. Badulin, S., Pushkarev, A., Resio, D., Zakharov, V.: Self-similarity of wind-driven sea. Submitted to *J. Fluid Mech.* (2005)
4. Battjes, J.A., Zitman, T.J. & Holthuijsen, L.H.: A reanalysis of the spectra observed in JONSWAP. *J.Phys.Oceanogr.* **17** (1987) 1288–1295
5. Donelan, M.A., Hamilton J., Hui W.H.: Directional spectra of wind-generated waves. *Phil.Trans.Roy.Soc.Lond.* **A315** (1985) 509–562
6. Donelan, M.A. & Pierson-jr., W.J.: Radar scattering and equilibrium ranges in wind-generated waves with application to scatterometry, *Journ.Geoph.Res.* **92**, C5 (1987) 4971–5029.
7. Gunson, J., Holt, M.: Diagnostics for rogue wave development from spectral wave model hindcasts. *Geophysical Research Abstracts* **4** (2002) EGS02-A-05665
8. Hasselmann, K.: On the nonlinear energy transfer in a gravity wave spectrum. Part 1, *J.Fluid Mech.* **12** (1962) 481–500
9. Hasselmann, K.: On the nonlinear energy transfer in a gravity wave spectrum. Parts 2 and 3. *J.Fluid Mech.* **15** (1963) 273–281; 385–398
10. Hasselmann, K., Barnett, T.P., Bouws, E., Carlson, H., Cartwright, D.E., Enke, K., Ewing, J.A., Gienapp, H., Hasselmann, D.E., Kruseman, P., Meerburg, A., Muller, P., Olbers, D.J., Richter, K., Sell, W. & Walden, H.: Measurements of wind-wave growth and swell decay during the Joint North Sea Wave Project (JONSWAP), *Dtsch.Hydrogh.Z.Suppl.* **12** A8 (1973)
11. Hsiao, S.V. & Shemdin, O.H.: Measurements of wind velocity and pressure with a wave follower during MARSEN. *J.Geoph.Res.* **88**, C14 (1983) 9841–9849
12. Holt, M., Fullerton, G., Li, J.-G.: Forecasting sea state with a spectral wave model. *Rogue Waves 2004 Brest*, 20-22 October 2004
13. Osborne, A. R., Onorato, M. & Serio, M.: The nonlinear dynamics of rogue waves and holes in deep water gravity wave trains. *Phys. Lett. A* **275** (2000) 386–393
14. Plant, W.J.: A relationship between wind stress and wave slope. *Journ.Geoph. Res.* **87**, C3, (1982) 1961–1967.
15. Pushkarev, A.N., Resio, D., Zakharov, V.E.: Weak turbulent theory of the wind-generated gravity sea waves. *Physica D: Nonlinear Phenomena*, **184** (2003) 29–63.
16. Resio, D. & Perrie, W.: A numerical study of nonlinear energy fluxes due to wave-wind interactions, *J.Fluid.Mech.* **223** (1991) 603–629
17. Snyder, R.L., Dobson, F.W., Elliot, J.A. & Long, R.B.: Array measurements of atmospheric pressure fluctuations above surface gravity waves, *J.Fluid.Mech.* **102** (1981) 1–59.
18. Stewart, R.W.: The air-sea momentum exchange, *Boundary-Layer Meteorology* **6** (1974) 151–167.
19. Toba, Y.: Local balance in the air-sea boundary processes. III. On the spectrum of wind waves, *J.Oceanogr.Soc.Japan* **29** (1973) 209–220.
20. Webb, D.J.: Non-linear transfers between sea waves. *Deep-Sea Research* **25** (1978) 279–298
21. Young, I.R.: *Wind Generated Ocean Waves*. Elsevier (1999)
22. Zakharov, V.E. & Filonenko N.N.: Energy spectrum for stochastic oscillations of the surface of a fluid, *Dokl.Acad.Nauk SSSR* **160** (1966) 1292–1295
23. Zakharov, V.E., Zaslavsky M.M.: The kinetic equation and Kolmogorov spectra in the weak-turbulence theory of wind waves, *Izv.Atm.Ocean.Phys.*, **18** (1982) 747–753.
24. Zakharov, V.E.: Theoretical interpretation of fetch limited wind-driven sea observations. 7th International workshop on wave hindcasting and forecasting, Banff, October 2002, (2002) 86–92

Spatial Extremes, Shapes of Large Waves, and Lagrangian Models

Hervé Socquet–Juglard and Kristian B. Dysthe, University of Bergen,
Karsten Trulsen, University of Oslo,
Sébastien Fouques, Jingdong Liu, and Harald E. Krogstad¹⁾, NTNU,
Trondheim

¹⁾ NTNU, Trondheim, Norway
harald.krogstad@math.ntnu.no

Abstract. The paper first states a simplified formulation of V. I. Piterbarg’s theorem about extremes of Gaussian fields, which together with the Slepian Model Representation is a general tool for analyzing the spatial characteristics of ocean waves. We then consider numerical simulations of random surface gravity waves carried out in space and time by means of modified nonlinear Schrödinger equations. It is demonstrated that high waves in the simulations are steeper and more asymmetric than predicted by the Gaussian theory. The last part of the paper discusses Lagrangian stochastic models as alternatives to the conventional Eulerian first and second order models.

Introduction

Today we are starting to obtain spatial measurements of ocean waves by remote sensing techniques (Schulz-Stelleneth and Lehner, 2004), and questions about spatial and even spatio/temporal extremes arise. For rogue waves the question naturally comes up whether such waves are truly exceptional, or whether they may actually happen somewhere or sometimes in a storm sea with considerable temporal and spatial extent.

Spatial data need tools from spatial statistics. The Slepian Model Representation (SMR) for Gaussian fields is well known [8]. In ocean engineering it forms the basis for *New Wave Theory* [17], the analysis of the shapes of extreme Gaussian waves [11], and the Boccotti theory of *Quasi Determinism* [1]. Another result of more recent origin is an explicit expression for the asymptotic extreme value distribution of a Gaussian field of arbitrary dimension derived by V. I. Piterbarg [14]. A simplified formulation of the theorem is given below.

The tools have been applied for analysis of spatial numerical simulations of random surface gravity waves of moderately narrow spectral bandwidth. The simulations utilize the Modified Nonlinear Schrödinger equations and produce the time development of sections of the ocean surface of the order 100×100 typical wavelengths and over 150 wave periods [18], [19]. Below we show a few results about the shape of the individual high waves. An extended discussion about extreme value distributions has been given elsewhere [16].

The final part reports from ongoing work investigating three dimensional second order Lagrangian stochastic models of the surface. Already at the first order, stochastic Lagrangian waves deviate significantly from linear Eulerian waves, and second order theory shows new and interesting features.

1 Gaussian Fields

Consider a zero mean homogeneous Gaussian field, $X(\mathbf{x})$, $\mathbf{x} \in \mathbb{R}^n$, with covariance function $\rho(\mathbf{x})$, $\rho(\mathbf{0}) = \sigma^2$, and spectrum $\Psi(\mathbf{k})$,

$$\rho(\mathbf{x}) = \int_{\mathbf{k}} e^{i\mathbf{k}\mathbf{x}} \Psi(\mathbf{k}) d\mathbf{k}. \quad (1)$$

We shall assume that the covariance matrix, Λ , of $\nabla X = \{\partial X / \partial x_i\}_{i=1}^n$ is non-singular. The covariance matrix may be expressed as

$$\Lambda = \int_{\mathbf{k}} \mathbf{k}\mathbf{k}' \Psi(\mathbf{k}) d\mathbf{k}. \quad (2)$$

By turning to the principal axis, Λ becomes diagonal and defines intrinsic spatial scales of the field, $\xi_k = 2\sigma / \nu_k^{1/2}$, $k = 1, \dots, N$, where ν_k is the k -th eigenvalue of Λ / σ^2 . The scales define a *unit cell* with volume $|V| = \xi_1 \times \dots \times \xi_n = (2\sigma)^n |\Lambda / \sigma^2|^{-1/2}$. When $n = 1$ and \mathbf{x} is time, the length of the unit cell is equal to the mean zero-upcrossing period, T_z . For $n = 2$ and $\mathbf{x} = (x_1, x_2)$, the scales are the mean wavelength, λ_0 , and the mean crest length, λ_c , and $|V| = \lambda_0 \lambda_c$. For the space-time case, (\mathbf{x}, t) , an additional correction term due to the space-time correlation is needed, $|V| = \lambda_0 \lambda_c T_z (1 - C_{0t}^2 - C_{ct}^2)^{-1/2}$. Here C_{0t} is the correlation between $\partial X / \partial x_0(\mathbf{0}, 0)$ and $\partial X / \partial t(\mathbf{0}, 0)$, and similarly for C_{ct} .

The *Slepian Model Representation* (SMR) follows from the general theory of multivariate Gaussian variables, where conditional expectations and prediction errors are expressed in terms of the covariance functions. We shall only use the result for the behavior around a high maximum at $\mathbf{x} = \mathbf{0}$, where $\nabla X = 0$:

$$X_s(\mathbf{x}) = \{X(\mathbf{x}) | X(\mathbf{0}) = a, \nabla X(\mathbf{0}) = 0\} = a \frac{\rho(\mathbf{x})}{\rho(\mathbf{0})} + \Delta(\mathbf{x}). \quad (3)$$

The residual process $\Delta(\mathbf{x})$ is Gaussian with $\mathbb{E}(\Delta(\mathbf{x})) = 0$, and

$$\text{Var}(\Delta(\mathbf{x})) = \rho(\mathbf{0}) - \frac{\rho(\mathbf{x})^2}{\rho(\mathbf{0})} - \nabla \rho(\mathbf{x}) \Lambda^{-1} (\nabla \rho(\mathbf{x}))'. \quad (4)$$

The approximation $X_s(\mathbf{x}) \sim a \frac{\rho(\mathbf{x})}{\rho(\mathbf{0})}$ is only reasonable when $\Delta(\mathbf{x})$ is small. In the present case this is at most for the extension of the unit cell centered at $\mathbf{x} = \mathbf{0}$, beyond which $\text{Var} \Delta(\mathbf{x}) \rightarrow \sigma^2$.

Piterbarg's Theorem ([14], Theorem 14.1) considers homogeneous Gaussian fields in \mathbb{R}^n and the asymptotic extreme value distributions for the maximum

of the field over subsets $T \subset \mathbb{R}^n$. We shall not bother about conditions on the shape of the subsets, and the rather strong regularity conditions on X required in the proof. Consider a subset T with volume $|T|$, or, recalling the unit cell V above, non-dimensional size $N = |T|/|V|$. Then the Piterbarg Theorem may be stated as

$$P \max_{\mathbf{x} \in T} X(\mathbf{x}) \leq u \sim \exp \left[- (2)^{\frac{n-1}{2}} e^{-u^2/2} H_{n-1}(u) N \right], \quad (5)$$

where H_n are Hermite polynomials w.r.t. to the standard Gaussian density ($H_0(u) = 1$, $H_1(u) = u$, $H_2(u) = u^2 - 1$, \dots). Some care should be exercised with the expression in Eqn. 5, since it obviously fails for small values of u .

In one dimension, Eqn. 5 reduces to the expression following from Rice's Formula and the Poisson property of high up-crossings. This is an excellent approximation for the distribution of the maximum of Gaussian processes with ocean wave-like spectra. Being an asymptotic expression, it becomes more accurate as N increases, but the theorem gives no hint of how large N is needed. A limited simulation study with realistic ocean wave spectra has shown an excellent agreement for N as low as 20 for $n = 2$. In general, when N increases, the distributions tend asymptotically to a Gumbel distribution, $G(u) = \exp(-\exp(-a(u - u_0)))$, where

$$u_0 = x_0 + \frac{(n-1) \log(x_0)}{x_0}, \quad a = u_0 - \frac{(n-1)}{u_0},$$

$$x_0 = \sqrt{2 \log N + (n-1) \log(2)}. \quad (6)$$

As an illustration, consider a uniform "storm" over an area 100×100 km, lasting for 6 hours. With a mean zero-crossing wave period of 10 s, assume a mean wavelength to be 200 m, and a mean crest length of 750 m. Within the two-dimensional storm area there are at each instant of time about $N_2 = 6.6 \times 10^4$ "waves", and hence $u_0 = 5.23$. With the significant wave height $H_s = 4$ m, the most probable extreme crest height is

$$(\text{Mode } C_{\max})_{\text{space}} = 1.31 H_s. \quad (7)$$

On the contrary, at a fixed location in space, $N_1 = 2160$, $u_0 = 3.94$, and

$$(\text{Mode } C_{\max})_{\text{time}} = 0.99 H_s, \quad (8)$$

Finally the over-all highest crest, assuming a rough estimate of the space-time coherence so that

$$|V| \approx 6 \lambda_0 \lambda_c T_z, \quad (9)$$

$N_3 = 2.4 \times 10^7$, and $u_0 = 6.73$. This results in

$$(\text{Mode } C_{\max})_{\text{space/time}} = 1.68 H_s, \quad (10)$$

The last value is quite high, and it may indeed be pertinent to ask whether *freak waves* are real outliers from the standard statistics, or merely being at the wrong place at the wrong time. In addition, second wave theory will increase the numbers above even further.

Numerical Simulations

We refer to [3] for a discussion about the numerical simulation model based on the Modified Non-Linear Schrödinger (MNLS) equation. The numerical simulations shown below are all based on the evolution of a stochastic wave field with initial wave spectra based on the JONSWAP form and a cos-directional distribution, $E(\omega, \theta) = S(\omega) D(\theta)$,

$$S(\omega) = \frac{1}{\omega^5} \exp \left[-\frac{5}{4} \left(\frac{\omega}{\omega_p} - 1 \right)^4 \right] \exp \left(-(\omega/\omega_p - 1)^2 / 2\sigma_J^2 \right), \quad (11)$$

$$D(\theta) = \begin{cases} \cos^2 \left(\frac{\pi\theta}{2} \right), & |\theta| < \theta_1, \\ 0, & |\theta| > \theta_1. \end{cases} \quad (12)$$

The corresponding wavenumber spectrum, truncated for $|\mathbf{k} - \mathbf{k}_0| > k_0$, is used for the initialization of the Fourier amplitudes. In all simulations, $k_p = 1$, and σ_J and θ_1 have the standard average JONSWAP-values. The spectrum is scaled with λ_p to an overall steepness $s = H_s/\lambda_p = 0.045$, typical for real ocean waves of some size. Only two different cases are shown below. For **Case A**, $\sigma_J = 0.7$, corresponding to a directional spread $\theta_1 = 14^\circ$, and for **Case B**, $\sigma_J = 0.35$, corresponding to $\theta_1 = 7.2^\circ$.

The simulated domain is square with sides $128 \times \lambda_p$, and the simulations cover a time span of $150 \times (2\pi/\omega_p)$. During this time period the spectrum changes slowly, and this has some impact on the mean wave and crest lengths of the fields.

The SMR gives a stochastic description of the spatial shape of high maxima for Gaussian processes. The upper pair of plots in Fig. 1 shows a color-coded graph of the surface, reconstructed to 3rd order, around the maximum along with the SMR prediction for a Gaussian field with the same covariance function. We observe that the simulation shows a definitely narrower crest in the wave propagation direction, whereas the crest length is comparable to the SMR prediction. The SMR prediction drops to 0 quite fast away from the maximum and the prediction error, $\Delta(\mathbf{x})$, takes over. This is illustrated in the lower plots, where we show cuts through the maximum crest along the wave propagation direction and in the orthogonal direction to that, the wave crest direction. Plus/minus 2 standard deviations of $\Delta(\mathbf{x})$ are shown along with the actual outcome of the simulation on top, and we observe that the SMR prediction quickly becomes of limited value away from the peak.

In order to draw more firm conclusions about the shape of the surface around the crest, it is therefore necessary to average the simulations over several maxima and compare the mean to the SMR prediction. This is, however, somewhat tricky since the spectrum and hence the covariance function and the SMR vary over the time span of the simulations. An example using Case A, which undergoes only a minor spectral changes, is shown in Fig. 2. It is obvious that the average crest from the simulations is narrower than the SMR prediction, and the extension of the surrounding troughs is larger. When inspecting individual realizations, as

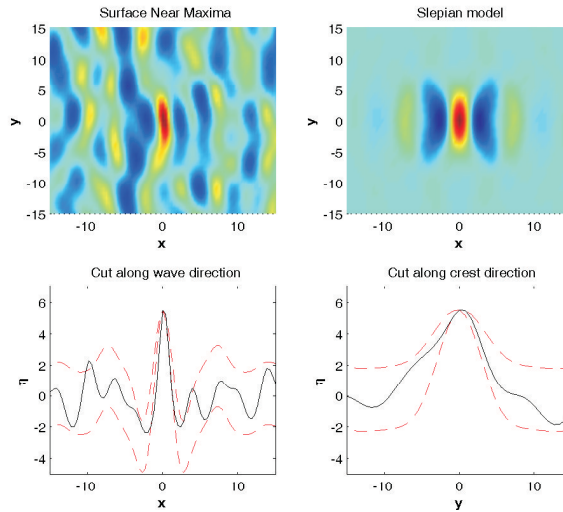


Fig. 1. Excerpt around the maximum peak of a simulation for Case A after $150T_p$. Top left: Color-coded surface elevation. Top right: SMR prediction. Bottom left: Cut through the maximum in the wave propagation direction. Black: Actual profile. Red: SMR prediction $\pm 2\text{std } \Delta(\mathbf{x})$. Bottom right: Cut in the orthogonal (crest) direction.

shown in Fig. 1, it is often seen that the crests are longer than predicted by SMR, but bent in various directions. On the average, the crest length in the direction orthogonal to the main propagation direction is similar to the SMR. Figure 3 demonstrates this for cuts in the wave and orthogonal crest directions for both Case A and B. Along the wave propagation direction, the waves are steeper than predicted by the SMR. Moreover, as a consequence of the second order contribution, the troughs on each side are significantly shallower than linear wave theory predicts. The wave as a whole is therefore more vertically asymmetric. The average difference in crest lengths is minor, but this is an average in the orthogonal direction to the wave propagation, and not the length of the actual crests, which, as noted above, tend to be bent.

2 Lagrangian Models

The traditional ocean surface wave theory is based on a perturbation expansion of the Eulerian equations of motion for an incompressible and inviscid fluid. This approach has been applied successfully to model gross features of the waves as long as their overall steepness remains small. However, issues such as the estimation of radar backscatter from the sea surface depend strongly on the slope and curvature of the ocean surface on many scales. This requires a description of the waves which is rather difficult to achieve through the Eulerian approach.

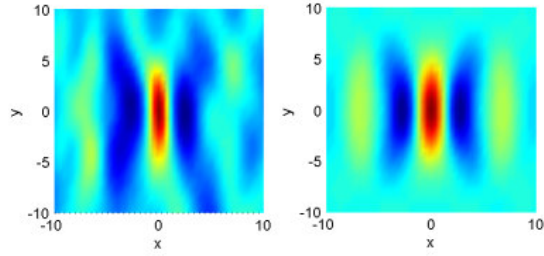


Fig. 2. Average surface shape around the maxima for Case A (left) compared to the SMR prediction, also averaged over the time span of the simulations (right).

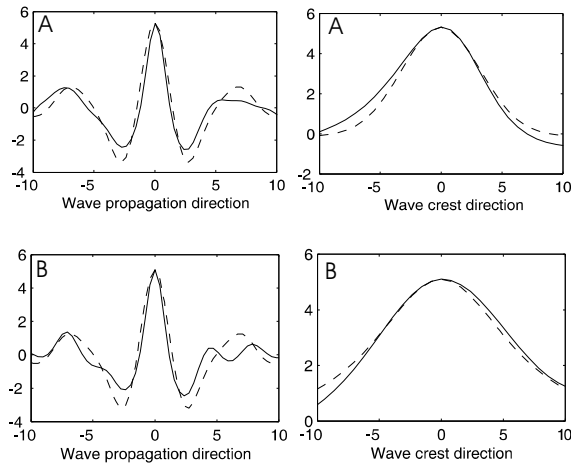


Fig. 3. Average cuts in the wave and crest directions for Case A (upper) and Case B (lower) . Solid: simulations, dashed: SMR prediction.

Recently, the interest for a Lagrangian description of ocean gravity waves has increased ([10], [2], [9], [5]). In this approach [6], one considers the motion of individual fluid particles, and the free surface is derived from the surface particles' positions [7]. As a result, the surface elevation is described through a parametric representation, which allows a larger flexibility as far as the wave shape is concerned.

In the Lagrangian model, the fluid is described through a set of fluid particles located at $\mathbf{X} = (x, y, z)^T$ at a given time t . The coordinate system has origin at the mean water level with z pointing upwards. Each particle is labelled by its reference position $\mathbf{X}_0 = (x_0, y_0, \delta)^T$. The fluid is assumed to be incompressible and inviscid, and the flow irrotational. The conservation of momentum can then be integrated to

$$\nabla_L \times (\mathbf{J}\mathbf{X}_t) = \mathbf{0}, \quad (13)$$

and the mass conservation reads [7]

$$\det(\mathbf{J}) = 1, \quad (14)$$

where $\mathbf{J} \equiv \nabla_L^T \mathbf{X}^T$, $\nabla_L \equiv (\partial/\partial x \ \partial/\partial y \ \partial/\partial \delta)$. The boundary conditions are

$$\begin{aligned} \delta &= 0 \quad \text{at the surface} \\ p &= 0 \quad \text{for } \delta = 0 \\ z_t &\rightarrow 0 \quad \text{for } \delta \rightarrow -\infty. \end{aligned} \quad (15)$$

A perturbation expansion of equations (13)–(15) has been carried out in [12] and [13]. According to dimensional analysis, the small parameter ϵ is proportional to $\|\mathbf{J} - \mathbf{1}\|$, where $\|\cdot\|$ is any matrix norm of $\mathbf{R}^{3 \times 3}$. Thus, ϵ is related to the Lagrangian gradient of the distance between the particles and their reference positions \mathbf{X}_0 . This differs from the Eulerian approach, where the small parameter of the perturbation expansion is the wave slope. The displacement of the particles is now written as $\mathbf{X} = \mathbf{X}_0 + \mathbf{X}_1 + \mathbf{X}_2 + \dots$, where $\mathbf{X}_n = O(\epsilon^n)$.

The first order solution is similar to the irregular extension of the Gerstner wave [4] given by Pierson (1961).

$$\mathbf{x}_1 = - \sum_p \frac{\mathbf{k}_p}{k_p} a_p e^{k_p \delta} \sin \Psi_p \quad (16)$$

$$z_1 = \sum_p a_p e^{k_p \delta} \cos \Psi_p \quad (17)$$

with $\Psi_p = \mathbf{k}_p \mathbf{x}_0 - \omega_p t + \phi_p$, and where $k_p = |\mathbf{k}_p|$ and $\omega_p^2 = g k_p$. The wave profiles show sharper crests and broader troughs. It is also capable of capturing some non-resonant wave-wave interactions such as the modulation of the crest-to-crest distance of short waves riding on the top of longer ones, as depicted in Fig. 4.

Besides, it can be shown that the interaction of two first order wave components with similar frequencies brings about a second order non-uniform current, whose main effect is to bend short crested waves. These so-called *horseshoe* patterns have also been observed to form in simulations based on the MNLS

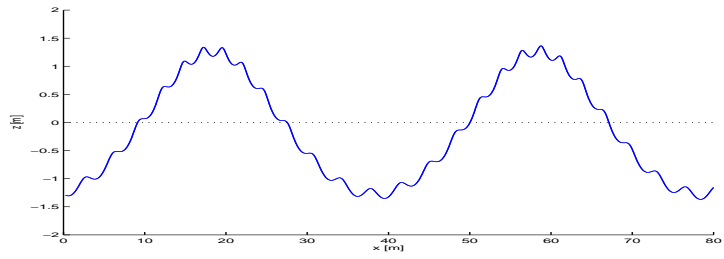


Fig. 4. First order bi-chromatic Lagrangian waves.

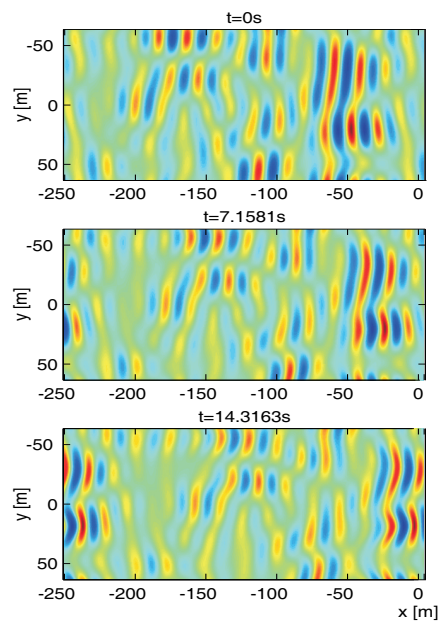


Fig. 5. Second order irregular Lagrangian waves in three dimensions developing "horseshoe patterns".

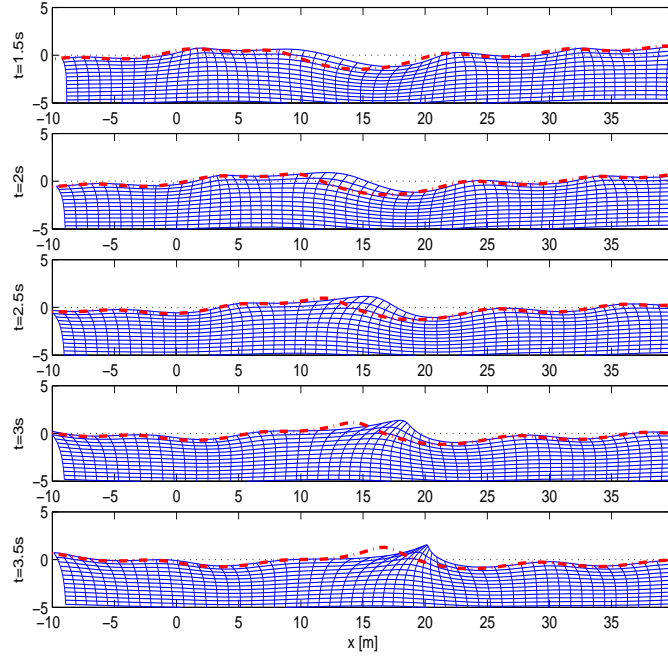


Fig. 6. Second order irregular Lagrangian waves (solid lines). Corresponding first order Lagrangian surface (dash-dotted line). The grid is regular in the reference coordinates.

equation [20], but are already seen at second order in the Lagrangian approach (see Fig. 5). The well-known Stokes drift is obtained from the second order interaction of a first order wave component with itself. Besides, for irregular waves, large horizontal displacement waves at the second order are responsible for asymmetric wave profiles with steep fronts, as shown in Fig. 6.

However, the second order mass transport induces an increase in the horizontal displacement of the fluid particles. Consequently, the small parameter of the perturbation expansion also grows towards infinity, and the duration of validity of the model is limited.

Conclusions

The Slepian Model Representation and Piterbarg's asymptotic extreme value distribution represent valuable tools for analyzing spatial fields. Piterbarg's Theorem gives a simple expression for the extreme values in Gaussian fields in any dimension, and may, in particular, answer questions about the maximum crest height in an area at a fixed time, or the overall highest crest in a spatially extended field lasting for some time.

The numerical simulations using the modified nonlinear Schrödinger equations give snapshots of the surfaces over a typical area 128×128 wavelengths and at time instances ranging from 0 to $150T_p$. During this time span, the simulated wave fields undergo some spectral change, as discussed in [3]. The simulated surfaces have been reconstructed to first, second and third order, and for the shape of the highest waves, the simulations show systematically steeper waves in the wave propagation direction and somewhat longer crests than the Gaussian prediction obtained from the SMR. Individual realizations often show that the crests bend. Simulated high waves are therefore significantly more vertically asymmetric than the corresponding Gaussian waves.

The Lagrangian stochastic models represent interesting alternatives to the conventional Eulerian models. Already at the first order, stochastic Lagrangian waves deviate significantly from linear Eulerian waves, and second order theory develops new and interesting features.

Acknowledgments

This research has been supported by the BeMatA programme of the Research Council of Norway (139177/431) and NTNU University Grant No. 70080000.

References

1. Boccotti, P. (2000), *Wave Mechanics for Ocean Engineering*, Elsevier, Amsterdam.
2. Chang, M.-S. (1969), Long-crested random gravity waves, *J. Geophys. Res.*, **74**(6), 1515–1536.
3. Dysthe, K. B., K. Trulsen, H. E. Krogstad, and H. Socquet-Juglard (2003), Evolution of a narrow band spectrum of random surface gravity waves, *J. Fluid Mech.*, **478**, 1–10.
4. Gerstner, F. J. (1809), Theorie der Wellen. *Gilbert's Annalen der Physik.*, xxxii.
5. Gjøvsund, S. H. (2003), A Lagrangian model for irregular waves and wave kinematics. *Trans. of the ASME, Journal of Offshore Mechanics and Arctic Engineering*, **125**, 94–102.
6. Lagrange, J. L. (1788), *Mécanique Analytique*, Jacques Gabay, Paris. Reprint 1989.
7. Lamb, H. (1932), *Hydrodynamics*, Cambridge University Press, 6th edition.
8. Lindgren, G. (1972), Local maxima of Gaussian Fields, *Arkiv för Matematik*, **10**, 195–218.
9. Moe, G., Ø. A. Arntsen, and S. H. Gjøvsund (1998), Wave kinematics based on a Lagrangian formulation. *Proc. of the 1998 International OTRC Symposium "Ocean Wave Kinematics, Dynamics and Loads on Structures"*, ASCE Press, 56–63.
10. Phole, F. V. (1950), *The Lagrangian equations of hydrodynamics: solutions which are analytic functions of the time.* Ph.D. Thesis, Graduate School of Arts and Science, New York University.
11. Phillips, O. M., D. Gu, and E. J. Walch (1993), On the Expected Structure of Extreme Waves in a Gaussian Sea. Part II: SWADE Scanning Radar Altimeter Measurements, *J. Phys. Ocean.*, **23**, 2297–2309.
12. Pierson, W. J. (1961), Models of random seas based on the Lagrangian equations of motion, *Tech. Rept. Contr. Nonr-285(03)*. College of Engineering, Research Division, New York University.

13. Pierson, W. J. (1962), Perturbation analysis of the Navier-Stokes equations in the Lagrangian form with selected linear solutions, *J. Geophys. Res.*, **67**(8), 3151–3160.
14. Piterbarg, V. I. (1996), *Asymptotic Methods in the Theory of Gaussian Processes and Fields*, AMS Transl. of Math. Monographs, **148**, Providence, R.I.
15. Schulz-Stelleneth, J. and S. Lehner (2004), Measurement of two dimensional sea surface elevation fields from complex synthetic aperture radar data, *IEEE Trans. Geos. Rem. Sensing*, **42**(6), 1149 – 1160.
16. Socquet-Juglard, H., K. B. Dysthe, K. Trulsen, H. E. Krogstad, and J. Liu (2004), Probability distributions of surface gravity waves during spectral changes, submitted to *J. Fluid Mech.*
17. Tromans, P. S., A. R. Anatürk, and P.M. Hagemeyer (1991), A new model for the kinematics of large ocean waves – applications as a design wave, in Proc. 1st Int. O shore and Polar Engng. Conf., Edinburgh, UK, **3**, 54–71.
18. Trulsen, K. and K. B. Dysthe (1996), A modified nonlinear Schrödinger equation for broader bandwidth gravity waves on deep water, *Wave Motion*, **24**, 281–289.
19. Trulsen, K., I. Kliakhandler, K. B. Dysthe, and M. G. Velarde (2000), On weakly nonlinear modulation of waves on deep water, *Phys. Fluids*, **2**, pp. 2432–2437.
20. Trulsen, K. (2004), Large horseshoe patterns of water surface waves, submitted *J. Fluid Mech.*

Wave crest statistics calculated using a fully nonlinear spectral response surface method

Richard Gibson[‡], Chris Swan[‡], Peter Tromans^{†‡} & Luc Vanderschuren[†]

[‡] Department of Civil and Environmental Engineering
Imperial College London
SW7 2AZ
United Kingdom

[†] Ocean Wave Engineering Ltd
Liss
Hampshire
GU33 7AT
United Kingdom

r.gibson@imperial.ac.uk, c.swan@imperial.ac.uk pt7185@hotmail.com,
luc.vanderschuren@skynet.be

Abstract. This paper is concerned with the calculation of the probability of exceedence of wave crest elevation. This has important implications for the design of both fixed and floating structures. In particular, the paper is interested in identifying sea-states in which so-called *freak*, or *rogue*, waves are intrinsically more likely to occur. This is investigated by ascertaining the effect that both the bandwidth and the directional spread of a spectrum has on the statistics of crest elevation. By combining a fully-nonlinear numerical wave-model with a spectral response surface method, statistics that include the full-nonlinearity of the wave-field can be determined very efficiently. It has been shown that whilst in unidirectional sea-states linear and second-order theory underestimates the probability of exceedence of crest elevation, this is not the case in most directionally spread wave-fields. Furthermore, by combining the short-term statistics relevant to sea-states with the long-term statistics of storms, the return period of the Draupner New Year's wave has been estimated.

1 Introduction

A knowledge of the statistics of wave crest elevation is fundamental for the design of most marine structures. For example, the occurrence of the largest waves determines the required air-gap and the maximum drag force on a fixed structure. Furthermore, it is important in the estimation of green-water inundation and the incidence of wave slam on floating structures. However, it has been suggested that some of the largest waves occur more often than would be predicted by linear, or second-order, theory. These waves are often referred to as *freak*, or *rogue*, waves. In this paper the short-term statistics of wave crest elevation are calculated by incorporating the fully nonlinear numerical wave-model of Bateman *et al.* (2001)

into a spectral response surface (SRS) method. The results of the short-term statistics have then been incorporated into the long-term statistical method of Tromans & Vanderschuren (1995) and the return period of a particular crest elevation at a particular location can be calculated. This method has been used to analyze hindcast data at the Draupner location and the return period of the January 1 1995 Draupner wave has been calculated. The paper begins in §2 by describing the theoretical basis and application of the SRS method. It continues in §3 by applying the method to calculate the short-term statistics of crest elevation in both unidirectional and directional sea-states. In §4 the SRS method is incorporated into that of Tromans & Vanderschuren (1995) and the return period of the Draupner wave is calculated. Concluding remarks can be found in §5.

2 SRS Method

The SRS method has been used in structural engineering to calculate the probability that a structure will fail when subjected to a number of statistically independent loads.

In this paper the SRS method is applied in order to calculate the probability of exceedence of crest elevation. A brief description of how this is undertaken follows; a more detailed description can be found in Gibson *et al.* (2005). The SRS method is applied by discretising the spectrum into a number of independent components, the statistical distribution of which is given by their variance, σ_n^2 . The components are directly related to the surface elevation, and therefore, in order to consider their phasing, must be divided into η_n :

$$\eta_n = a_n \cos(\omega_n t - \varphi_n), \quad (1)$$

and its Hilbert transform, $\tilde{\eta}_n$:

$$\tilde{\eta}_n = a_n \sin(\omega_n t - \varphi_n), \quad (2)$$

where a_n is the amplitude of the n_{th} component, ω_n its frequency and φ_n its random phase angle. These components are then standardised, by subtracting their mean and dividing by their standard deviation, σ_n . Figure 1 shows a surface, in this case a circle, of constant probability density in the space of the standardised variables x_n and \tilde{x}_n . The point A represents one particular event, its response is $R(x_n, \tilde{x}_n)$, and its probability density is directly related to its distance from the origin, $\beta = \sqrt{x_n^2 + \tilde{x}_n^2}$. A first order reliability method (FORM) can then be applied in order to estimate its probability of exceedence, this is given as:

$$Q = P(\text{Crest elevation} > R(x, \tilde{x})) = \exp\left(-\frac{\beta(x, \tilde{x})^2}{2}\right). \quad (3)$$

Therefore, each circle, or in more than two-dimensions each ‘hyper-sphere’, represents one probability of exceedence. A standard optimisation routine, such as that of Fletcher-Reeves (Press *et al.*, 1994), is then applied in order to find the

maximum value of the response that corresponds to a particular probability of exceedence. In this case the response is crest elevation, which according to linear theory is given by

$$R(x_n) = \sum_{n=1}^N (\sigma_n x_n). \quad (4)$$

However, the technique can be used for other responses, such as that of a structure subject to wave loading.

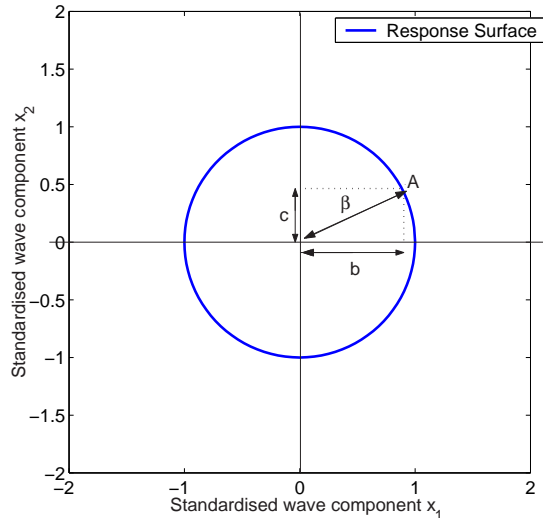


Fig. 1: A surface of constant probability density. The event A corresponds to $x_1 = b$ and $x_2 = c$ and has a probability density that is directly related to β .

3 Short-term statistics

The SRS method has been applied in order to calculate the probability of exceedence of crest elevation in both unidirectional and directional sea-states. This has been achieved using a first-order response function described in equation 4, a second-order response function based upon Sharma & Dean (1981) and described in Tromans & Vanderschuren (2002), and a fully-nonlinear response function obtained by incorporating the fully-nonlinear wave-model of Bateman *et al.* (2001) into the SRS method. The fully-nonlinear response function has been generated two ways. The first is by using the spectrum optimised linearly as the input to the wave-model and obtaining a fully-nonlinear correction to the crest elevation. This is an underestimate of the actual crest elevation as the

spectrum has not been optimised fully-nonlinearily. The second method addresses this short-coming and optimises the spectrum fully-nonlinearily. Unfortunately, this is an extremely time-consuming process as the wave model, whilst efficient, must be run many times for each wave component for each probability of exceedence. Accordingly, only a few probabilities of exceedence have been optimised fully-nonlinearily in the unidirectional sea-states, and only one in the directional sea-states.

3.1 Unidirectional Seas

The SRS method has been applied to two unidirectional spectra, J1D0 and J5D0. Both are JONSWAP spectra with peak period $T_p = 12.8s$; the former has a peak enhancement factor $\gamma = 1.0$, the latter a peak enhancement factor $\gamma = 5.0$. Figure 2 shows that the fully-nonlinear results give a substantial increase in crest elevation over the linear or second-order results. This is the result of the rapid evolution of the wave spectrum discussed in more detail in Gibson & Swan (2004) and Gibson & Swan (2005). Furthermore, the figure also shows that the more narrow-banded spectrum, J5D0, is more nonlinear than J1D0, and that it is only for this spectrum that a fully-nonlinear optimisation is required. The increase in nonlinearity with reduced bandwidth is confirmed in figure 3; this indicates that the fully-nonlinear optimisation of both J1D0 and J5D0 selects a spectrum that is more narrow-banded. Further discussion and an investigation of the physical mechanisms that are responsible for these results can be found in Gibson *et al.* (2005).

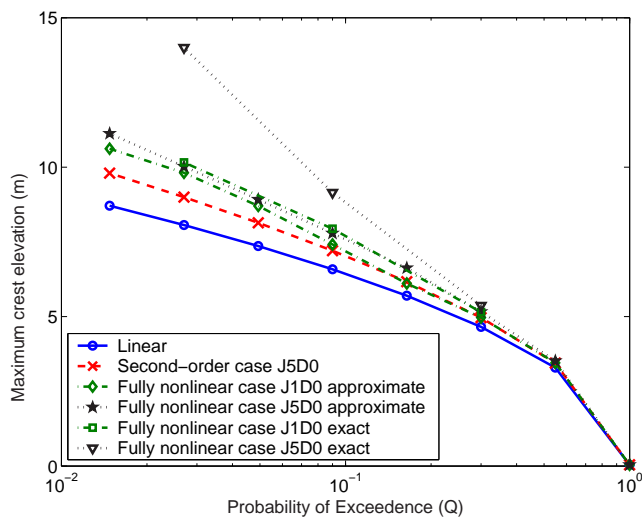


Fig. 2: The probability of exceedence of crest elevation in unidirectional seas.

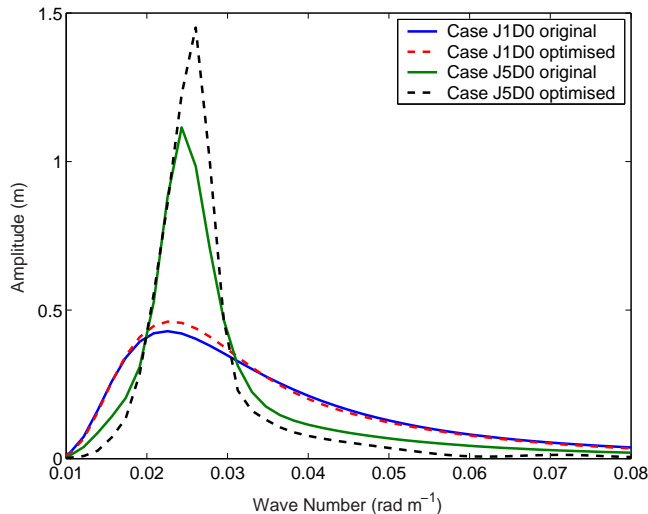


Fig. 3: The original and optimised spectra for cases G1D0 and G5D0. The spectra are coarsely discretised due to the time consuming nature of the optimisation process.

3.2 Multi-directional Seas

The SRS method has also been applied to two directional spectra, J5D10 and J5D30. Once again both are JONSWAP spectra with peak period $T_p = 12.8s$ and peak enhancement factor $\gamma = 5.0$; in the former the standard deviation of the wrapped normal directional spreading function is $\sigma_\theta = 10^\circ$, in the latter it is $\sigma_\theta = 30^\circ$. Figure 4 indicates that for both spectra the fully-nonlinear crest elevation is less than the second-order prediction. Furthermore, the fully-nonlinear optimisation of the wave spectra only marginally increases the crest elevation. This suggests that the focussing of wave components is not a mechanism by which *rogue* waves can form in sea-states characterised by a directionally spread JONSWAP spectrum. This is the result of the balance between the spectral evolution, involving changes in both the frequency and the directional spectrum, and the focussing of the wave components discussed in more detail in Gibson & Swan (2004) and Gibson & Swan (2005).

Figure 5 shows the probability of exceedence of crest elevation for a directionally spread Gaussian spectrum of $T_p = 16s$ and $\sigma = 5^\circ$, characteristic of swell-dominated sea-states. In this case the crest elevations are very much larger than those of the JONSWAP spectrum. However, figure 5 also shows that in mixed sea-states, those in which there is both a wind (JONSWAP) and a swell (Gaussian) component, the result is similar to that for a purely wind-dominated (JONSWAP) sea.

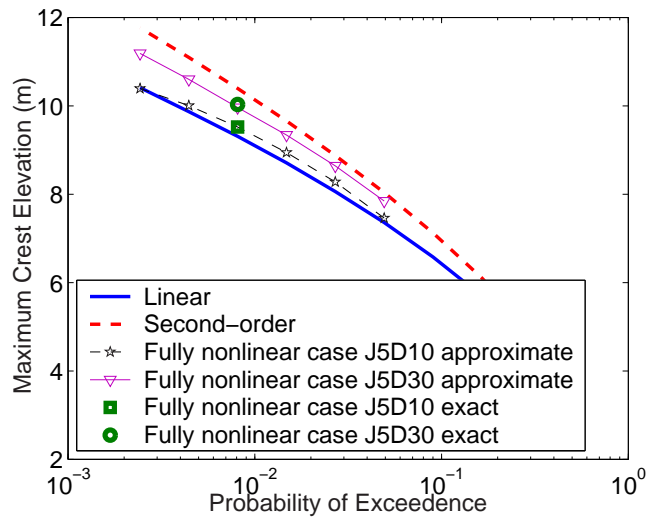


Fig. 4: The probability of exceedence of crest elevation in directional seas.

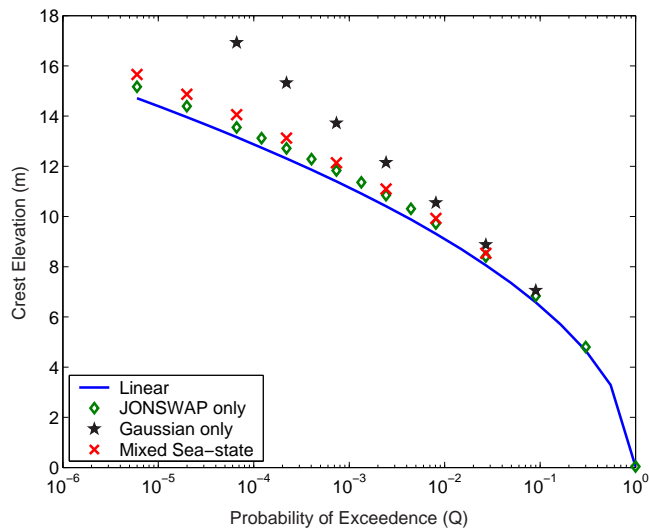


Fig. 5: The probability of exceedence of crest elevation in wind dominated, swell dominated and mixed directional-spread sea-states. In the case of the mixed sea the amplitude has been split evenly between the wind and swell components.

4 Long-term statistics

The results of the previous section relate to the short-term statistics of sea-states. However, the design of a marine structure typically requires knowledge of the long-term statistics at a particular location. This can be undertaken by applying Tromans & Vanderschuren (1995). The method considers storms as independent events and requires two types of distribution to be defined. The first is the long-term statistics of storms, which is calculated from measured or hindcast data. The second is the short-term statistics of waves within a sea-state, which can be calculated using the SRS method. Tromans & Vanderschuren (1995) has been applied, in conjunction with the SRS method and using hindcast data for the Draupner location, in order to calculate the return period of an 18.5m crest elevation; corresponding to the New Year Wave recorded on January 1 1995. The manner in which this has been undertaken is described below.

If the spectrum is assumed to be JONSWAP then it is possible to construct a transfer function from linear to nonlinear crest elevation:

$$C_{nl} = C_{lin} \cdot F(C_{lin}K_p), \quad (5)$$

where C_{lin} is the linear crest elevation, with a probability of exceedence defined by the Rayleigh distribution, C_{nl} is the nonlinear crest elevation and K_p is the wave-number of the peak of the spectrum. This ignores the parameters of the spectrum as previous results (Gibson & Swan, 2005) have indicated that, in directional seas, they have little effect on the distribution of crest elevation. The form of the transfer function, for a JONSWAP spectrum, is as follows:

$$F(C_{lin}K_p) = 1 + \beta(C_{lin}K_p)^p + \gamma(C_{lin}K_p)^q, \quad (6)$$

where p and q are approximately one and two respectively. Using these values, the β term corresponds to the second-order bound correction, whilst the γ term corresponds to the third-order resonant change to the amplitude of the underlying linear spectrum. The various coefficients are given in table 1 and the fit to the data described in figure 6.

Parameter	Second-Order	Fully-Nonlinear
β	0.50	0.87
γ	0.0	-1.63
p	1	1.17
q	2	1.92

Table 1: Parameters of the transfer functions from linear to nonlinear crest elevation using Equations 6

Tromans & Vanderschuren (1995) can now be applied using linear theory with a nonlinear transfer function utilised at each step. Figure 7 depicts the return

period of crest elevation at the Draupner location calculated using linear, second-order and fully-nonlinear theory. This shows that the best estimate for the return period of the New Year wave recorded at the Draupner platform wave is 800 years; which is greater than the 300 years calculated using a second-order model.

5 Concluding Remarks

In this paper both short- and long-term statistics of crest elevation have been considered. This has been undertaken by incorporating the fully-nonlinear wave-model of Bateman *et al.* (2001) into both the SRS method and that of Tromans & Vanderschuren (1995). The results have shown that whilst in unidirectional sea-states the fully-nonlinear crest elevations are significantly larger than those calculated to second-order, this is not necessarily the case in directional seas. Indeed, in broad-banded directionally spread seas, characterised by a JONSWAP spectrum, the fully-nonlinear crest elevations are in fact lower than those predicted to second-order. However, in narrow-banded swell-dominated seas, characterised by a Gaussian spectrum with a small spreading parameter, the results are similar to those of the unidirectional simulations; with crest elevations significantly higher than second-order theory. This suggests that it is in swell-dominated sea-states that *rogue* waves are intrinsically more likely to occur.

The SRS method has been used in conjunction with that of Tromans & Vanderschuren (1995) in order to calculate the return period of the Draupner wave. This has been undertaken by employing a transfer function from the linear to the fully-nonlinear results. The result gives a return period of a 18.5m crest elevation of 800 years.

Acknowledgement

The early stages of this work were undertaken within the project 'Reliability Based Structural Design of FPSO Systems', which involves Shell International, Instituto Superior Tcnico, DHI, Det Norske Veritas, Imperial College, Noble Denton and Oxford University. The project is partially funded by the European Union through the Energy Programme under contract ENK6-2000-00107. The later stages of the work were completed with support from the UK Engineering and Physical Sciences Research Council under grant number GR/R64971.

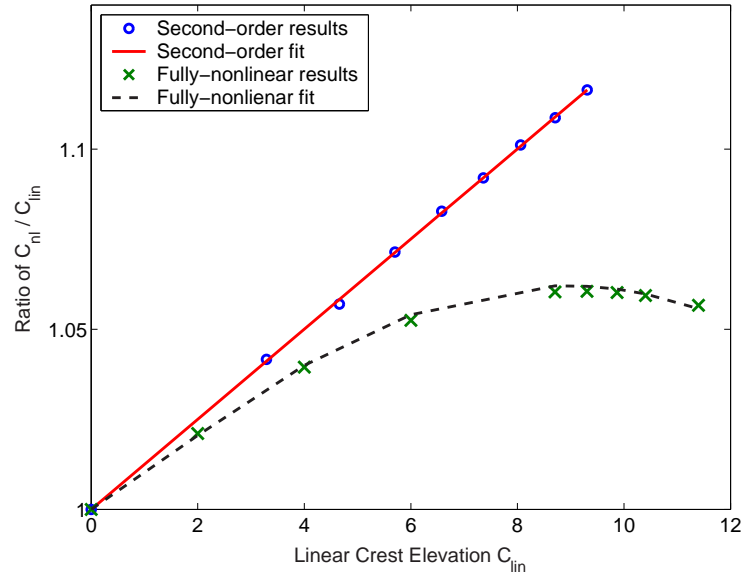


Fig.6: The fit to the nonlinear crest elevations. In terms of C_{lin} , the fitting function is parabolic for second-order results and cubic for the fully nonlinear results; the latter indicating the dominance of third-order terms.

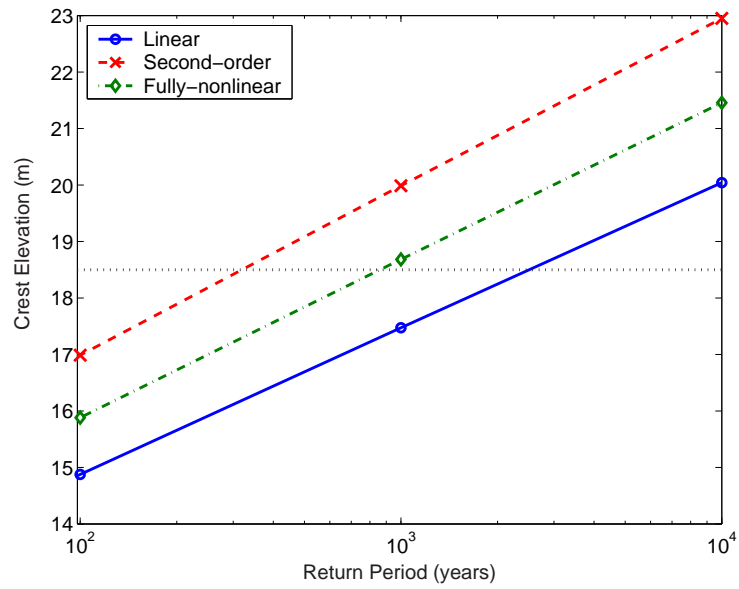


Fig. 7: The return period of crest elevation at the Draupner location.

Bibliography

- BATEMAN, W. J. D., SWAN, C. & TAYLOR, P. H. 2001 On the efficient numerical simulation of directionally-spread surface water waves. *Journal of Computational Physics* **174**, 277–305.
- GIBSON, R. S. & SWAN, C. 2004 The role of resonant wave interactions in the evolution of extreme wave events. *Rogue Waves 2004* .
- GIBSON, R. S. & SWAN, C. 2005 The evolution of large ocean waves: the role of local and rapid spectral changes. *Submitted to the Royal Society* .
- GIBSON, R. S., SWAN, C. & TROMANS, P. 2005 Fully-nonlinear statistics of wave crest elevation calculated using a spectral response surface method: Applications to unidirectional sea-states. *Submitted to the Journal of Physical Oceanography* .
- PRESS, W. H., FLANNERY, B. P., TEUKOLSKY, S. A. & VETTERLING, W. T. 1994 *Numerical Recipes in C—The Art of Scientific Computing*.. Cambridge University Press.
- SHARMA, J. N. & DEAN, R. G. 1981 Second-order directional seas and associated wave forces. *Society of Petroleum Engineering Journal* **4**, 129–140.
- TROMANS, P. S. & VANDERSCHUREN, L. 1995 Response based design conditions in the North Sea: application of a new method. In *OTC 7683, Offshore Technology Conference, Houston*.
- TROMANS, P. S. & VANDERSCHUREN, L. 2002 The statistics of wave crest elevation calculated to second order. In *Proceedings of OMAE02 Conference*.

Deterministic aspects of Nonlinear Modulation Instability

E van Groesen, Andonowati & N. Karjanto

Applied Analysis & Mathematical Physics, University of Twente,
POBox 217, 7500 AE, Netherlands
& Jurusan Matematika, Institut Teknologi Bandung,
Jl. Ganesha 10, Bandung Indonesia
groesen@math.utwente.nl, aantrav@attglobal.net,
n.karjanto@math.utwente.nl

Abstract. Different from statistical considerations on stochastic wave fields, this paper aims to contribute to the understanding of (some of) the underlying physical phenomena that may give rise to the occurrence of extreme, rogue, waves. To that end a specific deterministic wavefield is investigated that develops extreme waves from a uniform background. For this explicitly described nonlinear extension of the Benjamin-Feir instability, the soliton on finite background of the NLS equation, the global down-stream evolving distortions, the time signal of the extreme waves, and the local evolution near the extreme position are investigated. As part of the search for conditions to obtain extreme waves, we show that the extreme wave has a specific optimization property for the physical energy, and comment on the possible validity for more realistic situations.

Keywords: rogue waves, modulational instability, deterministic extreme waves, constrained minimal energy principle.

1 Introduction

In this contribution we describe various aspects related to modulational, Benjamin-Feir, instability that have been found in a detailed study of a family of wavefields. These aspects give rise to some understanding of phenomena that are observable in the downstream evolution of unidirectional waves, showing the spatial evolution from a slightly modulated uniform wave train to a position where large amplitude amplification occurs and extreme waves arise. Although these findings are for a special class of solutions in a simplified model, it is expected that at least some of the phenomena and underlying physics could be quite characteristic for more general situations in which extreme ('rogue') waves are observed. This is to be expected, since the family of wavefields studied are the deterministic description of the fully nonlinear evolution of the initially linear Benjamin-Feir instability with one pair of unstable sidebands. This family is known in the NLS model as the Soliton on Finite Background (SFB), given in [1]. Some of the results reported in detail in Andonowati e.a., [2], will be put in a broader perspective and, where possible, a link with research on stochastic elements will be

made. In fact, different from the statistical approach that envisages the occurrence of extreme waves as a very rare occasion for which it is not yet known if there are special circumstances that give rise to their occurrence, we start from the opposite direction: what are the basic underlying physical properties of extreme waves (as they appear in this family), and extract information from this that may be characteristic for more realistic cases too.

Slowly varying evolutions of a monochromatic wave with wavenumber and frequency (k_0, ω_0) satisfying the dispersion relation, are described in first order of the (small) wave elevations with a complex valued amplitude A like

$$\eta(x, t) \approx A \exp[i(k_0 x - \omega_0 t)] + cc$$

To study the spatial evolution, it is practical to describe the amplitude in variables with delayed time, with the delay determined by the corresponding group velocity V_0 , so $\xi = x, \tau = t - x/V_0$, where (x, t) are the (scaled) physical laboratory variables (we suppress the first order and second order scaling coefficients in τ and ξ respectively, just as we do in the amplitude). To incorporate dispersive and nonlinear effects in comparable order, A should satisfy in the lowest nontrivial approximation the NLS equation, given by

$$\partial_\xi A = -i [\beta \partial_\tau^2 A + \gamma |A|^2 A]$$

where β, γ are constants, depending on the monochromatic wave. For sufficiently large wavenumbers, both parameters have the same sign (positive say, without restriction since the sign of ξ can be changed). Then dispersive effects (broadening of linear wavegroups) can be balanced by focussing effects from nonlinearity; in this paper we consider only this case, the ‘deep water limit’.

In section 2 we present the basic observations of the family of SFB¹. We first present a description of the complete spatial evolution, using the envelope of the waves to illustrate the development of wavegroups, and the maximal temporal amplitude to depict the largest possible surface elevations at each point. We investigate the time signal, and its spectral properties, at the extreme position where the largest waves appear and describe how, as a consequence of the appearance of phase singularities, waves in one wavegroup are distinguished between extreme and intermittent waves that have opposite phase. Near the extreme position, the motion of the extreme waves is studied, showing the familiar nonlinear modification of the dispersion relation in the physical solution, and changes in the quadratic energy spectrum in second and higher order only. In section 3 we investigate what can be said about the maximal possible amplitude for signals obeying certain constraints. In particular we consider as constraints the simplest motion invariants of energy and momentum (constants during the

¹ Actually, in this paper we consider only the family with one pair of initial side bands: SFB(1); higher order families with n pairs of sidebands also exist, SFB(n). The case $n = 2$ shows phenomena like the interaction of two SFB(1) solutions, somewhat similar to interaction in NLS of two confined soliton wave groups .

down stream evolution), and show that the extreme signal has as remarkable property that it is a solution of a specific optimization principle. Remarks and conclusions about the relevance of the results obtained in this paper for more realistic situations will finish the paper.

2 Nonlinear modulation instability in the SFB family

This section is based to a considerable extent on the results presented in [2]; see this paper also for additional references. After some preliminaries, a global description of downstream running nonlinearly distorted waves according to SFB is presented, the extremal signal is studied, and the detailed dynamics near the extreme position is investigated.

2.1 Preliminaries

The explicit expression for the solution of the NLS equation called Soliton on Finite Background is given in [1]; we use the notation of [2]. The solution is given for the complex amplitude $A(\xi, \tau)$:

$$A(\xi, \tau) = r_0 e^{-i\gamma r_0^2 \xi} \left(\frac{\tilde{\nu}^2 \cosh(\sigma\xi) - i\tilde{\nu}\sqrt{2 - \tilde{\nu}^2} \sinh(\sigma\xi)}{\cosh(\sigma\xi) - \sqrt{1 - \tilde{\nu}^2/2} \cos(\nu\tau)} - 1 \right).$$

This describes actually a family of SFB solutions which depend on two essential parameters, r_0 and ν ; two other parameters are related to a shift in time and position: we will choose these such that the extreme wave will appear for normalized variables at $x = 0$, with maximal height at $t = 0$.

The parameter r_0 denotes (half of) the amplitude of the uniform wavetrain at infinity, while $\tilde{\nu}$ is a normalization of the modulation frequency ν of the given carrier frequency. In fact, with the notation from [2], we have $\tilde{\nu} = \sqrt{\beta/\gamma\nu}/r_0$. Compared to the definition of Benjamin-Feir Index BFI in [6], adapted for the case considered here, we have the relation $\tilde{\nu} = \sqrt{2}/BFI$ so that Benjamin-Feir instability takes place for $\tilde{\nu} < \sqrt{2}$, corresponding to $BFI > 1$. The parameter $\sigma = \gamma r_0^2 \sqrt{2 - \tilde{\nu}^2}$ happens to be the Benjamin-Feir growth factor of linear instability theory.

In the following we will use the notation SFB to denote the solution in physical variables, describing the surface elevation $\eta(x, t)$ of the physical waves without the second order Stokes effect. These second order effects can be added; they will contribute to the actual wave heights, and show modulations (with double modulation frequency) on the MTA described below, but will not essentially contribute to the basic phenomenon. The role of the second order effects in generating four wave interaction and resonance phenomenon is already accounted for (in the considered order of accuracy) by the NLS equation. Another important consequence of this is that in the following we deal mainly with the wave amplitudes which directly determine the waveheight as twice the amplitude.

In the following we will consider the spatial NLS-equation, in which case the SFB will be periodic in time, and soliton-like in the spatial direction, describing the spatial evolution of downstream running time-modulated waves.

For the deterministic SFB wavefield the significant waveheight H_s , a quantity that is fundamental in the statistical description of wave fields cannot well be defined. Yet, since the space asymptotics of the wave field is a uniform wavetrain, when considering the averaged amplitude of the one-third highest waves, the only consistent similar quantity would be the value $2r_0$. Adopting then the (seemingly arbitrary, but often used) definition of ‘rogue’ wave as waves of wave height larger than $2.2 * H_s$, this will give a rough idea in which cases in the following we are dealing with extreme waves.

2.2 Characteristic spatial evolution

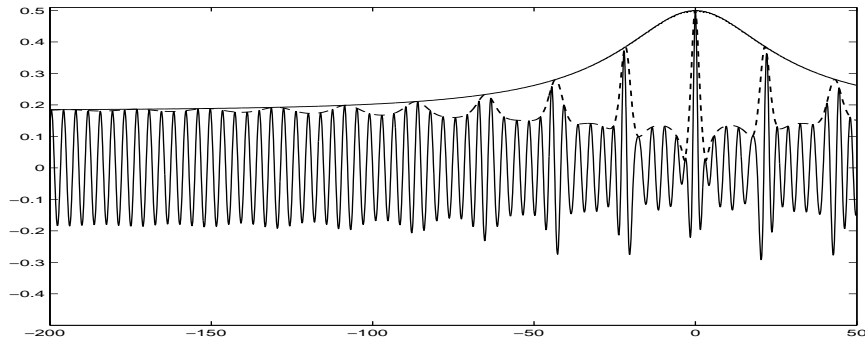


Fig. 1. Snapshot of the spatial wavefield SFB for $\tilde{\nu} = \sqrt{1/2}$. Shown are the individual waves, their envelope at that instant, and the time-independent MTA, maximal temporal amplitude. Physical dimensions are given along the axis: horizontally the distance and vertically the surface elevation in meters, for waves on a layer with depth of 5 meter.

Fig. 1 shows a plot of a snapshot of the spatial wavefield of waves running from left to right. At the left the slightly modulated uniform wave train (amplitude $2r_0$) is seen. This modulation clearly determines a characteristic modulation length that is maintained during the complete downstream evolution. While moving to the right, the modulations are amplified, creating distinct wave groups. At a certain position, called the *extreme position* (in scaled variables taken to be at $x = 0$), the largest wave appears, after which the reverse process sets in the decay towards the asymptotic harmonic wave train (with some phase change). Note that near the extreme position, the extreme wave is locally surrounded by waves of much smaller amplitude, as if the total energy in one wavegroup is conserved but with the energy redistributed between waves. In time, both

the waves and the envelope shifts to the right at different speed (the phase and group velocity respectively). Also shown in the plot is the so-called MTA, the *maximal temporal amplitude*: this is the (time-independent) curve determined by the maximal wave height at each point, the steady envelope of the wavegroups. Among other things, the MTA shows the global amplification factor, the ratio of the maximal and the asymptotic amplitude; this ratio is maximal 3, depending on $\tilde{\nu}$, but the local amplification factor near the extreme position can actually be much larger.

As is visible in Fig.1, the waves as they are running downstream, undergo increasingly large oscillations in amplitude. At a fixed position the maximal amplitude is given by the value of MTA, which is reached once every time period $T = 2\pi/\nu$. In between these successive maxima, the amplitude may be monotone, or (for sufficiently small values of $\tilde{\nu}$), non-monotone as is shown near the extreme position.

2.3 The extreme signal

The *extreme signal*, the time signal at the extreme position, has various special properties; we will denote the envelope by $S(\tau)$. First, this extreme signal is real, and its envelope is strictly positive for $\tilde{\nu} > \tilde{\nu}_{crit}$, while for $\tilde{\nu} < \tilde{\nu}_{crit}$ the envelope changes sign; here $\tilde{\nu}_{crit} = \sqrt{3/2}$. At times when the envelope vanishes, the phase experiences a π -jump, causing phase singularities. In any case we observe that at the extreme position all modes that make up the time signal are strongly phase correlated: either all having the same phase or some having opposite phase. More particularly, it was shown in [2] that the envelope S satisfies a Newton-type of equation and allows a simple phase-plane representation. Explicitly, the equation reads

$$\beta \partial_\tau^2 S + \gamma S^3 = \kappa S + \lambda \quad (1)$$

where κ, λ are positive constants (depending on $\tilde{\nu}$ and r_0). We will show in the next section that this is related to an optimization property.

For a characteristic value of $\tilde{\nu} < \tilde{\nu}_{crit}$, the time signal is plotted in Fig.2. We see that in one modulation period the wavegroup has been split in extreme waves and a number of intermittent waves of much smaller amplitude. The separation at times of a phase singularity, causes the intermittent and extreme waves to have opposite phase. In the spatial plot this shows itself in wave annihilation and wave creation at the successive singularities (see [2] for more details).

At the critical value $\tilde{\nu}_{crit} = \sqrt{3/2}$ for which the envelope vanishes at one point and is positive at the other times in the modulation period, the global amplification factor is precisely 2. To satisfy the ‘rogue wave’ definition of amplification larger than 2.2. the value of $\tilde{\nu}$ has to be smaller, i.e. will always correspond to the case when phase singularities are present; for instance, for $\tilde{\nu} = 1$, the amplification is $1 + \sqrt{2} \approx 2.4$.

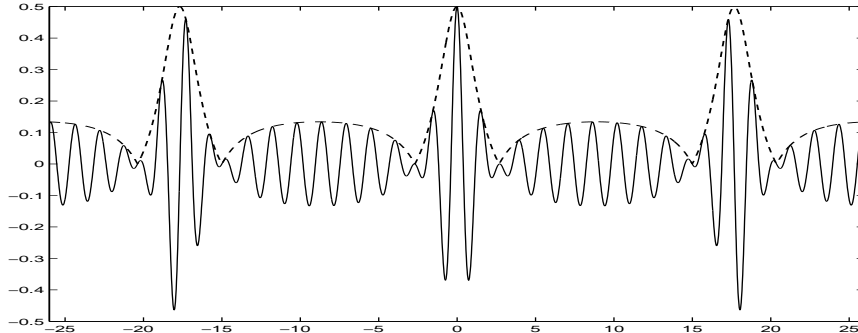


Fig. 2. The extreme signal, i.e. the time signal at the extreme position where the largest waves appear. For the same SFB parameters and scaling as in Fig.1 the horizontal axis is the time in seconds.

2.4 Spectral properties of the extreme signal

The spectral description of the time signal at a fixed position is for the asymptotic modulated wavetrain according to Benjamin-Feir instability: the major part of the energy in the central frequency and small contributions in one pair of sidebands. As is to be expected from the change of the spatial envelope, an increase of the number of relevant sidebands and large energy exchange between the modes takes place while approaching the extremal position; depending on the value of $\tilde{\nu}$ the energy of the central frequency may have been transferred to neighbouring sidebands, for $\tilde{\nu} = \sqrt{1/2}$ even completely.

Actually, the appearance in the extreme signal of the phase singularities, and the corresponding partitioning of the waves within one modulation period in extreme and intermittent waves, causes that large differences in the spectrum are observed while practically the same envelope for the extreme waves is obtained. The intermittent waves ‘modulate’ the spectral properties of the extreme waves. This can be seen by writing the envelope $S(t)$ in one period $[0, T_{mod}]$ as the sum of an envelope $f(t)$ of the extreme waves, and an envelope $g(t - T_{mod}/2)$ of the intermittent waves centered at $T_{mod}/2 = \pi/\nu$. Then the spectral Fourier components of the complete envelope $S(t) = f(t) - g(t - T_{mod}/2)$, the minus-sign to indicate the π -phase difference between the waves, are given by $S_m = \hat{f}_m - (-1)^m \hat{g}_m$, with \hat{f}_m, \hat{g}_m the spectral components of f and g in the m -th sideband respectively. The factor $(-1)^m = \exp(im\nu T_{mod}/2)$ is a consequence of the timeshift and has the modulational effect of decreasing and increasing the contributions in successive sidebands, starting with a decrease of the energy at the center frequency. In case the intermittent waves are such that $\sum |S_m|^2 < \sum |\hat{f}_m|^2$ this indicates that the presence of the intermittent waves makes it possible that the same maximal amplitude can be obtained for less energy. In Fig. 3 the spectra of the extreme signal are shown for three values of $\tilde{\nu}$.

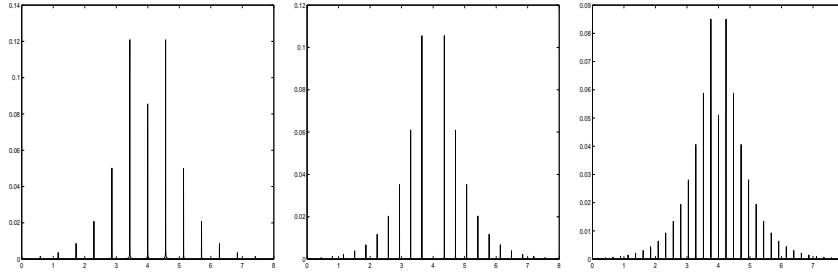


Fig. 3. The absolute value of the amplitude spectrum of the extreme signal for three values of $\tilde{\nu} = 1, \sqrt{1/2}, 1/2$ from left to right. Observe the vanishing contribution at the central frequency $\omega_0 = 4$ for $\tilde{\nu} = \sqrt{1/2}$.

The observation described here may be a warning when interpreting spectra for extreme waves, and just as well when looking for conditions on spectra to describe extreme waves. When background waves are present (the intermittent waves in the extreme signal may be considered like that), they will greatly disturb the spectrum related to the extreme waves and can increase the maximal possible amplitude at given energy.

2.5 Local evolution near the extreme position

We investigate the evolution of the signal and its spectral components in space near the extreme position. We show that the first order change in phase is described by a nonlinear modification of the dispersion relation with an additional quadratic term and a term of Fornberg-Whitham type. The change of the envelope, and of the quadratic spectrum, is shown to be of higher order.

The change of the amplitude near the extreme position is found from a direct Taylor expansion $A(\xi) = A(0) + \xi [\partial_\xi A]_{\xi=0} + \frac{\xi^2}{2} [\partial_\xi^2 A]_{\xi=0} + \dots$. Using the evolution equation and the equation for S one gets

$$A(\xi) = S + i\xi(-\kappa S - \lambda) - \frac{\xi^2}{2} [2\gamma\kappa S^3 + 3\lambda\gamma S^2 + \kappa^2 S + \lambda\kappa] + O(\xi^3).$$

In the plane of the complex amplitude A , the evolution in time at $\xi = 0$ is on the real axis, crossing the origin if there is a phase singularity. For small ξ the solution above can be described as $A(\xi) = e^{-i\kappa\xi} S - i\xi\lambda + O(\xi^2)$ which has the geometric interpretation of two successive actions: the solution at $\xi = 0$ that lies on the real axis is rotated around the origin over an angle $-\kappa\xi$ and then followed by a shift along the imaginary axis over a distance $-\lambda\xi$.

For the absolute value of the NLS solution we find up to third order

$$|A(\xi)|^2 = S^2 - \xi^2 [2\gamma\kappa S^4 + 3\lambda\gamma S^3 - \kappa\lambda S - \lambda^2] + O(\xi^3),$$

while, writing $A = |A| e^{i\phi}$, the first order change of the phase ϕ at $\xi = 0$ is

$$\partial_\xi \phi = -\kappa - \lambda/S + O(\xi),$$

indicating once again the singular behaviour at the times of phase singularity where S vanishes. For the phase of the physical solution, $\psi = \phi + (k_0 x - \omega_0 t)$, this leads to $\partial_x \psi = k_0 - (\kappa + \lambda/S)$. Invoking the governing equation for S , the result for the local wavenumber can be written like

$$k(x) = k_0 - \left(\gamma S^2 + \frac{\beta \partial_t^2 S}{S} \right) + O(x).$$

This can be interpreted as a nonlinear modification of the linear dispersion relation with a quadratic contribution and a homogeneous term of Fornberg-Withham type.

For the Fourier transformation with respect to time, we denote the spectral components of $A(\xi)$ by $A_m(\xi)$ according to $A(\xi, \tau) = \Sigma A_m(\xi) e^{-im\nu\tau}$. Using the fact that S is real we find

$$A_m(\xi) = S_m + i\xi \left(-\kappa S_m - \hat{\lambda} \right) - \frac{\xi^2}{2} \left[2\gamma\kappa \left(\widehat{S^3} \right)_m + 3\gamma\lambda \left(\widehat{S^2} \right)_m + \kappa^2 S_m + \kappa \hat{\lambda} \right] + O(\xi^3).$$

Here $\hat{\lambda} = \lambda \delta(m)$ is a contribution to the central frequency $m = 0$ only, while $\widehat{S^2}$ and $\widehat{S^3}$ denote convolution of second and third order respectively. For the absolute value we find up to third order

$$|A_m(\xi)|^2 = S_m^2 - \xi^2 \left[2\gamma\kappa S_m \cdot \left(\widehat{S^3} \right)_m + 3\lambda\gamma S_m \cdot \left(\widehat{S^2} \right)_m - \kappa \hat{\lambda} S_0 - \hat{\lambda}^2 \right] + O(\xi^3).$$

To relate this with the change of the physical quadratic spectrum, we get for the quadratic spectrum using $\eta(x, t) = \Sigma A_m(x) \exp[-i(\omega_0 + m\nu)t] + cc$:

$$P_m(x) = P_m(0) - x^2 \left[2\gamma\kappa S_m \cdot \left(\widehat{S^3} \right)_m + 3\lambda\gamma S_m \cdot \left(\widehat{S^2} \right)_m - \kappa \hat{\lambda} S_0 - \hat{\lambda}^2 \right] + O(x^3).$$

Writing $A_m = |A_m| e^{i\theta_m(\xi)}$ we find at $\xi = 0$ for the phase change of the spectral components of the amplitude $\partial_\xi \theta_m(0) = -\kappa - \hat{\lambda}/S_0$. For the phase of the physical solution η this modifies the change due to linear dispersion:

$$\partial_x \psi_m = -\kappa - \frac{\hat{\lambda}}{S_0} + k_0 + m\nu/V_0,$$

which is the spectral version of the nonlinearly modified dispersion relation.

3 Extremal formulations

This section addresses some aspects centered around the question when a wavefield (or envelope) attains its maximal value, depending on the constraints that are imposed. We will denote this symbolically for a signal $s(t)$ like

$$\max_s \{ \mathcal{A}(s) \mid \text{constraints} \} \text{ with } \mathcal{A}(s) = \max_t s(t)$$

In particular, the effect of prescribing the quadratic spectrum is considered first. Then we consider the case of relevance for the evolution of waves, when we take as constraints motion invariants (integral quantities), and describe that the extreme signal of the SFB solutions of the previous section arises as special signal when the constraints are optimally chosen.

3.1 Constrained maximal signal amplitudes

Here we consider real functions of given period T and $\nu = 2\pi/T$, or look at signals with continuous spectrum (using the notation of the latter). Any signal with given quadratic spectrum $P(\omega)$ is of the form

$$s(t) = \int \sqrt{P(\omega)} e^{i\theta(\omega)} e^{-i\omega t} d\omega$$

for some phase function $\theta(\omega)$. A completely focussed signal would have all phases the same, say zero, $s_{foc}(t) = \int \sqrt{P(\omega)} e^{-i\omega t} d\omega$, and produces the signal that for the given quadratic spectrum has the largest amplitude (at $t = 0$), and

$$\max_s \{ \mathcal{A}(s) \mid s \text{ has given quadratic spectrum } P(\omega) \} = s_{foc}(0) = \int \sqrt{P(\omega)} d\omega.$$

If we relax the constraints, the results critically depend on the constraints. For instance, if not the spectrum, but only the value of the integrated quadratic spectrum is prescribed, the related maximization problem has no finite solution. In Fourier language this is related to the fact that the energy is equally partitioned over all sidebands: equipartition of energy. We indicated in the previous section that intermittent waves can partly contribute to a better equipartition. If stronger norms that the integrated quadratic spectrum are prescribed, finite solutions will exist.

Most relevant seems to consider the maximization problem with constraints that are motivated by physics. To that end we introduce the following functionals that are related respectively to the approximation of the physical energy H , the physical momentum I and the ‘mass’ functional M defined by

$$H(s) = \int_0^T \left[\frac{\beta}{2} (\partial_t s)^2 - \frac{\gamma}{4} s^4 \right] dt, \quad I(s) = \int_0^T \frac{1}{2} s^2 dt, \quad M(s) = \int_0^T s dt,$$

and we investigate the optimization problem²

$$\max_s \{ \mathcal{A}(s) \mid H(s) = h; I(s) = g; M(s) = m \}. \quad (2)$$

² A very interesting statistically motivated variant of this maximization problem (without the linear mass-constraint) has been considered by Fedele [3]. He considers the initial value problem (evolution in time) and uses the Hamiltonian and quadratic invariant functionals that are related to the Zakharov equation, and takes as values of the constraints the values of a linearized wavefield at an initial time.

The resulting equation for (2) follows with Lagrange multiplier rule:

$$\sigma \delta \mathcal{A} = \lambda_1 \delta H + \lambda_2 \delta I + \lambda_3 \delta M \quad (3)$$

where we write the variational derivative of a functional K like δK (when equated to zero, $\delta K = 0$, this is precisely the Euler-Lagrange equation of the functional K). The multipliers are related to the values of the constraints; when the rhs doesn't vanish, the multiplier σ can be taken equal to one without restriction. Explicitly, the equation reads

$$\sigma \delta_{Dirac}(t - t_{\max}(s)) = \lambda_1 [-\beta \partial_t^2 s + \gamma s^3] + \lambda_2 s + \lambda_3$$

where $t_{\max}(s)$ is the time at which s attains its maximum, and δ_{Dirac} denotes Dirac's delta function. When the rhs vanishes, which is consistent with $\sigma = 0$, we recover the equation for the extremal signal of SFB described above. This is only the case if the constraint values g, h, m are chosen correctly; we show in the next subsection that this holds for the extremal signal.

For non-optimal constraint values, the multipliers will be different and $\sigma \neq 0$. Then formally the extremal signal can still be found explicitly but will not be a realistic physical signal since it contains a discontinuity in the derivative at the time of maximal amplitude as a consequence of the delta-function; the optimal solution is then obtained by pasting continuously together parts of a suitable extreme time signal. Although the signal itself may be non-physical, its value of the maximal amplitude provides an upperbound for any other signal satisfying the constraints.

3.2 Extremal property of the extreme signal

As stated above, among signals that satisfy constrained values of the functionals H, I, M the ones with maximal amplitude will be obtained when the constraints are such that these three functionals are linearly related (when $\sigma = 0$). We will now show that the extremal signals have this property.

Indeed, for suitable parameters ν, r_0 related to the constraint values g, m , the extreme signal will be a solution of the constrained optimization problem for the physical energy

$$\min_S \{ H(S) \mid I(S) = g, M(S) = m \} \quad (4)$$

Indeed, an extremizer of this optimization problem satisfies the Lagrange multiplier formulation

$$\delta H(S) = -\kappa \delta I(S) - \lambda \quad (5)$$

for some multipliers $-\kappa, -\lambda$. Written in full for the specific functionals, this is precisely the Newton equation (1) for the extreme signal. Actually, using the fact that H and I are restrictions to real-valued amplitudes of motion invariants for the complex amplitude of NLS, these values in (4) are immediately found from the asymptotic values at the uniform wavetrain; we will describe this in more detail in a forth coming paper [4].

4 Conclusions and remarks

We have studied a special class of wavefields and extracted several properties that may be useful for the understanding of the appearance of extreme waves in more realistic situations.

Although the wavefields are derived from the simple NLS-model and no rigorous mathematical proof of their validity can be given, at least it can be said that these wavefields seem to be realizable in practice, as was shown by actual experiments performed in large wavetanks at MARIN, see the contribution of Huijsmans e.a. [5] in these proceedings. The experimental verification is vital, in particular because most simplified models (and certainly NLS as has been used here) do not predict breaking phenomena. When breaking occurs, the deterministic predictions become useless, while if no breaking occurs it can be expected that the predictions have qualitative, and as has been shown in the experiments, also quite good quantitative, validity.

It is also appropriate to discuss the validity, the ‘robustness’, of the basic phenomena described here for extension to more realistic situations. In particular this concerns the optimization property of the extreme signal: can we expect such a property to hold in more realistic situations, without relying on any conviction that also in those cases ” la nature agit selon quelque principe d’un maximum ou minimum.” (Euler, 1746).

The optimization principle involves three functionals. Two of them have a clear physical meaning, although for NLS the complexified versions have to be considered. These are H , which is when complexified the Hamiltonian of NLS and is an approximation of the energy, and the quadratic functional I which in complex form is also an NLS invariant that can be interpreted for the real wavefields as the momentum. These functionals will also be present as invariants for reliable models that are more accurate than the NLS model, since the energy and momentum expressions are (approximations of) motion invariants for the full surface wave equations under the assumptions of non viscous fluid and translation symmetry. It can therefore be anticipated, or at least it can be hoped, that these two functionals will be relevant in any optimization principle for realistic large waves at the extreme position.

The major questionable point in the idea to generalize (4) is the role of the so-called ‘mass’ functional M that does not seem to correspond to a physically well understood invariant functional in more general situations. From its definition, $M(S)$ is seen to be precisely the square root of the energy in the central frequency, $M(S) = S_0$. It will be shown in [4] that this ‘mass’ turns up as a special case, valid only at the extreme position, in a variational principle that describes the complete SFB evolution as a relative equilibrium according to general Hamiltonian theory. That variational formulation depends on (the existence of) a higher order invariant functional, and this seems to be related to the special properties of the completely integrable NLS equation considered here. So the results presented here do not unambiguously support the idea that the optimization principle for the extreme signal can be expected to hold also in more

realistic cases. Yet it is tempting to look for such extremal formulations also in more realistic cases.

It may even be possible to investigate in a direct way the optimization principle for the extreme signal from experiments in a well-controlled laboratory environment. One possibility is to calculate the values of the relevant functionals from the measured signal at the extreme position, and investigate how close these values are near the optimal values from the minimizing property. Another, less robust (and therefore maybe more informative) method may be to use the fact that the extremizing property reflects itself in a simple phase-plane representation of the signal, see [2], so that the phase plane representation of the experimental extreme signals could give an indirect indication. Further research in this direction will be executed.

Acknowledgement

Regular discussions with Gert Klopman (UTwente) and Renee Huijsmans (MARIN) have been helpful. Special thanks to Francesco Fedele for referring to [3] and some useful discussions. Financial support from RUTI (Ministry of Research and Technology, Indonesia) in the project 'Wave motion and Simulation', and support for visits to ITB of EvG and NK by EU-Jakarta project SPF2004/079-057, and for visit of NK to 'Rogue Waves 04' by JMBurgers Centre, is acknowledged. This work is also part of project STW 5374 'Extreme Waves' from the technology division STW of NWO Netherlands.

References

1. N.N. Akhmediev and A. Ankiewicz, *Solitons, Nonlinear pulses and beams*, Chapman & Hall, 1997
2. Andonowati, N. Karjanto and E. van Groesen, Extreme wave phenomena in downstream running modulated waves, submitted July 2004.
3. F. Fedele, The occurrence of extreme wave crests and the nonlinear wave-wave interaction in random sea; *Proceedings XIV ISOPE Conference*, Toulon, France, May 2004..
4. E. van Groesen and Andonowati, Variational formulations for extreme waves, to be published.
5. R.H.M. Huijsmans, G. Klopman, N. Karjanto and Andonowati: Experiments on extreme wave generation based on Soliton on Finite Background; in *Proceedings 'Rogue Waves 2004'*, Brest France, October 2004.
6. P. Janssen, Nonlinear four-wave interaction and freak waves, *JPO* **33** (2003) 863-884

Dependence of Freak Wave Occurrence on Kurtosis

Nobuhito Mori¹ and Peter A.E.M. Janssen²

¹ Osaka City University,
Department of Environmental Urban Engineering,
3-3-138 Sugimoto, Sumiyoshi-ku, Osaka 558-8585, JAPAN
mori@urban.eng.osaka-cu.ac.jp

² European Centre for Medium-Range Weather Forecasts,
Shinfield Park, Reading RG2 9AX, UK
peter.janssen@ecmwf.int

Abstract. The occurrence probability of freak waves is formulated as a function of number of waves and surface elevation kurtosis based on the weakly non-Gaussian theory. Finite kurtosis gives rise to a significant enhancement of freak wave generation. For fixed number of waves, the estimated amplification ratio of freak wave occurrence due to the deviation from the Gaussian theory is 50%-300%.

1 Introduction

The last decade freak waves have become an important topic in engineering and science. Freak wave studies started in the late 80's [1] and the high-order nonlinear effects on freak waves were discussed in the early 90's [2, 3]. Due to many research efforts, the occurrence of freak waves, their mechanism and detailed dynamical properties are now becoming clear [4, 5, 6, 7, 8]). It was concluded that the third order nonlinear interactions enhance the freak wave occurrence and are the primary cause of freak wave generation in a general wave field except for the case of strong wave-current interaction or wave diffraction behind an island [9].

Numerical and experimental studies have demonstrated that freak-like waves can be generated frequently in a two-dimensional wave field without current, refraction or diffraction [2, 4, 6, 10]. Moreover, the numerical studies clearly indicate that a freak wave having a single, steep crest can be generated by the third order nonlinear interactions in deep-water [2]. Also, the theoretical background of freak wave generation has become more clear [5], but the quantitative occurrence probabilities on the ocean surface remain uncertain. In addition, it is still questionable how to characterize the dominant statistical properties of freak wave occurrence in terms of nonlinear parameters, spectral shape, water depth and so on.

Recently, Janssen [11] investigated the freak wave occurrence as a consequence of four-wave interactions including the effects of non-resonant four-wave

interactions. He formulated the analytical relationship between the spectral shape and the kurtosis of the surface elevation. These results have the potential to unify the previous freak wave studies covering nonlinear interactions, spectral profiles, nonlinear statistics, etc.

The purpose of this study is to investigate the relationship between kurtosis and the occurrence probability of freak wave in a unidirectional wave train. First, the wave height distribution is formulated as a simple function of kurtosis by the non-Gaussian theory. Second, the maximum wave height distribution is obtained from the wave height distribution as a function of kurtosis and number of waves. Finally, the dependence of the occurrence probabilities of freak waves on kurtosis and the number of waves will be analyzed and discussed.

2 Theoretical Formulation of Freak Wave Occurrence

Following a central limit theorem, linear, dispersive random waves have a Gaussian probability distribution function (PDF) for the surface elevation. Finite amplitude effects result, however, in deviations from the Normal distribution, as measured by a finite skewness and kurtosis. For narrow band wave trains it will be shown that the wave height distribution only depends on the kurtosis. Therefore, we shall formulate the relationship between wave height distribution and kurtosis to examine analytically the effects of kurtosis on freak wave occurrence.

We assume that waves to be analyzed here are unidirectional with narrow banded spectra and satisfy the stationary and ergodic hypothesis. Let $\eta(t)$ be the sea surface elevation as a function of time t and $\zeta(t)$ an auxiliary variable such that $\eta(t)$ and $\zeta(t)$ are not correlated. Assuming both $\eta(t)$ and $\zeta(t)$ are real zero-mean functions, we have

$$Z(t) = \eta(t) + i\zeta(t) = A(t)e^{i\phi(t)}, \quad (1)$$

$$A(t) = \sqrt{\eta^2(t) + \zeta^2(t)}, \quad (2)$$

$$\phi(t) = \tan^{-1} \frac{\zeta(t)}{\eta(t)}, \quad (3)$$

where A is the envelope of the wave train and ϕ the phase. For weakly nonlinear waves deviations from the Normal distribution are small. In those circumstances the PDF of the surface elevation can be described by the Edgeworth distribution, and the joint probability density function of η and ζ is known. The PDF of the envelope A now follows immediately from an integration of the joint probability distribution over the phase ϕ . It is then found that the first term gives the Rayleigh distribution, while the terms involving the skewness and etc, all integrate to zero because they are odd functions of the phase. The third term does give contributions to the probability distribution for the envelope and as a result we find

$$p(A) = Ae^{-\frac{1}{2}A^2} \left[1 + \frac{1}{4}(\kappa_{40} + \kappa_{22}) \left(1 - A^2 + \frac{1}{8}A^4 \right) \right], \quad (4)$$

where κ_{ij} is joint cumulant between η and ζ and we have used $\kappa_{40} = \kappa_{04}$, a relation that can easily be verified. Following Mori and Janssen [12], $\kappa_{22} = \kappa_{40}/3$ and the final result for the narrow-band approximation of the PDF of the envelope becomes

$$p(A) = Ae^{-\frac{1}{2}A^2} \left[1 + \frac{1}{3}\kappa_{40} \left(1 - A^2 + \frac{1}{8}A^4 \right) \right]. \quad (5)$$

From this result interesting consequences on the distribution of maximum wave heights may be obtained. In the narrow band approximation wave height H equals $2A$ and hence the wave height PDF becomes

$$p(H) = \frac{1}{4}He^{-\frac{1}{8}H^2} [1 + \kappa_{40}A_H(H)], \quad (6)$$

where $A_H(H) = \frac{1}{384}(H^4 - 32H^2 + 128)$. The exceedance probability $P_H(H)$ for wave height then follows from an integration of the wave height PDF from H to ∞ :

$$P_H(H) = e^{-\frac{1}{8}H^2} [1 + \kappa_{40}B_H(H)], \quad (7)$$

where $B_H(H) = \frac{1}{384}H^2(H^2 - 16)$.

We adopt a simple freak wave definition. A freak wave is thought to occur when the maximum wave height H_{max} exceeds twice the significant wave height $H_{1/3}$ of the wave train. The PDF of maximum wave height p_m in wave trains can be obtained once the PDF of wave height $p(H)$ and exceedance probability of wave height $P(H)$ is known [13], thus,

$$p_m(H_{max})dH_{max} = N_0[1 - P(H_{max})]^{N_0-1}p(H_{max})dH_{max}. \quad (8)$$

Substitution of Eqs.(6) and (7) into Eq.(8), gives the PDF of the maximum wave height, p_m ,

$$p_m(H_{max})dH_{max} = \frac{N}{4}H_{max}e^{-\frac{H_{max}^2}{8}} [1 + \kappa_{40}A_H(H_{max})] \times \exp \left\{ -Ne^{-\frac{H_{max}^2}{8}} [1 + \kappa_{40}B_H(H_{max})] \right\} dH_{max}, \quad (9)$$

and exceedance probability of the maximum wave height P_m ,

$$P_m(H_{max}) = 1 - \exp \left\{ -Ne^{-\frac{H_{max}^2}{8}} [1 + \kappa_{40}B_H(H_{max})] \right\}. \quad (10)$$

Eq.(9) is now evaluated as a function of N and κ_{40} (or μ_4). For $\kappa_{40} = 0$ results are identical to the ones following from the Rayleigh distribution. For simplicity it will be assumed that $H_{1/3} = 4\eta_{rms}$ (with η_{rms} the square root of the mean of the surface elevation variance). The freak wave condition therefore becomes $H_{max}/\eta_{rms} \geq 8$, and we obtain from Eq.(10) the following simple formula to predict the occurrence probability of the freak wave as a function of N and κ_{40} ,

$$P_{freak} = 1 - \exp[-N(1 + 8\kappa_{40})] \quad (11)$$

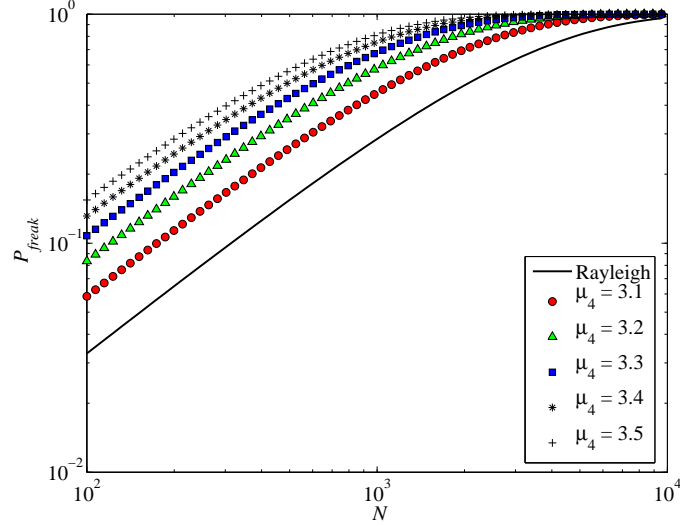


Fig. 1. Occurrence probability of freak wave as a function of number of waves N and kurtosis μ_4 .

where $\alpha = e^{-8}$.

Figure 1 shows for increasing μ_4 from 3.0 to 3.5 the comparison between the linear (Rayleigh) theory and present theory of the occurrence probability of the freak wave, P_{freak} , as a function of the number of waves N . For the case of $N=100$, the occurrence probability of the freak wave predicted by the linear theory is 3.3%, while it is 15.4% according to Eq.(9) with $\mu_4=3.5$, and for the case of $N=1000$, the occurrence probability of the freak wave is 28.5% by the linear theory, while it is 81.3% according to Eq.(9) with $\mu_4=3.5$. Thus, freak waves in a strong nonlinear field can occur several times more frequently than in a linear wave field, which obeys the Rayleigh distribution.

Figure 2 shows the ratio of freak wave occurrence probability R_{freak} predicted by the present theory and the Rayleigh theory, as a function of kurtosis μ_4 . For the case of a small number of waves $N \leq 250$, the ratio R_{freak} linearly depends on μ_4 . If μ_4 is 3.1 and $N = 500$, the occurrence probability of freak waves is 50% (two times) more than according to linear theory. On the other hand, the increment of R_{freak} decreases as the number of waves increases. This is because for very large number of waves even in linear theory the maximum wave height almost always exceeds $2 \times H_{1/3}$.

3 Conclusion

In this study, the kurtosis and related high-order cumulants were evaluated on the basis of Janssen's work [11]. Second, the wave height and the maximum wave

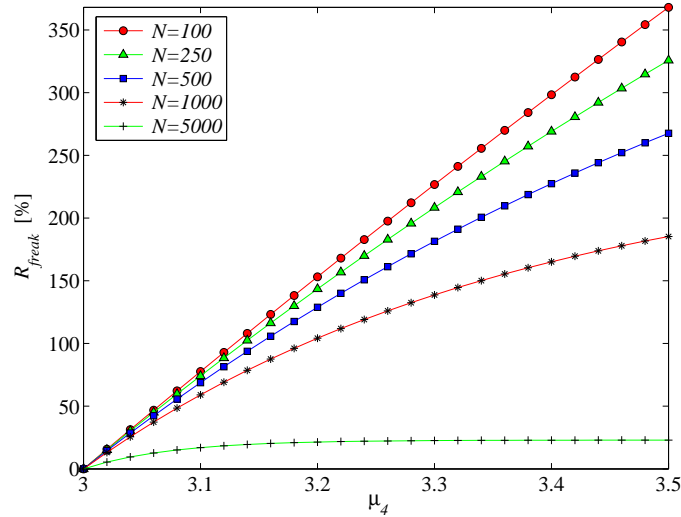


Fig. 2. Ratio of freak wave occurrence predicted by Eq.(11) to the Rayleigh theory.

height distribution were formulated as a function of kurtosis. Finally, the freak wave occurrence probability was formulated as a function of kurtosis and number of waves. From the theoretical frame work, we have the following remarks.

- The second order cross-cumulant between surface elevation and its envelope, κ_{22} , is 1/3 of the fourth cumulant, κ_{40} , of the surface elevation.
- The weakly non-Gaussian theory shows the dependence of the maximum wave height distribution on kurtosis.
- The occurrence probability of freak waves is significantly enhanced by the kurtosis increase as a consequent of the wave-wave interactions.

In order to check the validity of the theories developed here, systematic and continuous field measurement of freak waves will be critically required.

References

- [1] R.G. Dean. Freak waves: a possible explanation. In A. Tørum and O.T. Gudmestad, editors, *Water wave kinematics*, pages 609–612. Kluwer Academic Pub., 1990.
- [2] T. Yasuda, N. Mori, and K. Ito. Freak waves in a unidirectional wave train and their kinematics. In *Proc. of the 23th Int. Conf. on Coastal Eng.*, volume 1, pages 751–764, Venice, 1992. ASCE.
- [3] T. Yasuda and N. Mori. High order nonlinear effects on deep-water random wave trains. In *International Symposium: Waves-Physical and Numerical Modelling*, volume 2, pages 823–332, Vancouver, 1994.
- [4] K. Trulsen and K. Dysthe. Freak waves-a three-dimensional wave simulation. In *Proceedings of the 21st Symposium on Naval Hydrodynamics*, pages 550–558. (National Academy Press, 1997.

- [5] A.R. Osborne, M. Onorato, M. Serio, and S. Bertone. The nonlinear dynamics of rogue waves and holes in deep water gravity wave trains. *Physical Letter A*, (275):386–393, 2000.
- [6] Onorato M., A.R. Osborne, M. Serio, and S. Bertone. Freak waves in random oceanic sea states. *Physical Review Letter*, (86):5831–5834, 2001.
- [7] Sverre Haver. Evidences of the existence of freak waves. In M. Olagnon and G. Athanassoulis, editors, *Rogue Waves*, pages 129–140. 2001.
- [8] N. Mori, P. Liu, and T. Yasuda. Analysis of freak wave measurements in the Sea of Japan. *Ocean Engineering*, 29(11):1399–1414, 2002.
- [9] M. Olagnon and G. Athanassoulis, editors. *Rogue Waves*. IFRMER, 2000.
- [10] C.T. Stansberg. Extreme waves in laboratory generated irregular wave trains. In A. Tørum and O.T. Gudmestad, editors, *Water wave kinematics*, pages 573–590. Kluwer Academic Pub., 1990.
- [11] P.A.E.M. Janssen. Nonlinear four-wave interactions and freak waves. *J. Phys. Oceanogr.*, (33):2001–2018, 2003.
- [12] N. Mori and P.A.E.M Janssen. On kurtosis and occurrence probability of freak waves. *in preparation*, 2005.
- [13] Y. Goda. *Random Seas and Design of Maritime Structures*. World Scientific, 2nd edition, 2000.

Extreme Events in Field Data and in a Second Order Wave Model

Elzbieta Maria Bitner-Gregersen¹, and Anne Karin Magnusson²

¹ Det Norske Veritas, Veritasveien 1,
N-1322 Høvik, Norway
elzbieta.bitner-gregersen@dnv.com
² Norwegian Meteorological Institute, Allégaten 70,
N-5007 Bergen, Norway
a.k.magnusson@met.no

Abstract. The analysis is based on North Sea field data and on second order time domain simulations. Statistical properties of extreme waves are presented. Particular focus is given to the wave crest. Wave parameters obtained from the field data are compared with the values derived from the second order time domain simulations. Limitations of the 2nd order wave model to predict extreme events are shown. Uncertainties related to the field and numerically generated data are discussed.

1 Introduction

Abnormal waves, often called *rogue* waves or *freak* waves have been subject to much attention recently. These waves represent operational risks to ship and offshore structures, and are likely to be responsible for a number of accidents in the past. The completed (in 2003) EU research project MaxWave has made significant contribution to the understanding of freak waves; however, several important questions are still not answered. Too few data sets including freak events have been recorded making difficult to develop satisfactory physical and statistical models for prediction of these waves. Further, no consensus has been reached neither about a definition of a freak event nor about the probability of occurrence of freak waves. Finally, still more research is called for in order to investigate effects of these waves on marine structures.

The random nature of sea surface and non-linear effects are important when analyzing extreme events. Higher order solutions increase wave steepness, maximum crest and wave height compared to linear theory, and consequently also increase the probability of occurrence of extreme waves. As shown by several authors (i.e. [17], [9], [2]), freak waves in the “second order world” are pretty rare events. At the 100-year crest level the 2nd order models are expected to be of reasonable accuracy to predict extreme events, see [4].

The present analysis is based on North Sea field data and on second order time domain simulations using measured sea state parameters. The study focuses on statistical properties of extreme waves and on limitations of the 2nd order wave model to predict them. Main attention is given to the wave crest. Time series of wave elevations are generated using the Pierson-Moskowitz [16], JONSWAP [9] and two-peak Torsethaugen [19] frequency spectral shapes for long-crested seas and deep/intermediate water depth. Measured wave parameters are compared with values given by the second order time domain simulations. Sampling variability related to the data is discussed.

2 Field Data

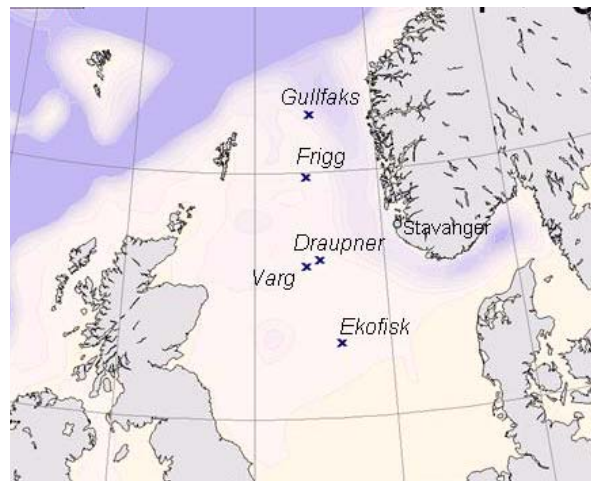


Fig. 1 The North Sea with locations of Ekofisk, Varg, Draupner, Sleipner, Frigg and Gullfaks.

Field data from two sites (Ekofisk and Draupner) in the North Sea are used. The following storms have been chosen as background for the study:

- (1) 25-26 October 1998: The ‘Stenfjell case’, using data at Ekofisk. The case is named after the bulk carrier *Stenfjell*, which arrived at Esbjerg (a harbour on West coast of Denmark) on the morning of 26 October 1998 with heavy weather damage to the wheelhouse, accommodation and electrical installations, reportedly due to freak waves. The ship was sailing from Hamburg to Tananger (near Stavanger, Western Norway). The ship experienced wind and waves from a low that had passed over the central North Sea, giving strong winds in a constricted area on the South of the low. The area moved from the East of Scotland towards the Danish coast passing over Ekofisk where a sharp increase in wave height ($H_s=10\text{m}$) was observed on the 25th. Some high crests are measured by lasers at two locations of the site and are analysed further herein.

(2) *27 December 1998*: A situation with close to 12m significant wave height with westerly winds at Ekofisk. High crests are observed in measured time series. The fetch is short from this direction and the increase is sharp.

(3) *5-6 February 1999*: The production ship (FPSO) at Varg (58N, 2E), operated by Saga Petroleum, experienced some damage due to ‘green water’ [5]. The wave damage caused the loss of a life buoy, a fire equipment storage locker torn from the connections and minor damages to cable gates occurred. All these items were located at the mid-ship. Time of incidence is not known. At Ekofisk, about 160 km further South, waves increased rapidly from 5 to 9m in a 6 hours period, with winds from between W and WNW. Wind speed stayed thereafter stable around 22-25 m/s during the night (a 12 hour period), slackening a little (to 20-23 m/s). At around 4 a.m. the 5th, wind direction veered to NNW and a high crest is recorded at Ekofisk at 04:40 UTC.

(4) *30 November 1999*: FPSO Varg B experienced some damage due to ‘green water’ [5]. Norsk Hydro reported damage to gas sensors, fire hose cabinets, doors on deluge stations for chemical injection module. Time of incident is not known, but records at Ekofisk also give some high crests. One record with $Crx/Hs = 1.4$ is used in this study, which occurred in the growing phase of the storm. The record is discussed further below.

(5) *29-30 January 2000*: the Petrojarl Varg ship, operated by Norsk Hydro, experienced damage on fore ship, midship and aft ship [5]. The incident is regarded as the most critical event so far on the Norwegian sector. The strong winds in the South area of the low pressure also influenced Ekofisk. Wave heights increased to about 11m. Some high crests are observed when wind speed is at its maximum (25 m/s from 17 to 21 UTC, from 280 deg). At that time it is most likely that waves are unidirectional.

(6) *1 January 1995*: The ‘Draupner wave’ with a crest height of 18.5 m above mean sea level is recorded by Statoil at the Draupner platform [11]. During this storm several wave heights (trough- to crest heights) more than twice H_s were observed at the Frigg platform operated by Elf Aquitaine. Analysis of weather maps indicates that there is swell added onto the wind sea from a slightly different direction.

The storms listed above have been selected from the MaxWave storm database [14]. Note that apart of the Draupner January 1 event all storms were recorded at the Ekofisk platform (see Fig.1). Sampling frequency used at Ekofisk is 2Hz, at Draupner 2.133 Hz. There are three sensors at Ekofisk: a waverider, and 2 downlooking lasers; the laser data are used herein. Wave data at Draupner are measured with a laser. The water depth for both platforms is 70m. One to two wave records (see Table 1) with the most extreme events present have been chosen from each storm and analyzed herein. In Table 1 H_{4std} denotes significant wave height calculated from the time series and is equal to 4 times standard deviation of the sea surface while H_{m0} represents significant wave height obtained from the zero-spectral moment of the whole time series. Although recognized

software is used to calculate H_{4std} and H_{m0} , a significant difference between the two estimators can be observed.

Table 1. Wave records selected for the study.

Case	Date and time	H_{4std} (m)	H_{m0} (m)	T_p (s)	T_{m02} (s)
1	25 Oct. 1998, 16:00 UTC	9.2	8.8	12.6	9.2
2	27 Dec. 1998, 06:40 UTC	11.6	10.4	14.6	10.6
3	5 Feb. 1999, 04:40 UTC	8.1	7.6	13.0	9.1
4	1 Dec. 1999, 02:20 UTC	6.5	7.2	11.3	8.7
5	29 Jan. 2000, 18:40 UTC	10.5	12.1	12.2	8.8
6	1 Jan. 1995, 15:20 UTC	11.9	11.2	16.7	10.8
7	1 Jan. 1995, 23:00 UTC	6.1	5.7	9.8	6.9

3 Second Order Simulations

A simulation program documented by Birknes and Bitner-Gregersen [1] is applied. Time series of wave elevations are generated using three empirical spectra: Pierson-Moskowitz [16], JONSWAP [9] and Torsethaugen [19]. The wave amplitudes are given by

$$a = \sqrt{2S(\omega, \theta)D(\theta)\Delta\omega\Delta\theta} \quad (1)$$

in the case of a directional sea state. Assuming single peaked frequency spectrum, e.g. JONSWAP, the spectrum can be given as $S(\omega, \theta) = S(\omega) D(\theta)$. For a two-peaked spectrum, we use $S(\omega, \theta) = S_1(\omega) D_1(\theta) + S_2(\omega) D_2(\theta)$. S_1 and S_2 may represent swell and wind sea frequency spectra and D_1 and D_2 are corresponding spreading functions.

Random wave amplitudes and random phases are generated for each wave component. The phases are assumed uniform distributed on the interval $[0, 2\pi]$, and the amplitudes are Rayleigh distributed with mean-square value given by

$$E[a^2] = 2S(\omega)\Delta\omega \quad (2)$$

The wave amplitude and phase define the complex wave amplitude through the following relation

$$A = a \exp(i\varepsilon) \quad (3)$$

A convenient model for combined seas is simply to add two frequency spectra

$$S(f) = S_{sw}(f) + S_w(f) \quad (4)$$

where $S_{sw}(f)$ is the swell spectrum and $S_w(f)$ is the wind sea spectrum.

The Torsethaugen two-peak spectrum applied herein was established primarily for one location (Statfjord, the Northern North Sea) but in qualitative terms is expected to be of much broader validity, and is currently used by the Norwegian industry for locations exposed to North Atlantic swell. The spectrum is an average wave spectrum derived by introducing various empirical factors, and therefore it should not be used uncritically for other locations. An attractive feature of the Torsethaugen spectrum is that only limited information about the sea-state is required as the spectrum is completely defined given the significant wave height and spectral peak period. The model splits the energy into a swell component and wind-sea component, using a modified JONSWAP spectrum for both peaks. It is noticed that even though including contribution from wind sea and swell the Torsethaugen spectrum does not necessarily need to have two *pronounced* peaks.

In the Torsethaugen model, each sea state is classified as *swell dominated* sea or *wind dominated* sea according to the criterion:

$$\begin{array}{ll} \text{swell} & \text{if } T_p > T_f \\ \text{windsea} & \text{if } T_p \leq T_f \end{array} \quad \text{where} \quad T_f = a_f H_{mo}^{1/3} \quad (5)$$

where T_p is the peak period, and $a_f = 6.6$ is adopted from the JONSWAP experiment [9]. If $T_p \leq T_f$, the local wind-sea dominates the spectral peak, if $T_p > T_f$ the swell dominates the spectral peak.

The statistical results presented herein are based on 350 simulations of a 1024 sec timeseries at 4Hz for the long-crested sea. A 1024 sec timeseries includes approximately 90-120 wave cycles. The chosen number of simulations gives reasonably stable results [3]. Typically the analyzed parameters evaluated from the simulations have approximately constant values for number of simulations $N > 250$. The calculations are carried out for the Torsethaugen spectrum and JONSWAP assuming peak enhancement factor γ equal to 3.3 and 1.0 (Pierson-Moskowitz). Results for deep/intermediate water depth are reported herein (water depth 70m).

4 Comparison of Wave Characteristics

Different definitions of freak waves are proposed in the literature. Often used as a characteristic is that the factor $H_{max}/H_s > 2$ (maximum crest to trough wave height factor). A ratio larger than 2 is seldom to be found in measured data, especially when measured by buoys due to the typical lack of skewness in these data [12, 13]. But this factor may not always be sufficient for an operational definition of an extreme or freak wave. Another commonly advocated definition of freak waves is a criterion based on the factor C_{max}/H_s , e.g. as suggested by Haver and Andersen [11] that $C_{max}/H_s > 1.2$ within a 20-minute sea elevation time series. Tomita and Kawamura [18] suggest that both a wave height and a crest height criterion be simultaneously fulfilled, with the height factor

higher than 2 and the crest factor higher than 1.3. Guedes Soares et al.[7, 8] argue that use of the height factor and the crest factor is not sufficient.

All wave records chosen for the present study include an event $c/H_s > 1.2$ and are shown in Figures 2-8. In each figure the top panel represents the 20 minutes time series sampled at 2Hz including the crest event analysed. Lower left panel shows the time history of significant wave height, maximum crest and trough in each 20minutes records during the storm. Lower right panel shows the frequency spectrum from the time series shown in top panel, using Blackman-Harris windowing and Fourier analysis on all data (nfft=2395, nb of samples), thereafter averaging the spectrum over 5 frequency bins (Nfa=5).

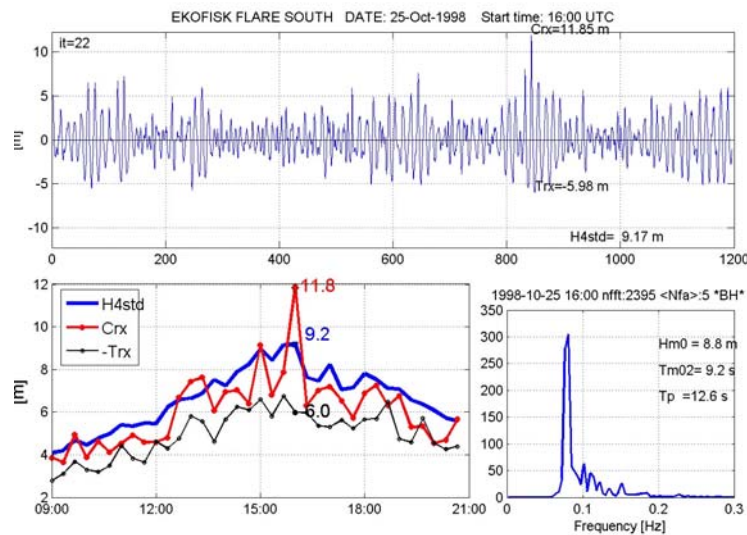


Fig. 2 Case 1: Measurements from laser at Flare South at Ekofisk during 25. October 1998. Lower left panel: Blue line: significant wave height using H4std, red line: max crest height (Crx) in each 20 minute record, black line: inverse of deepest trough (Trx) measured in each 20min record. $C_{\max}/H_{4std} = 1.29$ at 16:00 UTC

As seen in these figures the extreme events appear at different times of the storm histories, before, at, and after the significant wave height culmination (referred to here as part of storm with the highest H_s). Further, as shown in Table 2, by applying the Torsethaugen criterion (Eq.(5)) only the Draupner wave record (sea state 6, $T_p=16.7s$) represents clearly swell dominated sea. The sea state measured in case 2 (27 December 1998, 06:40 UTC) with $T_p=14.6s$, is very slightly swell dominated ($T_p > T_f$) when H_{m0} is used in calculation of T_f and wind dominated when H_{4std} is used. The relation between T_p and

T_f calculated from the spectra in the other cases (1, 3, 4, 5 and 7) indicates that the sea state is wind dominated following the Thorsethaugen criterion.

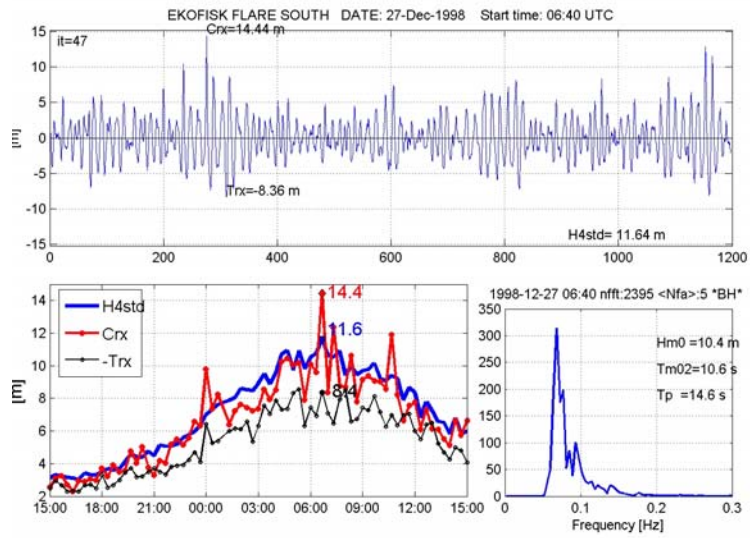


Fig.3 Case 2: 27 December 1998 storm . $C_{max}/H_{4std} = 1.24$ at 06:40 UTC.

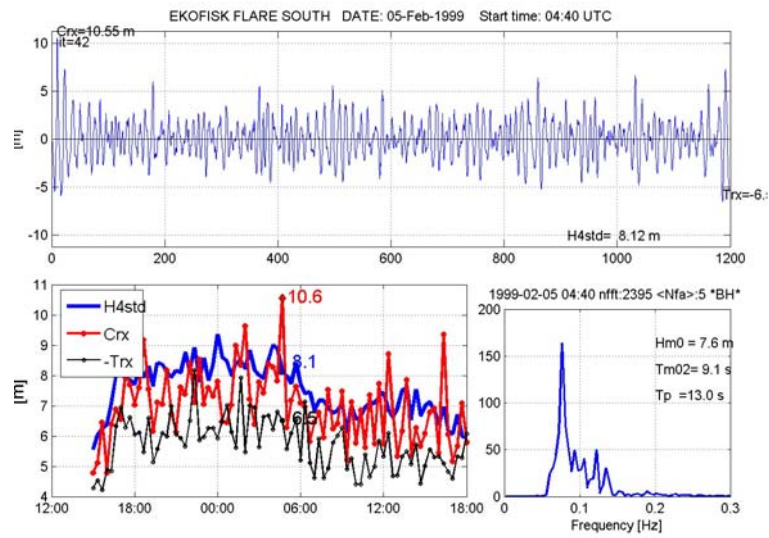


Fig.4 Case 3: 5-6 February 1999 storm. $C_{max}/H_{4std} = 1.31$ at 04:40 UTC the 6th.

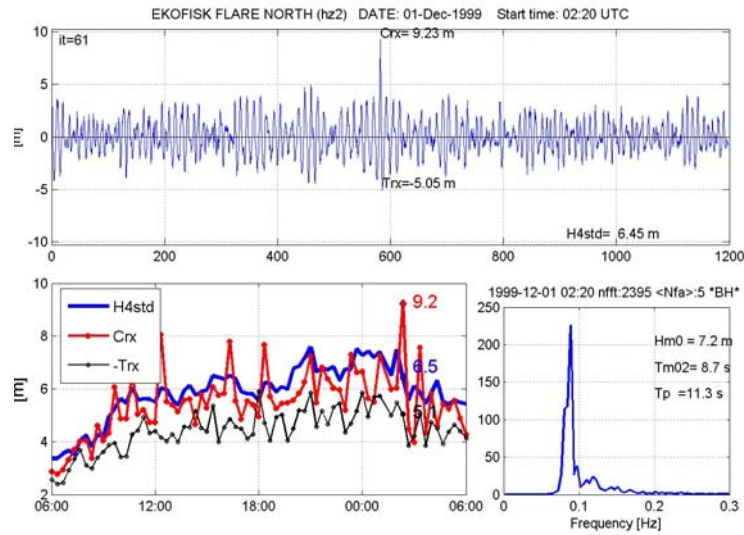


Fig.5 Case 4: 30. November – 1. December 1999 storm. Flare North measurements with $C_{max}/H_{4std} = 1.43$ at 02:20 UTC the 1st.

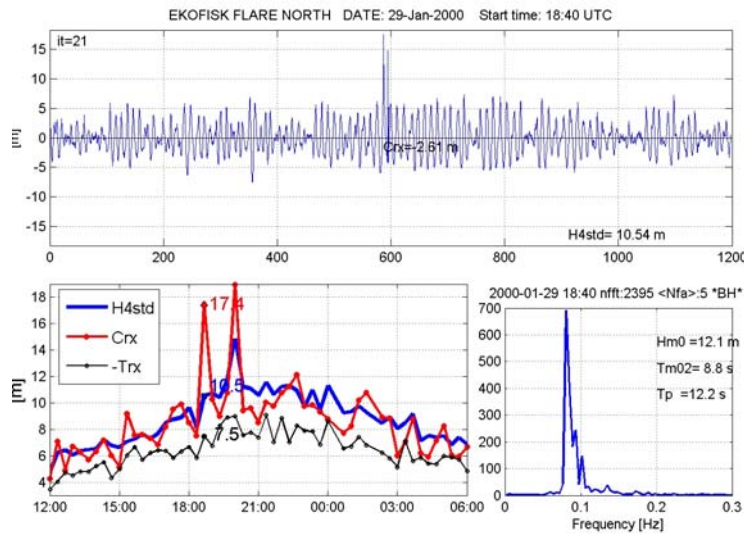


Fig. 6 Case 5: Flare North at Ekofisk, 29-30 January 2000. $C_{max}/H_{4std} = 1.65$ at 18:40 UTC the 29th.

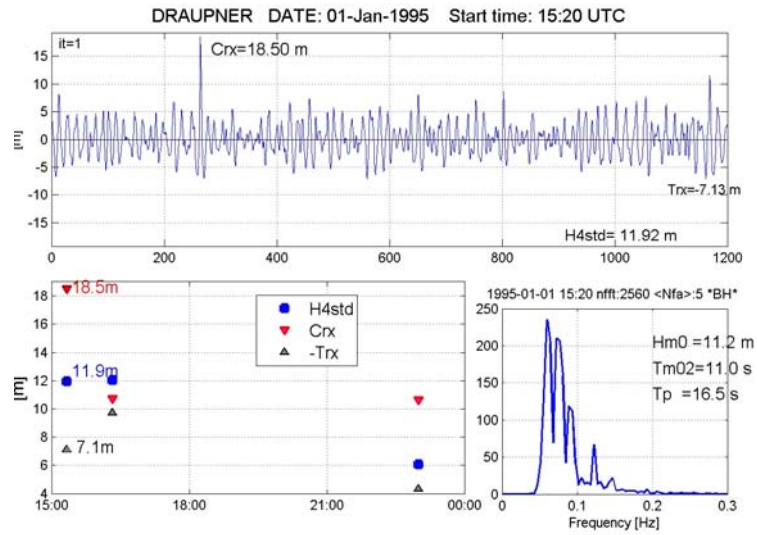


Fig. 7 Case 6: The Draupner “New year wave” recorded during the 1 Jan. 1995 storm, at 15:20UTC. Lower left panel shows the crest in detail. $C_{max}/H_{4std} = 1.55$

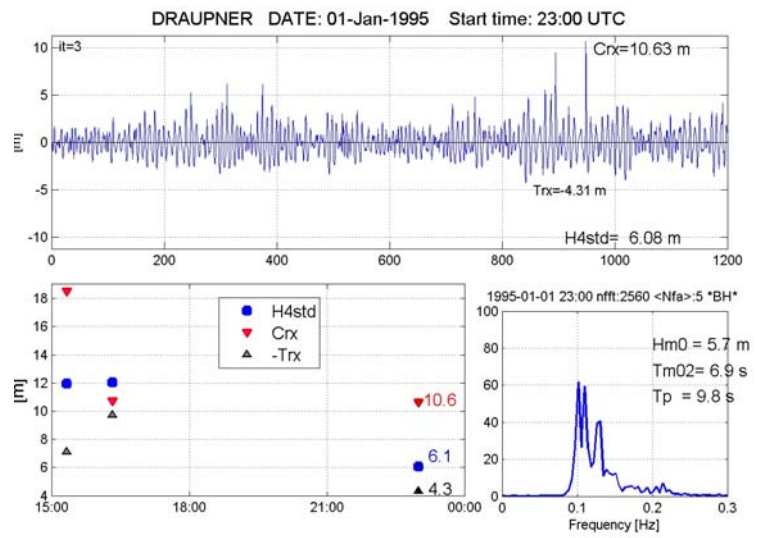


Fig. 8 Case 7: Second case from the Draupner platform on 1 Jan. 1995 storm, 23:00UTC. ($C_{max}/H_{4std} = 1.75$).

As expected (see Table 1) different crest to height ratios (C_{max}/H_s) are obtained using either H_{4std} or H_{m0} , and the difference between the ratios is significant for some wave records (see Table 2). Use of H_{4std} or H_{m0} may decide whether an event is classified as a freak event or not. Herein H_{4std} has been adopted because further discussions on which standard spectral analysis method to use is outside the scope of this paper.

Table 2. Sea surface characteristics.

Sea state	T_p (s)	T_f^* (s)	T_f^{**} (s)	Field data			Simulations – PM*		
				C_{max} (m)	C_{max}/H_{4std}	C_{max}/H_{m0}	$E[C_{max}]$	$\sigma_{C_{max}}$ (m)	$E[C_{max}]/H_{4std}$
1	12.6	13.8	13.6	11.8	1.29	1.34	8.47	2.91	0.92
2-w/sw d.	14.6	14.9	14.4	14.4	1.24	1.38	10.62	3.26	0.91
3	13.0	13.3	13.0	10.6	1.31	1.39	7.31	2.71	0.90
4	11.3	12.3	12.7	9.20	1.43	1.28	5.88	2.43	0.91
5	12.2	14.5	15.1	17.4	1.65	1.44	10.04	3.17	0.95
6-swell d.	16.7	15.1	14.8	18.50	1.55	1.65	10.53	3.25	0.88
7	9.8	12.0	11.8	10.63	1.75	1.86	5.76	2.20	0.95

* H_{4std} , ** H_{m0}

The second order simulations have been carried out using water depth of 70m, assumption of long-crested sea and H_{4std} and T_p as an input. T_p will depend on the averaging method used in the spectral calculations. In Table 2 results from simulations assuming a Pierson-Moskowitz (PM) spectrum are presented. Figs. 9 and 10 show results from simulations using all 3 types of spectral shapes (PM, JONSWAP and Thorsethaugen). In Fig.9 the mean and mean + 2*std of simulated extreme crests are compared with observations, while in Fig. 10 the mean and the maximum values of simulated maximum crests are compared with the maximum observed crests.

The JONSWAP spectrum with the factor γ equal to 3.3 gives lower mean extreme crest in comparison to the Pierson-Moskowitz and Torsethaugen spectrum in all cases. This can be attributed, in average, to larger spectral width for the two latter spectra, than the JONSWAP spectrum for the sea states considered, see also [4]. Further, we can see that the Torsethaugen spectrum increases slightly the extreme crests in average for the Draupner sea state 6, but, however, reduces the standard deviation. For the PM spectrum the mean extreme crest obtained from the 2nd order time domain simulations is up to 43% lower compared to the maximum observed crest. For the last 3 cases (5 (January 2000), 6 (Draupner 1995, 15:20UTC) and 7 (Draupner 1995, 23:00UTC)), the observed maximum crest is outside the interval range of the simulated mean of extreme crests plus two standard deviations of the extreme crest distribution, particularly for the higher sea states 5 and 6 (10.5m and 11.9m, compared to 6.1m in case 7). This confirms

the earlier findings presented in the literature; the freak wave observed at Draupner cannot adequately

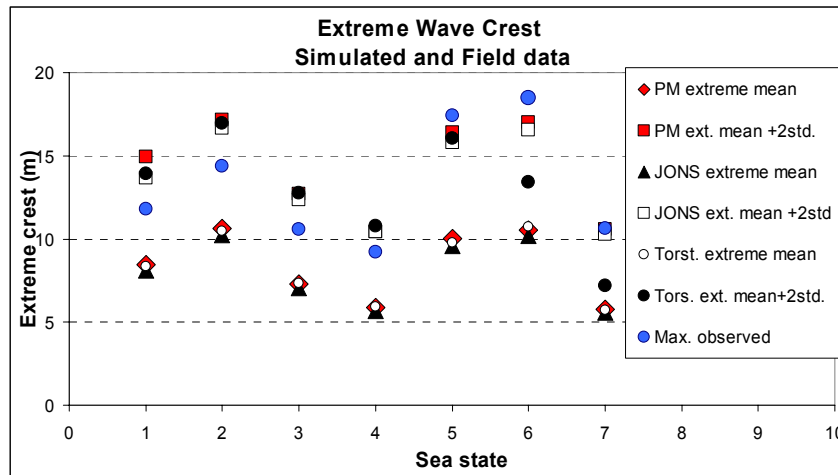


Fig. 9 Extreme wave crests in the 6 storm cases. Blue filled circles are observations. For simulations assuming Pierson-Moskowitz, JONSWAP and Thorsethaugen spectral shapes: given here are mean of maximum crests (points are all below observations) and its value + twice the standard deviation (see legend for symbol and color).

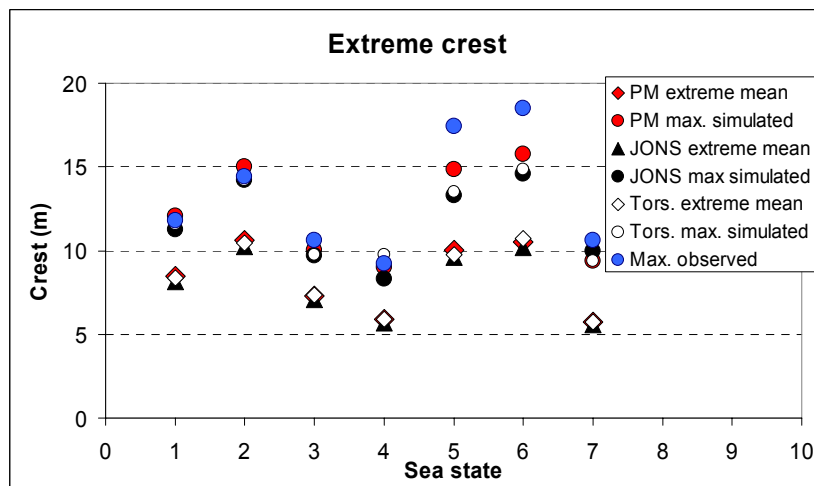


Fig. 10 As for Fig. 9, but simulation results are shown with mean and maximum values of maximum crest.

be accounted for by the 2nd order model. Note that the wave crest in the case 5 can be put in doubt due to the form (Fig. 11) of the wave behind the crest. However, for the less extreme events in cases 1 to 4 where $C_{max}/H_s < 1.45$, the 2nd order model ‘captures’ the observed maximum wave crest, thus the maximum observed crest is close to the crest extreme mean plus two standard deviations, see also [3].

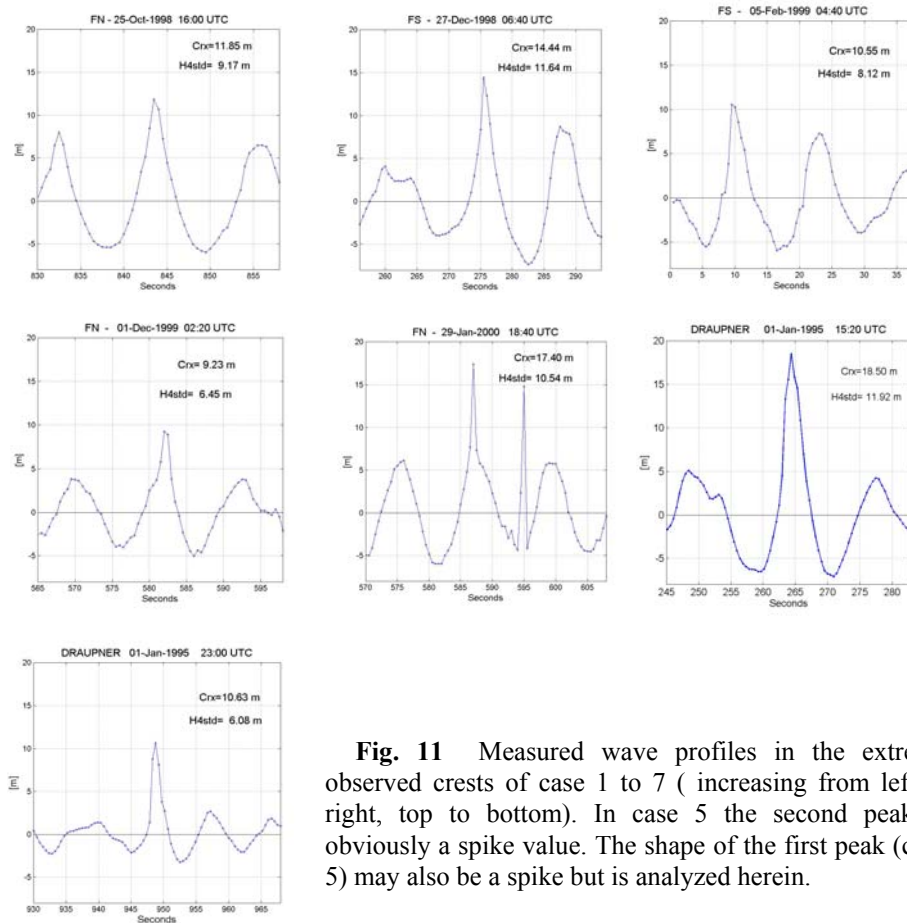


Fig. 11 Measured wave profiles in the extreme observed crests of case 1 to 7 (increasing from left to right, top to bottom). In case 5 the second peak is obviously a spike value. The shape of the first peak (case 5) may also be a spike but is analyzed herein.

The simulation results reported in Figs. 9 and 10 are based on the nominal (observed) significant wave height, $H_{s,nom}$. However, as pointed out by Bitner-Gregersen and Hagen [3] for a sample of 17 minutes time series there is a scatter in the spectral variance caused by sampling variability, which is accounted for in the simulations through random spectral amplitudes. For time series of 17 minutes duration, the coefficient of variation for significant wave height for a sample of realizations is in the range

5-7% (Olagnon & Magnusson [15] also showed H_{m0} calculated from simulations varied with up to 9%, in the mean 6%).

A high value of $C_{max}/H_{s,nom}$ may occur in a sea state in which also the simulated significant wave height is high ($H_{s,sim} = 4 \cdot \text{standard deviation of } 2048 \text{ simulated wave elevation values}$). In this case, $C_{max}/H_{s,sim}$ would be lower than $C_{max}/H_{s,nom}$. On the other side, a high crest observed in a 3 hour sea state may very well occur in a part of the sea state where the 20 minutes averaged significant wave height is substantially higher than the 3 hour averaged H_s , making the factor $C_{max}/H_{s,nom}$ low. In Fig. 10, the maximum simulated and observed wave crests are shown while Fig. 12 illustrates the difference between $C_{max}/H_{s,nom}$ and $C_{max}/H_{s,sim}$ for the PM spectrum. As can be observed, there is a clear difference, and this aspect should be kept in mind when evaluating freak criteria based on C_{max}/H_s or H_{max}/H_s ratios.

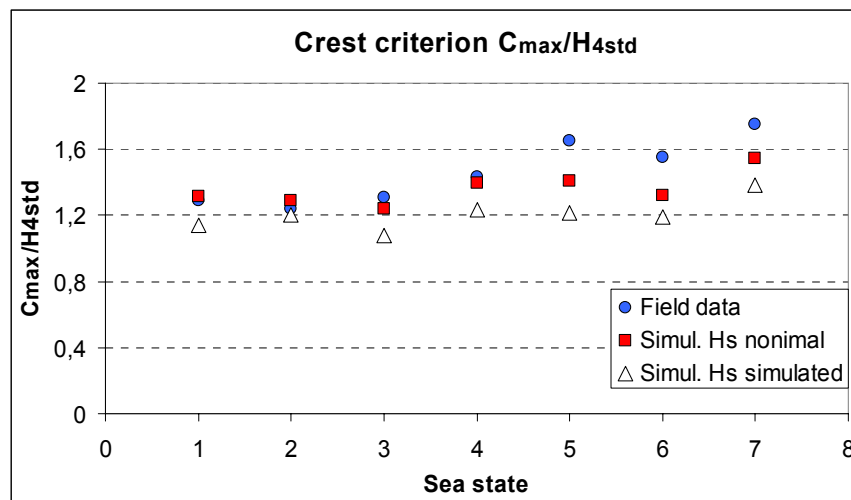


Fig. 12 Wave crest factor for nominal and simulated significant wave height using PM spectral shape.

5 Summary of Discussion

Cases analyzed herein show that the ratio C_{max}/H_s may vary significantly depending upon whether the significant wave height is calculated from the time series H_{4std} (4 times standard deviation) or from the zero-spectral moment H_{m0} . Which formulae is used may influence on deciding whether an event is classified as a freak wave or not. It is recommended to use both significant wave estimates with care, and investigate them further if significant difference between them is observed.

Cases 1 to 4 with the less extreme waves ($C_{max}/H_s < 1.45$) are well ‘captured’ by the 2nd order wave model. By capture it is meant here that the observed maximum crest is close to the simulated mean of extreme crests plus two standard deviations of the extreme crest distribution. This could be utilized in design by calibrating the extreme mean crest calculated by the 2nd order wave model. There is though no assurance that the observations have captured the most extreme waves in the area around Ekofisk due to changing profiles as waves evolve [13].

When $C_{max}/H_s > 1.45$, particularly for higher sea states with $H_s > 10.0\text{m}$, the observed maximum crest is outside the interval range of the simulated mean of extreme crests plus two standard deviations for the records characterized. Using the Thorsethaugen criterion [19] to define the sea state to be wind sea or swell, we find that two of these cases have been recorded in wind dominated sea (January 2000 storm, Draupner sea state at 23:00UTC) and the third one, the Draupner wave 1. January 1995 at 15:20UTC, in a swell dominated sea. Simulations of the Draupner wave assuming the Thorsethaugen spectral shape gives slightly higher mean values of the extreme crests as compared to PM or JONSWAP shapes.

In the first four cases, JONSWAP shapes give lower mean values, and PM shapes give highest extremes. Differences are though within decimetres.

The above leads to the conclusion that spectral shapes do influence results but a question is how significant these differences are. Further investigations are required to reach a firm conclusion.

It must be noted that of the 7 cases considered, the first 4 high crests occurred at end of the culmination period, when wind has relaxed to slightly lower speed, and wind direction is in a veering situation. This indicates that the sea state might be bi-directional at the event. Case 5, which is probably a spike, occurs in a strong growth phase of the storm (in which sea spray is highly probable). Cases 6 and 7 are a bit more difficult to define weatherwise (wavewise). Wind was around 20m/s all afternoon in the Northern North Sea, but analysis of weather maps also indicate the high crest events at both 15 and 23 occur in a slackening situation in the wind field as the wind direction is veering slowly towards North. Again one might find a spectrum with large spread or bi-directionality in these cases.

The present analysis is limited to long-crested sea. Further investigations including directional effects are called for.

Acknowledgement

The work presented was performed partially within the EU - Project “*Safety and Reliability of Industrial Products, Systems and Structures*” (SAFERELNET), which is described in <http://mar.ist.utl.pt/saferelnet/> and is funded partially by the European Com-

mission under the contract number G1RT-CT2001-05051 of the programme “Competitive Sustainable Growth”.

References

1. Birknes, J. and Bitner-Gregersen, E.M.: Non-linearity of the Second-order Wave Model for Directional Two-Peak Spectra. Proc. ISOPE'2003 Conf. Hawaii. (2003).
2. Bitner-Gregersen, E. M.: Sea state duration and probability of occurrence of a freak crest. Proc. OMAE'2003 Conf., Cancun, Mexico (2003).
3. Bitner-Gregersen, E.M. and Hagen, Ø.: Effects of Two-Peak Spectra on Wave Crest Statistics. Proc. OMAE'2003 Conf., Cancun, Mexico (2003).
4. Bitner-Gregersen, E. M., and Hage, Ø.: Freak Waves in the Second Order Wave Model. OMAE'2004 Proc., Vancouver, Canada (2004).
5. Ersdal, G. and A. Kvitrud,: Green water incidents on Norwegian production ships. Proceedings of ISOPE'2000 (2000).
6. Forristall, G. Z.: Wave Crests Distributions: Observations and Second-Order Theory. J. Physical Oceanography, vol.30. No.8. pp.1931-1943. (2000)
7. Guedes Soares, C., Cherneva, Z., and Antao, E.M., “Characteristics of Abnormal Waves in North Sea Storm Sea States. Accepted for publication in J. Applied Ocean Research (2004a).
8. Guedes Soares, C., Cherneva, Z., and Antao, E.M.: Abnormal Waves during Hurricane Camille. Accepted for publication in J. Geophysical Research (2004b).
9. Hasselmann, K. and Co-authors: Measurements of Wind-wave Growth and Swell Decay during the Joint North Sea Wave Project (JONSWAP). Dtsch. Hydrogr. Z.. Suppl. A. Vol.8. (1973).
10. Hagen, Ø.: Statistics for the Draupner January 1995 Freak Wave Event. Proc. OMAE-2002 Conference, Oslo, Norway (2000).
11. Haver, S. and Andersen O. J.: Freak Waves. “Rare Realizations of a Typical Population or Typical Realizations of a Rare Population.”. ISOPE' 2000, Seattle (2000).
12. Longuet-Higgins, M.S.: Eulerian and Lagrangian aspects of surface waves. J. Fluid Mech. 173, 683-707, (1986).
13. Magnusson, A. K, M. A. Donelan and W. M. Drennan: “On estimating extremes in an evolving wave field.” *Coastal eng.* **36**, pp 147-163 (1999).
14. Magnusson, A. K., Bitner-Gregersen, E.M. and Nieto Borge, J.C.: Analysis of Extreme Waves in the Maxwave Database. WMO Proc. Geneva (2003).
15. Olagnon, M, and A. K. Magnusson, 2004: “*Sensitivity study of sea state parameters in correlation to extreme wave occurrences*”. In proceedings of 14th international Offshore and Polar Engineering conf., ISOPE 3, (2004).
16. Pierson, W.J. and Moskowitz, L.: A proposed Spectral Form for Fully developed Wind Seas based on the Similarity Theory of t.A.A. Kitaigorodskii. J. Geoph. Res. Vol 69, pp 5181-5190 (1964).
17. Prevosto, M. and Bouffandeau, B.: Probability of Occurrence of a “Giant” Wave Crest. Proc. OMAE-2002 Conference, Oslo, Norway (2002).

18. Tomina, H. and Kawamura, T.: Statistical Analysis and Inference from the In-Situ Data of the Sea of Japan with Reference to Abnormal and/or Freak Waves. Proc. ISOPE'2000 Conf., Seattle, USA (2000).
19. Torsethaugen, K.: Model for Double Peaked Wave Spectrum. SINTEF Civil and Environmental Engineering, Rep. No. STF22 A96204, Trondheim, Norway (1996).

Spectral parameters to characterize the risk of rogue waves occurrence in a sea state

Michel Olagnon¹ and Anne Karin Magnusson²

¹ IFREMER Centre de Brest B.P. 70, F-29280 Plouzané, France

² Norwegian Meteorological Institute Allégaten 70, 5007 Bergen, Norway

Abstract. In a previous paper ([7]), we discussed the natural variability of some spectral parameters that may characterize a sea state, and concluded that deviations that might be observed close to occurrences of extreme waves were well within the natural range of variability. As a consequence, prediction of increased risk of rogue waves occurrence cannot be made from a simple local examination of the spectrum, but would require investigation of either simultaneous values of several parameters, or of the time history of a parameter over durations of the same order of magnitude as a storm.

In the present study, we investigate that second possibility, *i.e.* since the excursions on the time-scale of a sea-state are not decisive, we consider the next time-scale, that of a whole storm. To this aim, the Frigg database [4] is searched for storms, and an attempt is made to select within the set of storms a subset of “freaky storms” where there are observations of high crests with respect to the prevailing significant wave height. The histories of spectral parameters during the storms are then computed, and differences from histories in the subset and some other storms (since the other storms cannot all be “freaky”) are sought for.

Similarly to the previous study, those parameters are preferred that might be related to rogue wave occurrence. They were determined either from theoretical wave considerations (Benjamin-Feir instability indicators), or from meteorological ones (spectral front bandwidth, that might reveal “running fetch” situations).

1 Introduction

Significant wave height H_S , peak period T_p and main wave direction are sufficient to describe sea states for most practical purposes. However, that information is clearly not sufficient to detect increases in the risk of occurrence of unexpected rogue waves in a sea state. We thus study observations of additional parameters, in hope that on one hand they exhibit special properties when rogue waves occur, and that on the other hand they can be related to some theoretical mechanism of rogue wave generation and thus validate the assumption that the corresponding mechanism is active in nature on those occasions when rogue waves are observed.

It should be noted that in order to be useful, a parameter must have a characteristic change for some duration at a significantly larger time-scale than

that of the individual wave. Otherwise, the change in the parameter would merely be a detection of the rogue wave and could not be used for forecast, nor would it mean anything more than “the wrong place at the wrong time” and it thus could not fully validate a particular generation mechanism.

The next higher time-scale, that of a stationary sea state, was investigated in a previous paper ([7]). We concluded that sea state spectral parameters that exhibit sensitivity to rogue wave occurrences:

- do not depart from the normal range of aleatory variations but show only slight biases, and
- exhibit a high rate of false alarm.

We recommended that one try to find out criteria based on combined occurrence of several characteristics, including directional ones, or based on the next higher time-scale, *i.e.* the process or the time-history of characteristics over a whole storm duration.

The present study investigates the latter suggestion, that of characteristics derived from a whole storm.

Ersdal and Kvitrud ([1]) report on a total of 6 storms in the North Sea, and for two of them, damage was observed at two different locations. Similarly, damage was also reported at a BP platform during the storm of the famous “New Year Wave”. It is thus not unlikely that storms as a whole might have some characteristics related to an increase in the risk of occurrence of rogue waves.

2 Benjamin-Feir Instability indices

Many authors put forward non-linear focusing as a generating mechanism for rogue waves, and suggest to characterize it through an index of the Benjamin-Feir instability (BFI) computed by dividing steepness by adimensional bandwidth.

Results reported in [7], and recalled in figure 1, show that though sea state BFI indices are biased towards higher values when rogue waves occur, that bias is of little practical value since a small BFI index is no guarantee that rogue waves will not occur, and alerts for 80% of the rogue waves would require to send warnings more than half of the time.

Yet, the high natural variability of BFI index might be a consequence of the difficulty to obtain stable estimators when considering short *in situ* records, especially with respect to that part of spectral bandwidth that is relevant to the Benjamin-Feir instability and that is focused on the spectral peak.

Goda (1983) [2] recognizes that the narrowness parameter Q_p and the other ones that are based on spectral moments are sensitive, at least to some extent, to the tail of the spectrum and/or the cut-off frequency used in the measurements and analysis. He suggests the use of normalized peak height $\Phi_p = S(f_p)f_p/m_0$ as a measure of the sharpness of the spectral peak.

That measure of bandwidth has several advantages:

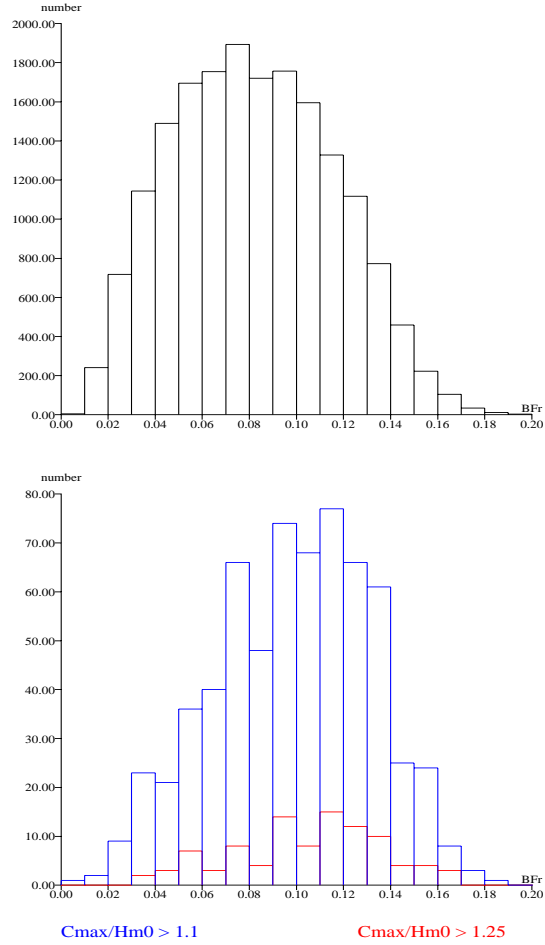


Fig. 1. Histogram of the robust Benjamin-Feir index values for 18000 sea states at Frigg

- it is not significantly affected by the cut-off frequency or a poor estimation of the spectral tail and of its shape;
- it enables to define in the same manner a “spectral front bandwidth” Φ_{fp} using the restriction of m_0 to $[0, f_p]$;
- it enables to define a spectral asymmetry coefficient that is also free from the influence of the spectral tail: $A_S = (\Phi_p - 2\Phi_{fp})/\Phi_p$.

That definition is often discarded because of the difficulties in estimating precisely S_{max} , especially for measured spectra. However, a reasonable amount of robustness may be achieved by using in such cases the weighted average of the

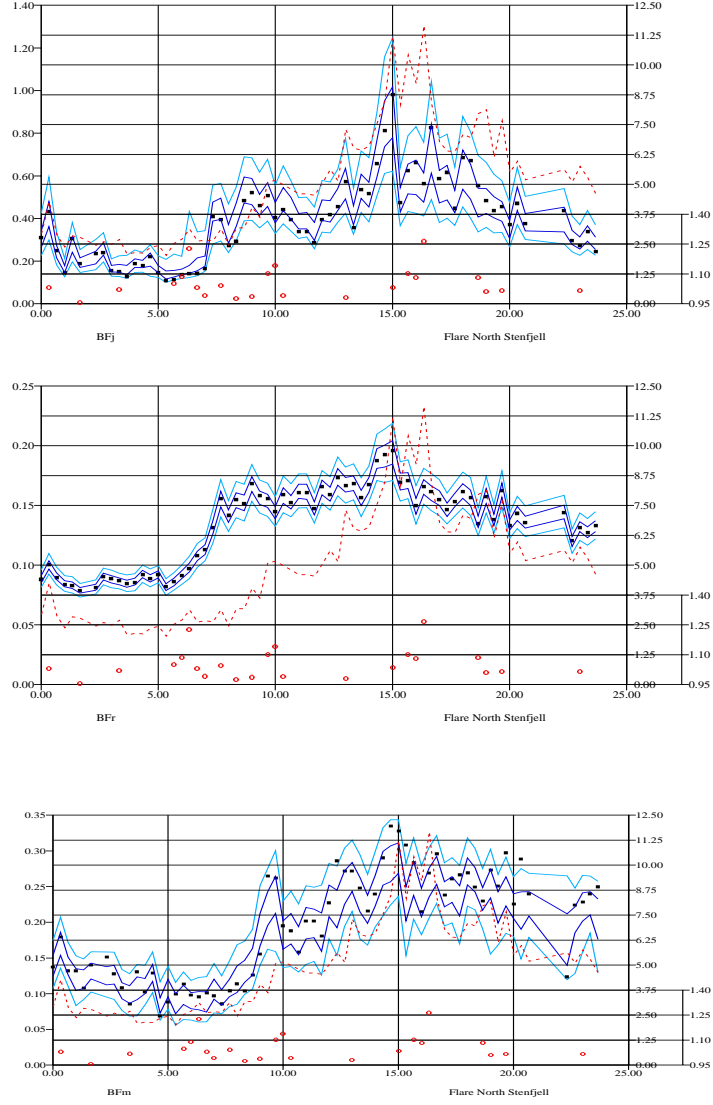


Fig. 2. Time-history of crests (dashed red), normalized crests (red circles), BF Index (black dots) and its 10, 30, 70 and 90% aleatory variability fractiles (solid blue)

peak value and of its two neighbours. The following relationships then hold:

$$S_{ave} = \frac{S(imax - 1) + S(imax) + S(imax + 1)}{3}$$

$$f_{max} = \delta f \left(imax + \frac{S(imax + 1) - S(imax - 1)}{S(imax - 1) + S(imax) + S(imax + 1)} \right)$$

$$\Phi_p = \frac{m_0}{S_{max}} = C \delta f$$

$$C_0 = \frac{m_0}{S_{ave} \delta f}$$

where δf is the frequency discretization interval.

For a triangular shape, we have the bandwidth at level S_{max} is zero and at level S_{ave} $\frac{2}{3}2\delta f$, thus:

$$\frac{S_{ave}}{S_{max}} = \frac{2\Phi_p - \frac{4}{3}\delta f}{2\Phi_p}$$

and replacing in the previous equations:

$$\frac{C}{C_0} = \frac{C - \frac{2}{3}}{C}$$

$$C = C_0 - \frac{2}{3} \frac{C_0}{C}$$

One can then solve the equation,

$$C^2 - C_0 C + \frac{2}{3} C_0 = 0$$

$$C = \frac{C_0}{2} \left(1 + \sqrt{1 - \frac{8}{3C_0}} \right)$$

Since C is close to C_0 , we have approximately

$$\Phi_p \approx \frac{m_0}{S_{ave}} - \frac{2}{3} \delta f$$

Figure 2 compares the time-history of the BFI index computed using Φ_p as a measure of bandwidth (bottom) to the robust BFI index defined in [7] (center) and to the common definition proposed by Janssen [3] (top), for the same Stenfjell storm measured at Ekofisk as in [7]. It can be seen that the use of Φ_p is acceptable, and that it exhibits a similar behaviour as the other versions of the BFI index, though its variability is much more of the order of magnitude of the Janssen version than of that of the robust one.

In order to make more emphasis on the storms where the spectrum rises steeply on the low-frequency side, which might be a token of a steep sea state and/or of a “running fetch” situation, we might want to base the BFI index on the spectral front bandwidth. The corresponding effect is shown on figure 3. Variability seems to be further increased, and to thus mask any possible detection of “running fetch” situations through the spectral front bandwidth based BFI index.

We could not identify on the time-histories of those Benjamin-Feir instability indices any special feature that might have some chances to be related to rogue wave occurrence.

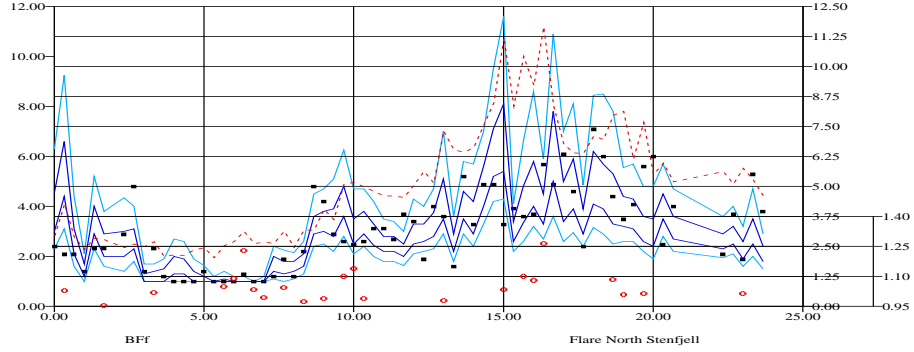


Fig. 3. Time-history of crests (dashed red), normalized crests (red circles), BF Index (black dots) and its 10, 30, 70 and 90% aleatory variability fractiles (solid blue)

3 Spectral bandwidth

In a previous study ([5]), we showed that no relation could be found between the average steepness of a sea state and rogue wave occurrence. Since Benjamin-Feir instability is characterized by steepness divided by bandwidth, the lack of influence of steepness might blur the effect of bandwidth by adding to the variability with no other consequence.

We may thus want to study bandwidth alone, *i.e.* look for changes in the spectral shape independantly of changes in the steepness of the sea state that varies for many reasons with the coming and going of wave systems and could thus be only a secondary cause for rogue waves.

Figure 4 shows the time-history of the spectral bandwidth (top) and of the spectral front bandwidth (bottom) for the same storm as previously. It may be noted that bandwidth exhibits a sharp decrease at the start of the storm, but that such behaviour could be observed on the arrival of any swell system, or even on any change from a confused sea state to a well-organized one.

On the particular storm that we studied, there does not seem to be much more to derive from the history of bandwidth parameters than from that of Benjamin-Feir Instability indices.

4 Comparison of storms

A characteristic feature may remain unnoticed for a single storm, yet it should appear on the study of a large number of such storms. The database used in [8] and complemented as reported in [7] was scanned for storms.

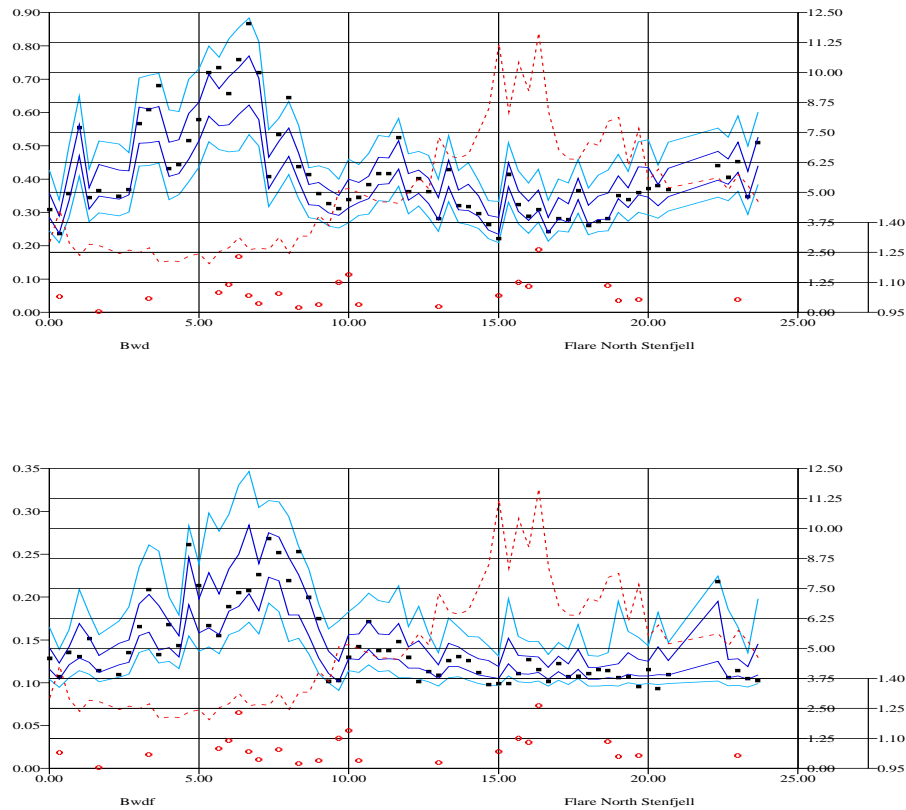


Fig. 4. Time-history of crests (dashed red), normalized crests (red circles), Bandwidth (black dots) and its 10, 30, 70 and 90% aleatory variability fractiles (solid blue)

Storms are defined as durations of at least 12 consecutive hours where significant wave height remains above 5 meters. Those storms were identified on the two different datasets of the database: the synthetic parameters computed by Oceanor on the measurements carried out on the field, and the values computed at Ifremer from the available time-series at QP. The Oceanor data cover the period from January 1979 to March 1989. That period contains 105 storms, 56 of which are also present in the data at Ifremer for which time-records of the water surface elevation are available with a 2 Hz sampling frequency, as measured with a radar distancemeter from the QP platform on the Frigg field.

A typical example of time-histories of the bandwidth parameters during a Frigg storm is given in figure 5. Comparison over several storms can be made

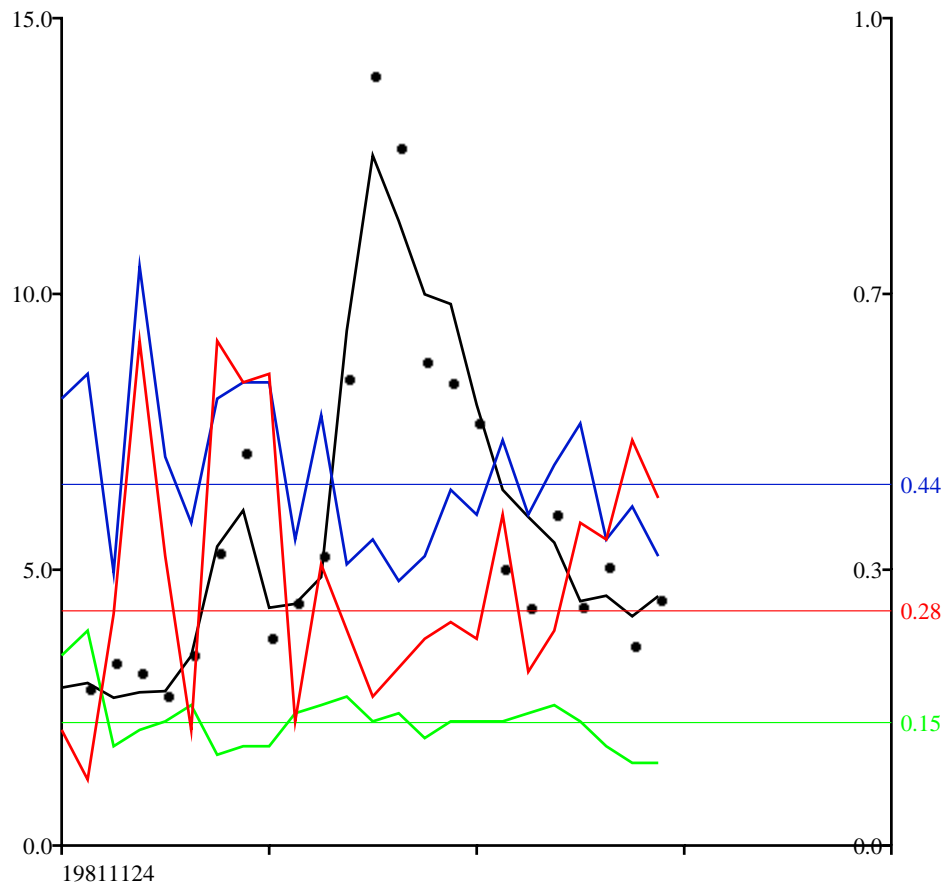


Fig. 5. Time-history of crests (black dots), significant wave height (black line), bandwidth Φ_p (blue line), spectral front bandwidth Φ_{fp} (green line), spectral asymmetry A_S (red line) and their averages over the storm

from figure 6. Those consecutive storms cannot but exhibit a variety of levels of risk with respect to rogue wave occurrence. Large crest to H_S ratios were observed for the two first ones. Yet, there is no visible relationship with the histories of the bandwidth parameters.

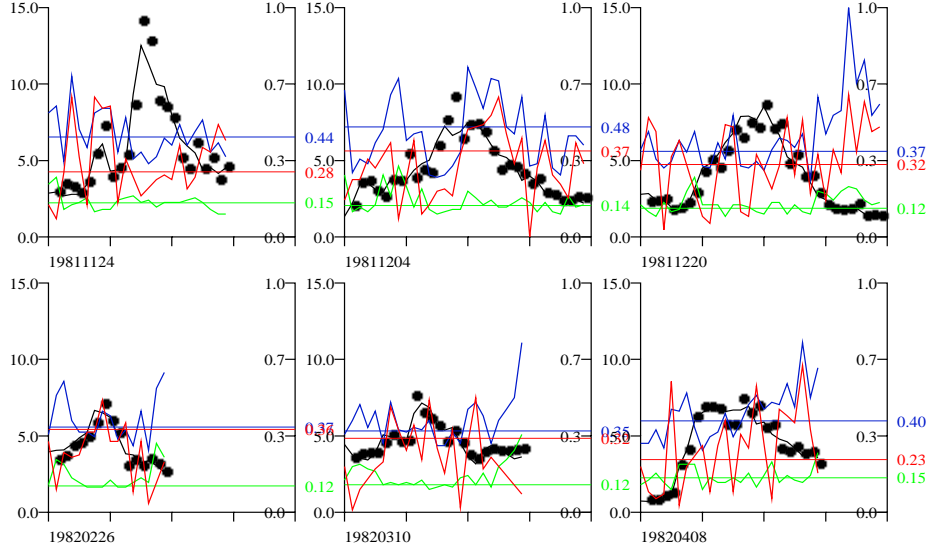


Fig. 6. Time-histories of crests (black dots), significant wave height (black line), bandwidth Φ_p (blue line), spectral front bandwidth Φ_{fp} (green line), spectral asymmetry A_S (red line) and their averages over the storms

5 Conclusions

The present study shows that dimensionless parameters related to spectral shape are rather constant over all storms in the database, as could be hinted from the results of another previous study [6].

As for the height and period (or steepness), it was shown at the previous Rogue Waves workshop[5] that steepness does not have any influence on the probability of rogue wave occurrence, and that significant wave height has only a limited one.

The time-history of spectral parameters evolution during a storm seems thus not to be a good candidate for the definition of warning systems. Furthermore, one may wonder about the validity of the assumption that some storms are more prone to extreme waves than others, or at least about the fact that such a characteristic would be reflected in the non-directional wave spectra.

Should the assumption be invalidated, *i.e.* extreme waves have no higher probability to happen in some storms than in any other, then either rogue waves would be normal extremes of the distribution, confirming some previous results

obtained by Robin & Olagnon [8] on a subset of the database investigated here, either it would mean that the dataset is still too small for the differences to appear, or that the storm characteristics that are related to abnormal extremes should be sought elsewhere than in the spectrum.

References

1. **Ersdal, G. & Kvitrud, A.** (1999) "Green sea on Norwegian production ships" *Proc. Airgap Workshop*, HSE/E&P Forum, London.
2. **Goda, Y.** (1983) "Analysis of Wave Grouping and Spectra of Long-travelled Swell" *Report of the Port and Harbour Research Institute*, Vol. 22, No 1, pp.3-41.
3. **Janssen, P.A.E.M.** (2002) "Nonlinear four wave interactions and freak waves" *Technical Memorandum ECMWF*, 366.
4. **Olagnon, M. & Krogstad, H.E.** (1998) "Observed short- and long-term distributions of wave steepness", *Proc. Int. Offshore and Polar Engineering Conf.*, Vol. 3, Montréal, pp. 63-70.
5. **Olagnon, M. & van Iseghem, S.** (2001), "Some Cases of Observed Rogue Waves and an Attempt to Characterize their Occurrence Conditions", *Proc. Rogue Waves 2000*, Ifremer, Actes de Colloques 32, pp. 105-116.
6. **Olagnon, M.** (2001), "Representativity of some standard spectral models for waves", *Proc. 11th International Offshore and Polar Engineering Conf.* ISOPE, 3, pp.92-99.
7. **Olagnon, M. & Magnusson, A.K.** (2004), "Sensitivity Study of Sea State Parameters in Correlation to Extreme Wave Occurrences", *Proc. 14th International Offshore and Polar Engineering Conf.* ISOPE, 3.
8. **Robin, A. & Olagnon, M.** (1991) "Occurrence of Extreme Waves with respect to Significant Wave Height" *Proc. Offshore Mechanics and Arctic Engineering*, OMAE Vol.2a, pp. 1-9.

Experiments on extreme wave generation using the Soliton on Finite Background

René H.M. Huijsmans¹, Gert Klopman^{2,3}, Natanael Karjanto³, and Andonawati⁴

¹ Maritime Research Institute Netherlands, Wageningen, The Netherlands,
e-mail: r.h.m.huijsmans@marin.nl

² Albatros Flow Research, Marknesse, The Netherlands

³ Applied Analysis and Math. Physics, Univ. of Twente, Enschede, The Netherlands

⁴ Jurusan Matematika, Institut Teknologi Bandung, Bandung, Indonesia

Introduction

Freak waves are very large water waves whose heights exceed the significant wave height of a measured wave train by a factor of more than 2.2. However, this in itself is not a well established definition of a freak wave. The mechanism of freak wave generation in reality as well as modeling it in a wave basin has become an issue of great importance.

Recently one is aware of the generation of freak wave through the Benjamin–Feir type of instability or self–focussing. Consequently the Non–Linear–Schrödinger (NLS) equation forms a good basis for understanding the formation of freak waves. However, the complex generation of a freak wave in nature within a sea condition is still not well understood, when the non-linearity of the carrier wave is not small. In our study we will focus on the Soliton on Finite Background, an exact solution of the NLS equation, as a generating mechanism for extreme waves.

Apart from a numerical investigation into the evolution of a soliton on a finite background also extensive detailed model tests have been performed for validation purposes in the hydrodynamic laboratories of the Maritime Research Institute Netherlands (MARIN). Furthermore, a numerical wave tank [12] is used to model the complete non-linear non-breaking wave evolution in the basin.

Properties of the Soliton on Finite Background

The NLS equation is chosen as a mathematical model for the non-linear evolution of the envelope of surface wave packets. For spatial evolution problems, it is given in non-dimensional form and in a frame of reference moving with the group velocity by

$$\partial_{\xi}\psi + i\beta\partial_{\tau}^2\psi + i\gamma|\psi|^2\psi = 0, \quad (1)$$

where ξ and τ are the corresponding spatial and temporal variables, respectively; β and γ are the dispersion and non-linearity coefficients. This equation has many

families of exact solutions. One family of exact solutions is known as the Soliton on Finite Background (SFB) and this is a good candidate for describing extreme waves. This exact solution has been found by Akhmediev, Eleonskii & Kulagin [3], see also [2] and [1].

This SFB solution describes the dynamic evolution of an unstable modulation process, with dimensionless modulation frequency ν . In the context of water waves, for infinitesimal modulational perturbations to a finite-amplitude plane wave, this process is known as Benjamin-Feir (BF) instability [5]. However, non-linearity will limit this exponential growth and the SFB is one (of many other) non-linear extension of the BF instability for larger amplitudes of the modulation. Extensive research on the NLS equation and the SFB solution, to obtain a better understanding of deterministic extreme-wave phenomena has been conducted in the past few years (see *e.g.* [10], [11], [4] and [9]).

An explicit expression for the SFB is given as the following complex-valued function

$$\psi(\xi, \tau; \tilde{\nu}, r_0) = A(\xi) \cdot \left\{ \frac{\tilde{\nu}^2 \cosh(\sigma\xi) - i [\sigma/(\gamma r_0^2)] \sinh(\sigma\xi)}{\cosh(\sigma\xi) - \sqrt{1 - \frac{1}{2}\tilde{\nu}^2} \cos(\nu\tau)} - 1 \right\}, \quad (2)$$

where $A(\xi) = r_0 e^{-i\gamma r_0^2 \xi}$ is the *plane-wave* or the *continuous wave* solution of the NLS equation, $\sigma = \gamma r_0^2 \tilde{\nu} \sqrt{2 - \tilde{\nu}^2}$ is the *growth rate* corresponds to the Benjamin-Feir instability, $\nu = \tilde{\nu} r_0 \sqrt{\frac{\gamma}{\beta}}$ is the modulation frequency, and $\tilde{\nu}$, $0 < \tilde{\nu} < \sqrt{2}$ is the normalized modulation frequency. This SFB reaches its maxima at $(\xi, \tau) = (0, \frac{2n\pi}{\nu})$, $n \in \mathbb{Z}$. It has a soliton-like form with a finite background in the spatial ξ -direction. The SFB is periodic along in the temporal τ -direction, with period $\frac{2\pi}{\nu}$. For $|\xi| \rightarrow \infty$, the SFB turns into the continuous wave solution $A(\xi)$. It possesses two essential parameters: r_0 and $\tilde{\nu}$.

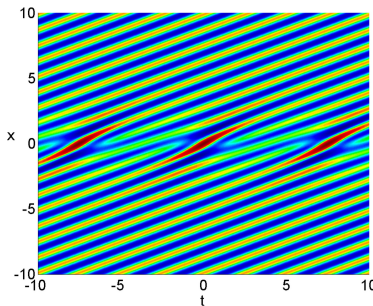


Fig. 1. Density plots of a physical wave packet profile according to an SFB envelope for $\tilde{\nu}_1 = 1$, showing the wave dislocation phenomenon.

The first-order part of the corresponding physical wave packet profile $\eta(x, t)$ for a given complex-valued function $\psi(\xi, \tau)$ is expressed as follows

$$\eta(x, t) = \psi(\xi, \tau)e^{i(k_0x - \omega_0t)} + \text{c.c.}, \quad (3)$$

where c.c. means the complex conjugate of the preceding term, the wave number k_0 and frequency ω_0 satisfy the linear dispersion relation $\omega = \Omega(k) \equiv \sqrt{k \tanh k}$. The variables (x, t) in the non-moving frame of reference are related to (ξ, τ) in the moving frame of reference by the transformation $\xi = x$ and $\tau = t - x/\Omega'(k_0)$. The modulus of ψ represents the wave group envelope, enclosing the wave packet profile $\eta(x, t)$. The dimensional laboratory quantities are related to the non-dimensional quantities by the following Froude scaling, using the gravitational acceleration g and the depth of the basin h : $x_{\text{lab}} = x \cdot h$, $t_{\text{lab}} = t \cdot \sqrt{\frac{g}{h}}$, $k_{\text{lab}} = k/h$, $\omega_{\text{lab}} = \omega \cdot \sqrt{\frac{g}{h}}$, and $\eta_{\text{lab}} = \eta \cdot h$.

In principle, the wave profile including the higher-order terms represents a good approximation to the situation in real life. To accommodate this fact, we will include higher-order terms up to second order. We apply an perturbation-series expansion (Stokes' expansion) to the physical wave-packet profile $\eta(x, t)$ and the multiple-scale approach using the variables ξ and τ , where $\xi = \epsilon^2 x$, $\tau = \epsilon(t - x/\Omega'(k_0))$, and ϵ is a small positive non-linearity and modulation parameter. The corresponding wave elevation $\eta(x, t)$, consisting of the superposition of the first-order harmonic term of $O(\epsilon)$ and a second-order non-harmonic long wave as well as a second-order double-frequency harmonic term of $O(\epsilon^2)$, is given by

$$\begin{aligned} \eta(x, t) = & \epsilon \left[\psi^{(10)}(\xi, \tau)e^{i(k_0x - \omega_0t)} + \text{c.c.} \right] \\ & + \epsilon^2 \left\{ \psi^{(20)}(\xi, \tau) + \left[\psi^{(22)}(\xi, \tau)e^{2i(k_0x - \omega_0t)} + \text{c.c.} \right] \right\}. \end{aligned} \quad (4)$$

We find from the multiple-scales perturbation-series approach that $\psi^{(10)}(\xi, \tau) = \psi(\xi, \tau)$ satisfies the spatial NLS equation and

$$\psi^{(20)}(\xi, \tau) = -\frac{1}{\Omega(k_0)} \frac{4k_0\Omega'(k_0) - \Omega(k_0)}{[\Omega'(0)]^2 - [\Omega'(k_0)]^2} |\psi^{(10)}(\xi, \tau)|^2 \quad (5)$$

$$\psi^{(22)}(\xi, \tau) = k_0 \frac{3 - \tanh^2 k_0}{2 \tanh^3 k_0} [\psi^{(10)}(\xi, \tau)]^2. \quad (6)$$

A similar derivation for the temporal NLS equation resulting from the KdV equation can be found in [8]. By including this second-order term, the wave signal $\eta(x, t)$ experiences the well-known Stokes' effect: the crests become steeper and the troughs becomes shallower [6].

The coefficients β and γ of the spatial NLS equation are given, in non-dimensional form, as:

$$\beta = -\frac{1}{2} \frac{\Omega''(k_0)}{[\Omega'(k_0)]^3}, \quad (7)$$

$$\gamma = \frac{\gamma_1 + k_0\alpha_U + \lambda\alpha_\zeta}{\Omega'(k_0)}, \quad (8)$$

where

$$\gamma_1 = k_0^2 \Omega(k_0) \frac{9 \tanh^4 k_0 - 10 \tanh^2 k_0 + 9}{4 \tanh^4 k_0}, \quad (9)$$

$$\lambda = \frac{1}{2} k_0^2 \frac{1 - \tanh^2 k_0}{\Omega(k_0)}, \quad (10)$$

$$\alpha_\zeta = -\frac{1}{\Omega(k_0)} \frac{4k_0 \Omega'(k_0) - \Omega(k_0)}{[\Omega'(0)]^2 - [\Omega'(k_0)]^2} \quad \text{and} \quad (11)$$

$$\alpha_U = \alpha_\zeta \Omega'(k_0) - \frac{2k_0}{\Omega(k_0)}. \quad (12)$$

These can be used to compute the SFB solution $\psi(\xi, \tau)$ from Equation (2).

Phase singularity and wave dislocation

By writing the complex-valued function ψ in a polar (or phase-amplitude) representation, it is found that for modulation frequency $\tilde{\nu}$ in the range $0 < \tilde{\nu} < \sqrt{\frac{3}{2}}$ a *phase singularity* phenomenon occurs. It happens when the real-valued amplitude $|\psi|$ vanishes and therefore there is no way of ascribing a value to the real-valued phase when it occurs. The local wave number $k \equiv k_0 + \partial_x \theta$ and local frequency $\omega \equiv \omega_0 - \partial_t \theta$, with $\theta(\xi, \tau) \equiv \arg(\psi(\xi, \tau))$, become unbounded when this happens. The corresponding physical wave packet profile $\eta(x, t)$ confirms this by showing a *wave dislocation* phenomenon. When the real-valued amplitude $|\psi|$ vanishes at that specific position and time, waves merge or split. For $\sqrt{\frac{3}{2}} < \tilde{\nu} < \sqrt{2}$, the real-valued amplitude is always definite positive, and thus there is no wave dislocation. Furthermore, in one modulation period, there is a pair of wave dislocations. Before or after this dislocation, the real-valued amplitude reaches its maximum value. Figure 1 shows the density plot of a physical wave packet profile $\eta(x, t)$. The wave dislocation is also visible in this figure. Figure 2 shows the evolution of the SFB from a modulated wave signal until it reaches the extreme position. We can see also in this figure that the amplitude $|\psi|$ vanishes at some moments for the extremal position $x = 0$, causing phase singularity.

The phase singularity is a well known phenomenon in physical optics. In the context of water waves, similar observations can be made, and also wave dislocations occur. Trulsen [13] calls it as *crest pairing* and *crest splitting* and he explains this phenomenon as a consequence of linear dispersion.

Maximum temporal amplitude

The maximum temporal amplitude (MTA) is a useful concept to understand long-time behavior of wave elevation. For wave propagation in the laboratory, it also gives a direct view of the consequences of an initial wave signal on the corresponding extreme-wave signal. It is defined as

$$\mu(x) = \max_t \eta(x, t), \quad (13)$$

where $\eta(x, t)$ is the surface elevation as a function of space x and time t . It describes the largest wave elevation that can appear at a certain position. For laboratory wave generation, it describes the boundary between the wet and dry parts of the wall of the basin after a long time of wave evolution.

Figure 3 shows the MTA plot of the SFB in the laboratory coordinates. In this example, the mean water depth is 3.55 m and the wavelength is approximately 6.2 m. The wave signal is generated at the left side, for example at $x_{\text{lab}} = -350$ m, and it propagates to the right and reaches its extremal condition at $x_{\text{lab}} = 0$. A slightly modulated wave train increases in amplitude as the SFB waves travels in the positive x -direction. Furthermore, in this example a SFB wave signal with initial amplitude around 0.19 m can reach an extreme amplitude of 0.45 m, an amplification factor of around 2.4. After reaching its maximum amplitude, the MTA decreases monotonically and returns to its initial value.

Experimental Result

For the validation of the proposed method we performed experiments in one of the wave basins of MARIN. The basin dimensions amounted to $L \times B \times D$ as 200 m \times 4.0 m \times 3.55 m. In the basin an array of wave probes were mounted as indicated in the set-up in figure (4). The predefined wave board control signal was put onto the hydraulic wave generator. The stroke of the wave flap was measured. Main characteristics of the model test experiments:

Carrier wave period is 1.685 sec. maximum wave height to be achieved (MTA) varies from 0.213m to 0.2485m

As a explanation the results for the tests with an MTA of 0.2485 will be shown, see figure(5) to figure(7).

Figure 8 shows the SFB signal based on the experiment at distance 150 m from the wave maker, where it is expected that the signal to be extreme. That figure also shows the phase singularity phenomenon when the local frequency becomes unbounded when the real-valued amplitude vanishes or almost vanishes. The experiment result shows asymmetric form of the extreme signal while the theoretical result of the SFB preserve the symmetry of the signal. It is suspected that if the modified NLS equation of Dysthe [7] is used as the governing equation for the wave signal evolution, then there are good comparisons with experimental measurements. The good comparisons are observed for the case of bi-chromatic waves, where the modified NLS equation predicts both the evolution of individual wave crests and the modulation of the envelope over longer fetch [14].

References

1. **Akhmediev, N.N. & Ankiewicz, A.** “*Solitons, Nonlinear Pulses and Beams*”, Optical and Quantum Electronic Ser., Vol. 5, Chapman & Hall, 1st edition, (1997).
2. **Akhmediev, N.N. & Korneev, V.I.** “Modulation instability and periodic solutions of the nonlinear Schrödinger equation”, *Theor. and Math. Phys.* Vol. 69, (1986), pp. 1089–1092.

3. **Akhmediev, N.N., Eleonskii, V.M. & Kulagin, N.E.**, “First-order exact solutions of the nonlinear Schrödinger equation”, *Teoret. Mat. Fiz.*, Vol. 72, No. 2, (1987), pp. 183–196. English translation: *Theoret. and Math. Phys.*, Vol. 72, No. 2, (1987), pp. 809–818.
4. **Andonowati, Karjanto, N. & van Groesen, E.**, “Extreme wave phenomena in down-stream running modulated waves”, submitted to *Math. Models and Meth. in Appl. Sc.*, July, (2004).
5. **Benjamin, T.B. & Feir, J.E.**, “The disintegration of wave trains on deep water. Part 1. Theory”, *J. Fluid Mech.*, Vol. 27, No. 3, (1967), pp. 417–430.
6. **Debnath, L.**, “*Nonlinear Water Waves*”, Academic Press, (1994).
7. **Dysthe, K.B.**, “Note on a modification to the nonlinear Schrödinger equation for application to deep water waves”, *Proc. R. Soc. London Ser. A*, Vol. 369, No. 1736, (1979), pp. 105–114.
8. **van Groesen, E.**, “Wave groups in uni-directional surface-wave model”, *J. Eng. Math.*, Vol. 34, No. 1-2, (1998), pp. 215–226.
9. **van Groesen, E., Andonowati & Karjanto, N.**, “Deterministic aspects of nonlinear modulational instability”, In: *Proc. ‘Rogue Waves’*, Brest, France, October, (2004).
10. **Osborne, A.R., Onorato, M. & Serio, M.** “The nonlinear dynamics of rogue waves and holes in deep-water gravity wave trains”, *Phys. Lett. A*, Vol. 275, (2000), pp. 386–393.
11. **Osborne, A.R.**, “The random and deterministic dynamics of ‘rogue waves’ in unidirectional, deep-water wave trains”, *Mar. Struct.*, Vol. 14, (2001), pp. 275–293.
12. **Westhuis, J.H.**, “*The numerical simulation of non-linear waves in a hydrodynamic model test basin*”, Ph.D. Thesis, University of Twente, (2001).
13. **Trulsen, K.**, “Crest pairing predicted by modulation theory”, In *J. Geophys. Res.*, Vol. 103, No. C2, pp. 3143–3147.
14. **Trulsen, K. & Stansberg, C.T.**, “Spatial evolution of water surface waves: Numerical simulation and experiment of bichromatic waves”, In *Proc. Eleventh Int. Offshore and Polar Eng. Conf.*, The Int. Soc. of Offshore and Polar Eng., (2001), pp. 71–77.

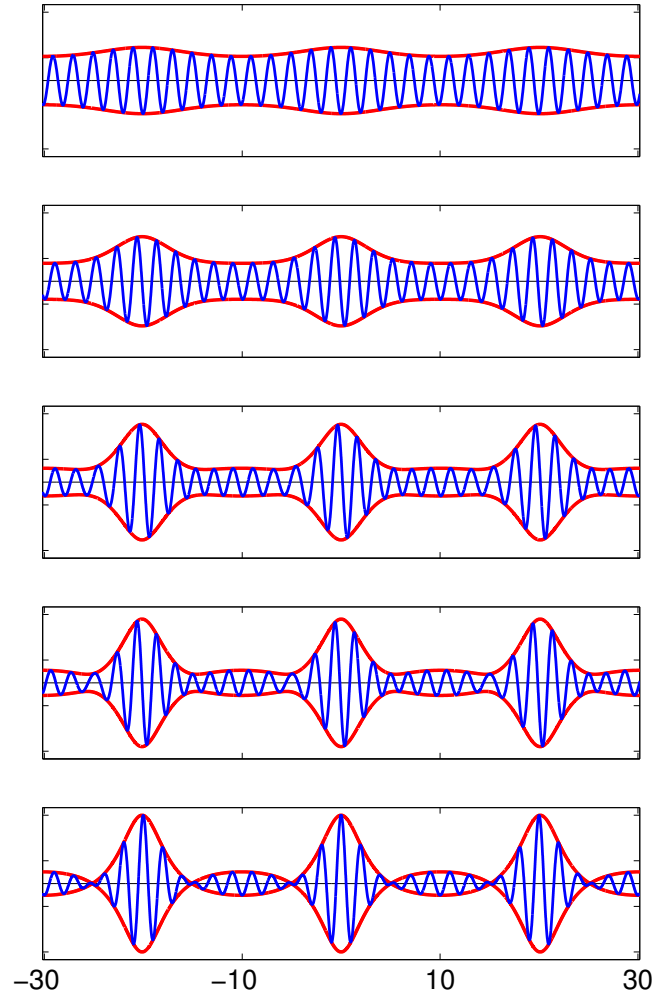


Fig. 2. The evolution of the SFB for $\tilde{\nu}_1 = 1$ from a modulated continuous wave signal into the extreme position. From top to bottom, the signals are taken at $x = -200$, $x = -100$, $x = -50$, $x = -30$, and $x = 0$.

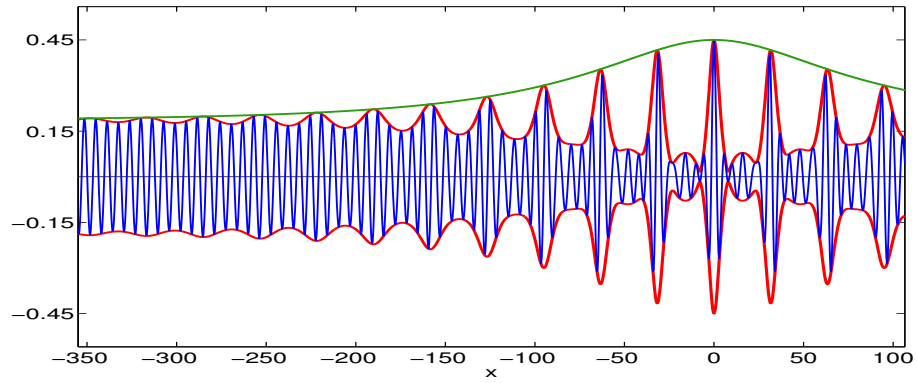


Fig. 3. The MTA plot of the SFB, the corresponding wave profiles at $t = 0$, and its envelope.

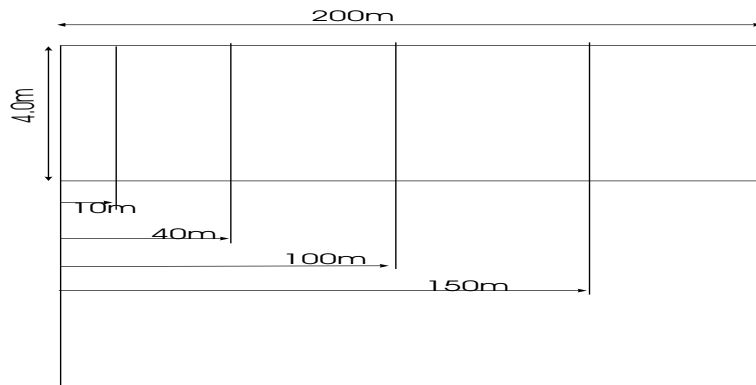


Fig. 4. The set-up of the wave probe array in the wave basin

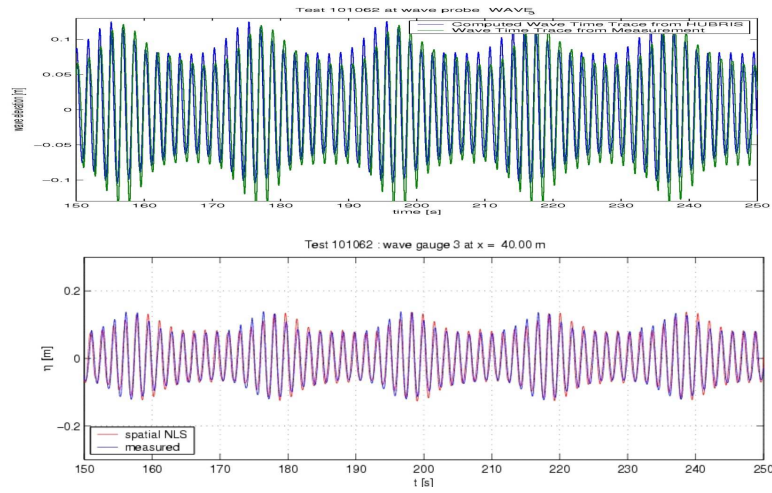


Fig. 5. Comparison Non-Linear Wave model HUBRIS with results from experiments and sNLS

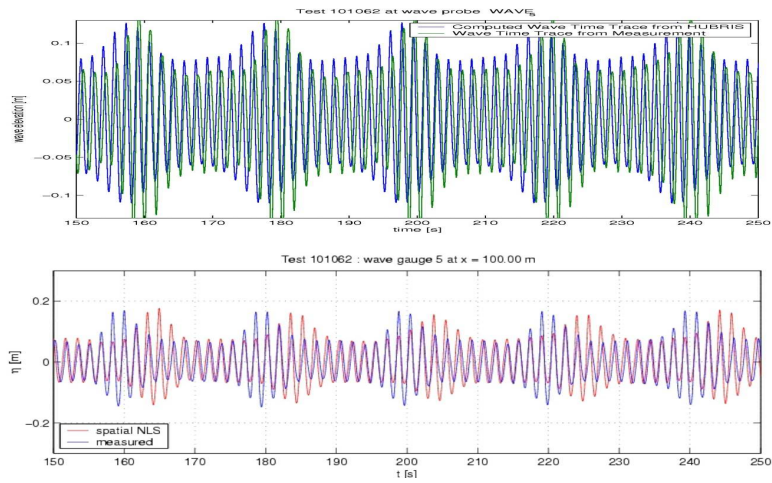


Fig. 6. Comparison Non-Linear Wave model HUBRIS with results from experiments and sNLS

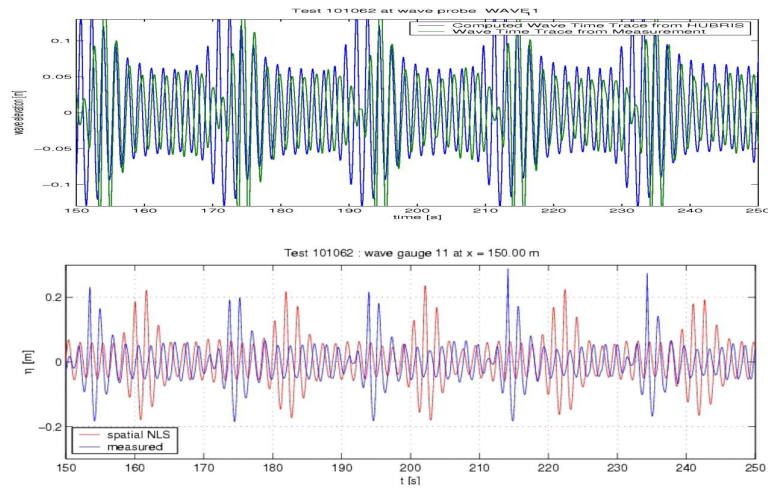


Fig. 7. Comparison Non-Linear Wave model HUBRIS with results from experiments and sNLS

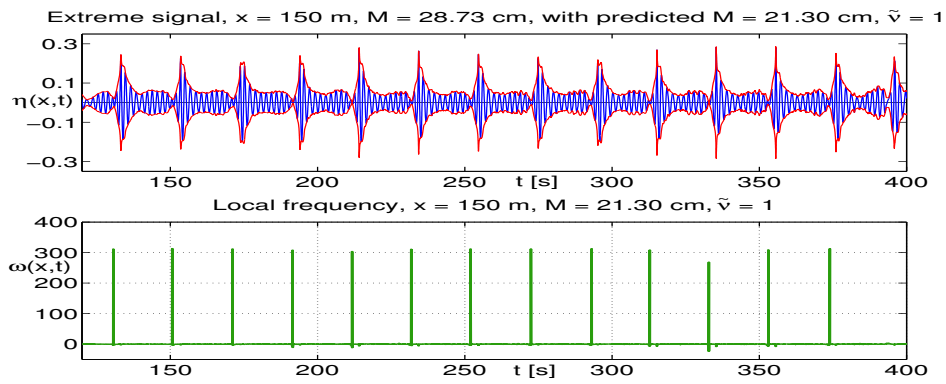


Fig. 8. The SFB signal plot based on the experiment at 150 m (top) and the corresponding local frequency plot (bottom).

Rogue waves and extreme events in measured time-series

Alastair D. Jenkins¹, Anne Karin Magnusson², Andreas Niedermeier³, Jaak Monbaliu⁴, Alessandro Toffoli⁴, and Karsten Trulsen⁵

¹ Bjerknes Centre for Climate Research, Geophysical Institute, Allégaten 70, N-5007

Bergen, Norway alastair.jenkins@bjerknes.uib.no

² Norwegian Meteorological Institute, Bergen, Norway

³ DLR, Oberpfaffenhofen, Wessling, Germany

⁴ K.U. Leuven, Belgium

⁵ Mathematical Institute, University of Oslo, Norway

Abstract. We report on the wave time-series data used in the MAX-WAVE project, with sample time series and statistics of wave height, crest height, and trough depth. Data are included from the Ekofisk and Draupner oil fields, and from Belgian coastal waters. As well as extreme value analysis, wavelet analysis has been performed. Studies were also made of buoy time series transformed by quasi-Lagrangian correction of the buoy motion, and of laser time series propagated to other locations with up to 220 m separation from the original measurement location using linear and nonlinear techniques.

The main conclusions of the study are as follows:

1. The extreme waves observed do not have an unusual shape: they tend to have sharp crests and round troughs, with a pronounced crest:trough asymmetry.
2. The statistics of individual wave height, crest height, and trough depth, are generally in agreement with Rayleigh or Weibull distributions, although particularly extreme events such as the Draupner 1995 New Year wave are highly unusual according to the normally-accepted Gaussian and non-Gaussian statistical models.
3. The wavelet analysis method can be useful for detecting ‘groupiness’ and individual large waves.
4. Analysis of the use of the quasi-Lagrangian correction method on Waverider time series for the Stenfjell case indicates that this method is insufficient to transform observational data into time series whose extreme values of crest height and trough depth are equivalent to observations using Eulerian measurement techniques.
5. ‘Propagation’ of wave observations to hypothetical locations different from where the wave measurements are made, in order to evaluate the risk of extreme waves larger than those actually observed, may be possible, but further study is required to determine the statistical reliability of the linear and nonlinear methods proposed.

Comparison of the Characteristics of Abnormal Waves on the North Sea and Gulf of Mexico

C. Guedes Soares, E. M. Antão
Unit of Marine Engineering and Technology, Technical University of Lisbon,
Instituto Superior Técnico
Av. Rovisco Pais, 1049-001 Lisboa, Portugal
{guedess, ewa}@mar.ist.utl.pt

Abstract

Abnormal waves that have occurred in various storms in more than one location in the North Sea and during a hurricane in the Gulf of Mexico, are considered here. This work compares the parameters that describe the characteristics of these abnormal waves and the sea states in which they occurred.

It was found that in general there were not major differences between the characteristics of the abnormal waves but some sea states that occurred during the hurricane Camille seem to show a higher degree of non-linearity than the ones in the North Sea.

1. Introduction

There has been much interest during last decade about abnormal or freak waves and various possible mechanisms for their generation have been identified, as reviewed by Kharif, and Pelinovsky (2003) and Guedes Soares et. al. (2004a), for example. However, the nature of abnormal or freak waves is not known yet, the wave generation mechanisms are not fully understood, and there is no generalized agreement about the criteria to classify one extreme wave as an abnormal one.

Dean (1990) has considered that freak waves are those that occur within a sequence of waves that have been identified as being higher than can be expected from the Rayleigh distribution of wave heights. He noted that the most probable maximum wave in a record of about 2000 waves is about 2 times the significant wave height according to

the Rayleigh distribution. Thus a freak wave in such a long record would need to have a height larger than that limit. Other definitions are based on the ratio between the crest of the maximum wave and significant wave, and different authors have chosen different level of this ratio (see e.g. Guedes Soares et al 2004a). Tomita and Kawamura (2000) have chosen a combination of the two ratios.

For this study the abnormal waves were selected according to definition given by Dean (1990) that is: the abnormality index ($AI = H_{\max}/H_s$) was higher than 2. As it is possible to calculate the abnormality index defining the wave heights from down-crossings and up-crossings of the mean sea surface, two possible definitions for AI were used. If any of the two possible abnormality indexes indicated a presence of a freak wave, the time series was included in this investigation.

This study builds upon results presented by Guedes Soares et al (2003) for North Sea waves and Guedes Soares et al (2004a) for waves that occurred during the Camille hurricane in the Gulf of Mexico. It considers the main properties identified in those abnormal waves and in the sea states in which they occurred, in order to determine if any significant differences exist in any of the parameters describing those data sets.

2. Description of the data

The raw data used in this study were collected at three different locations. One data set was recorded in Gulf of Mexico during hurricane Camille on 17th of August 1969. There are 6 time series chosen from all the data for further analysis. These contain records of freak waves satisfying condition: $AI_D > 2$ or $AI_U > 2$, where AI_D is the down crossing abnormality index calculated as $AI_D = H_{\max_D}/H_s$ and AI_U is the corresponding parameter for waves defined with zero up-crossings. As this is wave-by-wave analysis the H_s was calculated as the average height of the highest third of the waves. One of the 6 identified waves satisfies the Tomita and Kawamura condition for a freak wave.

Another time series considered in this study contains the well-known “New Year Wave” and was collected on Central North Sea on Draupner platform on 1st of January 1995 at 15:20 PM. The “New Year Wave” is a freak wave according to definition of Tomita and Kawamura.

Finally use is made of northern North Sea data recorded in the North Alwyn platform during the storm from 16 to 22 of November 1997. Among these data 25 time series were identified as having abnormal waves defined as in case of hurricane Camille.

Between these 25 waves 20 of them satisfy the Tomita and Kawamura condition. From the three data sets all together 32 records will be the basis for further analysis.

3. Results and discussion

To relate the occurrence of the abnormal waves with the stage of development of a storm the evolution of the significant wave height was plotted together with the occurrence of the abnormal waves. Figure 1 shows that the record of the hurricane Camille corresponds to a developing storm with very rapidly increasing H_s , until the recording equipment failed. During this period 6 abnormal waves were identified.

The record with the New Year Wave which was included in this investigation comes from a period in which there is a stable value of H_s , which might have coincided with the peak of the storm see (figure 2). In the case of North Alwyn (figure 3), abnormal waves have occurred both in the phase of storm development and of storm decay, although the majority of freak waves were registered after the storm peak.

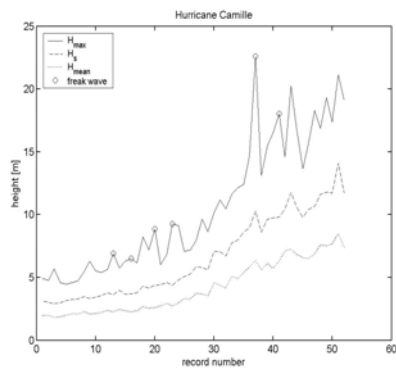


Figure 1. Time development of wave height characteristics during Hurricane Camille.

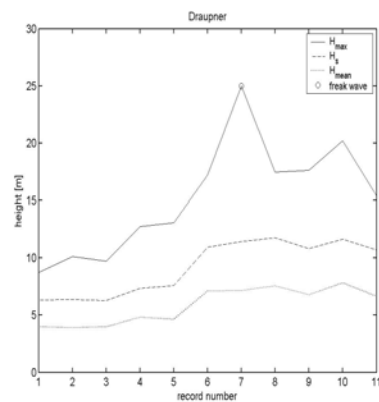


Figure 2. Storm recorded at the Draupner platform.

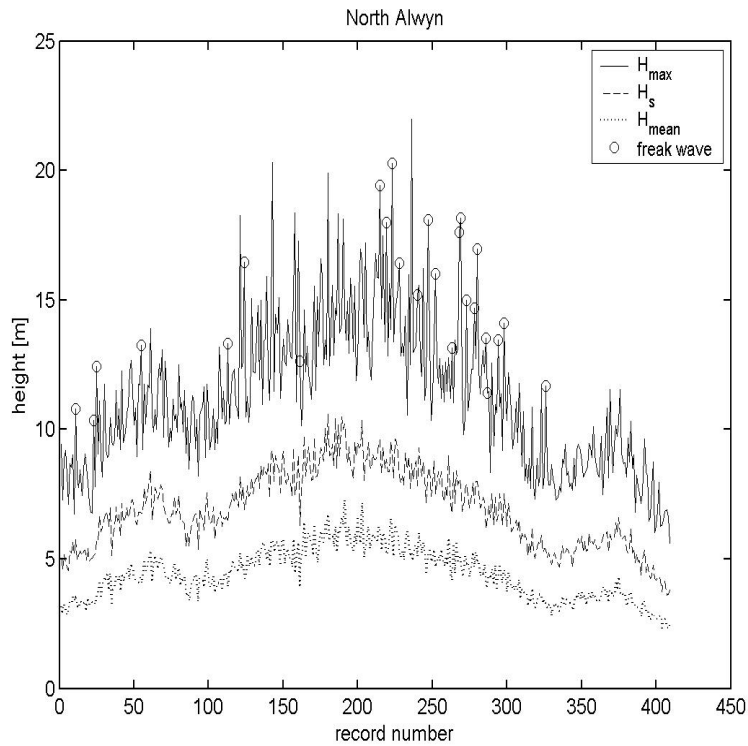


Figure 3. Time development of wave height characteristics during storm on North Alwyn.

Properties of the individual abnormal waves were studied and the correlation between various parameters has been analysed. Scatter plots of magnitudes which have shown the highest correlations are plotted in figures 4 a-d, which shown the individual wave steepness coefficient s_U , vertical asymmetry a_v , and maximum crest height as a function of the skewness of the sea state, as well as the relation between the vertical and horizontal asymmetry a_h . The definitions of different singular wave characteristics can be found in Guedes Soares et al. (2004b).

The differences between characteristics of the individual freak waves are not apparent and even hurricane Camille waves seem to follow behaviour of the rest of the North Sea freak waves.

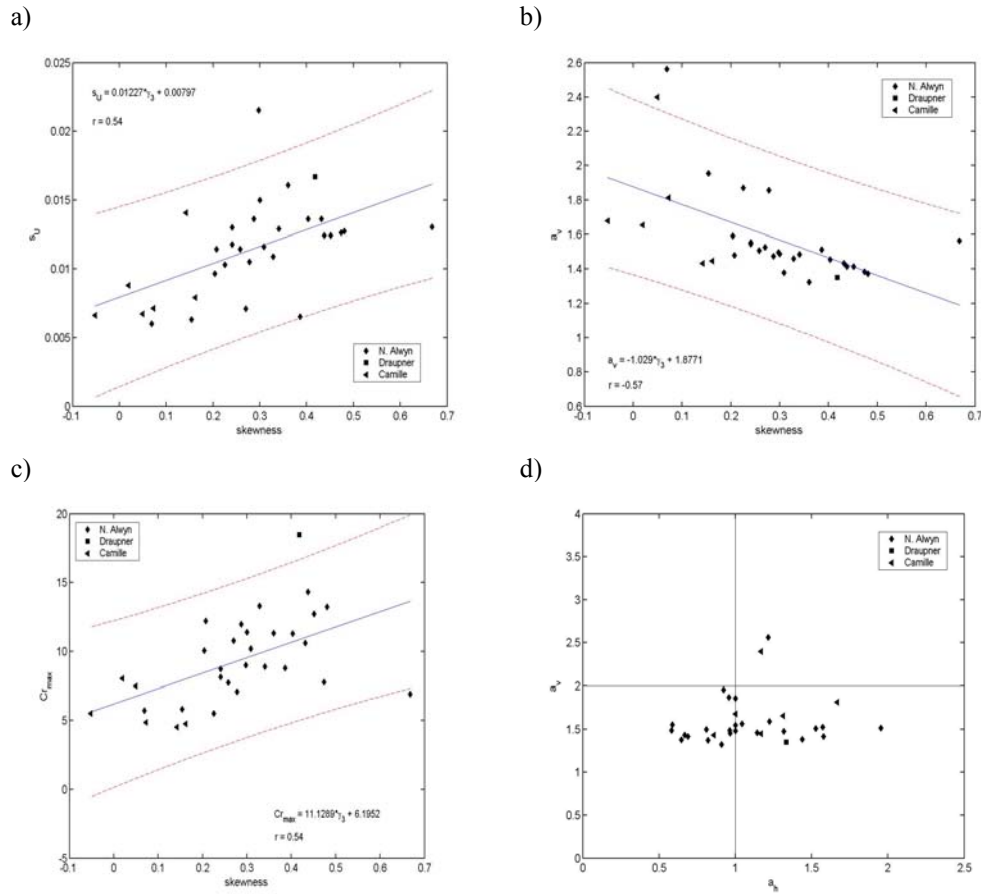


Figure 4. Characteristics of individual freak waves correlation between: a) down-crossing steepness and skewness of the sea state, b) vertical asymmetry and skewness, c) crest of the wave and skewness, d) vertical asymmetry plotted against horizontal one.

Since these large waves tend to occur in non-linear sea states, the degree of non-linearity was also studied. The non-Gaussian behaviour of wave record is reflected through its statistical moment-based parameters: skewness and kurtosis. In this study the excess kurtosis is used - that is sample kurtosis minus 3 – and from now on excess kurtosis will be called simply kurtosis. Table 1 shows mean values of different sea state parameters.

Skewness values indicate some differences between North Alwyn and hurricane Camille sea states: mean values differ significantly, being close to zero for Camille and clearly positive for the North Sea data. The Camille data also tends to have a lower value of the ratio of maximum crest height to H_s . The rest of characteristics shown in the table do not reveal major differences between the different locations.

	γ_3	γ_4	AI_{up}	AI_{down}	Cr_{maxD} / H_{sD}	H_{maxD}	Cr_{maxD} / H_{maxD}	H_{sD}/L_p
North Alwyn								
mean (N=25)	0,32	0,73	2,03	2,06	1,34	14,83	0,65	0,0356
standard deviation	0,13	0,45	0,18	0,15	0,20	2,83	0,08	0,0032
Draupner								
(N=1)	0.42	1.07	2.23	2.19	1.62	25.01	0.74	0.0379
Camille								
mean (N=6)	0,07	0,50	1,95	1,97	1,08	10,47	0,59	0,0257
standard deviation	0,08	0,31	0,21	0,17	0,24	4,42	0,10	0,0091

Total (N=32)								
mean	0,28	0,70	2,02	2,05	1,30	14,33	0,64	0,0338
standard deviation	0,16	0,43	0,19	0,15	0,24	4,01	0,09	0,0061

Table 1. Mean values and standard deviations for magnitudes calculated from time series with freak waves.

Figure 5 shows the scatter plot of kurtosis against skewness of all investigated time series. There are 3 time series recorded in hurricane Camille which do not follow the regression curve derived by Guedes Soares et al. (2003). Their skewness is close to zero and their kurtosis is high. There are also time series from hurricane Camille that have the same properties as time series from North Alwyn and Draupner.

It is reasonable to group the sea states in two sets: sea states with high kurtosis and skewness close to zero and these with existing correlation between kurtosis and

skewness. The sea states with high kurtosis and very small skewness cannot be described by a second order theory but could eventually fit a third order theory. On the other hand the rest of the sea states, which show both skewness and kurtosis different from zero exhibit the presence both of second order and third order interactions in the wave field as identified in Guedes Soares et al (2003).

Stansberg (1998) presented results from comparison of numerically simulated second-order waves with theory. Figures 7 and 8 show his results together with the sea data considered here. Only sea states with low values of kurtosis and middle values of skewness seem to obey the theory (see figure 8). Records with high kurtosis and almost zero skewness do not follow theoretical line for second order nonlinearities, what was to expect, and the sea state steepness is not in the region of highest values. Figure 7 shows comparison of vertical asymmetry and steepness of maximum waves and higher asymmetry of sea waves is visible very well.

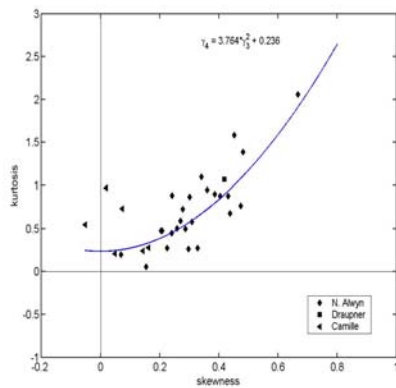


Figure 5. Relation between skewness and kurtosis for sea states with freak waves.

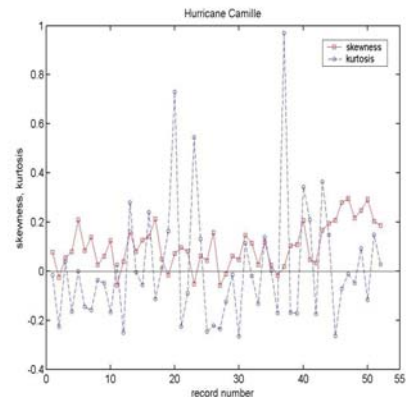


Figure 6. Time development of the coefficients of skewness and kurtosis, showing individual estimates and moving average trend - hurricane Camille.

The value of skewness shows increasing trend in case of all storms before the peak of the storm. However in the case of Camille the skewness very often drops below zero, what is not typical for the other storms. Hurricane Camille data was recorded before peak of the storm with quite a big distance from the storm (23 km) and as skewness is

proportional to the wave steepness (Huang and Long, 1980) one would expect rather slow growth of the skewness value as it is in case of Draupner and North Alwyn wave records.

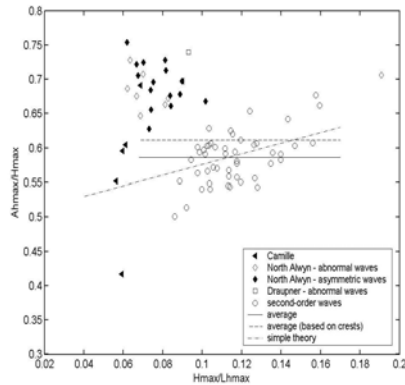


Figure 7. Comparison between vertical asymmetry of in-situ data and second-order theory and simulations.

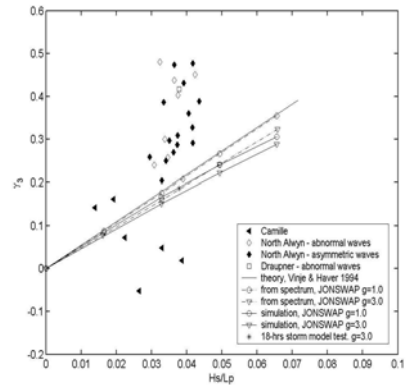


Figure 8. Skewness from second order simulations of sea states, theory and measurements in the North Sea.

Mori and Yasuda (2002) showed that the value of kurtosis is directly proportional to the probability of the occurrence of large waves in a wave record. Storm waves have high steepness and the majority of the water elevation records analysed have high kurtosis, as is visible in figure 5 and table 1. Surprisingly, the correlation coefficient of kurtosis with wave height (maximum, mean, or significant - calculated for up- and down-crossing waves) is very low. Nevertheless storm waves are higher than calm water waves and kurtosis higher than zero can be an indicator of that.

Conclusions

The analysis of data from the North Sea and Gulf of Mexico indicates that the difference between the characteristics of the individual freak waves do not seem to be significant, although the Camille waves tend to have a lower ratio of maximum crest to significant wave height. However these conclusions must be considered with care as the length of records and the number of abnormal waves considered is not very large.

There appears to exist a clear difference between the characteristics of the sea states in which freak waves occur in North Sea storms and in the Gulf of Mexico hurricane, namely in North Sea records did not appear clear cases of clean third order nonlinearity, while they appeared in records from Camille. This may be associated with the nature of hurricanes that induce a very high transfer of energy locally and this may lead to a higher degree of non-linearity of the generated sea states.

Analysis and comparison of storm waves with second order simulations and theory indicates discrepancies that could be associated with the presence of third order nonlinearities, especially visible in case of hurricane Camille sea states with skewness close to zero.

Acknowledgements

This work has been performed in the scope of the research project "Freak Wave Generation in the Ocean" which is partially financed by European Commission, under the Contract INTAS 01-2156.

The data used in this work has been collected during the research project "Rogue Waves – Forecast and Impact on Marine Structures (MAXWAVE)", partially funded by the European Commission, under the programme Energy, Environment and Sustainable Development (Contract no. EVK3:2000-00544). The authors are grateful to BP for having provided the data relative to hurricane Camille, to STATOIL for providing the Draupner data and to Herriot-Watt University for having shared the North Alwyn data.

References

Dean, R., (1990), "Freak waves: a possible explanation", *Water Wave Kinematics*, Tørum, A. and Gudmestad, O. T. (Eds), Kluwer Academic Publishers; Norwell, Mass, pp. 609-612.

Guedes Soares, C., Cherneva, Z. and Antão, E., (2003), "Characteristics of abnormal waves in North Sea storm sea states", *Applied Ocean Research*, N° 25, pp. 337-344

Guedes Soares, C., Cherneva, Z. and Antão, E., (2004a), "Abnormal waves during Hurricane Camille", *Journal of Geophysical Research*, Vol. 109, C08008, doi:10.1029/2003JC002244

Guedes Soares, C., Cherneva, Z. and Antão, E., (2004b), "Steepness and asymmetry of the largest waves in storm sea states", *Ocean Engineering*, Vol. 31, pp.1147-1167

Huang, N., E., Long, S., R., (1980), "An experimental study of the surface elevation probability distribution and statistics of wind-generated waves", *J. Fluid Mech.*, Vol. 101, pp. 179-200

Kharif, C., and Pelinovsky E., (2003), Physical mechanisms of the rogue wave phenomenon, *European Journal Mechanics / B - Fluids*, Vol. 22, pp 603-634.

Mori, N., Yasuda, T., (2002), "A weakly non-gaussian model of wave height distribution for random wave train", *Ocean Engineering*, Vol. 29, pp. 1219-1231

Stansberg C., (1998), "Non-Gaussian extremes in numerically generated second-order random waves on deep water", *Proceedings of 8th ISOPE Conference*, Montreal, Canada, Vol. III. p. 103-10.

Tomita, H., and T. Kawamura, (2000), "Statistical analysis and inference from the in-situ data of the Sea of Japan with reference to abnormal and/or freak waves", *Proceedings of the 10th ISOPE Conference*, Seattle, USA, pp. 116- 122,

Climatic wave spectra and freak waves probability

Alexander V. Boukhanovsky^{1,2}, Leonid J. Lopatoukhin¹, Carlos Guedes Soares²

1 – St. Petersburg State University, St. Petersburg, Russia

2 – Unit of Marine Technology and Engineering, Technical University of Lisbon,
Instituto Superior Técnico, Av. Rovisco Pais, 1049-001 Lisbon, Portugal

avb@csa.ru, leonid@LL1587.spb.edu, guedess@mar.ist.utl.pt

Abstract. Long-term ensembles of hindcasted sea wave spectra are analyzed in order to provide a statistical description of spectral wave climate. The possibility to identify situations of high probability of freak wave occurrence is considered by analyzing the situations in which there has been rapid transitions between types of wave spectra as classified in the climatic spectra evaluation.

1 Introduction

Nowadays the main source of wave climate information is based on the results of hydrodynamic simulation of wave generation by past wind fields (in other words hindcasting). Spectral models, mainly WAM, Wavewatch and SWAN are being widely used. The result of hindcasting is a set of wave fields described by directional spectra at selected grid points. Normally the statistics that are determined, based on the moments of directional wave spectra, are the significant wave height h_s , mean period $\bar{\tau}$, and the mean wave direction $\bar{\theta}$. These parameters contain the general information about the intensity of the waves, but they do not describe the spectral structure of complex sea states so completely as the spectra do.

The first attempt to analyze the long-term variability of sea wave spectra was made by Scott [14]. The average wave spectra were computed using 204 wave records at OWS “I” in the North Atlantic. Buckley [1] analyzed more than 2 million spectra that were measured during 12 years at 13 buoys located in coastal waters of the USA. All the wave situations were subdivided down into twelve types, based on the values of significant wave height.

The main methodological approach to provide average spectra that can be considered a spectral wave climate description is connected with principles of “averaging” of both the frequency and directional spectra, for which there are many different techniques. For instance, Vincent & Resio [16] represent the spectral ensemble using the expansion with respect to empirical orthogonal functions, but the interpretation of the principal components sometimes is not clear. Ochi [12] analyzed 800 spectra and showed that the most general representation would be the composition of one-peaked spectra with the simple set of parameters. Statistical models of long-term variability of multi-peaked spectra were considered by Guedes Soares *et al.* [4,7] and Lopatoukhin *et al.* [8,9] for omni-directional case.

The principal goal of this paper is the development of a parametrical statistical model for climatic multi-peaked directional wave spectra, and to suggest the possibility to use these results for estimation of freak wave probability arising [11]. Freak (or rogue) waves are one of the main hazards at sea. Most existing freak wave measurements are recorded in some point of the sea, but most short-term statistics do not show such phenomena. The directional spectrum of wave record does not reveal the existence of freak wave and consequently the results of hindcasting for any specific time also do not display any suspicion of such type of waves. However synthesis of hindcasted spectra, i.e. their long-term (climate) features opens the perspective to identify situations of higher probability of occurrence of the freak wave phenomena as will be shown in the last section here.

2 Initial dataset and problem to solve

Statistical models of directional wave spectra may be developed for any sea or part of the Ocean. The North Sea was selected for this study as being one of the most investigated areas, where many wave measurements and data are available. The information about long-term distributions of spectral parameters are known and published.

The data used here is the continuous ensemble of the hindcasted sea wave fields from 1983 till 1998 (each 3 hours), obtained with the help of Wavewatch III (version 2.22) model for a grid of 15×15 miles. The NCEP/NCAR reanalysis wind speed (at 10-m level) was used as input. In each point the directional sea wave spectrum $S(\omega_i, \theta_j)$ has 24 values in direction θ_j (step 15°) and 25 in frequency ω_i . The total number of the sea grid points is more 1500. Thus, the integral size of the output data (arrays of the directional wave spectra) is enormous. Total number of spectra is more than 65 millions, and the bulk of data is $4 \cdot 10^{10}$ numbers.

The main problem to solve is the statistical generalization of such data, taking to account the physical features of sea waves and specifics of the data representation. High dimension of these values and the complexity in interpretation induces one to adopt some simplifications in calculations of wave climate statistics and in particular in the form of spectra. This simplification is based on the parameterization of the each directional spectrum

$$S(\omega, \theta) = S(\omega, \theta | \Xi(\vec{r}, t)), \quad (1)$$

which is defined as a deterministic function of random arguments $\Xi(\vec{r}, t)$. Thus, the formulation (1) allows reducing all the results of statistical modeling to a space of spectral parameters.

There are some challenges in the achievement of a clear result in statistical modeling of directional wave spectra. A *methodological* challenge is caused by the fact, that the traditional techniques for statistical formalization of sea wave spectra (e.g. principal component analysis, clustering without learning etc.) are not adequate to problem solving, because they not take into account both the physical features of sea waves

and data specifics. Therefore, the alternative statistical approaches highlighting the physics of $\Xi(\vec{r}, t)$ are needed.

A *performance* challenge reflects the strong requirement to computational procedure due to high amount of data. In spite of these challenges, the formulation (1) allows one to achieve the main objectives of spectral wave climate investigations:

- to select classes of wave spectra and to estimate their probability;
- to propose a parameterization which allows one to justify a choice of difference between the various classes (i.e., the selection of discriminant variables);
- to approximate the ensemble $\{S(\omega, \theta)\}$ in terms of its probabilistic characteristics;
- to elaborate a stochastic model of the spectral wave climate;
- to analyze the association between climatic wave spectra and rare events (the possibility of freak waves).

The problems of the classification and the discriminant analysis of climatic wave spectra were considered in [10]. Here only the problems of statistical modeling of spatio-temporal variability and approximation of the statistical characteristics are considered. Using of climatic wave spectra as the base of freak wave probability forecasting is discussed.

3 Statistical parameterization of directional spectra

In the present study, parameters of the spectrum related to wave height, spectral shape, the frequency of the spectral peak, ω_{\max} , and the main wave direction, θ_{\max} , are selected as parameters in Ξ . The single peaked model spectrum may be written as $S(\omega/\omega_{\max}, \theta - \theta_{\max}, \Xi)$, where Ξ signifies the set of the spectral parameters.

The more general multi-peaked spectrum $S(\omega, \theta)$ are obtained as

$$S(\omega, \theta) = m_{00} \sum_{p=1}^{n_{fields}} \kappa_p S_p(\omega, \theta | \omega_{\max}^{(p)}, \theta_{\max}^{(p)}), \quad (2)$$

where m_{00} , the 0th moment of the spectrum, is equal to the total variance of wave field, n_{fields} is the number of wave fields (peaks in the spectrum), and κ_p are weight

factors for each system so that $\sum_{p=1}^{n_{fields}} \kappa_p = 1$.

Guedes Soares [3] has proposed that two-peaked spectra could be represented by a combination of two JONSWAP components, which was also adopted by Torsethaugen [15] and more recently confirmed by Ewans et al [2]. However, in view of the heavy computational demand, a simpler frequency model spectrum - the Gamma-spectrum – was adopted both for wind sea and swell.,

$$S_{\Gamma}(\omega, \omega_{\max}, n) = \frac{n}{\omega_{\max}} \left(\frac{\omega}{\omega_{\max}} \right)^{-n} \exp \left(- \left(\frac{n}{n-1} \right) \left(\frac{\omega}{\omega_{\max}} \right)^{1-n} \right). \quad (3)$$

Note, that $\int_0^{\infty} S_{\Gamma}(\omega, \omega_{\max}, n) d\omega = 1$, and that the spectral peak occurs for $\omega = \omega_{\max}$. For the directional distribution, a well known one was adopted with the form:

$$Q_0(\theta, \theta_{\max}, m) = C_m \cos^m(\theta - \theta_{\max}), \quad |\theta - \theta_{\max}| < \pi/2, \quad (4)$$

where C_m is a normalizing parameter such that $\int_0^{2\pi} Q_0(\theta, \theta_{\max}, m) d\theta = 1$, and the m parameter determines the width of the angular distribution.

The model of one-peaked directional spectrum used below is therefore

$$S_p(\omega, \theta | \omega_{\max}, \theta_{\max}, n, m) = S_\Gamma(\omega, \omega_{\max}, n) Q_0(\theta, \theta_{\max}, m) \quad (5)$$

This means that the building blocks of S_p are defined in terms of four parameters ω_{\max} , θ_{\max} , n , and m . The full spectrum shown in (2) is completely defined by specifying the overall energy in the waves, m_{00} , the weights κ_p , and the parameters for each system, $\{\omega_{\max i}, \theta_{\max i}, n_i, m_i\}$. From these expressions one can derive the marginal spectra, $S(\omega)$ and $Q(\theta)$, defined from the integration of the expression in Eqn. (2) over direction and frequency, respectively.

The parameters m_{00} , $\omega_{\max 1}$, and $\theta_{\max 1}$ are determined directly from the spectra for the main peak. These values define the total energy of the spectrum, and the location and number of the prevailing wave fields.

The secondary wave systems are characterized by parameters $\omega_{\max i}$ and $\theta_{\max i}$, $i = 2, 3, 4, \dots$; but their definition are not obvious everywhere. Lopatoukhin et al [10] have considered the simplified case, where all wave systems $(\omega_{\max i}, \theta_{\max i})$ correspond to the clear separate peaks in the directional spectrum. But in fact, there are some situations, where the summary spectrum of wind sea and swell have only one single clear peak with the broad peak corresponding to the input of a secondary wave system. To reveal such cases the parameterization procedure of [11] was modified on the base of sequential conditional optimization technique. The brief algorithm considers the minimization of the functional, called ‘‘the deviation index’’:

$$DI = \sum_i \sum_j \frac{|S(\omega_i, \theta_j) - S_{ij}^*|}{S_{ij}^* m_{00}} \frac{1}{\langle \kappa_k, \omega_{\max k}, \theta_{\max k}, N \rangle} \rightarrow \min, \quad (6)$$

with the conditions

$$\sum_{p=1}^{n_{fields}} \kappa_p = 1; \quad |\theta_{\max i} - \theta_{\max j}| \geq \Delta_\theta \vee |\omega_{\max i} - \omega_{\max j}| \geq \Delta_\omega, \quad i, j = \overline{1, N}. \quad (7)$$

where S_{ij}^* are the values of the model output (for frequency ω_i and direction θ_j). Sensitivity values Δ_θ and Δ_ω are driving the algorithm calibration; in this work the values adopted were $\Delta_\theta = 30^\circ$ and $\Delta_\omega = 0.1$ (rad/s). Solving of the problem in equations (6,7) was done by means of adaptive Monte-Carlo approach for $n_{fields} = 2, 3, \dots$ in sequence. The computations were finished when the $\kappa_{n_{fields}} < \Delta_\kappa$, where Δ_κ is the sensitivity parameter (in this case, $\Delta_\kappa = 0.05$, i.e., the secondary wave system was considered negligible, if its energy input in m_{00} less than 5%).

Thus, any directional spectrum in the ensemble may be parameterized in terms of model (2-5), using the optimization procedure (6,7). But the different number of wave systems n_{fields} in (2) lead to spectra with the principally different shapes that may be described by means of statistical classification.

4 Spatio-temporal statistics of climatic wave spectra

4.1. Occurrence of the spectral classes

The model (2) allows one to distinguish one-, two- and multi-peaked (by variables ω and θ) spectra. Hence, a generic classification may be presented as shown in Fig. 1 for the SW part of the North Sea. The details of the classification procedure are published in [10].

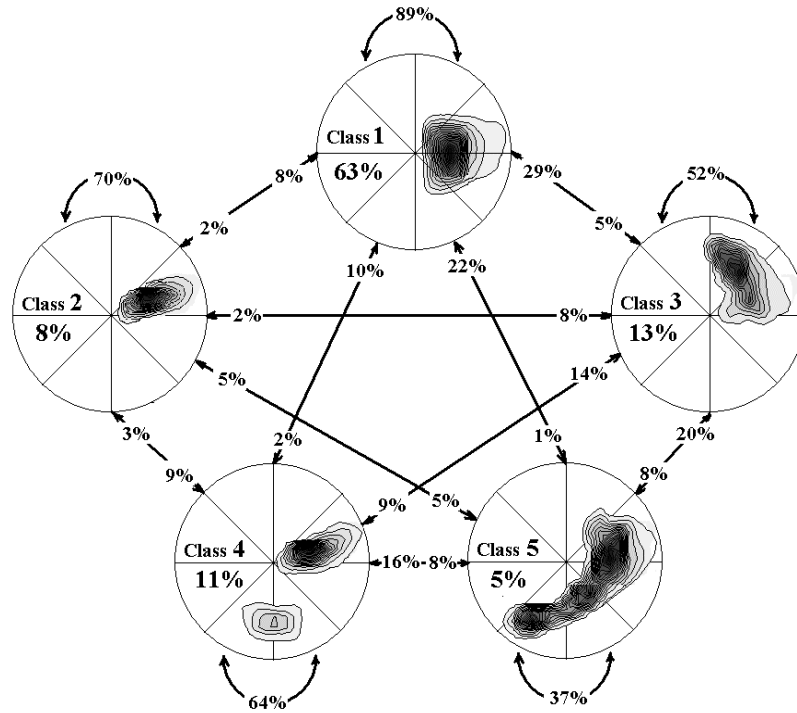


Fig. 1. Classification and transient “star” diagram for directional spectra variability. SW part of North Sea.

The following five classes of wave spectra are selected:

One-peaked spectra ($n_{fields} = 1$)

- Wind waves ($k=1$);
- Swell ($k=2$);

The separation between wind waves and swell is based on the non-dimensional steepness defined as

$$\delta = \frac{g_{\max}^2}{h_s} = \frac{\pi^2 g}{\sqrt{m_{00}} \omega_{\max}^2}, \quad (8)$$

If $\delta > 300$, then spectrum belongs to a swell, otherwise to wind waves.

Double-peaked spectra ($n_{fields} = 2$)

- Wind waves and “young” swell with close frequencies ($k=3$); It means, that in (7) may be $|\omega_{\max i} - \omega_{\max j}| < \Delta_\omega$.
- Wind wave and “old” swell separated both by frequency and direction ($k=4$);

Multi-peaked spectra ($n_{fields} \geq 3$).

- Wind waves and swell without separation (complicate sea) ($k=5$).

The spatial distribution of occurrences of each class of the spectra in the North Sea is shown in the Fig. 2. It is seen, that the wind waves are prevailing all over the sea. The occurrence of complex sea with “fresh” swell is decreased from North to South.

4.2. Markov transitions probabilities between classes

Associating each class with the stable state of the sea with number k , the synoptic variability of sea waves may be presented as the Markov chain $k = k(t)$ with the transient probability matrix $p_{ij}^{(t,t+1)} = P\{k^{(t+1)} = i | k^{(t)} = j\}$, $i, j = \overline{1, m}$ and limit probability vector $\pi_j = P\{k^{(t)} = j\}$, $j = \overline{1, m}$. In Fig. 1 the transitions between classes are also shown as a “star” diagram, where the arrows correspond to different transient probabilities. E.g., the probability of transition during 3 hours from *Wind waves* (Class 1) to *Wind waves and “young” swell* (Class 3) is 5%, and 29% - return. The probability of the cases with the same class after 3 hours, is pointed on the arcs; e.g. for the *Wind waves* this value is 89%.

4.3. Approximation of spectral statistics

The model (1) allows one to estimate the probability characteristics of directional spectra $S(\omega, \theta)$ – mean value, r.m.s, probability, tolerant and probability intervals by means of the statistical linearization. The mean spectrum is:

$$\bar{S}(\omega, \theta) = S(\omega, \theta, \bar{\Xi}), \quad (8)$$

the $p\%$ quantile spectrum is:

$$S_p(\omega, \theta) = S(\omega, \theta, \Xi_p), \quad (9)$$

spectral variance is:

$$D_S(\omega, \beta) \cong \sum_{i=1}^n \left(\frac{\partial S(\omega, \beta)}{\partial \xi_i} \right)_{\xi=\bar{\xi}}^2 D_{\xi_i} + 2 \sum_{i>j} \left(\frac{\partial S(\omega, \beta)}{\partial \xi_i} \right)_{\xi=\bar{\xi}} \left(\frac{\partial S(\omega, \beta)}{\partial \xi_j} \right)_{\xi=\bar{\xi}} \text{cov}(\xi_i, \xi_j). \quad (10)$$

Here $\bar{\Xi}, \Xi_p$ – are the sets of mean or quantile parameters of spectra, $D_{\xi_i}, \text{cov}(\xi_i, \xi_j)$ the variance and the covariance of these parameters. For example, in Fig. 3 the results of the estimation of mean spectra with 70% probability intervals for each class, for

SW part of the North Sea, are presented. All the directions are showed in Wavewatch III notation (zero is the East, and rotation counter clockwise).

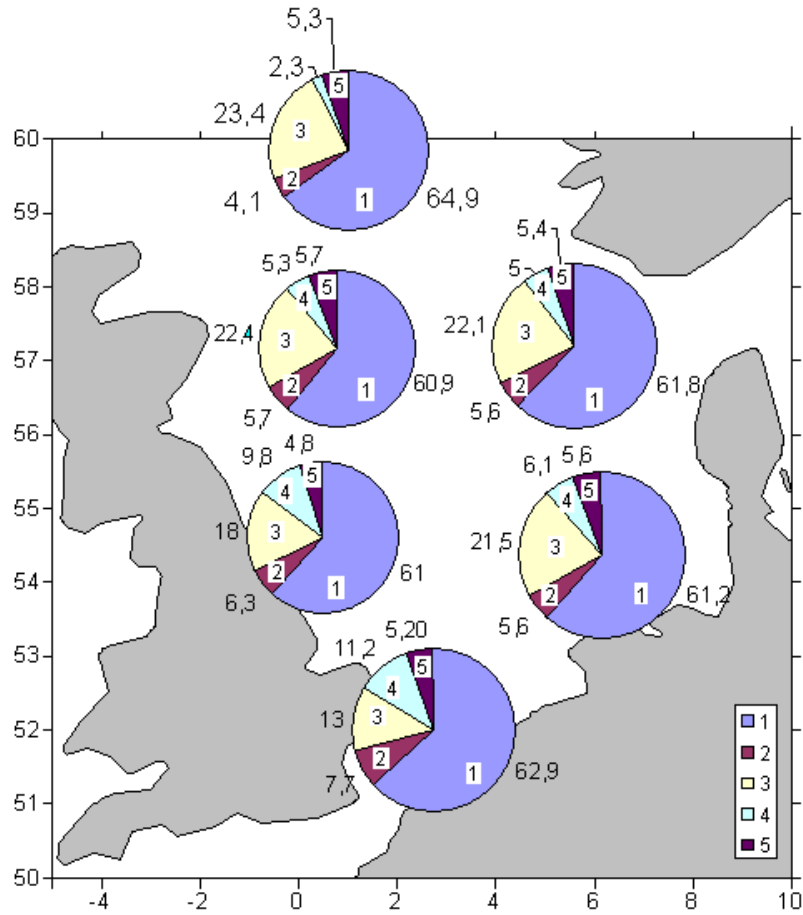


Fig. 2. Spatial distribution of the occurrence of 5 classes of directional spectra in the North Sea. 1-5 are the classes of spectra. The probability (%) shown near the pies.

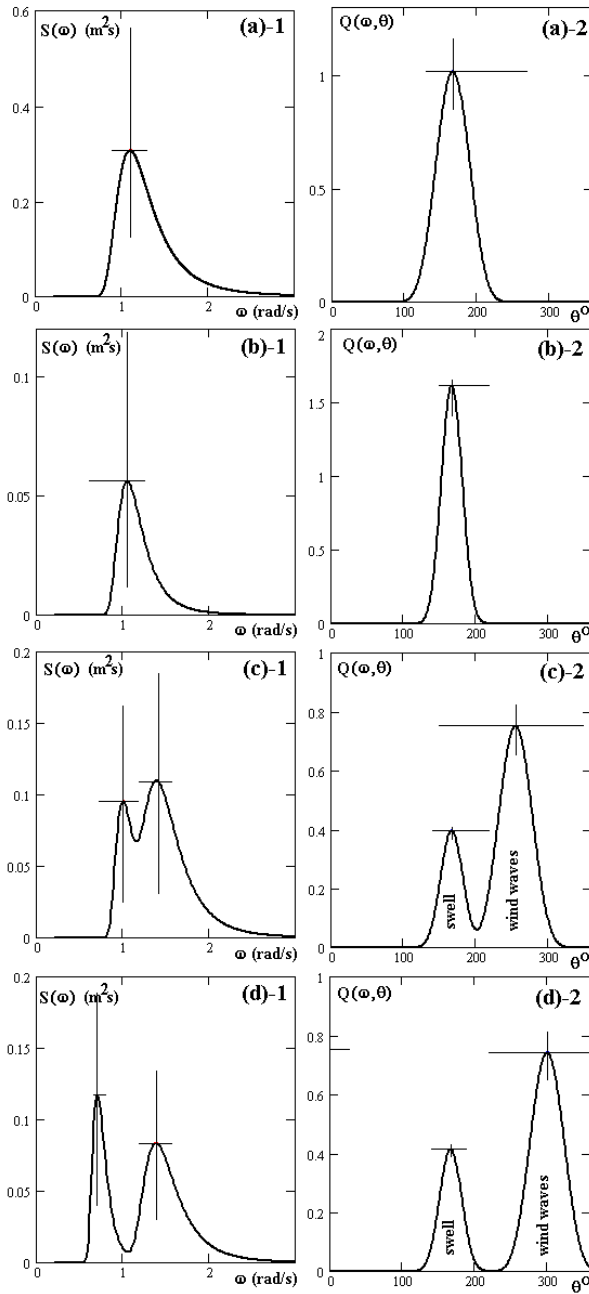


Fig. 3. Mean values and 70% probability interval for frequency spectra and angular distributions of directional spectra in Eq. (2). Classes 1-4, SW part of the North Sea.

5 Rapid sea state transitions and the occurrence freak wave

At the present state of knowledge the prediction of individual freak wave occurrence seems to be impossible. Nevertheless, the situations with increased freak wave probability may be described [11]. Comprehensive list of external and internal scenarios of freak wave generation are published elsewhere (e.g. [13]).

One of the metocean scenarios leading to freak waves generation are rapid changing of wave conditions. Using the data from climatic wave spectra this is a situation with jump from one class of spectra to another and returning back to initial situation. The most suspicious jumps related to this situation are the ones from class 1 to class 5 and back (with probability $P_{151} = \pi_1 p_{15} p_{51}$), and the jumps from class 1 to class 3 (with probability $P_{131} = \pi_1 p_{13} p_{31}$).

Markov transient probabilities were calculated both for time and space domain. In the time domain the highest probability is on the diagonal of the matrix. This means, that at least during 3 hours, the class of spectra remains the same. The next one in terms of probability is the transition from class 1 (*wind waves*) to class 3 (*wind waves and fresh swell*) is 22-27% for all the regions. The lowest probability is for transition from any class to class 5 (*wind waves and swell without separation*). Such situations are quite rare, but their probability is not infinitely small.

The plots with those probabilities are shown on the Fig. 4. It is seen that the probability P_{131} has a maximum in the West side of the North Sea, and the probability P_{151} increase from the North part of sea to South.

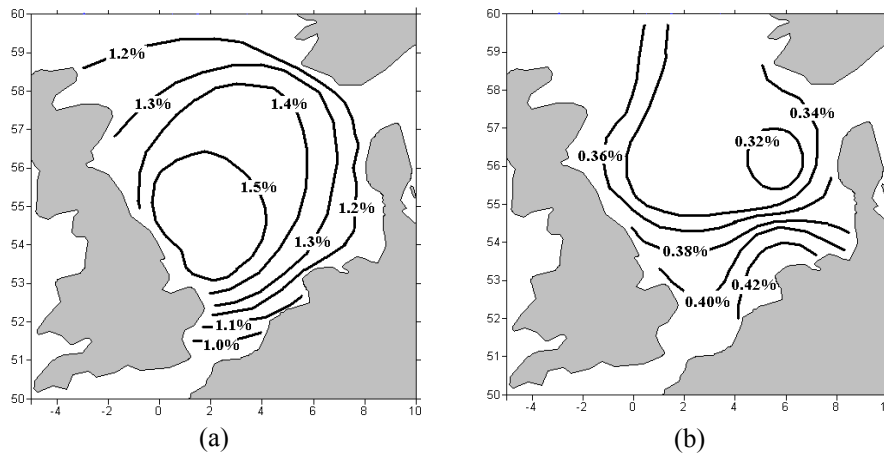


Fig. 4. Probability of the “spectral jumps” (from wind waves to complicated sea and back): (a) - P_{131} , (b) - P_{151} .

As has been pointed out, the probability of freak wave occurrence increases in the cases of jumping from one class spectra to another. This is confirmed by comparing the present climate results with wave measurement in some points in Northern North Sea.

Cases where freak waves were recorded in the North Sea were analyzed by Guedes Soares et al [5,6] respectively for North Cormoran and for North Alywn and Draupner. These situations have been studied by investigating in the database of hindcast wave spectra the transitions that have occurred between types of spectra at the time of occurrence of the freak waves. The results are presented in Table 1. In the same table (row 3) jumps between different classes of spectra (1÷5) are shown.

Additionally, in this table the instrumental measurements in the Black sea [8,11], where the freak waves were recorded, are considered. The result confirms that in all cases of freak wave recording, there happened sudden change of classes of spectra.

From Fig. 4 it is seen that for case of jump 1-3-1 the most dangerous is the Eastern part of the sea (probability 1.5%). In the case of jump 1-5-1 – the most dangerous is Southern part of the sea (probability 0.4%).

Forecasting of wave conditions for the North Sea is a routine experience. This means, that changing of wave conditions are also known. Therefore prediction of spectral jumps may be one of warning to the possibility of freak wave arising.

Table 1. Dates and types of spectral jumps from the one class to another (in comparison with the wave measurements in the North Sea and the Black Sea).

Position	Date	Sequence of classes (each 3 hours)
North Alwyn, N. Sea	16.11.1993	1 1 3 3 3 1 1 1
“	18.11.1993	1 1 1 1 3 3 3 1
N. Cormorant, N. Sea	04.01.1993	1 5 5 3 1 1 1 1
“	12.01.1993	3 3 3 3 1 1 1 1
“	18.01.1993	1 3 3 3 3 3 1 1
“	12.03.1996	1 1 1 1 1 1 1 1
Draupner, N. Sea	01.01.1995	1 1 1 3 3 1 1 1
Gelendzik, Black Sea	16.12.2000	4 3 3 1 1 3 1 3
“	22.11.2001	4 3 3 3 3 1 3 1

6 Conclusions

An approach for the statistical modeling of climatic directional wave spectra is proposed. Probabilities of occurrence of each class of spectra, and of the transitions between classes for the North Sea are estimated (see Fig. 1, 2). Jumps from one class of spectrum to another have been studied for the time in which cases of freak wave measurements in the North and Black sea were reported. It is suggested that those types of rapid jumps may be regarded as an indication of increased freak wave probability.

Acknowledgements

This research is partially funded by INTAS grant 2001-2156 "Freak waves generation in the ocean".

References

1. Buckley W.N. Extreme and climatic wave spectra for use in structural design of ships. *Naval Engineering Journal Soc.* (1988), pp. 36-57.
2. Ewans, K. C.; Bitner-Gregersen, E., and Guedes Soares, C. Estimation of Wind-Sea and Swell Components in a Bimodal Sea State. *Proceedings of the OMAE Specialty Conference on Integrity of Floating Production, Storage & Offloading (FPSO) Systems*; 30 Aug 2-2004 Sep 2; Houston, TX. (2004), Paper OMAE PFSO'04-0045
3. Guedes Soares, C. Representation of Double-Peaked Sea Wave Spectra. *Ocean Engineering.* (1984); Vol. 11, pp 185-207.
4. Guedes Soares C. On the occurrence of double peaked wave spectra, *Ocean Engng., Vol. 18, No 1/2*, (1991), pp. 167-171.
5. Guedes Soares, C.; Cherneva, Z., and Antão, E. M. Characteristics of Abnormal Waves in North Sea Storm Sea States. *Applied Ocean Research.* (2003), Vol. 25(6), pp 337-344.
6. Guedes Soares, C.; Cherneva, Z., and Antão, E. M. Steepness and Asymmetry of the Largest Waves in Storm Sea States. *Ocean Engineering.* (2004), Vol. 31, pp 1147-1167.
7. Guedes Soares, C. and Nolasco, M. C. Spectral Modelling of Sea States with Multiple Wave Systems. *Journal of Offshore Mechanics and Arctic Engineering.* (1992), Vol. 114, pp 278-284.
8. Lopatoukhin L.J., Boukhanovsky A.V., Rozhkov V.A., Divinsky B.V. Climatic wave spectra of the Black Sea, *Proc. Int. MEDCOAST Conf. «Wind and wave climate of the Mediterranean and the Black sea», Antalya, Turkey*, (1999) pp. 97-109.
9. Lopatoukhin L.J., V.A.Rozhkov, V.E.Ryabinin, V.R.Swail, A.V. Boukhanovsky, A.B. Degtyarev. Estimation of extreme wind wave heights. *World Meteorological Organization. WMO/TD-No 1041*, (2000), 76 p
10. Lopatoukhin L., Rozhkov V., Boukhanovsky A., Degtyarev, A., K. Sas'kov, G. Athanassoulis, Ch. Stefanakos, H. Krogstad. The spectral wave climate in the Barents sea. *Proceedings of Int. Conf OMAE'02, Oslo, Norway, June 23-28*, (2002), (CD-version).
11. Lopatoukhin L.J., Boukhanovsky A.V. *Freak waves generation and their probability. Int. Shipbuild. Progress*, 51, 2-3, (2004), pp. 157-171.
12. Ochi M.K. Wave statistics for the design of ships and ocean structures. *Trans. Soc. Naval Architects and Mar. Eng. Vol.86*, (1978), pp. 47-76.
13. Olagnon, M, Athanassoulis, M., *Proceedings of the Rogue waves Workshop, Ifremer. Brest, France.* (2000).
14. Scott J.R. Some average sea spectra. *Quarterly Transactions Royal Institution of the Naval Architects*, v.110, N 2, (1968) pp. 233-245.
15. Torsethaugen, K. (1993), "A Two Peak Wave Spectrum Model", *Proc. of the 12th Int. Conf. on Offshore Mechanics and Arctic Engineering*, Vol. 2, pp. 175-180.
16. Vincent C.L, Resio D.T.. An eigenfunction parameterization of a time sequence of wave spectra. *Coast. Eng. Vol. 1*, (1977) pp. 185-205.

**Ship Design Rules and Regulations
- An overview of major themes**

Gil-Yong Han
International Association of Classification Societies (IACS)

Abstract: This paper provides an insight into the ship safety legislation issues relating to ship design that has evolved in recent years, with a brief background on the risk-based approach that the shipping industry has adopted.

It outlines the roles of classification societies in ensuring that the ships are designed, built and maintained in good condition.

It also provides an overview of the development of the Goal-Based Standards and the common Structural Rules. Some critics even suggest that the discussion on the development of the Goal-Based Standards should have taken place some decades ago. Nevertheless, a good degree of progress is being made with participation from the flag states and industry organizations. The goal-based regulatory framework is expected to begin with goal-setting at the top-level, followed by breaking down the goals on the sub-levels. It means that once the Goal-Based Standards are developed, classification societies will develop detailed standards on ship structure and machinery by which the so-determined safety goals are achieved.

Major issues surrounding the development of the Common Structural Rules will be introduced.

Finally, the results of the Maxwave Project are discussed from the ship designer's point of view with the following summary:

- IACS Recommendation No. 34
- Analysis of shipping casualties
- Design parameters such as probability of encounter and return period
- Difference between shipping and offshore industry
- Voluntary reduction of ship speed

1. Introductory remarks

Ladies and Gentlemen,

I would like to thank you for inviting me to take part in this workshop. At the beginning of this year, the final reports of the Maxwave Project were published. The Senior Advisory Panel (SAP) finalized its report with recommendations for ways forward. As the cover note of the SAP report suggests, the Project has found its way to raise awareness of users in various sectors of the Society. Therefore, perhaps this might be a timely occasion on which to look at how the ship safety is addressed both at IMO and IACS and see what they have achieved – and then to look to the challenges ahead. Finally, I will suggest how the findings of the Maxwave Project should be carried forward.

As I understand, the main objective of this section of the workshop is to openly exchange our views and search for the answers to a few fundamental questions:

- First of all, to what extent will the findings of the Maxwave Project influence the shaping of the future ship design practices ?

- The answer to the first question is directly connected to the second issue: are the current ship design practices and ship construction rules, including the classification societies' requirements, adequate to the new times – and if they are, then to what extent? Do they respond to the new needs and are they an effective instrument for preventing and countering any perceived risks which modern ships are subject to.

I hope that this workshop provides an opportunity to understand what other stakeholders do play in their roles and to have an insight over these issues.

2. Roles of classification societies¹

At the outset, it might be helpful if I were to update you as to what roles classification societies do play, and what is IACS in relation to IMO.

Classification societies have been subjected to much criticism, some constructive and some not. Constructive criticism is always welcome; however, to be truly constructive, it should be based on a full understanding of the roles of the Classification Societies and their considerable contribution to ship safety in the setting and maintaining standards for hull structures and shipboard engineering systems.

IACS Member Societies produce rules for hull structural design and essential shipboard engineering systems and apply them by means of appraisal of the design and survey of the ship and its systems. Additionally, the Societies apply the requirements of the IMO Conventions on behalf of more than 100 Administrations, also by means of design appraisal and survey.

¹ IACS and IMO, the established relationship (JRG Smith J D Rose, IACS, 2001)

Therefore, it is important to have a clear understanding of the separate but related functions of the Societies and the International Maritime Organization (IMO) in producing safety and pollution prevention rules and regulations for ships, and the functions of the Societies in applying them. It highlights the fact that compliance with Classification rules for hull structures and essential shipboard engineering systems is a requirement of the 1974 Safety of Life at Sea Convention (SOLAS 1974)².

Each Member of IACS can be defined as a Classification Society having comprehensive classification rules compiled on the basis of sound research and development, a worldwide network of well qualified surveyors' efficient and effective feedback of significant technical data via surveyors' reports and an internationally recognized quality management system. Their classification rules have been in a constant state of evolution and development, in some cases for over 200 years, and have traditionally addressed hull structures and shipboard engineering systems. Complying with these rules will ensure the provision of adequate overall or global strength, together with adequate local strength of individual components. For overall strength, a ship's hull must be capable of withstanding design values of still water and wave induced loads within specified stress criteria. Local strength, to resist modes of buckling, fatigue, yielding or brittle fracture, is obtained by compliance with the rules' material requirements and scantling formulations. In addition, the rules provide for the determination of scantlings of primary members (such as girders, floors, stringers) direct calculation procedures and permissible stress criteria.

A strength of the classification concept is that the societies act as independent bodies, giving an independent assessment of the status of the structure and machinery of a ship.

However, classification societies are not guarantors of safety of life or property at sea or the seaworthiness of a vessel in the sense that they have not full control over how the vessel is operated and maintained in between the periodic surveys. Further, proper and effective construction of the ship lies in the hands of the designer and shipbuilder. Human errors and poor workmanship may occur. Safe operation of a ship for its intended service depends principally upon the shipowner, the shipowner's representatives and the crew who operates and maintain the ship on a day to day business³.

IMO Conventions, on the other hand, concentrate on other safety issues, such as the computation of load lines and conditions of assignment, stability, security, fire safety, life saving appliances, navigation lights and equipment and radio communication. IMO, as a specialized agency of UN, enables Member States to meet collectively for the purpose of producing international Conventions, instead of producing their own safety and pollution prevention requirements individually and in isolation.

² SOLAS 1974 Reg.II-1/3-1 states that in addition to the requirements contained elsewhere in SOLAS 1974 As amended, ships shall be designed, constructed and maintained in compliance with the structural, mechanical and electrical requirements of a classification society which is recognized by the Administration in accordance with the provisions of regulation XI/1 or with applicable national standards of the Administrations which provides an equivalent level of safety.

³ classification societies – what they do and do not do (IACS, 2004)

Despite records of achievement by IACS and IMO, regrettably, accidents do occur, no matter how much we seek to make ships built and operate safely. The circumstances that follow any major shipping accidents will inevitably have an impact on the image of the shipping industry as a whole. Therefore, there is a demand for more robust ships that will be safer and more productive for longer.

IACS initiated the Common Structural Rules program in June 2003 to improve transparency in rule making, and clearly define the rule objectives, thereby removing competition among classification societies based on specific rules, nor seeking to optimize steelwork to the detriment of the longevity of the ship. This is a huge step forward in the ship design rule making history where all the technical expertise of the classification societies is combined with the feed back input from the ship owners.

IACS plans to extend common rules approach to other vessel types, with container ships in the list.

The common rules have been developed with goal-based standards (GBS) in mind which are currently being laid down by the IMO. The objective of GBS is that a ship is built in accordance with rules that ensure a safe operating life for a particular type of ship over a specific period in certain prevailing sea conditions. Once such standards are set, classification societies with feedback from ship owners and operators, are to establish common rules to achieve the goals. Therefore, it can be safely said that classification societies would not compete on the necessary minimum scantlings. Instead, focus will be given to service delivery to their customers after the ship is built.

3. Improvements in ship safety legislation

It is often said that more than 80 % of accidents at sea are the results of human errors. It does not mean that for only 20 % of those marine accidents, interest parties other than ships' crew such as the ship designers, owners and regulators are accountable. From the design stage, ships shall be built to withstand the most probable worst damage scenarios in a hostile environment. However, in many instances, improvements in safety have been driven by accidents. This is not a proper way to deal with improving ship safety because decisions are not taken solely on a basis of sound technical analysis. The urgent need to introduce new requirements tailored to address the specific problems overrides.

Following a series of high profile accidents at sea such as Piper Alpha(offshore), Herald of Free Enterprise, Exxon Valdez, Scandinavian Star, and Estonia in 1980-1990s, the shipping industry was called on to adopt a risk-based approach in ship design and operation as other industries had practiced for years³.

3.1 Risk-based approach

Having recognized a more holistic approach is needed in place of a piece-meal approach, and in response to the call for risk-based approach from various sectors, the IMO, supported by IACS, has introduced a more structural risk analysis process through a now so famous

³ In an attempt to answer the question "Is safety given sufficient weight in ship design and technology ?", UK House of Lords Science & Technology Committee (Report 2992-92, 2nd report, 1992) recommended that UK should advocate the adoption of performance standards rather than prescriptive standards wherever possible.

“Formal Safety Assessment” procedure, and regulators are encouraged to examine potential areas and introduce appropriate risk reduction measures before a tragedy occurs. A number of FSA studies have been undertaken, with bulk carriers FSA studies heading the list.

Many of classification societies also are moving towards the application of risk methodologies to the establishment of classification rules for both the design and operational maintenance of ships’ hulls, machinery and marine structures. This risk-based approach will *supplement* the traditional prescriptive approach, allowing variation from prescriptive rules provided that the system (ship) risks are maintained at acceptable levels ⁴

The advantages are: a systematic method is put in place to seek to establish ship safety regulations on the basis of assessment of risks, costs and benefits. Further, this method is characterized by being both rational and systematic, thus generating confidence that regulatory decisions based upon its use should be robust and defensible.

In addition, classification societies introduce a reliability-based method for ship hull structures that can be expressed in a special format such as the Load and Resistance Factor Design (LRFD) format.

All these efforts stem from the shared understanding that changing rules in immediate reaction to casualties prior to discovering main causes is an inadequate way of addressing the ship safety issues, and from the demand of the shipping industry as a whole that ships are to be built more robust and operate more safely.

3.2 Common Structural Rules (CSR)

IACS Joint Tanker & Bulker Project teams are currently developing the new rules under the IMO’s “goal-based standards” principles. What this means in practice is that classification societies will agree common structural rules enabling robust tankers and bulkers to be built, fit for purpose and effective and safe operation, to last for a period of 25 years, corresponding to 10⁸ wave induced load cycles. Differences in scantlings or longitudinal strength requirements will be removed so that new ships conform to common standards, whichever Classification Societies oversee their construction. Matters of significant importance are as follows:

- The ship’s hull girder strength should be sufficient enough to withstand North Atlantic ocean conditions for 25 years (25 year return period). The North Atlantic is regarded as the most severe. The 25-year significant wave height is equal ca. 16.0m which corresponds to ca.31.0 m individual wave height.;
- Net Thickness Approach (as opposed to gross scantling approach)
The net scantling approach (i.e. excluding nominal design corrosion margins) is intended to ensure that, with protective coating and good maintenance, the minimum global and local strength requirements to resist all the failure modes will be met over the ship’s intended service life.
Under the older rules, the corrosion margin is given as a percentage figure of steel plate thickness but the new rules will give an absolute minimum figure corrosion margin.
- Fatigue assessment and fatigue details catalogue

⁴ MSC 72/16, Decision parameters including risk acceptance criteria, Norway, 2000

Survey procedures – renewal criteria for explicit wastage allowances. Similarly to the net thickness approach, the fatigue life of structural details is based on a 25 years unrestricted service at the North Atlantic sea conditions.

This initiative utilizes in the best way the combined experience and know-how of all IACS members.

To fill the gap between design appraisal and survey during construction, IACS is, in parallel, developing a standard procedure for survey and inspection during new building construction.

3.3 Goal-Based Standards(GBS)

Based on a proposal by The Bahamas and Greece, the IMO Council agreed to include the development of Goal-Based Standards for shipbuilding into its Strategic Plan⁵.

The basic principles of the proposed goal-based regulatory framework, as shown in Fig.1, are:

- The goal-based standards should represent the top tiers of the framework, against which the ship safety should be verified both at design and construction stages, and during ship operation.
- The goals are not intended to set prescriptive requirements or to give specific solutions. However, they should be clear, demonstrable, verifiable and long-standing and capable of adapting to changes in technology.
- The goals should be achieved either by compliance with published technical standards or by means of alternative solutions providing an equivalent level of safety;
- The requirements developed and applied by national Administrations or Classification Societies acting as Recognized Organizations should be capable of demonstrating compliance with the goal-based standards.

⁵ IMO Strategic Plan (MSC 78/6/2, February 2004)

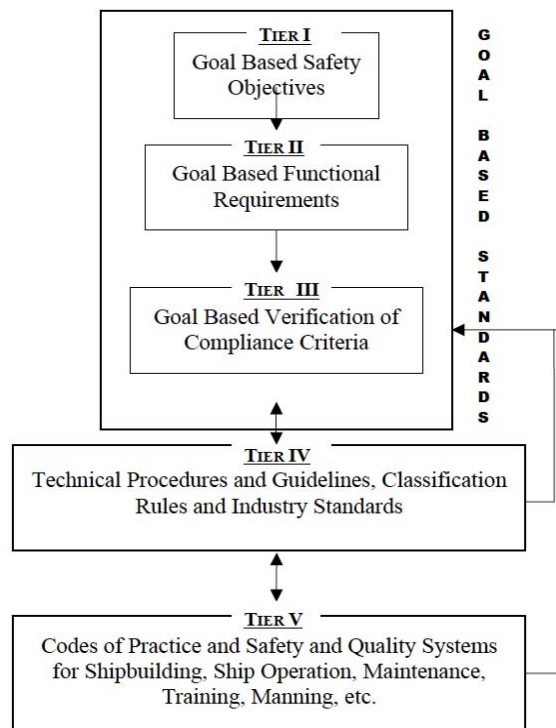


Figure 1. Goal-Based Regulatory Framework⁶

The mechanism by which the goal-based standards will be put in place are as follows:

- IMO sets the goals;
- IACS develops classification rules and regulations that meet the so-determined goals;
- Industry, including IACS, develops detailed guidelines and recommendations for wide application in practice.

It should be, however, noted that even at the time of this writing, IMO members governments and non-governmental organizations are voicing their views on how the discussion on GBS shall be carried forward. Though IMO is currently focusing its attention on the GBS for the design and construction of new ships, the scope of application of the GBS will soon be extended to cover quality and uniformity on how ships are to be surveyed during construction, another important aspect of ship safety prior to the delivery of the ship.

Figure 2 is an example showing how the classification rules would stand under the IMO's goal-based standards.

⁶ MSC 78/6/2, Goal-Based Standards, The Bahamas, Greece and IACS, 2004

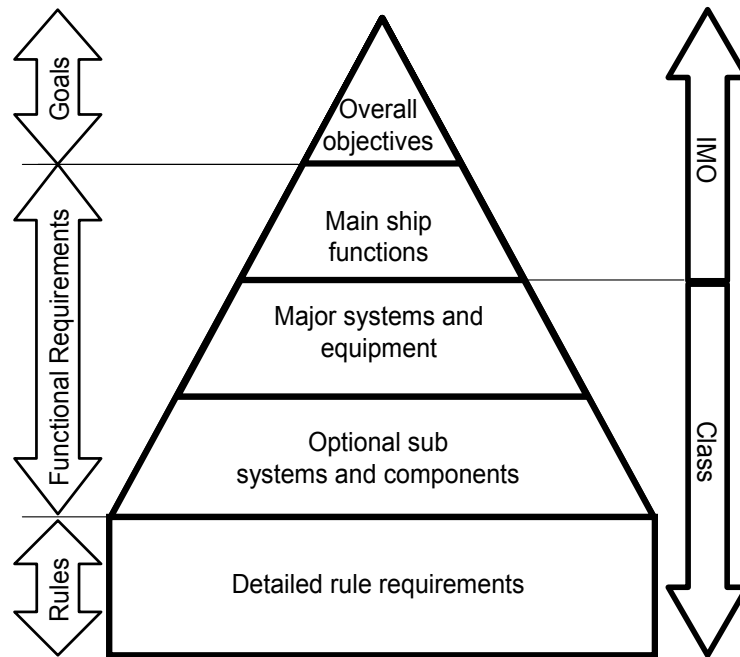


Figure 2. GBS and class rules

4. Freak Waves

4.1 General

Waves which influence the behavior of ships at sea exhibit a notably random behavior in nature. For engineering purpose, waves need to be described by probabilistic models. One of the important tasks in ship design is the estimation of an extreme design wave from the recorded wave data. In other words, a good degree of understanding of the random seas enables designers to predict ship motions, wave-induced forces, bending moments of ships and dynamic pressures at sea, or, more generally speaking, prognosticate wave loads. These engineering disciplines are well established in naval architect, ocean engineering, offshore engineering and coastal engineering.

IACS standard wave data⁷ is applied as a standard probability of sea states for long-term prediction, while wave data for representative worldwide trading routes can be applied, using the Global Wave Statistics, North Pacific wave data and Walden's North Atlantic wave data. It recommends the Bretschneider or two parameter Pierson-Moskowitz spectrum for the North Atlantic which includes the most important factors in ship design: significant wave height and wave directional spectrum.

For the purpose of ship design, information is needed not only on the severity of sea states that the ship is expected to encounter during her life time (e.g. 25 years), but also on the frequency of occurrence of sea conditions, the former being most commonly represented by significant wave height and the latter being important for fatigue analysis.

IACS Recommendation, by its definition, is of recommendatory nature. IACS Members are not bound by it, however, it provides at least guidance as to the use of wave data, determination of return period (RP) and probability of exceedance.

⁷ IACS Recommendation No. 34 – Standard Wave Data, 2001

4.2 Freak Waves

Notably, Draper. L suggested two aspects of freak waves⁸, which were followed by other researchers (M.Ochi, R. Dean, etc) to continue using the term “freak waves” and develop a theory for application to a real ocean wave spectrum.

At this stage, no authoritative definition of “freak waves” which represents the observed abnormal waves such as the New Year Draupner wave yet exists. Even the terms for such waves vary ! The commonly used criteria to define freak waves, $H_{max}/H_s > 2.0$, a ratio between maximum wave height and significant wave height, is still challenged due to its shortcomings in representing the full spectrum of the surrounding sea states.

Even if it is the correct definition of a freak event, the question of highly non-linear lifetime maximum responses of a ship to freak waves has to be addressed with caution.

It is noted that recent advances in wave generation and measurement techniques have led researchers and oceanographers to investigate the existence of the so-called “freak waves” and their physical/statistical characteristics. “Maxwave” project was a most recent collaborative research program.

Careful follow-up of the researches in the Maxwave project makes of impressive findings⁹:

- Traditionally, this type of waves have been observed only occasionally under unexpected condition. However, by virtue of an advance mode of measurement and data analysis techniques, the occurrence of freak waves has been analyzed and measured.
- Better understanding of the mechanism generating such waves was gained.
- Most importantly, the analysis of shipping casualties is expected to lead to the development of a mechanism by which shipmasters will be alerted of an occurrence of freak waves, so as to enable them to take precautionary actions.

With respect to the areas of future study as a result of the Maxwave project, I wish to add the following comments:

- The design practice is moving towards a more consistent probabilistic approach, for example, extremes are determined for a given return period (e.g expected lifetime of the structure). In order to consider the effect of freak waves in ship design, the probability of occurrence and also the probability of a ship encountering such waves need to be quantified. This involves a rigorous analysis of shipping casualty database. It is not unusual that the lack of casualty data, or more precisely speaking, lack of information on the core causes of the reported casualties, can lead to a misleading or unfounded conclusion. Therefore, a degree of accuracy in data analysis in dealing with uncertainty needs to be assured and the process needs be made transparent.

The findings of the Maxwave Project indicate that freak waves, due to their extreme steepness, normally last for very short periods before breaking. Hence, the probability of a ship or platform meeting such waves is even significantly lower than the probability that these waves occur in the ocean.

⁸ Draper.L, freak ocean waves, 1964

⁹ Maxwave Senior Advisory Panel (SAP) report, 2004

Further, shape of freak wave profiles both in space and time including their kinematics and ship responses to freak waves should be analyzed and be well documented.

- A distinction is to be made between ship structures and offshore structures.

Offshore structures normally operate at fixed locations and often require a unique design. Unlike offshore platforms, ships have forward speed. The methods applied for wave load calculations are different between ships and offshore structures. Master's practice to adapt ship, course and heading to extreme environmental conditions need to be taken into account. Offshore structures cannot actively avoid heavy weather in the same manner as shipmasters do¹⁰.

In that sense, it is very encouraging to see that the Maxwave Work Package.8 reported that Manual of Marine Met services could provide additional information on abnormal waves in the list of potential parameters for warning. A software tool in support of the master's decision-making under abnormal wave conditions has also been shown in various occasions¹¹.

- The validity of a non-linear wave theory and mathematical model for freak waves developed in the Maxwave Project should be verified, i.e. how well the prediction of the theory agrees with the actual measurements. I believe that this is an area for further research as one of recommendations of the Maxwave project.

5. Concluding remarks

With 95% of world trade dependent upon maritime transportation in one form or another, a massive increase in shipping transportation may occur over the next 25 years¹².

Whether this prediction is accurate or not remains outside of the scope of this workshop. However, these figures compel us to an ever increasing need to ensure that ships are built to the highest standards and operate safely for their intended life-time.

Now, challenges lie ahead. It is important to note that whatever level of quantifiable risk we deem acceptable today will without doubt be declared unsatisfactory by the media and public once that level is exceeded in an accident involving a catastrophic consequences. Though our responsibility is to learn from the incident and find a means of preventing it from happening again, it is equally important to bring the risk-based safety standards to practice as a means of addressing the ship safety from a much broader perspective.

In addition, new knowledge gained from the advanced technology shall be fed into the design rules whenever found necessary.

I hope that the updates on the current major themes in the shipping industry that I have provided will assist you in the application to your own fields of interest. Finally, it is

¹⁰ The classification rules presuppose that the ship will be operated and maintained by a competent and adequately trained crew. Together with the making timely and precise decisions to change the ship's heading, the magnitude of voluntary speed reductions in extreme sea-states has been part of the art of seamanship.

¹¹ Shipboard Routing Assistance (H. Rathje(GL), Design & Operation for Freak Waves, 2003, London)

¹² US Department of State, Blue Water Project, 2003

encouraging to see that the scientific researches on the freak waves continue and have entered into a Post-Maxwave phase with more tailored research objectives.

* * *

Comparison of Present Wave Induced Load Criteria with Loads Induced by an Abnormal Wave

C. Guedes Soares, N. Fonseca, R. Pascoal

Unit of Marine Engineering and Technology, Technical University of Lisbon,
Instituto Superior Técnico
Av. Rovisco Pais, 1049-001 Lisboa, Portugal
{guedess, nfonseca, rpascoal}@mar.ist.utl.pt

Abstract.

In this work, values determined from existing design load criteria are compared with loads determined by a first principles based method that has the novelty of using a wave trace including an abnormal wave from a real field measurement. A time domain seakeeping code is used in the linear and non-linear variants to solve the equations of motion and assess the structural loads for oceangoing vessels. Linear and nonlinear calculations are compared in time domain for the S-175 containership with speed of advance. Nonlinear time domain computations are compared with experimental results from physical model tests with a moored FPSO. For both, the S-175 and the FPSO, probability domain comparisons are made between long-term probability distributions, experimental results and minimum rule requirements. The uncertainty associated even with methodologies strongly based on first principles is also discussed.

1 Introduction

In order to build safer and more cost efficient ocean structures, there should be a continuous strive to increase the confidence level at all stages of design. One of the major sources of uncertainty are the loads themselves and therefore a complementary method is sought and compared with existing criteria.

The more traditional design criteria originate in some kind of statistical analysis of existing data or a probability based methodology that attempts to replicate this type of analysis. Statistical analysis is possible and useful when there are existing data that can characterize the wave loads within a desired confidence level. This means that, when compared to the vessels from which the data sets have originated, the new design should not have significant specificity of any type, be it for instance on the hydrodynamic behavior, climatology it must encounter or cargo distributions. In order to be useful, appropriate low order multivariate regression models are derived. The result of this methodology is easiest to use because it omits the analysis steps and can provide intuitive and pragmatic relations between wave loads and vessel main particulars for instance. Rules minimum values are a good example of this more pragmatic approach that can easily provide starting values in the design spiral.

More direct analysis depends on determining long-term distributions based on calculations with an underlying principle of linearity of responses. The main

hydrodynamic calculations are then performed in the frequency domain and after the needed estimators are calculated, appropriate probability distributions are used to determine the design value at the desired probability level, sometimes referred to a return value. Probably the most common form of this calculation is the long-term distribution determined as the sum of linear short term distributions ([1], [2]). The short term distributions are determined for each seastate of interest and the weighted sum gives the result for any return period. All seastates may be used or just those over a certain threshold.

Some variants of the probability based calculation aim to further simplify the procedure by reducing the number of calculation steps. As examples of such there is the use of a design seastate and also the environmental contour line method ([3]). Attention should be given however, to the fact that these seastates must be carefully chosen or else it can give bad estimates. For instance in case of a system with a very narrow band response, the worst loads may not be at the more energetic seastate but at one with a different period. Other variants attempt to explicitly include the nonlinearity due to vessel hydrodynamic response, as for instance in [2] and [4] by the use of form functions to correct for the nonlinearity, or more recently by direct use of nonlinear pseudo transfer functions as in [5].

Here, following previous work on the subject ([6], [7], [8] and [5]), it is proposed that measured sea surface elevations containing abnormal wave events become data for advanced time domain codes and the result from these be used in parallel with current design procedures, making it possible to assess if design load values are reasonable and to alert for problems. This methodology arises because there is an understanding that current design procedures do not account for abnormal wave events and available data can be used directly to eliminate the need for heavy data fitting, with all the problems that can arise. Easily, data fits will include failure to acknowledge the existence of special events such as is the case of abnormal waves, which have come to be considered as an important design survival case (see [9]). Furthermore, this method makes way to assess a whole new design with more confidence and detail.

The variability of results deriving from the uncertainty in climate, from different approaches to perform first principles hydrodynamic calculations, etc, may be alleviated if deterministic weather traces, which may include waves and other meteorological data, also have to be used to assess a design, at least as better assurance that the vessel survives such a combination.

2 Time Domain Seakeeping Code

2.1 General Description

The seakeeping code used in this investigation is based on a time domain formulation and the hydrodynamic forces are represented by a strip theory approach. The method assumes that the nonlinear contribution to the vertical bending moment is dominated by hydrostatic and Froude-Krilov forces and therefore these components are calculated over the instantaneous hull wetted surface. Radiation and diffraction forces are linear. Green water loads on the deck, which contribute to the calculation of motions and global loads, are represented by the momentum method.

The exciting forces due to the incident waves are decomposed into a diffraction part and the Froude-Krilov part. The diffraction part, which is related to the scattering of the incident wave field due to the presence of the moving ship, is kept linear. Since this is a linear equation and the exciting waves are known a priori, it can be solved in the frequency domain and the resulting transfer functions be used to generate a time history of the diffraction heave force and pitch moment. The Froude-Krilov part is related to the incident wave potential and results from the integration at each time step of the associated pressure over the wetted surface of the hull under the undisturbed wave profile.

The hydrostatic force and moment are calculated at each time step by integration of the hydrostatic pressure over the wetted hull under the undisturbed wave profile. The radiation forces, which are calculated using a strip method, are represented in the time domain by infinite frequency added masses, radiation restoring coefficients (which are zero for the zero speed case), and convolution integrals of memory functions. The convolution integrals represent the effects of the whole past history of the motion accounting for the memory effects due to the radiated waves.

The vertical forces associated with the green water on deck, which occurs when the relative motion is larger than the free board, are calculated using the momentum method. The mass of water on the deck is proportional to the height of water on the deck, which is given by the difference between the relative motion and the free board of the ship.

A detailed presentation of this solution to the hydrodynamics problem is given in [10] and [11].

2.2 Code validation for ships with forward speed

In order to perform code validation for vessels with speed of advance, a segmented and instrumented model of the S-175 containership has been subject to extensive experimental tests at El Pardo seakeeping basin.

The model was sectioned at $\frac{1}{4}$ and $\frac{1}{2} L_{pp}$ from the forward perpendicular in order to measure the cross sectional loads at these positions and subject to regular and irregular wave trains. Table 1 presents the ship main particulars and figure 1 shows the model whilst undergoing tests at the basin. In [12] and [13] are presented details of this experimental program and the analysis of results, while some of the comparisons with numerical results are reproduced here.

Figure 1 to Figure 3 present some results of the experimental program plotted together with the results of the numerical simulation using the aforementioned time domain code. These are results for the vessel advancing at a Froude number of 0.25 in an irregular seastate with significant wave height of 6.13m and a peak period of 11.5s.

Figure 1 presents the empirical cumulative distribution function for positive and negative maxima of the heave motion. Very good general agreement is found, with the numerical model, as compared with the experiments, having slightly

S-175 Containership		
Length betw. perp.	$L_{pp}(m)$	175.0
Beam	$B(m)$	25.40
Draught	$T(m)$	9.50
Displacement	$\Delta(\text{ton})$	24742
Long. posit. of CG	$LCG(m)$	-2.43
Pitch rad. of gyr.	K_{yy}/L_{pp}	0.24

Table 1 S175 main particulars

overestimated the number of larger positive and negative peaks. Opposite behavior is found for the smaller peaks.

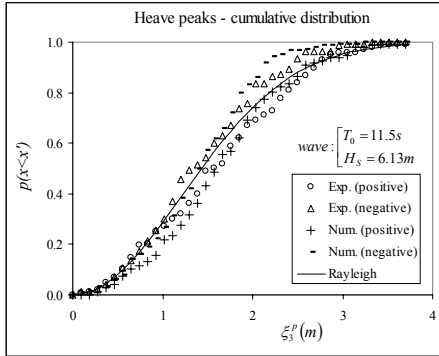


Figure 1 Empirical cumulative distribution function for heave motion maxima at $F_n = 0.25$.

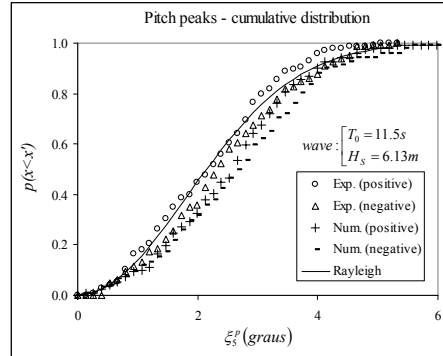


Figure 2 Empirical cumulative distribution function for pitch motion maxima at $F_n = 0.25$.

The results for pitch, represented in Figure 2, show that the numerical model slightly underestimated the number of pitch peaks over most of the range. The underestimation in pitch may have a direct explanation by considering that 3D flow effects are not taken into account in the numerical code and thus any higher order moment of the pressure loads amplify the effects of this simplification. In this case the simplification probably resulted in a lower pitching moment due to 3D effects at the vessel fore and aft ends.

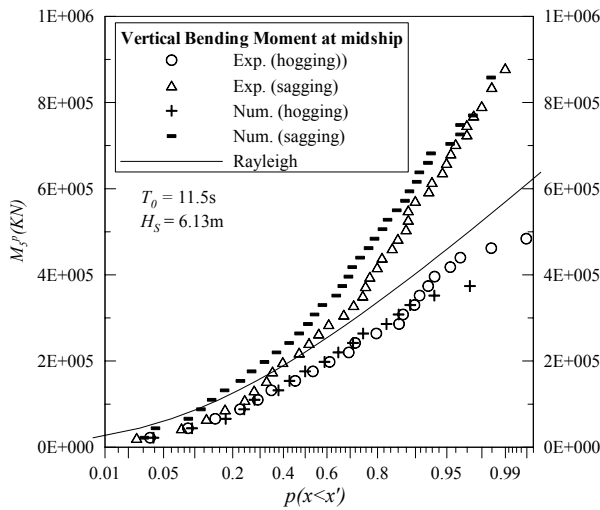


Figure 3 Vertical Bending Moment at $F_n = 0.25$.

Figure 3 shows the vertical bending moment cumulative distribution function for the midship section. Hogging peaks from the experiments and numerical results are in

excellent agreement, the sagging peaks are in very good agreement with the code slightly underestimating the number of values below a given level.

3 Simulation of Abnormal Wave Records and Time Domain calculations

In order to conduct experiments with abnormal waves, they must be generated within the test area. The Technical University of Berlin (TUB) has developed the necessary software for numerical processing of real wave records and the adequate control laws to use the processed data to generate them within a test basin ([14], [15] and [1516]). TUB's test basin has been used to perform experiments with zero speed of advance.

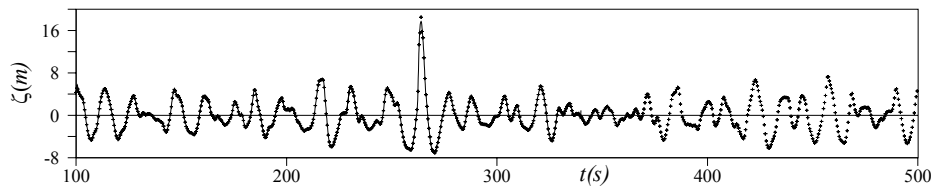


Figure 4 Time trace with 4 minutes duration using the 100 largest harmonics superimposed with the original trace (symbols).

Real data can also be numerically processed in such a way that it provides high level inputs for time domain codes such as the one described herein. Draupner “New Year Wave” time trace, which has been reported the first time in [17], has been processed using an FFT algorithm and the most important harmonic components have been used within the time domain code in such a way that, to a desired degree of approximation, the numerical model of the vessel is subject to the same wave time trace as in the tank. In order to have a spatial description of the wave field, a deep water wave dispersion relation has been used in the numerical simulation. It is important to stress that only the wave elevation at a fixed point in space has been verified at this time, because no other wave kinematics has been recorded. In Figure 4 is an example of how the numerical code uses a prescribed number of harmonics to adequately reproduce the wave trace. All calculations have assumed long crested head waves.

4 S175 Containership in the “New Year Wave”

A time domain calculation has been performed specifically for the S-175 advancing over the “New Year Wave” time trace at a reduced ship speed of 13 knots. There exist no experimental results for this specific trace, but the numerical code has shown good estimation with the previous tests so it is expected that results are at least qualitative. The numerical simulation was carried out using the non-linear and linear versions of the numerical code and it is possible to see in Figure5 that linear code fails to account for on-off events related to greenwater and for the memory effects resulting thereof. The bending moment determined from the non-linear code shows

the effect of a strong greenwater event as the vessel passes the large crested wave and plunges into the trough and the next incoming crest.

Table 2 presents the results of rule minimum requirements, linear and non-linear long-term distributions calculated with the same procedure as in [5], calculated for European Area 8 (see [18]) and for the 1E-8 probability level, along with the absolute maximum hogging and sagging bending moments in the “New Year Wave” time trace. Very large disparity is found even though the same hydrodynamic code has been used, but it is evident that the first principles based methodologies estimate that the sagging bending moment will be larger than minimum requirements, anywhere from 1.5 to 2.7 times.

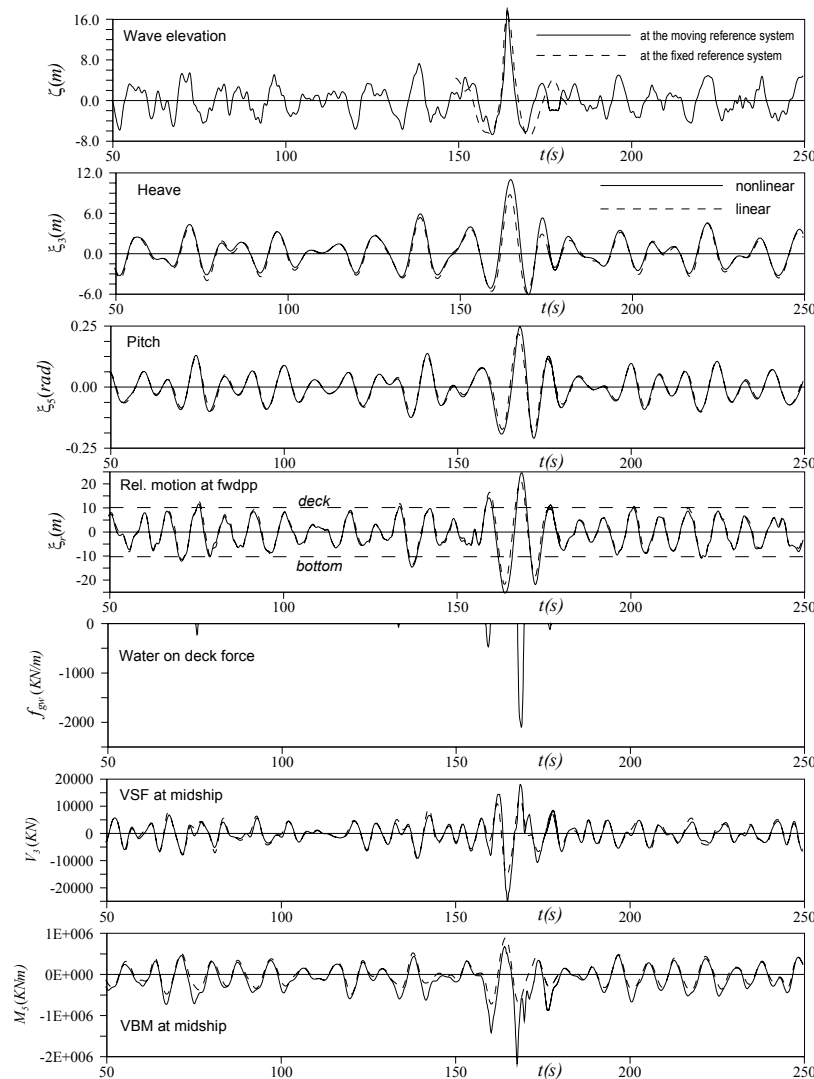


Figure 5 Time domain simulations for the “New Year Wave” at $F_n = 0.16$.

	Sagging [GNm]	Hogging [GNm]	Sagging normalized by Rule Value [-]	Hogging normalized by rule value [-]
Linear ($p = 10^{-8}$, 20 years)	1.504	1.504	1.48	1.91
Nonlinear ($p = 10^{-8}$, 20 years)	2.73	-	2.69	-
Rules minimum	1.0163	0.7879	1.0	1.0
New Year Wave	2.1796	0.6758	2.14	0.86

Table 2 Values of bending moment determined from several procedures.

The fact that long term distribution calculations give significantly larger vertical bending moments than rule values have been identified before (see [19] for instance). What is interesting to note here is that is that the maximum bending moments in this extreme wave are lower than those from the non-linear long term distribution. Since both results are based on calculations from the same nonlinear time domain code, the conclusion seems to be that during its operational life time the ship will encounter wave conditions (non abnormal) that result in larger bending moments than those induced by the “New Year Wave”

4 FPSO in the “New Year Wave”

This section presents some results for a FPSO ship, which include experimental data and time domain simulations in the “New Year Wave” trace, linear and nonlinear long term distributions and rule values.

A model of the FPSO has been subject to experimental tests at TUB’s test tank. The model was sectioned at $\frac{1}{4}$ and $\frac{1}{2}$ L_{pp} from the forward perpendicular in order to measure cross sectional loads at these positions. The vessel main particulars are given in Table 1. Details of the experimental program, the complete set of experimental data and comparisons with numerical results have been presented in [5]. This section presents a couple of graphs from those publications.

Some results of the experimental campaign and the corresponding numerical simulations for the moored vessel excited by a replica of the “New Year Wave” time trace are plotted in Figure 6. It can be observed that the general agreement is very good, with the numerical code slightly underestimating the motions and presenting a phase advance. Because the model had the possibility of rolling and the measurement methodology is ideal for heave-pitch only, the experimental heave motion measurement may have been lightly corrupted and thus the large difference at some points with no special particularity, such as between 500 and 550s. As for the bending moment, very good agreement is achieved with the only relevant mismatch being found around the very large wave.

There was also simulation of the “New Year Wave” such that it occurred at different longitudinal positions relative to the vessel’s midship section. These results are presented in Figure 7 and it is observed that with these different positions of occurrence, interestingly enough, there is no significant change of the maximum values of the bending moment.

280m FPSO		
Length between perp.	$L_{pp}(m)$	259.8
Beam	$B(m)$	46
Draught	$T(m)$	16.67
Displacement	$\Delta(ton)$	174000
Block coefficient	C_b	0.87

Table 1.- Main particulars of the FPSO vessel.

Table 4 presents results from the linear and non-linear long-term distributions for the 1E-8 probability level, together with the maximum values of bending moment from the “New Year Wave” simulation, and the rules minimum requirement. The long-term distributions have been calculated for European area 8 ([18]) which encompasses the measurement point of the “New Year Wave”.

For the FPSO the maximum bending moments in the “New Year Wave” are smaller than those required by the rules. Comparing the results in the New Year Wave with the long term distributions values, one concludes, again, that this abnormal wave will not induce the largest bending moment during the ship operational life time.

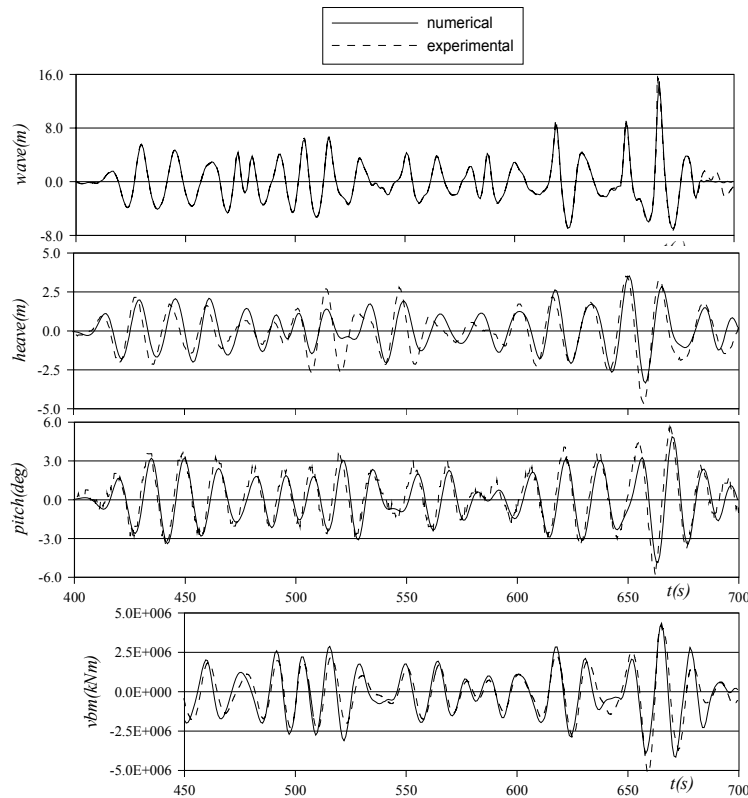


Figure 6 Time domain and experimental time traces for the “New Year Wave” record with FPSO at zero advance speed.

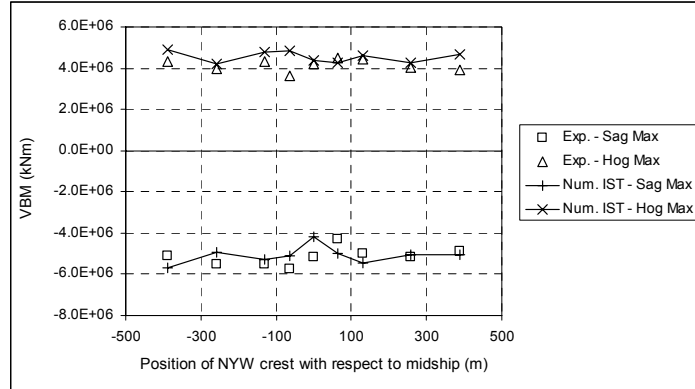


Figure 7 Maxima for different positions of occurrence of the “New Year Wave” relative to midship.

	Sagging [GNm]	Hogging [GNm]	Sagging normalized by rule value [-]	Hogging normalized by rule value [-]
Linear ($p = 10^{-8}$, 20 years)	7.3	7.3	1.30	1.38
Nonlinear ($p = 10^{-8}$, 20 years)	8.1	-	1.45	-
Rules minimum	5.6	5.3	1.00	1.00
New Year Wave	5.1	4.5	0.91	0.85

Table 2 Values of bending moment determined from several procedures.

5 Discussion and Conclusions

There is published material that has dealt with the various degrees of uncertainty arising from both the initial climate data and from the procedures themselves. In [20] it is reported that a 14% uncertainty in the final values of design bending moment due to use of different climates, while according to [19] a 15% variability in the final results arises simply from comparison of strip and panel methods and 9% if only strip theories are considered.

Here it has been shown that the uncertainty of first principles based design values is large, especially visible when comparing probability based calculations performed with linear and nonlinear pseudo transfer functions. It remains to establish the degree of detail to be included in the short term calculation such that the values can readily compare with the design values that the shipbuilding industry uses.

The direct time domain calculation for the S-175 containership estimates wave induced bending moments that are much larger than the rules minimum requirements, while the FPSO would survive this abnormal “New Year Wave” simply by having met the rules minimum requirements. It was noted earlier that long term distribution

calculations give significantly larger vertical bending moments than rule for conventional ships. What has been concluded by this investigation is that such an extreme wave like the “New Year Wave” will not induce the largest bending moment for these two ship hulls during their operational lifetimes, although its relative effect is significantly different for the containership and FPSO.

Finally, it is considered that when data exists for a specific region and there are exceptional wave events, like the “New Year Wave”, there should be an effort to evaluate the behavior and survival capability of structures that are being designed to cross or that will be fixed at the location, as if such an encounter were to happen. This method should then be taken to accompany the evolution of software in such a way that climate records become an integral part of the design stage.

6 Acknowledgements

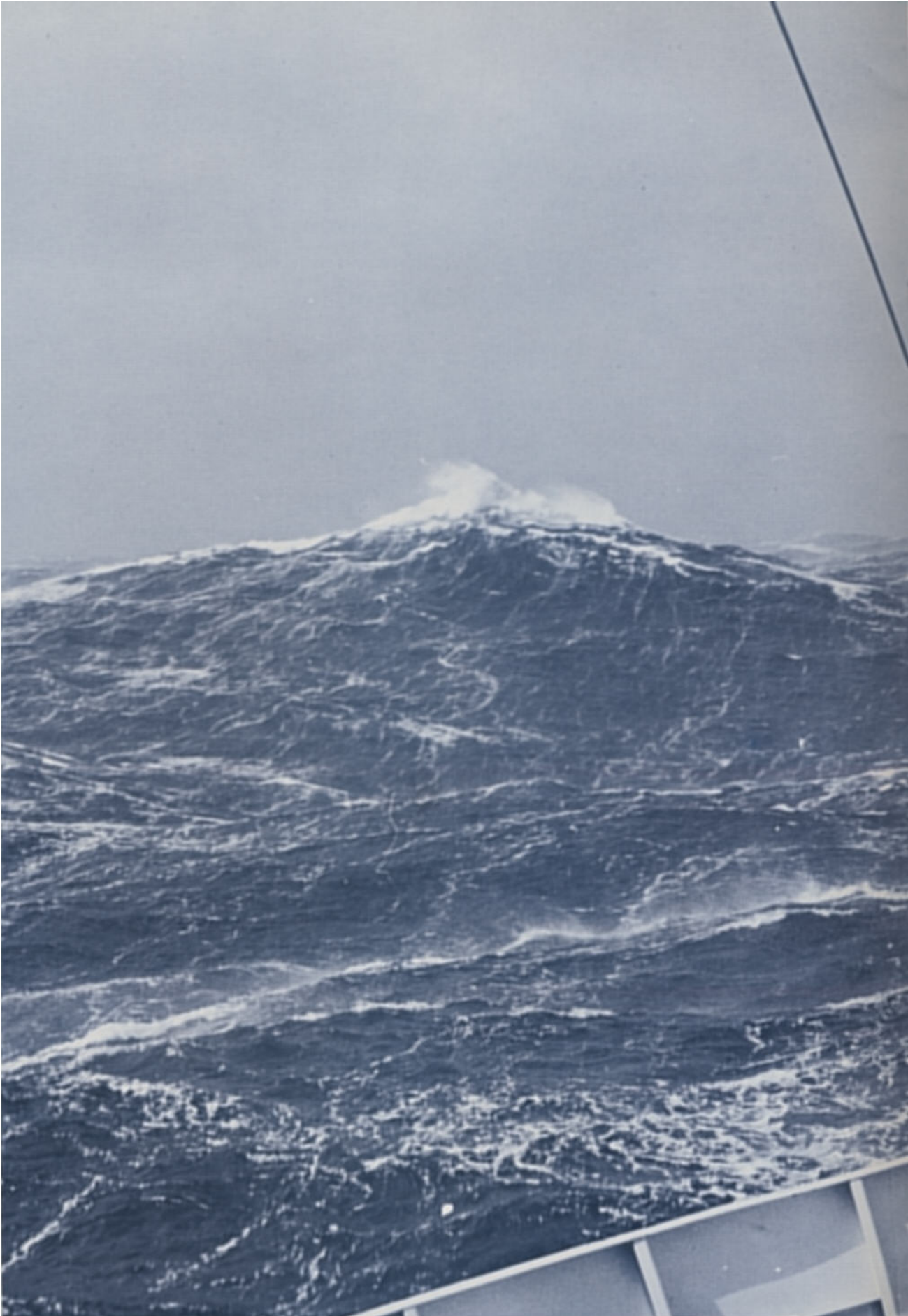
This work has been performed in the scope of the research project “Rogue Waves – Forecast and Impact on Marine Structures (MAXWAVE)”, partially funded by the European Commission, under the programme Energy, Environment and Sustainable Development (Contract no. EVK3:2000-00544).

Work of the third author has been financed by grant SFRH/BD/10527/2002 of Fundação para a Ciência e a Tecnologia.

References

1. Fukuda, J., 1967, “Theoretical Determination of Design Wave Bending Moments”, *Japan Shipbuilding and Marine Engineering*, Vol. 2, No. 3, pp. 12-22.
2. Guedes Soares, C., 1993, “Long-Term Distribution of Non-Linear Wave Induced Vertical Bending Moments”, *Marine Structures*, Vol. 6, pp. 475-483.
3. Sagli, G. and Moan, T., 2001, “Application of Contour Line Method to Estimate Extreme Ship Hull Loads Considering Operational Restrictions”, *Journal of Ship Research*, Vol. 45, No. 3, 228-240.
4. Guedes Soares, C. and Schellin, T. E., 1998, “Nonlinear Effects on Long-Term Distributions of Wave-Induced Loads for Tankers”, *Journal of Offshore Mechanics and Arctic Engineering*, Vol. 120, n° 2, pp. 65-70.
5. Guedes Soares, C., Fonseca, N., Pascoal, R., Clauss, G.F., Schmittner, C.E. and Hennig, J., 2004, “Analysis of Wave Induced on a FPSO due to Abnormal Waves”, *Proc. of OMAE Specialty Conference on Integrity of Floating Production, Storage & Offloading (FPSO) Systems*, Houston, TX.
6. Fonseca, N., Guedes Soares, C. and Pascoal, R., 2001, “Prediction of Ship Dynamic Loads in Ship in Heavy Weather”, *Proceedings of the Conference on Design and Operation for Abnormal Conditions II (RINA)*, London, United Kingdom, pp. 169-182.
7. Guedes Soares, C., Fonseca, N. and Pascoal, R., 2003, “An Approach for the Structural Design of Ships and Offshore Platforms in Abnormal Waves”, *Proceedings of the Maxwave Workshop on Rogue Waves – Forecast and Impact on Marine Structures*, Geneva.
8. Clauss, G., Schmittner, C., Hennig, J., Guedes Soares, C., Fonseca, N. and Pascoal, R., 2004b, “Bending Moments of an FPSO in Rogue Waves”, *Proceedings 23rd International Conference on Offshore Mechanics and Arctic Engineering (OMAE2004)*, paper OMAE2004-51504.

9. Faulkner, D. and Buckley, W. H., 1997, "Critical Survival Conditions for Ship Design", *Proceedings International Conference on Design and Operation for Abnormal Conditions*, RINA, paper no. 6, pp. 1-25.
10. Fonseca, N. and Guedes Soares, C., 1998a, "Time-Domain Analysis of Large-Amplitude Vertical Motions and Wave Loads", *Journal of Ship Research*, Vol. 42, n° 2, pp. 100-113.
11. Fonseca, N. and Guedes Soares, C., 1998b, "Nonlinear Wave Induced Responses of Ships in Irregular Seas", *Proceedings 17th International Conference on Offshore Mechanics and Arctic Engineering (OMAE'98)*, ASME, New York, paper OMAE 98-0446.
12. Fonseca, N. and Guedes Soares, C., 2004a, "Experimental Investigation of the Nonlinear Effects on the Vertical Ship Motions and Loads of a Containership in Irregular Waves", *Journal of Ship Research*, Vol. 48, No 2, June 2004, pp. 118-147.
13. Fonseca, N. and Guedes Soares, C., 2004b, "Experimental Investigation of the Nonlinear Effects on the Vertical Ship Motions and Loads of a Containership in Regular Waves", *Journal of Ship Research*, Vol. 48, No 2, June 2004, pp. 148-167.
14. Clauss, G., and Kühnlein, W., 1995. "Transient wave packets – an efficient technique for seakeeping tests of selfpropelled models in oblique waves". *Proceedings Third International Conference on Fast Sea Transportation*, pp. 1193–1204, Vol. 2.
15. Kühnlein, W., Clauss, G., and Hennig, J., 2002. "Tailor Made Freak Waves Within Irregular Seas", *Proceedings 21st International Conference on Offshore Mechanics and Arctic Engineering (OMAE2002)*, paper OMAE2002-28524.
16. Clauss, G., Hennig, J., Schmittner, C., and Kühnlein, W., 2004a. "Non-linear Calculation of Tailored Wave Trains for the Experimental Investigation of Extreme Structure Behaviour", *Proceedings 23th International Conference on Offshore Mechanics and Arctic Engineering (OMAE2004)*, paper OMAE2004-51195.
17. Haver, S. and Karunakaran, D., 1998, "Probabilistic description of crest heights of ocean waves", *Proceedings 5th International Workshop of Wave Hindcasting and Forecasting*, Melbourne, Florida.
18. Hogben, N., da Cunha, L.F. and Olliver, H.N., 1986, *Global Wave Statistics*, Brown Union London.
19. Guedes Soares, C., 1999, "On the uncertainty in long-term predictions of wave induced loads on ships", *Marine Structures*, Vol. 12, pp. 171-182.
20. Guedes Soares, C., 1996, "On the Definition of Rule Requirements for Wave Induced Vertical Bending Moments", *Marine Structures*, Vol. 9, pp. 409-425.
21. Guedes Soares, C., and Moan, T., 1991, "Uncertainty in the Long Term Distribution of Wave Induced Bending Moments for Fatigue Design of Ship Structures", *Marine Structures*, Vol. 4, pp. 294-315.



'Freak' Ocean Waves

Exceptionally high waves are not curious and unexplained quirks of Nature. Their occurrence can be calculated with an acceptable degree of precision.

By L. DRAPER

STORIES abound of monstrous waves; every sailor has his tale of how a great wave arose from nowhere and hit his ship leaving a trail of damaged lifeboats and shattered crockery. Estimates of the heights of the highest waves which can be encountered at sea vary widely. Cornish reported a freak wave 70 feet from crest to trough seen in the North Pacific in 1921, and waves of 80 feet and possibly higher in the North Atlantic in 1923. More recently, in 1956, Captain Grant of the cargo vessel 'Junior' reported a wave estimated to be 100 feet high about 100 miles off Cape Hatteras. There must be many more reports of similar waves in the history of the seas. As early as 1826 Captain Dumont d'Urville, a French scientist and naval officer in command of an expedition, reported encountering waves 80 to 100 feet high. The poor fellow was openly ridiculed for making such an outrageous report, even though three of his colleagues supported his esti-

mate. Perhaps the most famous reliable report was that of the wave encountered by U.S.S. 'Ramapo' in the North Pacific in 1933; that wave was estimated to be 112 feet high, a monster indeed.

Although such events happen only rarely, this does not mean that their likelihood of occurrence is not predictable. There are two aspects of this problem. One concerns what happens on a sea when a large number of wave components each with its own period and height, are traveling along together at slightly different, but constant, speeds. As the components continually get into and out of step with each other they produce the groups of high waves followed by brief intervals of relatively quiet water which are characteristic of all sea waves. Every now and then, just by chance, it so happens that a large number of these components get into step at the same place and an exceptionally high wave ensues. The life of such a wave is

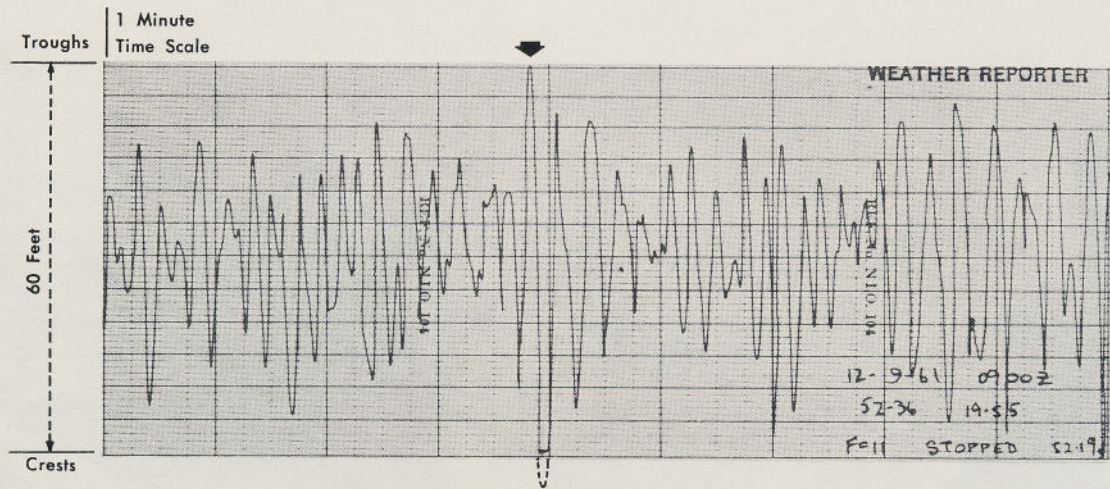
Waves

only a transient one, being not much more than a minute or two. Because each wave component is traveling at its own characteristic speed, the faster ones will escape from the others and the monster wave will die just as surely as it was born. The energy it contains belongs to its component wave trains, which still exist and travel on, taking their energy with them. Somewhere else in the storm at some other time some other wave trains will, again just by chance, coincide and produce another large wave which will have its brief moment of glory before disappearing forever into the random jumble of the sea. Although we are never likely to be able to predict just where and when an exceptionally high wave will appear, because the instrumentation problems involved are immense, the probability of occurrence of any such wave is finite and can be predicted; its calculation has the apparently contradictory title of Statistics of a Stationary Random Process. Using this theory, it has been shown that whilst one wave in 23 is over twice the height of the average wave, and one in 1,175 is over three times the average height only one in over 300,000 exceeds four times the average height.

The second aspect of the problem, also concerned with the prediction of the occurrence of exceptional waves, has a different basis. The probability of occurrence of unusual events such as severe storms, heavy rainfall, or hot summers, can be predicted by the Statistics of Rare Events. This technique has been used extensively by meteorologists in the study of natural phenomena and has proved to be a useful tool. The probability of occurrence of storms of any severity can therefore be calculated. From a series of recordings of wave conditions over a period of time such as a year, it is possible to estimate how often waves of any given size will occur by using these two methods. The longer the time over which the recordings have been made the more reliable will be the prediction.

MR. DRAPER is a physicist who, since 1953, has worked mainly on ocean waves at the National Institute of Oceanography in Great Britain.

It is only about thirteen years since it became possible to measure waves in the open sea from a ship with acceptable accuracy, and so provide a check on whether or not the stories of monstrous waves were to be believed. One of the British Ocean Weather Ships, operating in all weathers in the North Atlantic, has carried such a shipborne wave recorder for twelve years. As the ship is on station for about two-thirds of the time, the National Institute of Oceanography now has a long series of wave records which were taken for fifteen minutes every three hours. At first the scale of the instrument could record waves 50 feet high from crest to trough, but very soon it was found that waves higher than this were not uncommon and the scale was increased to 60 feet. This proved to be adequate for about nine years, but on September 12, 1961, 'Weather Reporter' lay close to the track of the dying hurricane Betsy, and as she made her routine recording at 0900 hours the pen dipped and touched the lower edge of the chart and then rose rapidly and "hit the stops" at the top — a wave over 60 feet high. A crest was fitted to this wave and it is estimated that the true height of the wave was not less than 67 feet from crest to trough. The period of this wave was 15 seconds, which meant that the weather ship was lifted over 60 feet in $7\frac{1}{2}$ seconds and then dropped almost as far in the succeeding $7\frac{1}{2}$ seconds! The probability that we actually recorded the highest wave which hit the vessel is fairly small, because the instrument is operated for only about 8% of the time. Using the first method described above one can compute that the highest wave which was felt by the weather ship during that storm was probably about 80 feet from crest to trough. At the present time the wave which 'Weather Reporter' measured is the highest one which



has ever been recorded by an instrument — conservatively estimated to be 67 feet from crest to trough.

Because the proportional area of an ocean which is occupied by vessels is incredibly small, it follows that only a minute proportion of the exceptional waves which must occur each year in an area such as the North Atlantic are ever noticed by man. It therefore seems reasonable to suppose that with only one vessel equipped with a wave recorder regularly at sea in the North Atlantic, the chance that our 67 foot wave is the highest which ever occurred is small indeed. We must by no means claim that the report from the 'Ramapo' was exaggerated.

Although one is inevitably surprised when an exceptional wave appears to rise from an apparently ordinary rough sea, and everyone who sees or feels it labels it as a freak, it is fair to say that no miracle is being witnessed; the chance of this occurring does seem to obey well established physical laws, so that the probability of occurrence of a wave of any specified height, or the probable height of the highest wave which will occur in any specified length of time, can be calculated with an acceptable degree of precision. After all, the latter problem is raised by every good engineer who hopes to build a structure in the sea, and oceanographers are expected to provide the answer!

Severe Wave Conditions at Sea

Laurence Draper

1. INTRODUCTION. Perhaps the most surprising thing about sea waves is that they come in a vast range of shapes and sizes. The casual observer on a ship in waters not exposed to an ocean, for example the southern North Sea, may rightly think that the waves he can see have all been generated

by the same wind blowing over some particular stretch of water for a fixed length of time. It then seems almost logical to deduce that all the waves ought to be of the same height, length and shape. Unfortunately this is not the case, the energy of sea waves is locked in wave components spread over a wide range of wave periods, each of which travels at a speed dictated by its period. Considering the very simple case of a sea with only two wave components, when a crest of one component overtakes the other, a higher wave will ensue. As a result of this process, high waves come in groups; during the time in which the components gradually get into phase the wave height builds up giving a train of waves of increasing height, which then decreases as the faster component travels away, until when they are out of phase the sea is temporarily fairly calm. This is the reason why it is commonly said that every seventh wave is the highest, although whether it is every fourth or every fourteenth depends on the relative speeds of the components.

2. THE HEIGHT OF WAVES. In the sea there are not two components but an infinite number, and their continual interplay makes it difficult to ascribe meaningful numbers to wave height. However, there is one parameter, named significant wave height, and defined as the average height of the highest one-third of all the waves, which is a useful one to have. It is a meaningful parameter to the theoreticians, and it has the additional virtue that on average it is very close to the value which an experienced seaman would give if asked to estimate the wave height. It has been shown by both theory and measurement that if the sea is watched for the duration of about 60 waves, typically about 10 minutes, the height of the highest wave which appears is about 1.60 times the significant height and if the sea is watched for 3 hours the height of the highest individual wave will be about twice that of the significant height. The same theory, due largely to Cartwright and Longuet-Higgins, tells us that whilst one wave in 23 is twice the height of the average wave, one in 1175 exceeds it by three times and only one wave in over 300,000 exceeds four times the average height (300,000 waves is equivalent to about once a month at sea). It is perhaps important to stress that this refers to the average height, which is about 0.63 times the significant height.

These improbable events are, of course, very rarely experienced, and almost never recorded by an instrument. However, there is in existence one record (Fig. 1), taken by the Commissioners of Irish Lights with a Shipborne Wave Recorder on *Daunt* light-vessel off Cork, showing a wave 4.1 times the average height. According to theory, this is likely to occur only once in about 700,000 waves, or one record in about 10,000. The actual height of this wave was about 42 feet, at a time when the significant height was 16.5 feet.

An important characteristic of individual waves is their lack of longevity; once again, it is simply because the really big wave is the result of a chance superposition of many components overtaking each other at one point in space and time. Before long, perhaps two or three wave

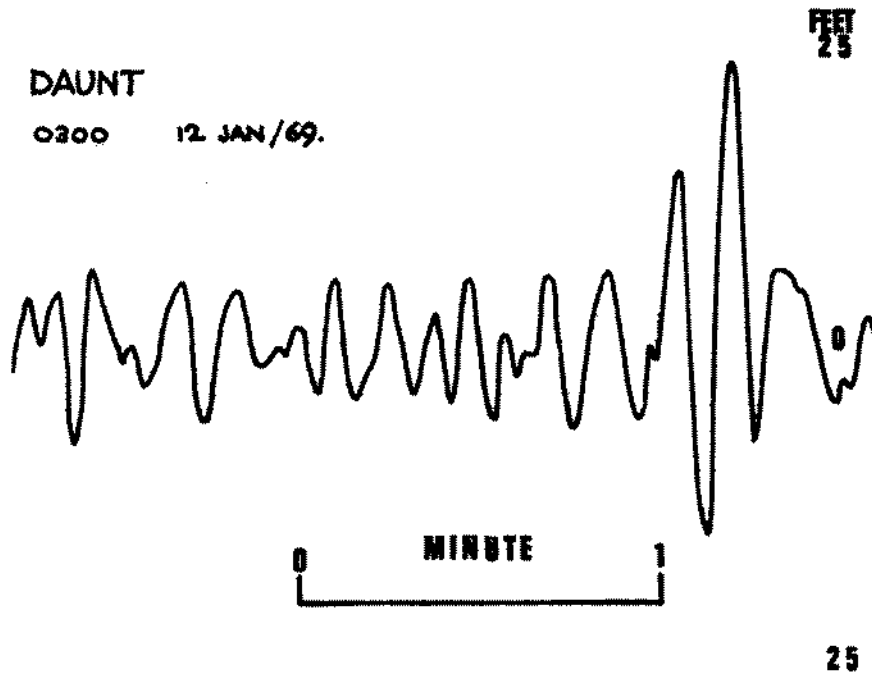


FIG. 1. Wave recorder trace taken on light-vessel *Daunt* off Cork

periods and over a distance of less than a mile, the height of any large individual wave has decreased and it is no longer distinguishable from any other wave.

It might be of interest to mention some of the large storm waves which have been reported. In 1826 Captain Dumont D'Urville, a French scientist and naval officer in command of an expedition, reported meeting waves 80 to 100 feet high, but he and three colleagues who supported him were openly ridiculed. There is an interesting report by Captain (later Admiral) Robert Fitz-Roy in the *Narrative of the Surveying Voyages of H.M.S. Adventure and Beagle, 1826-36*, London, 1839, Appendix to vol. II, p. 297.

'In H.M.S. *Thetis*, during an unusually heavy gale of wind in the Atlantic, not far from the Bay of Biscay, while between two waves, her storm try-sails were totally becalmed, the crest of each wave being above the level of the centre of her main-yard, when she was upright between the two seas. Her main-yard was sixty feet from the water-line. I was standing near her taffrail, holding by a rope. I never saw such seas before, and have never seen any equal to them since, either off Cape Horn or the Cape of Good Hope.'

This is an objective and unemotional report by an experienced sailor, and if there were several waves higher than 60 feet then the highest of all would have been appreciably higher than this. The 112 foot wave experienced by the U.S.S. *Ramapo* in the North Pacific in 1933 still seems

to be the highest reliably observed wave. In the last few years perhaps the highest claimed is the 90–100 foot wave which hit a drilling rig off Vancouver Island about 3 years ago. There is a Russian stereophotograph of the Antarctic sea surface in which the vertical distance between the highest and lowest points appears to be 82 feet, although if these two points are not on the line of travel of the wave energy it may not necessarily be justified to refer to this as a wave height.

An interesting point is that there is just as much likelihood of an unusual trough occurring as there is of an unusual crest, but of course these are not as likely to be seen unless an unfortunate vessel happens to fall into one. Nevertheless, such things have been experienced, for example, the report by the Master of the *Edinburgh Castle*, Commodore W. S. Byles, R.D., that in 1964 his vessel 'charged, as it were, into a hole in the ocean at an angle of 30° or more'. This report prompted Commander I. R. Johnston, R.N. (retd.), to recount his startling experience in the cruiser *Birmingham* during the Second World War when his vessel fell into a similar hole. The interesting thing is that, to the author's knowledge, such holes have only been reported off South Africa; there seems to be no obvious explanation for such a geographical preference, as these phenomena ought to occur at any place if waves are present.

3. HIGH WAVES IN BRITISH WATERS. Out in north-eastern parts of the open North Atlantic, the highest wave likely to be experienced each year at any location will be about 70 or 80 feet in height, and even a few miles off Land's End there will probably be a wave of over 50 feet in height almost every year. In the north-eastern Irish Sea, the eastern end of the English Channel and the southern North Sea, the highest wave each year at any open-water point is likely to be in excess of 30 feet.

As one goes northwards in the North Sea, extreme wave conditions become more severe. Structures such as those which are being operated by the hydro-carbon companies are designed to survive, for example, the 50-year wave. At places where waves have been recorded, such as Smith's Knoll, this can be estimated in two ways. One is to extrapolate the measured wave data, and this yielded an estimate of 56 feet as the height of the highest wave occurring in 50 years. The second method is to use the estimates of extreme wind speeds made by H. C. Shellard of the Meteorological Office and to apply these to a wave forecasting technique, and if one does this with the National Institute of Oceanography's technique, one ends with a figure of 53 feet as the height of the highest wave likely to be exceeded once in 50 years. The apparent agreement is better than one can expect if one considers the errors at play in both methods. In the extreme north of the North Sea conditions are approaching those of the North Atlantic. In its first winter, 1969/70, a Shipborne Wave Recorder on the Norwegian rescue and weather ship *Famita*, 160 miles east of Peterhead, recorded a wave 61 feet high, and the estimated height of the highest wave in the storm was 76 feet. More recently, in the storm of 18–21 October 1970, during which time the wind was mainly from

between west and north, the highest waves seemed to have been reported from the more easterly areas of the sea, and there were several visual observations of waves of over 70 feet in height, although the highest wave actually recorded by *Famita* in the storm was only 51 feet high.

Over the last quarter century the understanding of sea waves has improved tremendously, theory has helped us understand the processes and factors at play, and measurements have enabled us to determine with a fair degree of accuracy the sizes of the waves. It is of interest that far from ridiculing the old sailors' stories about enormous waves, modern research has confirmed that such monsters can occur, and that wave heights can exceed by an appreciable amount the maximum values which have been accepted in responsible circles.

4. ACKNOWLEDGMENT. I am indebted to Miss Margaret Deacon for bringing to my attention the report of Captain Fitz-Roy.

REFERENCE

Byles, W. S. (1965). The one from nowhere, *British and Commonwealth Review*, Feb. (This article is quoted in *The Marine Observer*, 35, 210, October 1965, together with the comments from Commander I. R. Johnston, R.N. (retd.).)

The Glorious Three

Commandant Frédéric-Moreau,
translated by Michel Olagnon¹ and G. Anderson Chase²

¹ IFREMER Centre de Brest
B.P. 70, F-29280 Plouzané, France
Michel.Olagnon@ifremer.fr
WWW home page: <http://www.ifremer.fr/metocean/>
² Department of Maritime Transportation
Maine Maritime Academy
Castine, ME04420, USA
achase@mma.edu
WWW home page: <http://www.mainemaritime.edu/>

Abstract. We were given the present note by a former cadet who went on his round-the-world cruise in 1963, and given its relevance, we decided to translate it and publish it together with the Rogue Waves 2004 proceedings.

A few explanations may be useful as to the context;

- The “Glorious Three” is the name that was given in French History to 27th, 28th and 29th of July 1830. On 25th of July, King Charles the Xth had taken four ordinances. The first two ones suspended freedom of press and the ballot law. The other two dissolved the newly elected Parliament and organized new elections. On 27th of July, workers and people of the Paris suburbs started to erect barricades. On 28th, the Arsenal, the Hôtel de ville (City Hall), Notre-Dame were taken by crowds following the tricolour flag. On 29th, Charles X offered to withdraw the ordinances; too late, and on 30th the Duke of Orleans was appointed by the Parliament King of the French People under the name of Louis-Philippe.
- The *Jeanne d’Arc* has been for many years the ship on board which French cadets of the Naval Academy sail on their round-the-world training cruise. In 1963, she was the second of that name, and was only one year from her last voyage and her replacement by the helicopter-carrier *la Résolue* who is currently the third *Jeanne d’Arc*, and close to her replacement once again. When the event occurred, the port propeller shaft had recently broken from fatigue and the propeller been lost. That was no wonder, since the ship was built in 1930 and had been sailing since 1931.
- The *Jeanne d’Arc* had a displacement of 9,200 tons and could sail at 25 knots. She was armed with 4 double 155 mm turrets, 4 75 mm-, 6 40 mm- and 20 20 mm guns. She could accomodate 156 cadets in addition to 28 regular officers and a crew of 620.

Aboard, at sea, 6th of February, 1963

Cruiser "JEANNE D'ARC"

COMMUNICATION

The morning of 4th of February was marked by a "sea event" of short duration (less than 30 seconds overall) but that nevertheless deserves a few comments to the intent, especially, of all those who were submitted to its effects without being in an appropriate position to observe the cause.

To this aim, I distribute the attached sheet that briefly presents the proceeding of the event as could be observed from the Bridge.

Some of you may have wondered: could it have made a nasty end ? It may be answered to that question:

- The *Jeanne d'Arc* should be able to withstand a 40° heel or so, and it did not quite reach 35°;
- to roll 40°, we would need to face significantly higher waves; and the height of the "Glorious Three" (15 to 20 meters) was absolutely abnormal, since even during a typhoon, it is very unusual for a wave to overpass 20 meters;
- and of course, the best way to avoid any risk of "sea event" is to remain on the shore. . .

Attention: all personnel on board.

Commander FREDERIC-MOREAU
Executive Officer

NOTE

Be reminded that "to heave to" means "to take such heading and speed as to allow the ship to ride out bad weather conditions the best she can", that is within acceptable roll and pitch limits.

"Hove-to course" depends on the kind of ship; in general, the ship should head at an angle between 30° and 50° with the waves direction, for the *Jeanne d'Arc*, "hove-to heading" is between 30° and 40°.

"Hove-to speed" depends of the waves celerity and of the distance between two consecutive crests; it should always be rather low, but still sufficient to maintain rudder efficiency. Under such conditions, the ship, who is in addition submitted to wind and wave action, progresses very slowly and drifts significantly.

Being limited to our starboard propeller makes the ship pay off to port. We were thus led to heave-to on the port tack, *i.e.* receiving wind and waves on our port side, so that the action of the propeller would add to that of the rudder and refrain the ship from paying off to starboard under the joint action of wind and waves.

Had we hove-to on the starboard tack, the action of the propeller would have added to that of wind and waves, and the rudder would probably not have sufficed to avoid the ship falling beam to the sea.

Board, at sea, 5th of February, 1963

Cruiser "JEANNE D'ARC"

Object: Clearing by the /Jeanne d'Arc/ of a "train" of three high waves on 4/th/ of February, 1963.

1 Situation

Ship position at 0945 K: about 430 nautical miles South-East of Tokyo¹.

Weather: very strong westerly gale

Wind: westerly, Beaufort 5 to 6 (speed 30 to 40 knots)

Sea: 7, westerly swell, wave height 7 to 8 meters

Course: ship hove-to on the port tack, receiving swell from two points on port side, ordered course 245° to 250° (the helmsman had great difficulties to correct yaw).

Speed: Starboard engine: 130 rpm (the ship had only her starboard propeller line remaining operative). Estimated bottom speed: 4 knots.

2 Description of the event and of action taken

2.1

At about 0947, a group of large breaking waves was sighted straight ahead, just beyond an area of relative calm water (4 to 5 meters waveheight).

The Captain ordered immediately "25° to the left", to make the ship meet them with a better heading and to protect the propeller.

The *Jeanne* paid off by about 15 degrees, allowing her to meet the first wave two points to port. The height of that wave has been estimated around 15 meters.

It heaved the ship and added to her sway to the left in such a manner that she fell into the trough with a significant trim (about 15°) and leaning greatly to starboard (heel has been estimated to 30°), then she continued paying off for about twenty degrees.

To counter that trend, the Captain ordered "Helm amidships", and then "25 to the right".

During the interval of about 100 meters in-between the first and the second wave, the *Jeanne* had time to return approximately to its waterline, but she was soon heeled over to starboard by the second wave, until the angle reached about 35° (the inclinometer of the safety H.Q. reached its block at 30° while the ship was still continuing her rolling motion).

During clearance of those two waves, the freeboard deck and the quarterdeck were submerged in turn, the sea covered the catwalks of the first deck, water

¹ Approximate position obtained from LORAN Q=31° 40' N, G=146° 50' E

reaching the top of the bulkheads at the time of maximum heel. The man on watch at the SILAS buoys, that were fixed at the height of second deck could see the buoys floating, one of the floats of the port buoy was torn away.

The third wave was cleared in similar conditions, but with not as large amplitude motions, its height being slightly less than that of the two first ones.

2.2

The total duration to clear the three waves was 30 seconds at most.

The manoeuver action that was taken has avoided that the ship take the waves head on, which would have raised the risk of serious damage to the Bridge and upper decks, and also of submitting the hull to very high stresses, especially if the ship had come to “ride over” the crest of one of the waves.

On the other hand, the ship rode her way over each of the obstacles, gliding into the troughs and never pounding nor ramming.

As a consequence, only minor damage was experienced to equipment as well as to the crew. It is noteworthy that all access to the decks had been prohibited for more than 24 hours, thanks to that no casualty was suffered.

3 Remarks

3.1

The phenomenon was characterized by 5 abnormal features:

1. The exceptional height of the waves (crest-trough height between 15 and 20 meters) and their remarkably vertical front.
2. The shortness of the gap between two consecutive waves (about one hundred meters).
3. The travelling direction of the group that came at an angle of twenty to thirty degrees from the main swell.
4. The high velocity of the wave group (about 20 knots).
5. The shapes of the waves, that showed a short crest front (600 to 800 m) with a steep decrease at both ends.

Thanks to that extraordinary shape and to their exceptional height, the waves contrasted with the still rough sea and could be detected in just sufficient time to change the ship’s heading to an appropriate course.

3.2

It should be noted that the *Victor Schælcher* which was hove-to abaft the beam at about two nautical miles and saw the *Jeanne d’Arc* disappear on three occasions into the troughs, did not have to face the wave train.

3.3

In the absence of other explanation, it may be assumed that the wave train arose from a resonance between the swell and the wind, or more probably, between two wave systems, one resulting from the wind prevailing before the passage of the cold front, the other, about 60° from the first, created by the wind blowing after the passage of the front.



Fig. 1. The *Jeanne d'Arc*, 1931-1964



Fig. 2. The Glorious Three: Liberty leading the People, painting by Eugène Delacroix

*de Gault*COMMUNICATION

La matinée du 4 Février a été marquée par un "événement de mer" de courte durée (moins de trente secondes au total...) mais qui mérite cependant de faire l'objet de quelques commentaires à l'intention, notamment, de tous ceux qui en constateront les effets sans être en bonne position pour en observer la cause.

Dans ce but, je diffuse la Fiche jointe qui expose sommairement le déroulement de l'événement tel qu'il a été observé depuis la Passarelle.

Certains d'entre vous se sont peut-être demandé : est-ce que cela aurait pu mal finir ?

À cette question on peut répondre :

- la "JEANNE D'ARC" doit pouvoir étaler sans danger une gîte de 40° environ ; or elle s'est arrêté avant 35° ;
- pour rouler de 40°, il est fallu se mesurer avec des vagues occasionnellement plus hautes ; or la hauteur des "vagues glorieuses" (de 15 à 20 mètres) était tout à fait exceptionnelle, puisque même au cours des cyclones, il est très rare que des lames atteignent 20 mètres ;
- enfin, il est certain que la manière la plus sûre d'éviter les "événements de mer" consiste à ne jamais quitter la terre ferme...

Diffusion : tous présents à bord.

Le Capitaine de Frégate FREDERIC MORAU
Commandant en Second,

P.M.

NOTA

Je rappelle que "prendre la Cape" signifie "adopter la Route et la Vitesse qui permettent au bâtiment d'étaler le mauvais temps dans les meilleures conditions, c'est-à-dire dans des limites acceptables de roulis et de tangage.

La "Route de Cape" dépend du type de bâtiment ; en général, le bâtiment doit faire avec la direction des lames un angle compris entre 30° et 50° ; pour la "JEANNE D'ARC", la Route de Cape est comprise entre 30° et 40°.

La "Vitesse de Cape" dépend notamment de la vitesse des lames et de la distance séparant 2 crêtes successives ; elle est toujours assez faible, mais elle doit être suffisante pour que le gouvernail reste efficace. Dans ces conditions, le bâtiment, qui de plus est freiné par le vent et les lames, avance très lentement et dérive beaucoup.

N'ayant que notre hélice Babord, l'action de celle-ci tend à faire abattre le bâtiment sur Tribord.

Ceci a conduit à adopter la Cape "Tribord Amures" (c'est-à-dire de manière à recevoir le vent et la mer par Tribord), afin que l'action de l'hélice, s'ajoutant à celle du gouvernail, empêche le bâtiment d'abattre sur Babord sous l'action conjuguée du vent et des lames.

Avec une Cape "Babord amures", l'action de l'hélice se serait ajoutée à celle du vent et de la mer : le gouvernail n'aurait sans doute réussi à empêcher le bâtiment de venir par de travers.

F I C H E

Objet : Franchissement par la "JEANNE D'ARC" d'un "train" de trois grosses lames, le 4 Février 1963.

-1-

1. SITUATION

Position du bâtiment à 0945 K : à 430 Neutiques environ dans le Sud-Est de TOKYO (1).

Temps : très gros temps d'Ouest.

Vent : Ouest, force 5 à 6 (vitesses de 30 à 40 nœuds).

Mer : forée 7, houle d'Ouest, creux de 7 à 8 mètres.

Route : bâtiment à la Cape Tribord amirauté reçoit la houle par deux quarts Tribord, cap ordonné : 245° à 250° (l'homme de barre éprouvant de grandes difficultés à corriger les embardées).

Vitesse : - Allure de la Machine Babord : 130 T/en (le bâtiment n'a plus que sa ligne d'arbre Babord),
- vitesse estimée sur le fond : 4 nœuds.

2. DESCRIPTION DE L'EVENEMENT ET DE LA MANOEUVRE EFFECTUEE

2.1 Vers 0947, on aperçoit droit devant de grosses lames déferlantes à un demi-nautique environ, juste derrière une zone de "calme relatif" (4 à 5 mètres de creux).

Le Commandant ordonne aussitôt "à gauche 25°", afin de présenter le bâtiment dans une meilleure position et protéger l'hélice. La "JEANNE" abat d'une quinzaine de degrés, ce qui lui permet de prendre la première lame par environ deux quarts Tribord. La hauteur de cette lame a été évaluée à une quinzaine de mètres.

Elle soulève le bâtiment en précipitant son abattée sur la gauche, de telle sorte qu'il retombe dans le creux avec une "pointe" accusée (15° environ) et en se couchant fortement sur Babord (la gîte est estimée à 30°) - puis effectue une abattée supplémentaire d'environ vingt degrés.

Pour contrarier cette tendance, et ne pas tomber plus en travers des lames suivantes, le Commandant ordonne "Zéro la barre", puis "à droite 25°".

Dans l'intervalle d'environ cent mètres qui sépare la deuxième lame de la première, la "JEANNE" a le temps de revenir à peu près dans ses lignes d'eau, mais elle est aussitôt couchée à nouveau sur Babord par la deuxième lame, jusqu'à prendre une gîte d'environ trente-cinq degrés (l'inclinomètre du P.C. Sécurité vient sur sa butée à 30° tandis que le bâtiment poursuit son mouvement de roulis).

(1) Point approximatif obtenu par LORAN : Q = 31°40' N G = 146°50' E

.../...

Au cours du franchissement de ces deux lames, la Flage Avant et la Flage Arrière sont successivement submergées ; la mer recouvre les Passavants du 1er Pont, l'eau atteignant, au moment du roulis extrême, le haut des cloisons. Le fonctionnaire des bouées GILAS qui sont fixées à hauteur du 2ème Pont voit les bouées flotter ; un des flotteurs de la bouée Tribord est arraché.

La troisième lame est franchie dans les mêmes conditions, mais avec des mouvements moins amples, sa hauteur étant légèrement inférieure à celle des deux premières.

- 2.2 La durée totale du franchissement des trois lames a été de 30 secondes au maximum.

La manœuvre effectuée a permis d'éviter que le bâtiment ne prenne les lames de bout, ce qui aurait risqué de provoquer des avaries sérieuses à la Passerelle et aux Ponts supérieurs, et, d'autre part, de soumettre la coque à des efforts extrêmement importants, notamment si le bâtiment s'était trouvé "à cheval" sur l'une des crêtes de lames.

Bien au contraire, le bâtiment a frayé son chemin en se roulant sur chacun des obstacles, en se coulant dans les creux sans jamais tasser, sans subir le moindre coup de bélier.

Aussi les dégâts subis ont-ils été mineurs, tant en ce qui concerne le matériel que le personnel, à noter que toute circulation était interdite sur les Ponts depuis plus de 24 heures, grâce à quoi il n'y eût pas à déplorer de pertes.

3. REMARQUES

- 3.1 Le phénomène a été caractérisé par 5 anomalies :

- (1) la hauteur exceptionnelle des lames (creux compris entre 15 et 20 mètres), et leur verticalité remarquable ;
- (2) le faible écart séparant deux lames successives (une centaine de mètres) ;
- (3) la direction du "train" qui présentait avec la direction générale de la houle une incidence de vingt à trente degrés ;
- (4) la grande vitesse de propagation du train de lames (de l'ordre de 20 nœuds) ;
- (5) la forme de la lame, qui se présentait qu'un front très court (500 à 600 mètres) terminé à chaque extrémité par une chute abrupte.

C'est grâce à cette forme extra-ordinaire et à leur hauteur exceptionnelle que les lames, se détachant sur une mer encore "grosse", ont pu être décalées avec le préavis juste suffisant pour faire abattre le bâtiment jusqu'à la Route convenable.

- 3.2 Il convient de noter que le "VICTOR SCHELCHER", qui naviguait à la coque sur l'Arrière du travers à 2 nautiques environ et a vu la "JEANNE D'ARC" disparaître totalement à 3 reprises dans les creux, n'a pas eu ensuite à affronter lui-même le train de lames.
- 3.3 A défaut d'autre explication, on peut admettre que ce train de lames est né d'un phénomène de résonance entre la houle et le vent ou, mieux, entre deux systèmes de houle, l'un créé par le vent régnant avant le passage du "front froid", l'autre incliné à 60° environ par rapport au premier, et dû au vent régnant après le passage du front.

A Possible Freak Wave Event Measured at the Draupner Jacket January 1 1995

Sverre Haver

Marine Structures and Risers, Statoil ASA, N-4035 Stavanger, Norway
svha@statoil.com

Abstract. A brief informal description of the weather conditions at the Draupner platform January 1. 1995 is given. During this day a wave with a majestic crest height, often referred to as *the New Year Wave* or *the Draupner Wave*, was measured by a down-looking laser. The crest height is clearly an outlier in view of what is expected for that sea state and is considered as a possible freak wave event.

1 Introductory remarks

As a response to a request for some info on this subject during the summer 2003, a brief description of the wave event and the conditions January 1 1995 at the Draupner field is given below. The description has been updated and modified several times during the last year.

The platform in the front (the platform with living quarter) is Draupner S, which was installed in the mid-eighties, while the aft platform, Draupner E, was installed during the summer 1994. Draupner E is the first platform build with a bucket foundation and in order to verify the bucket loading and bucket behaviour, the platform was instrumented for that purpose during the first winter. The instrumentation involved a down looking laser based wave sensor. The wave sensor is said to be located at a platform corner, Haver and Karunakaran (1998). Presently I do not remember which corner, but it is most likely the northern platform corner. The well-known Draupner wave was measured at the wave sensor on the Draupner E platform, i.e. the unmanned platform. It is seen that the platform is rather transparent, i.e. wave measurements are not likely to be much disturbed by the platform legs.

2 The Weather Situation January 1

The weather situation in the North Sea January 1 at 12UTC is indicated in Fig 1. The weather pattern is dominated by a major low with center in Southern Sweden causing a strong northerly wind field over the whole North Sea and Norwegian Sea. In addition to the major low, a smaller low has been moving southwards in the North Sea during the morning hours and in Fig. 1 it is indicated to be located close to

Skagerak. The effect of this smaller low is to strengthen the wind field in the western North Sea. As the smaller low moved southwards, the area with the strongest wind field moved southwards as indicated in Fig. 2. The wind conditions seemed to peak at hurricane level wind between 12UTC and 18UTC. The Draupner platform is located more or less straight west of the southern tip of Norway midway between Norway and Scotland. This means that the platform was outside the area where the wind conditions seem to have been most extreme.



Fig. 0. The Draupner S and Draupner E platforms in the North Sea,
Photo: Øyvind Hagen, Statoil.

The England – Norway ferry “Color Viking” was hit by this storm event on its way over the North Sea. In an interview, the ship master told he had never experienced such weather during his years as a ship master of Color Line ferries. The bridge of this ferry is about 30m above sea level when floating on even keel. In the same interview the ship master said that in connection with the highest waves, those on the bridge looked upwards on the wave crests approaching the vessel. Although it may be somewhat difficult relate observations to a horizontal base line in this sort of weather conditions due to ship pitching and rolling, the statement clearly suggests that a number of rather extreme wave crests seem to have occurred in a certain area of the storm event.

One interesting aspect of the overall situation is the local enhancement of an underlying strong wind field by the secondary low moving southwards. It may well be that this will result a significant increase of sea state steepness over certain areas. In

turn this may represent conditions being favourable regarding non-linear wave phenomena.

A more detailed discussion of the weather pattern that particular day can be obtained by contacting e.g. The Norwegian Meteorological Institute in Bergen.

3 Wave Conditions at Draupner

At Draupner the wave conditions started increasing late in morning. The significant wave height reached 11 –12 m just after noon and stayed at that level until early evening, Haver and Andersen (2000). For a significant wave height we will expect the maximum wave height (height from trough to crest) to be about 20, but occasionally it may well be 10-15% higher. The maximum crest height (height from still water level until wave crest) would be expected to be about 15m. We have a number of 20-minute observations of the wave condition during peak level of the storm. Most of these show nothing particular, see e.g. Fig. 3, which is rather representative for most of the 20-min. time histories. (It should be noted that we merely have one 20-min record every hour, i.e. no measurements are made for 2/3 of the time.)

The 20-min. wave history collected at about 15:20, however, did include a very extreme wave event bearing in mind the sea state conditions. The time history is shown in Fig 4, and a closer look at the extreme wave is given in Fig. 5. The maximum wave height is close to 26m. For the actual area, the wave with an annual probability of 10^{-2} (i.e. the so-called 100-year wave height) was estimated to be around 27m. This means that the wave height in itself is not that extreme, but we did not expect the wave height to be realized in a sea with a 12m significant wave height. It is more likely to be experienced in a sea state with 13-14m significant wave height.

The wave spectrum for the time history shown in Fig. 4 is shown in Fig.6. Although the estimated spectral ordinates are associated with a considerable statistical uncertainty, the estimated spectrum clearly suggests the existence of two sea systems. This is in agreement with the previous description of the weather scenario January 1 1995.

The extreme pattern of this wave event is its asymmetry about the still water level. The crest height reaches about 18.5m above still water level. For the actual area, the crest height occurring with an annual probability of 10^{-4} (i.e. 10000-year crest height) was at that time estimated to be 19.5m. This means that the crest event was not beyond design parameters, but we did not expect such a wave to occur for a significant wave height of 12m. None of our basic engineering approaches suggest the possibility of such a crest height for a 12m sea state. We think the measured event is of good quality. Of course some uncertainties may be associated with the crest height, but the uncertainties or possible biases cannot bring the wave event into the class of typical (slightly non-Gaussian) wave events. The measured structural loads do also

suggest that a big wave hit the structure, but the loads are relatively speaking not as bad as the observed crest height. Although the crest height is well beyond the 10^{-2} probability crest height, the maximum platform loads do not exceed that level. This suggests that the shape of the wave do differ from our typical design waves. As the wave passed the structure, it was rather close to a temporary deck and as I remember being told some minor damage was reported to equipment located on that deck.

To my knowledge, people onboard the next neighbour platform, see Fig. 0, did not particularly note the wave event as it happened. But of course during those weather conditions nobody will be out on the open deck area. It is said in the platform daily journal that all work on deck was stopped at 15:00 due to very strong wind.

4 Freak waves

A number of people and institutions have been given access to the Draupner time history. I think there is a general agreement that the wave event can be referred to as a freak event, i.e. an event that would not be expected under our typical engineering models for extreme wave predictions. I think there is competing ideas regarding explaining the event and not least regarding modeling it mathematically, but my favourite theory involves self-focusing of energy of a wave group into one majestic wave event, i.e. the big event steal energy from its neighbours. The major challenge from my point of view is to understand when and why this strongly non-linear self-focusing process is turned on.

5 References

Sunde, Alv (1995): "Kjempebølger i Nordsjøen" (Extreme Waves in the North Sea), Paper is written in Norwegian, Vær & Klima, Nr.1, 1995.

Haver, S. and Andersen, O. J. (2000): "Freak waves – Rare Realizations of a Typical Population or Typical Realizations of a Rare Population?", ISOPE'2000, Seattle.

Haver, S. and Karunakaran, D. (1998): "Probabilistic description of crest heights of ocean waves", Proceedings 5th International Workshop of Wave Hindcasting and Forecasting, Melbourne, Florida, January 1998.

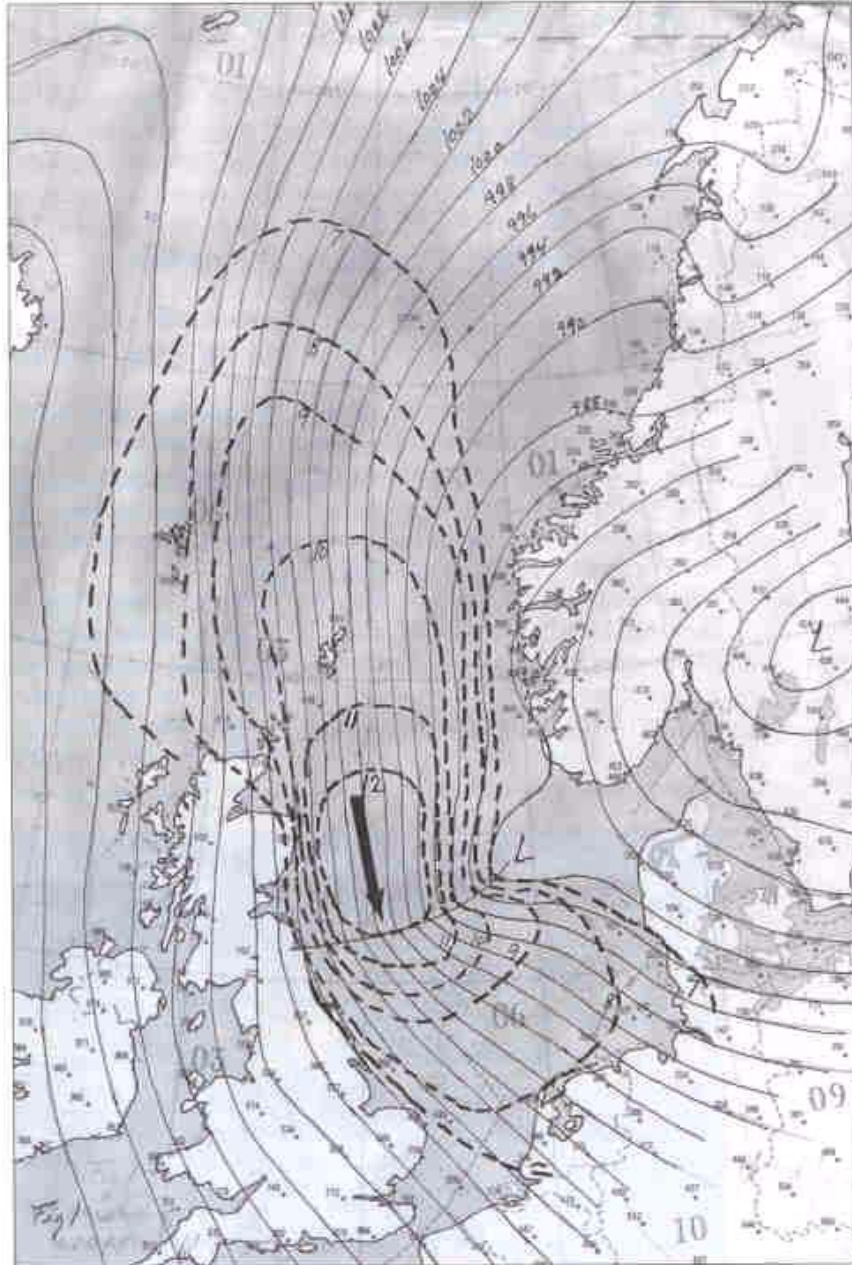


Fig. 1. Weather situation in the North Sea, Januar 1 at 12 UTC, Sunde (1995)

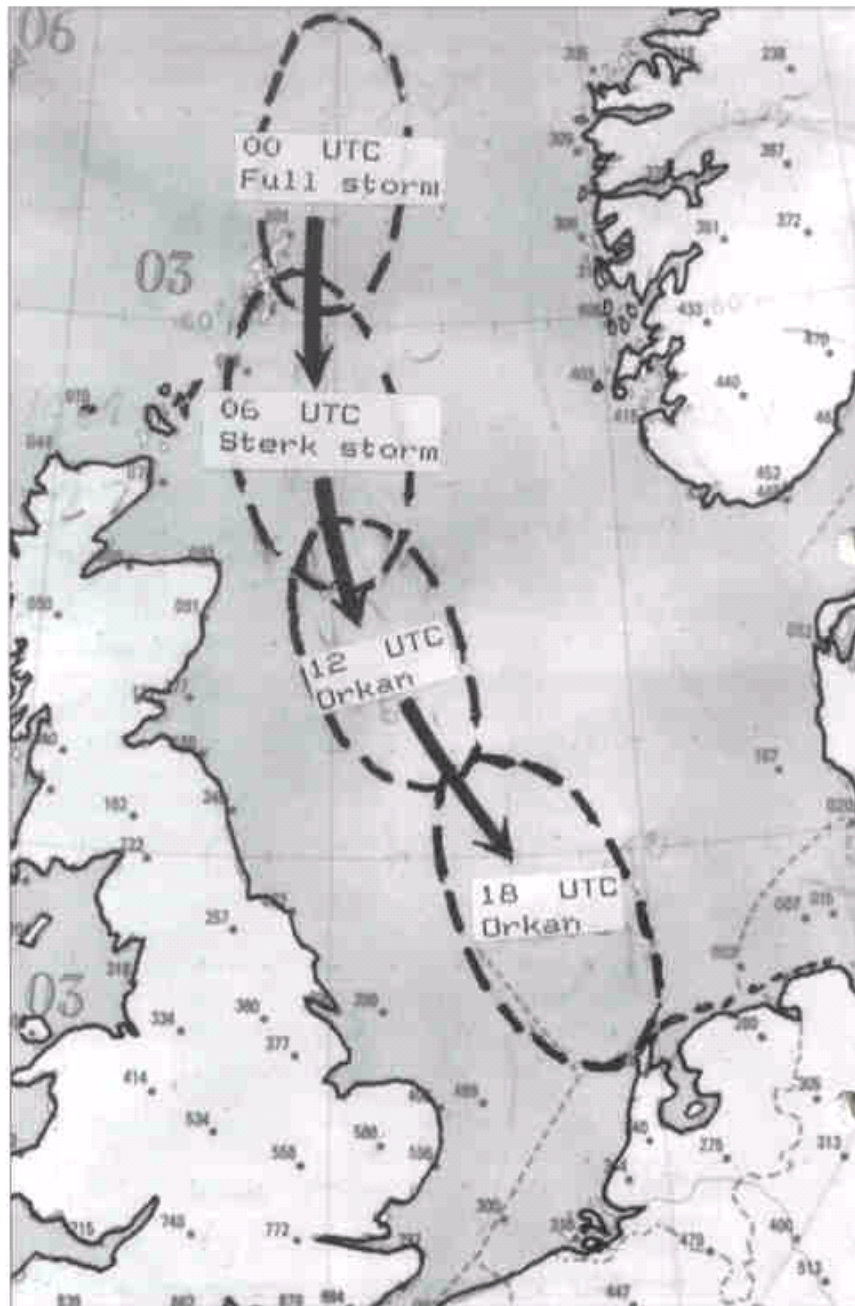


Fig. 2. Area with most severe wind during January 1, Sunde (1995).

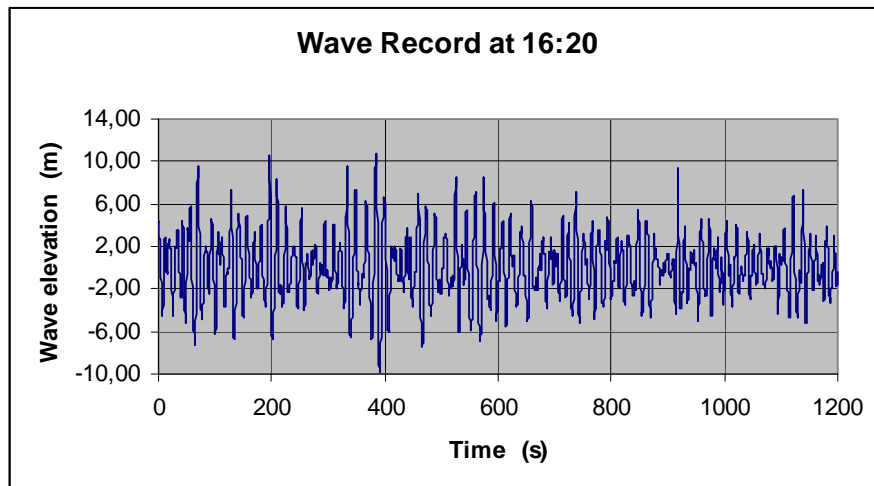


Fig. 3. A typical 20-min. time history of surface elevation during the storm.

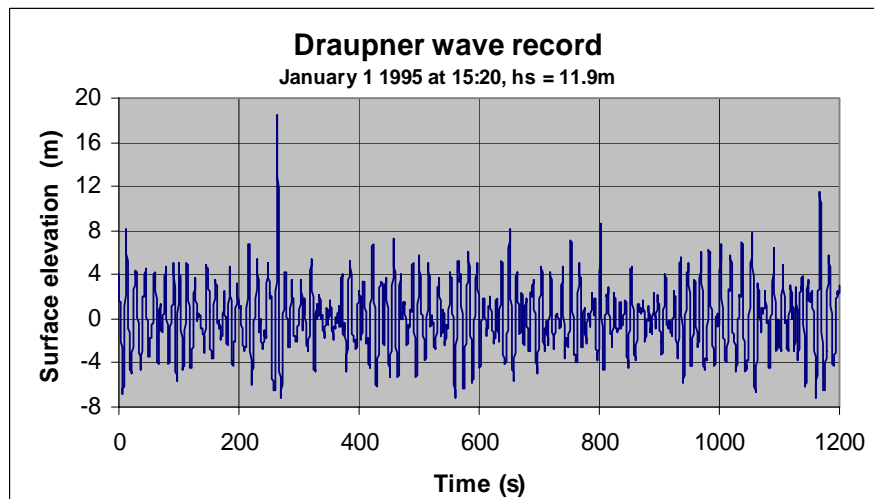


Fig. 4. Time history including an possible freak wave event

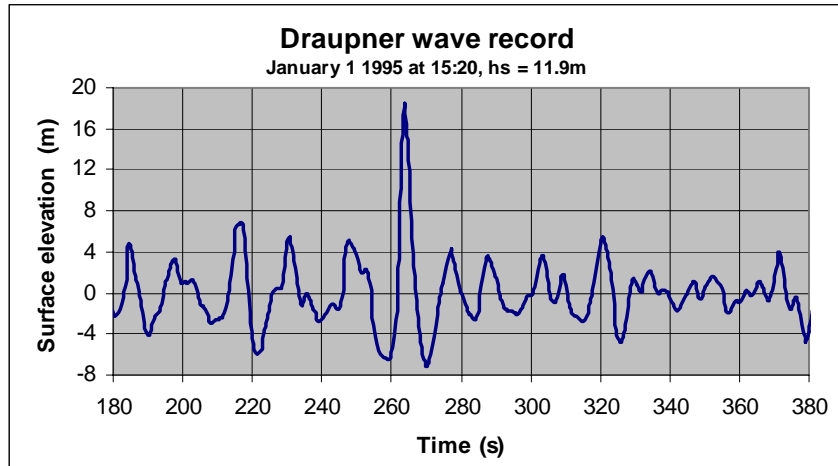


Fig. 5. A closer look at the possible freak wave event.

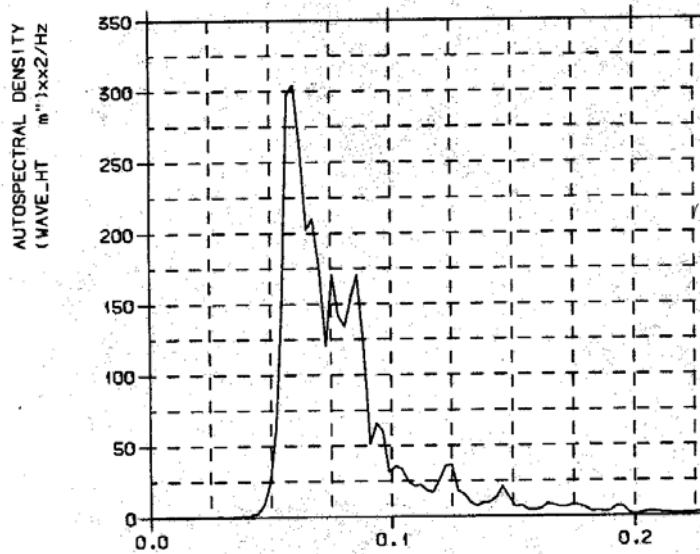


Fig. 15 Wave spectrum for the time history in Fig. 13.

Fig. 6. Estimated wave spectrum for the 15:20 wave time history, Haver and Karunakaran (1998)

Achevé d'imprimer sur les presses de Cloître Imprimeurs

ISSN 0761-3962

ISBN 2-84433-150-5 / Dépôt légal 3^e trimestre 2005

All rights reserved - © 2005, Ifremer.

No part of the material protected by this copyright notice may be reproduced or utilized in any form or by any means, electronic or mechanical including photocopying, recording, or by any information storage and retrieval system, without written permission from the copyright owner.

Rogue waves 2004 Brest, 20-21-22 October 2004

Since the Rogue Waves 2000 workshop, significant advances have been made in the proposition of models and descriptions that may improve our understanding of rogue waves. Questions arise now on how those results should influence standard practices in the shipbuilding and offshore industries, and whether they allow to improve forecast and warning systems. The Brest Rogue Waves 2004 workshop gathered again many scientists and engineers to an opportunity to confront and discuss their views on the subject.

Keywords: ocean waves, extremes, rogue waves, freak waves.

Rogue waves 2004 Brest, 20-21-22 octobre 2004

Depuis le colloque Rogue Waves 2000, des avancées significatives ont été réalisées dans la description et la proposition de modèles susceptibles d'améliorer notre compréhension des vagues scélérates. Les questions qui se posent maintenant concernent l'influence que ces résultats doivent avoir sur les normes et pratiques de la construction navale et offshore, et s'ils apportent des possibilités d'amélioration pour les systèmes de prévision et d'alerte. Le colloque Rogue Waves 2004 de Brest a de nouveau rassemblé de nombreux scientifiques et ingénieurs qui ont pu y confronter et discuter leurs positions sur le sujet.

Mots-clés : vagues, extrêmes, vagues anormales, vagues scélérates.

Ifremer

actes de colloques

39

Éditions Ifremer

BP 70, F-29280 Plouzané
tél. 33 (0)2 98 22 40 13
fax 33 (0)2 98 22 45 86
mél : editions@ifremer.fr

DIFFUSION :

INRA Éditions

RD 10, F-78026 Versailles Cedex

VENTE PAR CORRESPONDANCE :

tél. 33 (0)1 30 83 34 06

fax 33 (0)1 30 83 34 49

mél :

Inra-Editions@versailles.inra.fr

VENTE AUX LIBRAIRES ET ASSIMILÉS :

tél. 33 (0)1 30 83 34 01

fax 33 (0)1 30 83 31 58

mél : foucher@versailles.inra.fr

ISSN 0761-3962
ISBN 2-84433-150-5

35 €

 **Brest**
métropole océane
COMMUNAUTÉ URBAINE

